Characterising the anti-convulsant effects of CBD and CBDV on layer II of the medial entorhinal cortex of rat and human brain tissue *in vitro*

Benjamin Henley

Doctor of Philosophy

Aston University

March 2018

Aston University

Characterising the anti-convulsant effect of CBD and CBDV on layer II of the medial entorhinal cortex of rat and human brain tissue *in vitro*

Benjamin Henley, Doctor of Philosophy

March 2018

Epilepsy is a common and serious neurological disorder, which manifests in seizures, and has an incidence of approximately 1% of the world population. In developed nations, most instances are relatively well controlled through the use of anti-epileptic drugs (AEDs). For around a third of cases, AEDs are ineffective, resulting in poorly maintained seizures otherwise known as refractory, or drug-resistant epilepsy (DRE).

Currently, treatment of DRE often requires neurosurgery to be performed to resect seizure generating foci. Historically, such treatment was used as a last resort due to the invasive and higher risk nature of neurosurgery. More recently, however, surgical intervention has been performed much earlier in order to achieve better long-term patient outcomes. Notwithstanding this, DRE presents a major and as of yet, unmet clinical need for new and effective anti-epileptic drugs to be found.

In vitro and *in vivo* electrophysiological methods have been used investigate epilepsy for many years. Neuronal network oscillations and single cell patching recordings between physiological and pathophysiological samples provide a basis to compare alterations between normal and epileptic brain tissue. In terms of electrophysiological approaches, the hippocampus and entorhinal cortex (EC) are two of the most commonly studied areas of the brain, especially in relation to temporal lobe epilepsy (TLE).

Plant derived cannabinoids – phytocannabinoids – have been proposed as effective AEDs for DRE cases. In particular the non-psychoactive phytocannabinoids cannabidiol (CBD) and cannabidivarin (CBDV), with recent clinical trials supporting this claim.

The present study is an investigation into whether CBD and CBDV are suitable and effective AEDs, and to identify their mechanism(s) of action. Electrophysiological recordings of medial entorhinal cortex (mEC) layer II principal cells have been studied due to their relative importance and participation in TLE. Alterations in oscillatory rhythms and single cell responses were compared between RISE afflicted epileptic rats (SE rats) and wild type, age matched controls (AMC). Experiments on human tissue resected from children with TLE were also performed, concurrent with the rodent experiments.

Key findings from this project show CBD(V) suppressant effects on induced gamma oscillations, in an age- and disease-dependent manner in rat tissue, suggesting damping of neuronal network excitability. Further to this, CBD induces increased GABA inhibition onto rat medial entorhinal principal cells as evidenced by increases in mean median decay times and inhibitory charge transfer across the postsynaptic membrane, while CBDV did not show this effect. The effects of CBD were effectively blocked by both $GABA_AR$ and NMDAR antagonists, suggesting interaction with both of these receptors to exert the response. CBD also showed additive effect to low-dose benzodiazepine and barbiturate agonists and a ceiling effect at higher doses, suggestive of an allosteric action on the $GABA_AR$. Similar effects were also noted in the human tissue cells, suggestive of an analogous mechanism of action in humans.

Hence, we postulate that CBD is acting at both postsynaptic $GABA_ARs$, as a positive allosteric modulator (PAM) and, at pre-/postsynaptic NMDARs, either directly or indirectly, to positively influence GABA signalling mechanisms causing an increase in inhibitory activity at postsynaptic principal cells resulting in decreased neuronal excitability.

Keywords: oscillations, gamma, GABA, interneurons, phytocannabinoids

Acknowledgements

First and foremost, I would like to express my gratitude to my supervisor Prof. Gavin Woodhall, whose continuing guidance and support enabled me to thoroughly enjoy my PhD. I would also like to thank my associate supervisor Prof. Ian Stanford for his help throughout my project. Alongside this, I would also like to thank Dr. Stuart Greenhill who provided ideas and support especially with regards to the data analysis.

I would also like to extend my gratitude to the staff of the biomedical facility at Aston University who were always on hand to provide assistance, my thanks especially to Wayne and Matt who were particularly supportive.

Of course, I also wish to thank all my past lab mates who made working in the lab such a good experience including, Swetha, Sukhe, Max, Darshna, Nick, Jane, Mazhar, Katy and Becky.

I should also like to thank the Henley lab at the University of Bristol for allowing reproduction of certain figures, especially Hope Needs and Sonam Gurung.

Finally, I wish to thank my family for their enduring support throughout my moaning.

TABLE OF CONTENTS:

LIST OF FIGURES:

LIST OF TABLES:

LIST OF ABBREVIATIONS:

μM - Micromolar

2AG - 2-Arachidonoyl glycerol

aCSF – Artificial cerebral spinal fluid

saCSF – Sucrose-based artificial spinal fluid

AD – Afterdischarges

AEA – Anandamide

AEDs – Anti-epileptic drugs

AMC – Age-matched control

AMPA - α-amino-3-hydroxy-5-methyl-4-isoxazolepropionic acid

AP – Action potential

(n)AUC – (Normalised) Area under the curve

BZ - Benzodiazepine

CA - Cornu ammonis (1/2/3)

Ca^{2+} - Calcium ion

cAMP - Cyclic adenosine monophosphate

CBD – Cannabidiol

CBDV – Cannabidivarin

CBN – Cannabinol

CBR – Cannabinoid receptor

CCK – Cholecystokinin

Cl^- - Chloride ion

CNS – Central nervous system

DG – Dentate gyrus

DMSO - Dimethyl sulfoxide

DRE – Drug resistant epilepsy

eCB – Endocannabinoid

(N)ECT – (Normalised) Excitatory charge transfer

EEG - Electroencephalogram

ECoG – Electrocorticography

(s)EPSCs – (Spontaneous) Excitatory postsynaptic currents

EPSP – Excitatory postsynaptic potential

FAAH - Fatty acid amine hydrolysis

FCD – Focal cortical dysplasia

FFT – Fast Fourier transform

g - Grams

GΩ – GigaOhm

GABA(R) - γ-aminobutyric acid (receptor)

GPCR – G-protein coupled receptor

hrs - Hours

HFO – High frequency oscillations

HT – Human tissue

(N)ICT – (Normalised) Inhibitory charge transfer

I/M – Intramuscular

IEI – Inter-event interval

ING – Interneuron-network gamma

(s)IPSCs – (Spontaneous) Inhibitory postsynaptic currents

IPSPs – Inhibitory postsynaptic potentials

K^+ - Potassium ion

KA – Kainic acid

KAR – Kainate receptor

LFP – Local field potential

LiCl – Lithium chloride

M1 – Muscarinic acetylcholine receptor subtype 1

mACh – Muscarinic acetylcholine

MAGL - Monoacylglycerol lipase

mEC – Medial entorhinal cortex

MEG – Magnetoencephalography

Mg^{2+} - Magnesium ion

mGluR – Metabotropic glutamate receptor

MF – Mossy fibres

mIPSC - Miniature inhibitory postsynaptic currents

min - Minutes

mM – Millimolar

mnths - Months

MOA – Mechanism of action

ms – Milliseconds

Na^+ – Sodium ion

NaCl – Sodium chloride

NAM – Negative allosteric modulator

NATS - N-acyltransferases

NArPE – N-arachidonoyl-phosphatidyl-ethanolamine

nM – Nanomolar

NMDA(R) - N-methyl-D-aspartate (receptor)

NO – Nitric oxide

NPY - Neuropeptide Y

NREM – Non-rapid eye movement (sleep phase)

PAM – Positive allosteric modulator

PCA – Principal component analysis

PHR – Parahippocampal region

PING – Pyramidal-cell interneuron-network gamma

PLI – Pyramidal looking interneurons

PNS - Peripheral nervous system

PSBB – Post status behavioural battery

PSP – Postsynaptic potential

PV – Parvalbumin

RISE – Reduced intensity status epilepticus (model)

sec - Seconds

S/C – Subcutaneous

SE – Status epilepticus

SEM – Standard error of the mean

SLE – Seizure-like events

SOM – Somatostatin

SRS – Spontaneous recurrent seizures

TA - Temporoammonic pathway

THC - Δ^9-tetrahydrocannabinol

TL – Temporal lobe

TLE – Temporal lobe epilepsy

VIP - Vasoactive intestinal polypeptide

VFO – Very fast oscillations

VPA – Valproic acid

VSO – Very slow oscillations

wks - Weeks

Chapter 1

Introduction

1.1 Aims and objectives

Given the relative paucity of investigation in the effect of both CBD and CBDV *in vitro*, we were first interested to uncover whether any effect was visible on neuronal oscillations in the mEC layer II in normal brains. The mEC was chosen due to its importance and connections to the hippocampus as well as its role in temporal lobe epilepsy. Alongside this we were interested in the possible anticonvulsant effect of CBD(V) in epileptic brains. As such, we could compare the responses of each to look if any disease specific effects of CBD(V) were present. Further to this, study into any effect of CBD(V) on single pyramidal cells in the mEC layer II was also investigated. As such the following set of aims was produced:

- Uncover whether an effect of CBD and CBDV was present on induced gamma oscillations in the mEC layer II
- Produce dose-response curves for each phytocannabinoid for three defined age ranges of epileptogenesis and normal rats (24-hours post SE, 1-week post SE, 3-months post SE)
- Characterise any effect of CBD on single pyramidal cells of mEC layer II
- Assess whether any effect could be modulated or inhibited, and if so, by what
- Investigate human tissue principal cell responses to CBD

1.2 The temporal lobe

The temporal lobe (TL) is one of four major lobes of the brain, situated within the cerebrum, the others include: frontal, parietal and occipital (visible in **Figure 1.1**). Its functions are largely sensory input processing for visual memory, language comprehension and emotional association (Squire et al., 2004).

Figure 1.1 Schematic showing general subdivisions of the human brain into the four major lobes. Lobes are colour coded and labelled: frontal lobe (blue), parietal lobe (yellow), occipital lobe (red) and, temporal lobe (green). Adapted from (Gray and Lewis, 1918).

The lobe is generally divided between two cortices: the neocortex and the allocortex. The neocortex is postulated to be the most evolutionary recent area of the mammalian brain, with neocortex translating to “new cortex” (Rakic, 2009). The neocortex is heavily involved in sensory perception and behavioural response, i.e. the generation of motor commands. Further split into two cortices, the true isocortex and the pro-isocortex, the structure and function of the neocortex is relatively well defined. The true isocortex has clear and well defined laminar structure and spans across much of all the four brain lobes, covering structures from the parahippocampal region and cingulate gyri as well as the insula (Zilles, 1990). The pro-isocortex acts a transitional region between the true isocortex and the allocortex (Moser et al., 2014).

The allocortex contains the phylogenetically older parts of the cerebral cortex (Creutzfeldt, 1995) including, for example, both the olfactory system and hippocampus. It contains three subdivisions: the archicortex, encompassing the hippocampus and subiculum, the paleocortex, essentially the olfactory system, and periallocortex, containing the entorhinal

regions. The periallocortex is the section of allocortex that has historically been viewed as the transitional section between the neocortex and the allocortex. The pro-isocortex of the neocortex and periallocortex of the allocortex are split by the rhinal fissure, which acts as a physical border for the regions, providing a transition between the two cortical divisions (Creutzfeldt, 1995).

The neocortex is comprised of either five or six layers whereas the allocortex is characterised as having three or four layers, this allows each cortex division to be relatively easily identified (Creutzfeldt, 1995). Intervening between these subsections is the transitional area of pro-isocortex and periallocortex, where the layers increase from three to six (Moser et al., 2014). Where the two cortices meet encompasses the parahippocampal region, including the entorhinal cortex, postrhinal and perirhinal cortices, where the cortical layers increase from 3 in the hippocampal region to 6 in the parahippocampal region (Moser et al., 2014).

Figure 1.2 Schematic showing the location of the temporal lobe in rodents and humans. The colours highlight different structures. Red – CA3, light blue – CA1, light green – Perirhinal cortex (PrC), dark green – Postrhinal/parahippocampal cortex (rodent/humans) (POR/ParaHIP), yellow – LEC, dark blue – MEC. Taken from (Sauvage et al., 2013).

In rodents and other small mammals, the cortices are smooth, however in primates and larger mammals, the cortex is rugose, with grooves (sulci) and ridges (gyri) providing a dramatically larger surface area, as can be observed in **Figure 1.2**.

1.2.1 The hippocampal formation

Figure 1.3 Schematic of the structures of the hippocampus.
Structures include: DG, CA3, CA1 and entorhinal cortex (EC). Prominent connections between these regions are noted. Input emanating from the EC terminate in the DG (1) and CA3 (2). Mossy fibres (MF) connect the DG and CA3 (3). Schaffer collaterals shown between the CA3 and CA1 (SC; 4). Output from the CA1 passes back to the EC via the subiculum (S). CA3-CA3 recurrent collaterals are not shown. Taken from (Patten et al., 2015)

The hippocampus's name is derived from the Latin for sea horse and is so-named due to the resemblance between the two. It is a component of the limbic system, a set of structures including: the amygdala, the olfactory bulbs, fornix, nucleus accumbens and, the hypothalamus (Hopper and Vogel, 1976). The limbic system is ascribed as being vital to a variety of functions such as, short-term memory, emotion, motivation and olfactory processing. The hippocampus is situated in the medial temporal lobe, beneath the cerebral cortex. Due to its connections with the entorhinal cortex it is able to communicate with all areas of the neocortex (Amaral & Lavenex, 2007).

The hippocampal formation includes all constituent members of the hippocampus proper: *cornu ammonis* – literally translated to "Amun's horns", a reference to the Egyptian god Amun, a ram, of which the hippocampus bears a likeness to - (CA) 1, CA2, CA3, the dentate gyrus (DG), plus the subiculum. All are included within the allocortex due to their enduring presence in more primitive brain types (Hopper and Vogel, 1976).

The DG is a single cell layer consisting of tightly packed granule cells which encircle the CA3 region of the hippocampus. The DG is divided into two – the fascia dentata and the hilus. The fascia dentata is credited as being the oldest formation of the hippocampus. It receives the majority of its input via the perforant pathway from superficial EC layers (see **Section 1.1.2.1**)

and, receives GABAergic and cholinergic input from the medial septum (Amaral et al., 2007). It is estimated that rat fascia dentata contains 1,000,000 granule cells, from which mossy fibres emerge and synapse onto the hilus and CA3, receiving feedback from reciprocal mossy cells from the hilus (Amaral et al., 2007).

The CA3 region is the “pacemaker” of the hippocampus as it provides the internal rhythm, described as a spontaneous gamma oscillation generator (Jackson et al., 2011). CA3 contains mostly pyramidal cells and receives input from the mossy fibres of granule cells in the DG. A majority of input in the CA3 is received from the perforant pathway emanating from superficial EC layer II and passing through the DG, via the tri-synaptic loop (Amaral and Witter, 1989). Aside from input provided by DG and EC cells, CA3 cells have recurrent connections – CA3-CA3 – marking it apart from other hippocampal regions (Miles and Wong, 1986). CA3 outputs most notably via Schaffer collaterals that extend to the CA1, passing information along the perforant path (Arrigoni and Greene, 2004).

The CA2 is a generally described as a transitional region between CA3 and CA1 due to its small size (Ishizuka et al., 1990; Woodhams et al., 1993). It does receive some input from the perforant pathway via mEC LII pyramidal cells, and also from CA3 Schaffer collaterals. Despite this, it is not thought to have a significant role in hippocampal function, though this view is now being challenged as further investigations into the CA2 region are underway (Arrigoni and Greene, 2004; Mercer et al., 2007).

CA1 receives significant input from the CA3 Schaffer collaterals, and sends output to both the subiculum and layer V of the entorhinal cortices via the tri-synaptic pathway. Alongside this, layer III + V of the EC are able to interact directly with CA1 via the temporoammonic pathway (TA), described in a later section (**Section 1.1.3**). CA1 provides the main output of information to the cortical regions of the brain (Van Groen and Wyss, 1990).

1.2.2 The parahippocampal region

The parahippocampal region (PHR) encompasses the area surrounding the hippocampus and, it too, is part of the limbic system (Hopper and Vogel, 1976). Generally, the PHR is divided into 5 disparate regions: the entorhinal cortex (EC), subdivided into medial and lateral entorhinal cortex (mEC/ lEC), the perirhinal cortex (PER), the postrhinal cortex (POS), the presubiculum (PrS) and parasubiculum (PaS). It is distinguishable from the structures of the hippocampal formation through two major features: the clear laminar organisation and increased number of cellular layers (6); and differences in connectivity, with PHR structures typically displaying more reciprocal connections.

There is some debate as to how to correctly categorise these two formations with some including the entorhinal cortices in the hippocampal formation (Schultz and Engelhardt, 2014), however for the purposes of this thesis, I shall be following the definitions of Moser et al, set out in the review and described above (Moser et al., 2014).

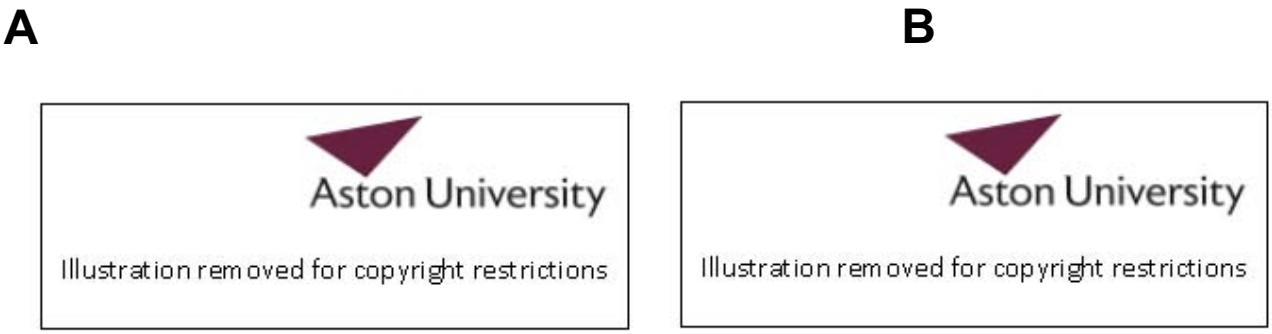

Figure 1.4 Schematic showing hippocampal location in the rodent brain.
A) Indicates the position of both the hippocampal and parahippocampal structures within the rodent rat brain on 3-axes, rostral-caudal, dorsal-ventral and lateral-medial (labelled). Left panel shows lateral view and right, caudal. Colour coding corresponds as follows: dentate gyrus (DG; dark brown), CA3 (middle brown), CA2 not shown, CA1 (orange), subiculum (Sub; light brown), presubiculum (PrS; light blue), parasubiculum (PaS; dark blue), medial entorhinal cortex (MEC; light green), lateral entorhinal cortex (LEC; dark green), perirhinal cortex (split in Brodmann's area A35 (pink) and A36 (purple)), postrhinal (POS; blue-green). B) Transverse slice taken from rat brain, showing connected hippocampal-entorhinal structures. Hippocampal formation limited to: DG, CA1, CA3, subiculum; parahippocampal therefore includes: pre-and para-subiculum, mEC and lEC and postrhinal cortex. Cortical layer indicated by Roman numeral. Adapted from van Strien et al., 2009.

1.2.3 Hippocampal and parahippocampal connectivity

The major hippocampal circuit is the tri-synaptic pathway, which describes the flow of information around the hippocampus, also sometimes known as the 'hippocampal loop'. First described by Ramón y Cajal in the early twentieth century using Golgi staining techniques, the tri-synaptic pathway consists of three synaptic junctions covering the whole hippocampal region (Amaral and Witter, 1995).

The basic pathway is as follows:

Synapse 1: Pyramidal cell axons located within the superficial layers of the EC project down and synapse onto granule cells of the DG.

Synapse 2: Mossy fibres from the DG synapse onto CA3 pyramids.

Synapse 3: Schaffer collaterals from CA3 project onto pyramidal cells of the CA1, thus completing the loop of the hippocampal formation. Cells within CA1 are able to interact and synapse onto layer V cells of the EC but are also able to output to cortical regions as well.

High amounts of multimodal information are delivered to the hippocampus mainly along the perforant pathway (PP), the pathway that connects the entorhinal cortex regions to the

hippocampus proper and subiculum (Witter et al., 2000; Vago and Kesner, 2008). Axons from the glutamatergic stellate and pyramidal cells in the superficial layer II, and also possibly from small pyramidal cells deep in layer VI, project through the subiculum - hence the name PP. These axons terminate as synapses onto granule cells and mossy cells of the DG, as well as CA3 and CA1 and, possibly pyramidal cells of CA2 (Andersen et al., 1966, 1971; Amaral et al., 1990; Yeckel and Berger, 1990). This pathway forms the basis of the tri-synaptic pathway. The PP is split between medial and lateral depending on which part of the EC the axon originates from (either mEC or lEC), to give either medial PP (MPP) or lateral PP (LPP) (Bliss and Lømo, 1973; McNaughton and Barnes, 1977). The PP is crucial in memory consolidation and spatial learning and memory and, has been implicated in animal-based models of depression (Remondes and Schuman, 2004; Kallarackal et al., 2013).

Axonal fibres from layer III, and also deep layer V, are able form a slightly altered pathway, branching off in the subiculum to form the temporoammonic (TA) pathway, which terminates in the CA1 (TA-CA1 pathway) (Aksoy-Aksel and Manahan-Vaughan, 2013). The TA-CA1 pathway has been shown to be crucial in spatial memory consolidation and has also been implicated in some models of depression (Lisman and Otmakhova, 2001; Treves, 2004; Hasselmo and Eichenbaum, 2005; Rolls and Kesner, 2006).

Efferent output from CA1 and the subiculum project to layer V cells of the mEC (Woodhams et al., 1993; Witter et al., 2000; van Groen et al., 2003). These connectivity pathways are identical for outputs from the lEC, with the single neuronal targets being the same as those of the mEC in CA2, CA3 and DG, but different in CA1 and subiculum (Moser et al., 2014). mEC outputs originate in the PrS and PaS. The majority of the EC neurons synapse onto excitatory pyramidal cells in the DG and CA3 regions of the hippocampal formation, allowing for an excitatory/positive, forward feedback loop to be formed between the hippocampus and the PHR (represented in **Figure 1.5**). Some neurons project and synapse onto inhibitory interneurons, which produces an inhibitory or negative feedback loop between the two regions (Buzsaki, 2011).

The destination and processing of information from the EC to the hippocampus are likely determined through the dynamic balance of inhibitory and excitatory synapses and level of neuronal excitability at each layer of the EC (Jones and Buhl, 1993; Witter et al., 2000).

Figure 1.5 Feed-forward excitatory pathway between regions of the EC and hippocampus. Alternating recurrent circuits (EC2, CA3 and EC5) and parallel-organised circuits (granule cells, CA1 and EC3) provides ample opportunity for the disassembly and integration of multimodal information. The main sources of input/output of information are indicated with arrows. Sub-cortical output is mainly handled by the subiculum (include the sub-c, as is the pre- and para-subiculum), while cortical output by the CA1. Taken from (Buzsaki, 2011). EC – entorhinal cortex, gc – granule cell, PFC – prefrontal cortex.

Figure 1.6 Schematic of the tri-synaptic pathway.
Typical participating cells, connections and direction of information flow all depicted. The PP is shown, where signal is passed from Layer II EC pyramidal cells to the DG (green path). The tri-synaptic pathway is completed with flow to the CA3 (blue path), then CA3-CA1 and CA1 to EC Layer V cells (blue path), passing through the subiculum. Layer II EC are capable of synapsing directly onto CA3 cells, while layer III EC cells are able to synapse directly to CA1, bypassing the DG and CA3, to compose the TA pathway (shown in pink from EC3 to CA1). Simplified connections are visualised in the simplified arrow connections (bottom right) with the pathways indicated by coloured lines and participating cell types colour coded (bottom). Taken from (Aimone et al., 2014).

A

B

Figure 1.7 Schematic of parahippocampal and hippocampal connectivity.
A) Left: sections showing the hippocampal formation and several regions of the parahippocampal region, colour coded and labelled, from rat hemisected brain. Right: shows a mid-sagittal view of the rat brain, again with major regions colour coded and placed in the estimated locations. B) Shows a more detailed account of the neuronal connections between the parahippocampal region and the hippocampal formation. The reciprocally connected entorhinal layers are indicated with the double-headed arrows. Layer II projects to CA3, CA2 and DG, while layer III to CA1 and subiculum (green and grey lines). Both the mEC and lEC pathways converge onto the same single neurons from the layer II projection but are different in layer III projections. Taken from (Moser et al., 2014).

1.2.4 Entorhinal cortex connectivity

As highlighted in the parahippocampal region section above (**Section 1.1.2**) the EC lies on the border between allocortex and neocortex, indeed, it was once described as a simple transitional region between the two cortices. Further research into the area, however, revealed its highly connected nature. A multitude of intrinsic and extrinsic connections became apparent, as too, did its role as a key partner of the hippocampus controlling the flow of information to and from it.

As stated, the EC is composed of the lateral EC (lEC), the triangular shaped region located rostrolaterally, and the medial EC (mEC) composed of the caudiomedial section of EC. Both divisions of the EC have 6 independent layers. Each of these layers is distinct and comprised of different cell types and intrinsic and extrinsic connections. The functional differences of the regions and the precise targets of their extrinsic outputs split the two.

The cell types of the entorhinal cortex were first described in 1933 using Golgi-silver impregnation staining techniques, which allowed neurons to be classified based on their morphology (Lorente de Nó, 1933). As techniques have improved, novel ways to classify neurons have too, with chemical markers and electrophysiology used alongside morphology as means to differentiate cell types.

In the present study we are focused on the mEC, though more detail on the differences in cell types across the layers and their functional consequences between the mEC and lEC shall be briefly discussed here:

1.2.4.1 Superficial EC layers

1.2.4.1.1 *Layer I*

The most superficial layer of the EC, layer I is relatively sparsely populated, however it has been noted to contain two distinct type of cells; non- or sparsely-spiny multipolar neurons (MPNs) and horizontal cells (Lorente de Nó, 1933; Germroth et al., 1989). The majority of the cells within layer I are the former, and often stain positive for calretinin (CR) and GABA (Wouterlood et al., 2000). The processes of these MPNs have been observed radiating throughout layer I, occasionally branching into layer II (Miettinen et al., 1997; Wouterlood et al., 2000). The axons are described as travelling towards layer II/III, possibly to provide feedforward inhibition for the principal cells in these layers (Canto et al., 2008).

Of the horizontal cells, most are relatively spine free, with their dendritic trees spreading laterally across layer I into layer II. Many horizontal cells are located in the transitional area between layers I/II. Horizontal cells are GABAergic and therefore the source of inhibition within layer I. Indeed, there are differences between medial and lateral horizontal cells, with mEC dendritic terminals staining positive for cholecystokinin (CCK) while lEC for vasoactive intestinal polypeptide (VIP) (Kohler and Chan-Palay, 1983; Schwerdtfeger et al., 1990).

1.2.4.1.2 *Layer II*

Layer II of both subdivisions of EC are densely packed with medium and large pyramidal and other principal cells. There are, however, marked differences in the cellular make up of Layer II in the lEC and the mEC with regards to the principal neurons found in each.

In the mEC the most abundant neuron type are the principal stellate cells, with a relative abundance of 65% (Klink and Alonso, 1997) which morphologically can have a star-like soma – with Lorente de Nó dubbing them as such after observing the soma shape in his Golgi-silver staining experiments (Lorente de Nó, 1933) – though this shape is no longer considered compulsory for a cell to be defined as a stellate cell (Canto et al., 2008). The main distinguishing feature of stellate cells is their highly spiny dendritic tree. Stellate cells are preferentially located in superficial and mid-level positions of layer II, with their dendritic arbor spread widely and evenly, extending up to and, running parallel with the pial surface. The axons of stellate cells are relatively thick, branching off into collaterals that encompass and co-localise with the dendritic tree to form a "net" around it (Kohler and Chan-Palay, 1983; Germroth et al., 1991). 1-3 branching collaterals are sent towards the deeper mEC layers III-VI and another 1-3 collaterals pass through the subiculum heading to the DG and CA3 (forming the perforant pathway) (Canto et al., 2008). The vast majority of stellate cells found in the mEC are glutamatergic (White et al., 1977; Yoshida et al., 1987; Mattson et al., 1988; Xie et al., 1991) and stain for calbindin (Jones, 1994; Wouterlood, 2002).

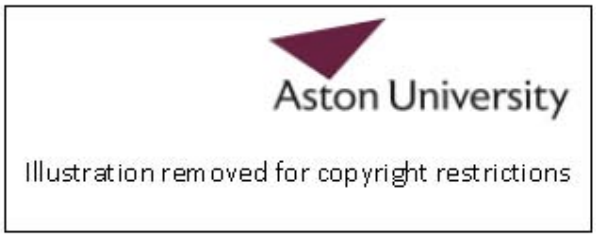

Figure 1.8 A stellate cell from a juvenile Long-Evans rat (P14).
Filled with Alexa Fluor 488 displaying typical stellate morphology. Visible are strong primary dendrites extending superficially to the pial surface, dendritic spines, and perisomatic axon collaterals (the so-called "net"; arrowheads). The axon ramifies from a basal primary dendrite, extending collaterals to deeper layers III and VI (cropped). Taken from (Burton et al., 2008).

Stellate cells can also be grid cells. Layer II has been demonstrated to contain the highest density of grid cells throughout the EC, and when depolarised spike to produce loose phase-locked theta oscillations (Alonso and Llinás, 1989; Alonso and Klink, 1993; Klink and Alonso, 1997; Sargolini et al., 2006). Grid cells are cells within the superficial layers of the EC that are activated upon entry into specific spaces (i.e. spatial representation) and, are represented and spaced upon an abstract lattice formation (Hafting et al., 2005). Theta rhythms are produced and, therefore, are argued as being important in grid cell activation and function (Blair et al.,

2007; Burgess et al., 2007; Giocomo et al., 2007). Layer II is the most prominent site for theta oscillations across the EC (Quilichini et al., 2010).

Separate to stellate cells, other non-stellate principal cells are found in the mEC. The majority of these cells are pyramidal-like principal cells, usually of medium size located in the deeper regions of layer II. Similar to stellate cells the dendritic trees of the pyramidal cells extend into the superficial layers of layer III. The axons extend down and branch into collaterals that spread across layers I-III, again similar to stellate cells, though less profuse (Jones, 1994; Canto et al., 2008).

In contrast with the abundance of stellate cells in the mEC, they are relatively sparse in the lEC, whereas the comparable “fan” cells are highly abundant (Lingenhohl and Finch, 1991; Tahvildari and Alonso, 2005). Fan cells are similar, in that they are composed of large somas and have thick primary dendrites, though they are sparsely spiny. Fan cells differ morphologically to stellate through their shallower, smaller descending dendrites.

Though layer II is densely packed with excitatory neurons there is also a myriad of diverse interneurons. One being the bipolar horizontal interneuron, a sparsely spiny interneuron that straddles the border between layer I and II and synapses in either of the layers (Germroth et al., 1991). Alongside horizontal bipolar cells, vertical bipolar cells are also present, displaying a spindle shape soma with thin projections including one ascending and one descending dendrite that ramify distally (Wouterlood et al., 2000).

Another important interneuron class is the fast-spiking basket cell, shown to be present in layer II by Jones & Bühl, (1993), which possesses thin dendritic projections that process into layer I to ramify. The axonal projections, however, are mainly contained in layer II and move to encapsulate somas of neighbouring cells – stellate or pyramidal cells – in a basket formation providing symmetrical inhibitory synapses (Kohler et al., 1986; Jones and Buhl, 1993). Basket cells have been found to stain extensively across all areas of the EC for parvalbumin (PV); it has been suggested that all basket cells in the EC are PV positive, therefore basket cells are commonly called PV+ basket interneurons (Kohler et al., 1986; Jones and Buhl, 1993; Wouterlood et al., 1995).

Chandelier cells are another important GABAergic interneuron found in both layer II and III. Chandelier cells lack a consistent cell body shape, though are generally of medium size and stain positive for PV and, are distinguished by superficial vertical aggregations of axonal boutons, aptly named “candles”, a lack of dendritic branching and lack of spines. They can be either horizontal or vertical, with vertical cells usually being slightly smaller (Soriano et al., 1993). They generally display bipolar (2 projections) or bitufted (3 projections) dendritic arbors

that remain in layer II/III to form symmetrical synapses with the early axonal segments of stellate/pyramidal cells (Somogyi, 1977; Freund et al., 1983; De Felipe et al., 1989; Hendry et al., 1989).

1.2.4.1.3 *Layer III*

Differences in the electrophysiological and morphological characteristics of cells in the mEC and lEC are not as pronounced in layer III as in layer II (Tahvildari and Alonso, 2005). Previously, authors investigating the mEC have split pyramidal cells of layer III into two separate groups: spiny pyramidal cells (SPCs) and non-spiny pyramidal cells (NSPCs) – whereas in the lEC only sparsely SPCs were observed (Germroth et al., 1989).

This work was initially developed by Gloveli et al, (1997), who instead split the mEC cells into 4 differing types (type 1-4); type 1 and 2 are excitatory cells whose axons project to the deep EC layers toward CA1, forming the TA-CA1 pathway (Amaral and Witter, 1989) (type 1 being the spiny pyramidal and type 2 being non-spiny). In these classifications type 1 cells have long apical dendrites that extend to the cortical surface and ramify extensively. The basal dendrites are always spiny and branch further horizontally than vertically, often by a factor of 2. The non-spiny type 2 cells are similar morphologically to type 1, excepting a lack of spines, though their dendrites branch closer to the cell body. The axons of these cells normally extend into the deeper layers of EC. Types 3 and 4 are assumed to be local circuit cells, with type 3 cells possessing similar morphological structure to type 1 – a small pyramidal soma with circular, extending, branching non-spiny apical and basal dendrites, that do not reach the cortical surface with slightly less horizontal spread. These type 3 cells have been classified as interneurons that resemble pyramidal cells, and as such are named pyramidal looking interneurons (PLIs). The axons of these cells remain within layer III, highly suggestive of a role in regulation of local circuitry (Gloveli et al., 1997). Type 4 resembles type 2 cells, with compact basal dendrites and an apical dendrite that reaches the cortical surface. Axons of these cells remain in the superficial layers, again suggesting a role in local circuitry (Gloveli et al., 1997).

Stellate cells have also been recorded within layer III, always in the upper portion of the layer close to layer II. The stellate cells have variable somata morphologies, which confer some morphological differences onto the dendrites of the cells. Noted cell body shapes include: spherical, elongated and polygonal – with the first conferring evenly distributed spiny dendrites that enclose the soma, the other two shapes show either one or two spiny basal dendrites with ascending apical dendrites that terminate in layer I. The axons of each extend into the white matter, with collaterals ramifying in layer III and IV (Germroth et al., 1989). Alongside PLIs are bipolar interneuron cells, with extending ascending dendrites that transverse layer II to reach layer I. The axon ramifies from the basal dendrite and extends throughout layer III and into layer IV. Bipolar interneuron cells most commonly stain for CR in the lEC and VIP in the mEC

(Miettinen et al., 1997; Wouterlood et al., 2000). Slow wave oscillations are most frequently and strongly observed within layer III, with those waves being akin to cortical up and down states (Cunningham et al., 2006).

Figure 1.9 Cell types of the superficial EC layers
Split into lEC (top) and mEC (below), showing preferential location of different cell types and the common projections of both dendrites and axons shown. Dendrites and cell bodies in black whilst axons in red. Layers labelled with Roman numerals and colour coded. Taken from Canto et al., 2008.

1.2.4.1.4 *Layer IV (Lamina Dissecans)*

Layer IV is predominantly free of cells and normally ascribed as the layer that separates the superficial and deep layers of the EC. Layer IV is noted as being a densely packed layer of fibres.

That is not to conclude that layer IV is completely devoid of any cells, as occasionally pyramidal or fusiform cells can straddle the border between layer IV and layer III or V. These cells always have the characteristics of the cell layer they are closest too (LIII or V) (Lingenhohl and Finch, 1991; Canto et al., 2008).

1.2.4.2 Deep EC layers

1.2.4.2.1 *Layer V*

Layer V is a layer packed with pyramidal cells, normally possessing large somata at the surface of the layer, while deeper portions contain more medium and small pyramidal cells (Canto et al., 2008).

Principal neurons of layer V are consistent across both mEC and lEC, with an apical dendrite extending upwards toward the superficial layers of the EC, often reaching Layer II or the pial surface. Normally the basal dendrites ramify within the deeper layers while the axons travel toward the subiculum (Hamam et al., 2000, 2002). The large pyramidal cells observed at the surface of the layer consistently have large, thick apical dendrites that tuft in superficial layers II and III, while the thin basal dendrites spread extensively across the extent of layer V and VI (Lingenhohl and Finch, 1991; Gloveli et al., 2001).

Deeper, smaller pyramidal cells are more densely spiny, with thin basal dendrites that preferentially remain in the deep layers, while the axons project to the dentate gyrus via the subiculum, while collateral axons also terminate in layer IV and even layer II/III (Hamam et al., 2000, 2002; Gloveli et al., 2001).

A second principal neuron is observed in layer V, an offshoot of horizontal cells, it extends with thin sparsely spiny dendrites upward towards layer I and the pial surface, while its axons collateralise in layer V and VI (Lingenhohl and Finch, 1991; Hamam et al., 2000, 2002; Witter and Moser, 2006). A third, polymorphic MPNs are reported to be present in layer V, with axon bundles that project to the dentate gyrus, again via the subiculum (Hamam et al., 2000, 2002; Gloveli et al., 2001).

In addition to these cell types, layer V also contains both fusiform and bipolar cells (Lingenhohl and Finch, 1991; Wouterlood et al., 2000). Both cells axons project toward the hippocampus and dentate gyrus. The dendrites of bipolar cells are spiny and extend on one side toward the hippocampus and on the other toward layer I and the pial surface, as does the ascending dendrite of the fusiform cells (Lingenhohl and Finch, 1991; Gloveli et al., 2001). Previous work suggests the bipolar/multipolar cells stain positively for GABA, neuropeptide Y (NPY) and somatostatin (SOM) (Kohler et al., 1986).

Layer V is likely to contain conjunctive head direction cells, another cellular subtype proven to be integral to spatial memory and navigation processes (Witter and Moser, 2006). Alongside this, Layer V cells are either unable or reluctant to participate in slow-wave oscillatory events observed in the superficial layers II and III and, as a whole, the layer is less likely to produce either pharmacologically induced gamma or theta rhythms when compared to the superficial layers (Cunningham et al., 2003, 2006; Quilichini et al., 2010).

1.2.4.2.2 *Layer VI*

Layer VI borders the white matter and, has been shown to contain both MPN and small pyramidal cells (Lingenhohl and Finch, 1991). This layer is not a commonly investigated EC area and, as such, much is still unknown about its cell types and function.

Several conclusions can be formed from the data available about the differing cell types of the entorhinal layers. Firstly, the differences, both morphological and electrophysiological, between the principal neurons of layer II mEC and lEC, as well as the interneuronal populations of layer I, are highly suggestive of separate microcircuits in each area. The differences wane in the deeper layers of the EC, with layer III and V cell populations becoming more uniform both in a morphological and electrophysiological sense, across the mEC and lEC.

This data is suggestive of differential wiring, distribution and functions at the superficial layers, with the deeper layers having a more functionally similar role. Caution must be applied to these conclusions, however, as the data is reliant on pieced together conclusions from disparate experiments and applied as a whole. Whole entorhinal layering and circuitry is still an area of intense interest and further research may shed new light on the differing roles of the mEC and lEC.

Figure 1.10 Cell types of the deep layers of the EC.
Preferential locations of different cell types in lEC (top) and mEC (below), and the common projections of both dendrites and axons. Cell bodies and dendrites coloured black, axons red. Layers indicated with Roman numerals. Taken from (Canto et al., 2008).

1.2.5 Intrinsic organisation of the entorhinal cortex

The EC is a large and evolutionary important region of associative connections with a primary purpose of linking the hippocampus to multiple regions of the brain. The extensive connections between the EC and the hippocampus probably relates to their reciprocal importance in spatial memory processes with place cells being located in the CA1 and CA3 and, grid cells in the superficial layers of the EC (Witter and Moser, 2006).

The intrinsic organisation of the EC involves the intraentorhinal connections clustering into distinct bands (normally 3) The bands are comprised of associational connections and are orientated rostrocaudally, while connections linking these bands are sparse (Kohler, 1986; Witter et al., 1986; Dolorfo and Amaral, 1998a; Chrobak and Amaral, 2007).

Anatomical tracing experiments have shown that projections occurring within the superficial layers II/III terminate within the superficial layers, whereas projections originating in the deeper layers terminate at both deep and superficial layers (Kumar and Buckmaster, 2006). This incidence of superficial-superficial innervation has been shown to be extensive, with both inhibitory and excitatory connections described in layer II (Kumar and Buckmaster, 2006). Collateral innervation has been described as rare in layer II, while layer III principal neurons, on the other hand, are highly collaterally innervated (Dhillon and Jones, 2000). Tracing experiments provided evidence for highly connected layers but do not describe whether these connections are excitatory or inhibitory in nature. Further work has shown that these specific bands of the EC are connected to specific regions of the hippocampus, with, in rats, interconnected areas between mEC and lEC including: close to the rhinal fissure – connected to dorsal hippocampal formation; in the intermediate band of EC – connected to intermediate portions of the hippocampal formation; the medial band of EC is connected to the ventral portion of the hippocampus. These bands in the EC provide associational connections to cells contained within that band, but have not, as yet, been shown to have any substantive connections with cells outside of these bands, highly suggestive information integration and input specific responses at these regions. (Witter, 1989; Witter et al., 1989; Dolorfo and Amaral, 1998a, 1998b).

The layers of the EC are highly interconnected, as described in previous sections, with Ramón y Cajal the first to describe the nature of some of these connections, identifying cells from deep layers projecting and collateralising in the superficial layers (Kohler, 1986, 1988; Dolorfo and Amaral, 1998a; Hamam et al., 2000, 2002). Further detailed anatomical work performed on the intrinsic EC connections has shown connections arising from deep layers and terminating in the superficial layers are split equally between pyramidal and interneurons and are most likely excitatory over inhibitory, providing evidence for both feedforward inhibition pathways as

well as excitatory pathways (van Haeften et al., 2003). Many pyramidal cells from each layer branch dendritically into layer I, which is reminiscent of cells in the neocortex, though it has not yet been established if they possess functionally similar roles. Layer I in the neocortex is responsible for receiving feedback projections and input from subcortical brain regions, whereas layer I in the EC is the main input layer from cortical structures and deeper layers of the EC (layers II, III and V especially) (Wouterlood and Nederlof, 1983; Room et al., 1984; Douglas and Martin, 2007).

It has been speculated that back propagating action potentials may arise from the connections between CA1 and layer V pyramidal cells, with back propagating action potentials moving up the layer V dendrites into the superficial layers of the EC. Evidence of back propagating action potentials has been documented in both CA1 and the neocortex though as of yet not in the EC (Kloosterman et al., 2003). Overall, connectivity between the layers of the entorhinal is much more noticeable from the deep layers connecting up to the superficial layers, while the superficial layers mainly interconnect amongst themselves, with only rare axons directly connected to deeper layers (Iijima et al., 1996; Kajiwara et al., 2003).

Research into the electrophysiological properties of each of the layers of the EC has been ongoing for many years, with inhibition and excitation balance (I/E) across the layers of particular interest. To do so, spontaneous background synaptic activity has long been monitored to assess the I/E balance of the networks and used as a measure of neuronal excitability. Spontaneous release of glutamate has been shown to play an important role in overall neuronal network function and synchrony, as well as modulation of neuronal excitability, observed in the form of spontaneous EPSCs (sEPSCs) (Paré et al., 1998a, 1998b; Destexhe and Pare, 1999; Harsch and Robinson, 2000; Ho and Destexhe, 2000; Stacey and Durand, 2000, 2001). Spontaneous background inhibition is also present in the form of spontaneous GABA release manifesting as spontaneous IPSCs (sIPSCs) (Otis et al., 1991; Mody et al., 1994; Salin and Prince, 1996). Background inhibition has been shown to decrease network excitability, and thus works to balance the effects of background excitation (Soltesz et al., 1995; Hausser and Clark, 1997; Paré et al., 1998b; Stevens and Zador, 1998; Harsch and Robinson, 2000). Indeed, these principles apply to all areas of the cortex, including the hippocampus and entorhinal cortex.

Excitation was found to disperse into a clear rank, with LV displaying the highest amounts of background excitation, followed by LIII and then LII. LV neurons showed larger sEPSC amplitude, a greater tendency for high frequency bursting and a greater NMDAR contribution to EPSCs than observed in LII (Berretta and Jones, 1996). All these factors have been speculated as playing a role in the greater propensity for synchronisation observed in LV over LII. In the layers where background excitation levels were high, inhibitory levels were still

higher, displaying the overall inhibited nature of the EC as a structure (Berretta and Jones, 1996; Bailey et al., 2004; Jones and Woodhall, 2005; Woodhall et al., 2005; Greenhill and Jones, 2007, 2010, Greenhill et al., 2012, 2014). Further evidence has shown that inhibition exhibits a clear hierarchy of across the layers, with an order of LII>LIII>LV (Greenhill et al., 2014).

Background synaptic activity has also been suggested to highlight the processing of efferent, reentrant and afferent information within the EC (Paré et al., 1998a; Destexhe and Pare, 1999; Ho and Destexhe, 2000; Shu et al., 2003). This I/E balance therefore has an important role in the control of network excitability, as well as in epileptogenesis (Otis et al., 1991; discussed further in **Section 1.4)**.

The overall outline of the EC therefore, as we currently understand it, is in agreement with the research previously performed by Gloveli et al, (1997) and (2001), postulating that superficial layers are massively dominated by inhibition, while deeper layers are much less so (Jones, 1993). Alongside the background synaptic activity work previously discussed a greater number of inhibitory terminals are present in the superficial layers, as shown by immunocytochemical approaches (Kohler et al., 1985).

Further research into the exact functional and morphological differences between the divisions of the EC (mEC/lEC) and the effect they have on the overall scheme of the EC are required, as too is further work to establish the roles of the layering and the connections between the layers before a full picture of the complex role the EC has into cortical and subcortical flow of information.

1.3 Receptors of the entorhinal cortex

1.3.1 Glutamatergic receptors

Glutamate is the most abundant excitatory neurotransmitter in the brain (Meldrum, 2000). Receptors sensitive to glutamate are excitatory in nature and are said to be glutamatergic. Excitatory receptors are divided into two families: ionotropic receptors and metabotropic receptors. Ionotropic receptors include: α-amino-3-hydroxy-5-methyl-4-isoxazolepropionate receptors (AMPARs), N-methyl-D-aspartate receptors (NMDARs) and kainate receptors (KARs), all of which have a reverse potential of ~0mV. Metabotropic glutamate receptors are G-protein coupled receptors known as mGluRs that effect responses through second messenger signal transduction systems. These signal transduction mechanisms are slower than ionotropic receptor mediated ion movement into neurons. As we are mainly interested in phasic responses to stimuli the next section shall be focussed on ionotropic receptors.

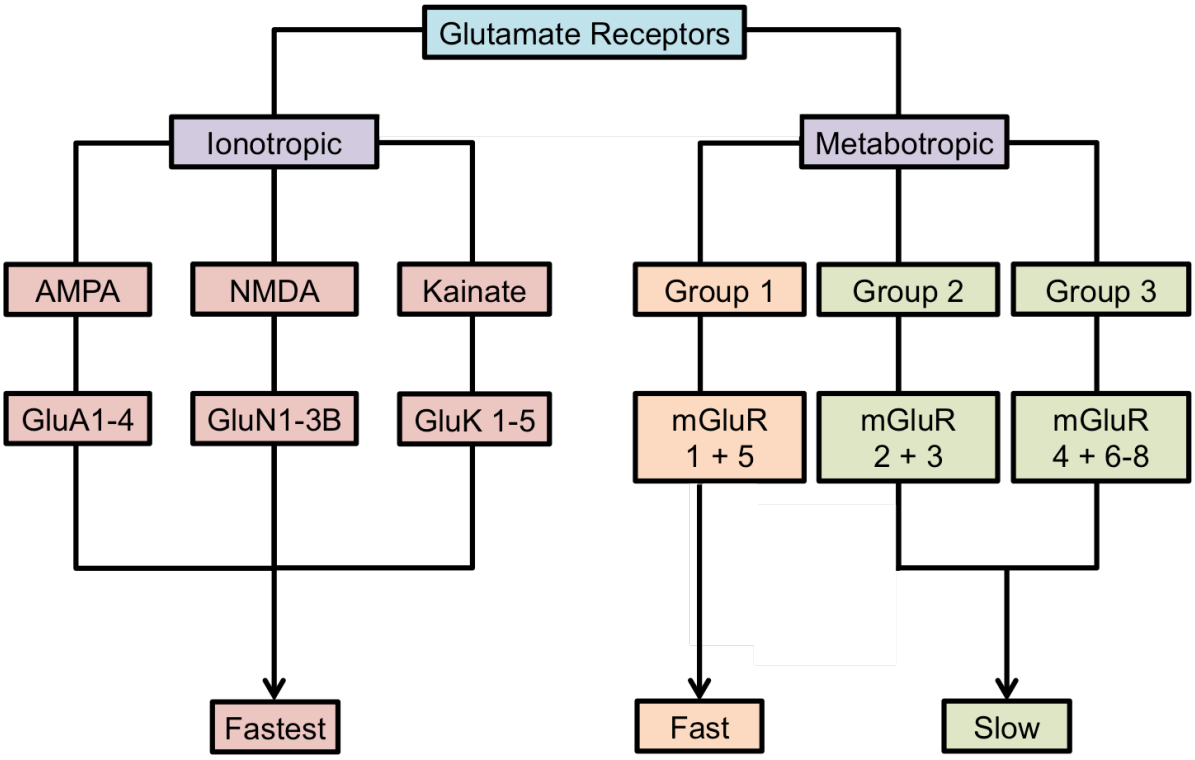

Figure 1.11 Flow chart showing the different glutamate classifications.
Receptor types and the subunits that compose them are shown. The general activation response time is shown for each receptor type. Metabotropic receptors are further divided into groups, which perform slightly different functions. Group 1 activates PLC when stimulated, whereas groups 2 + 3 are known to inhibit the enzyme adenylyl cyclase reducing cAMP production, among other transduction pathways (Pinteaux-Jones et al., 2008).

1.3.1.1 AMPA receptors

AMPARs are usually heteromeric tetramers, composed of a combination of 4 subunits from GluA1-4 (GluR1-4 in old terminology). Homomeric AMPARs, however, have been described in the literature though are exceedingly rare in nature (Lu et al., 2009). AMPARs are widely

distributed throughout the CNS and are commonly postsynaptic receptors, though there is evidence of their presence at the presynaptic terminal (Pinheiro and Mulle, 2008).

Activation of AMPARs requires two L-glutamate molecules to bind. The binding of L-glutamate effects conformational change of the receptor, opening the central pore, allowing ionic transfer into the postsynaptic bouton. Entry of positive ions into the cell generates fast excitatory postsynaptic currents (EPSCs), increasing the membrane potential a small amount with one EPSC, due to rapid activation and deactivation of the receptor. Multiple summed EPSCs can elicit an action potential if threshold potential is reached.

AMPAR function and ionic permeability depends on the specific subunit composition of the receptor. The vast majority of AMPAR are Ca^{2+} impermeable, with Ca^{2+} entry wholly dependent on whether GluA2 is present or not, with its presence denying Ca^{2+} entry (Derkach *et al.*, 2007). The majority of AMPARs in the mammalian CNS, especially in the CA1/CA3 of the hippocampus, are GluA2 containing tetramers, as GluA2 is preferentially incorporated into AMPARs (Sans et al., 2003; Derkach et al., 2007). Ca^{2+} entry, therefore, is unusual and can act as one the distinguishing factors between AMPARs and NMDARs, as NMDARs are perpetually Ca^{2+} permeable. AMPAR variants are seemingly differentially distributed throughout the brain, suggesting a link between subunit composition and location (Martin et al., 1993).

To add, GluA2 incorporation into AMPARs is not always exclusive of Ca^{2+} permeability. Glutamine/arginine (Q/R) site RNA editing of the GluA2 subunit mRNA is required for AMPAR Ca^{2+} impermeability. Q/R editing refers to a post-transcriptional modification that alters a glutamine encoding codon to an arginine encoding codon (Hollmann et al., 1991; Hume et al., 1991). Without this modification AMPAR containing GluA2 are permeable to Ca^{2+}, though unedited GluA2(Q) containing AMPARs are relatively rare, with less than 1% of grey matter mRNA encoding for unedited GluA2 subunits (Kawahara et al., 2003). The function of unedited GluA2(Q) AMPARs are relatively unknown as they do not seem to have a role in brain function or disease, though have recently been linked to regulating excitotoxic neuronal cell death in ischemia and motor neurone disease (Kwak and Kawahara, 2005; Kwak and Weiss, 2006; Liu and Zukin, 2007; Kwak et al., 2010).

AMPARs are heavily implicated in both synaptic plasticity and, learning and memory (Rioult-Pedotti et al., 2000; Dragoi et al., 2003; Whitlock et al., 2006).

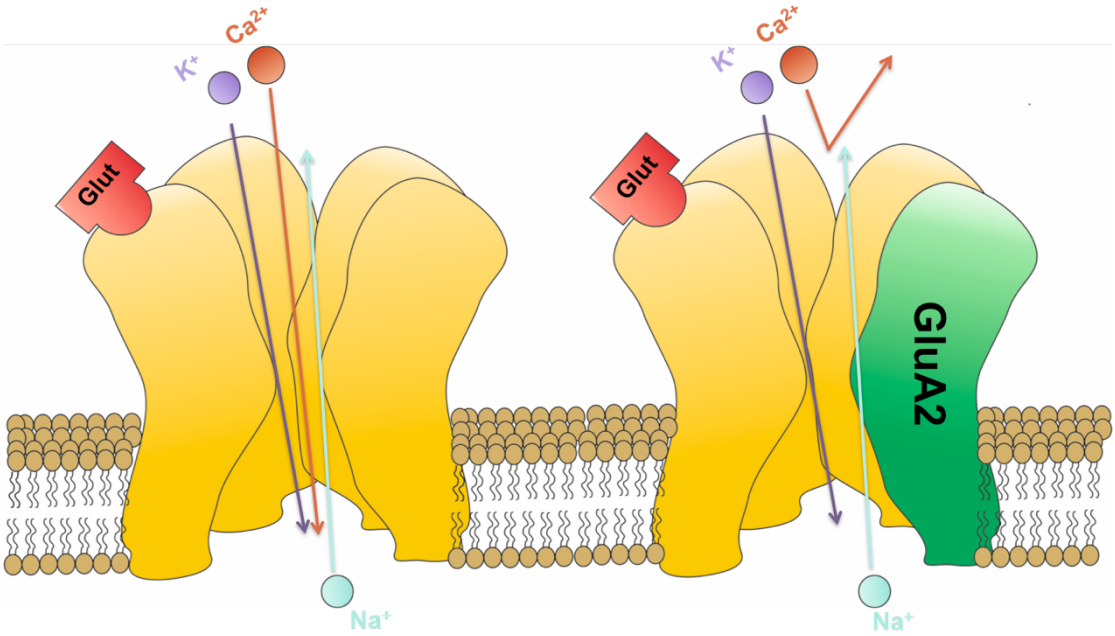

Figure 1.12 Schematic of AMPARs showing the tetrameric structure.
Inclusion of the edited GluA2 subunit in AMPARs impedes Ca2+ permeability of the receptor. Binding of glutamate or another agonist causes a conformational change allowing Na^+ (and $Ca2^+$ if GluA2 not present) into the neuron – causing depolarisation and excitation.

1.3.1.2 NMDA receptors

NMDARs are glutamatergic receptors formed of tetramers, generally composed of two GluN1 and two N2 subunits (formally NR subunits), in a dimer of dimers formation (commonly 1-1-2-2). A third subunit type is known, GluN3, though this subtype has been shown to have inhibitory effects on NMDA receptors. GluN1 is obligatory for the formation of a functional NMDAR, usually in collaboration with one or more of the N2 subunits (Schorge and Colquhoun, 2003; Furukawa et al., 2005), with the most common tetramer widely believed to contain 2 GluN1 subunits, with 1 of both the N2A and N2B subunits (Parsons and Raymond, 2014). GluN3A-B must co-assemble with a GluN1 subunit to form a functional receptor, where, if present a reduced permeability to Ca^{2+} is noted (Pérez-Otaño et al., 2001). Recombinant homomeric GluN1 NMDARs have been demonstrated to be functional in *Xenopus* oocytes with low conductance and amplitude, with affinity values for agonists and partial agonists 4- to 16-fold weaker, but with a higher affinity for glycine (Grimwood et al., 1995).

Within these subunit types there are many isoforms, with eight splice variants of GluN1 produced by alternative splicing of GRIN1 (Durand et al., 1992, 1993; Sugihara et al., 1992; Hollmann et al., 1993; Mori and Mishina, 1995). There are four known isoforms of GluN2 (A, B, C and D) encoded by GRIN2A-D, while 2 isoforms of GluN3 are known, those being N3A and N3B, encoded by GRIN3A-B respectively (Moriyoshi et al., 1991; Meguro et al., 1992; Monyer et al., 1992; Mishina et al., 1993; Ciabarra et al., 1995; Sucher et al., 1995; Nishi et al., 2001). Each subunit possesses a distinctive intracellular C-terminal domain, of differing amino acid lengths, which allow interaction with alternative signalling molecules.

The GluN2 subunits display differential developmental expression, with the embryonic brain expressing only GluN2B and N2D. Major alterations in expression rates are observed in the first two post-natal weeks, with GluN2A showing a rise immediately after birth and remains constant through to adulthood, while GluN2D falls to a low expression rate after birth. GluN2B expression remains relatively constant throughout, while GluN2C shows expression only on post-natal day 10 (P10) (Akazawa et al., 1994; Monyer et al., 1994; Sheng et al., 1994). In terms of GluN3 expression, expression is only noted post-natal, with GluN3A showing expression immediately before declining, while GluN3B rises slowly throughout development, with high expression in motor neurons. The expression profiles of GluN2B and ND, as well as GluN3A, suggest roles in synaptogenesis and synapse maturation (Henson et al., 2010; Pachernegg et al., 2012). The adult brain, meanwhile, shows predominant expression of GluN2A and N2B in the hippocampus among other regions, suggesting an integral role in synaptic plasticity (Watanabe et al., 1992; Akazawa et al., 1994; Monyer et al., 1994).

GluN2A have been found to be express across all brain areas, in mature adult rat brains, while GluN2B was contained mostly in the forebrain. GluN2C was restricted to the cerebellum, olfactory bulb and thalamus areas, while GluN2D was constrained to the brain stem, mesencephalic and diencephalic structures. This data suggest GluN2A is the most predominantly expressed NMDAR subunit expressed throughout the brain, while the other GluN2 subunits appear to be more region specific in expression. The overlap of subunit expression highlights the possibility of multiple GluN2 subunits being present in a single NMDAR (Wenzel et al., 1995).

GluN1 and GluN3 subunits bind to glycine, while GluN2 subunits bind glutamate. NMDARs are characterised by the voltage-dependent magnesium (Mg^{2+}) block and the high permeability to Ca^{2+}. The Mg^{2+} blockade of the central pore inhibits ionic transfer until the membrane potential threshold has been met through depolarisation of the neuron by AMPAR, the co-binding of glutamate to N2 subunits and, D-serine or glycine to the linked binding site present on N1 subunits causing the voltage-gated Mg^{2+} to be removed. Upon activation Ca^{2+}, Na^{+} and K^{+} ions flow into the intracellular membrane, with Ca^{2+} entry triggering certain intracellular signalling molecules. An allosteric binding site for zinc is present and a known modulator of NMDARs (Rachline et al., 2005). NMDARs are the predominant receptors involved in synaptic plasticity and memory, cortical circuitry development and, synaptic function (McBain and Mayer, 1994; Tsien et al., 1996; Cull-Candy et al., 2001; Perez-Otano and Ehlers, 2004; Lau and Zukin, 2007).

.

Figure 1.13 Schematic of the NMDARs
NMDARs are composed of tetrameric assemblies of, generally, two GluN1 and two GluN2 subunits expressing glycine and glutamate recognition sites, respectively (Hirai et al., 1996; Laube et al., 1997). Binding of and co-agonists are required for receptor activation. Mg2+ block the central pore of NMDARs, relying on voltage change of the membrane to allow ion flux. Antagonist such as D-AP5 are competitive and as such compete for the agonist binding site with glutamate and NMDA. Ifenprodil is a N2B specific antagonist, while PEA-QX (not shown) is a N2A selective antagonist. In addition, most NMDA receptors are influenced by Zn^{2+} ions in a voltage-independent manner. Taken from (Parsons et al., 2007).

1.3.1.3 Kainate receptors

KARs are also ligand-gated ionotropic tetramers, assembled from a pool of 5 subunit types (GluK1-3 + GluK4-5), able to form either homomers or heteromers. Like AMPARs, KARs mediate rapid excitatory transmission (Jane et al., 2009). KARs are expressed both on the pre- and postsynaptic terminals. Presynaptic KARs regulate both excitatory and inhibitory neurotransmission by interacting with coupled G-proteins and protein kinase C signalling mechanisms, while at postsynaptic locations, KARs enrich synaptic responses (Jane et al., 2009).

KARs are associated in various processes such as seizure generation and CA3 NMDAR-independent long-term potentiation (Bortolotto et al., 1999; Fritsch et al., 2014).

1.3.2 GABAergic receptors

γ-amino butyric acid (GABA) is the primary inhibitory neurotransmitter in the CNS, with receptors sensitive to it known as GABAergic receptors. These receptors include $GABA_A$ and $GABA_B$, and formally $GABA_C$, though these have now been reclassified into a specific type of $GABA_A$ receptor (Olsen and Sieghart, 2008).

1.3.2.1 $GABA_A$ receptors

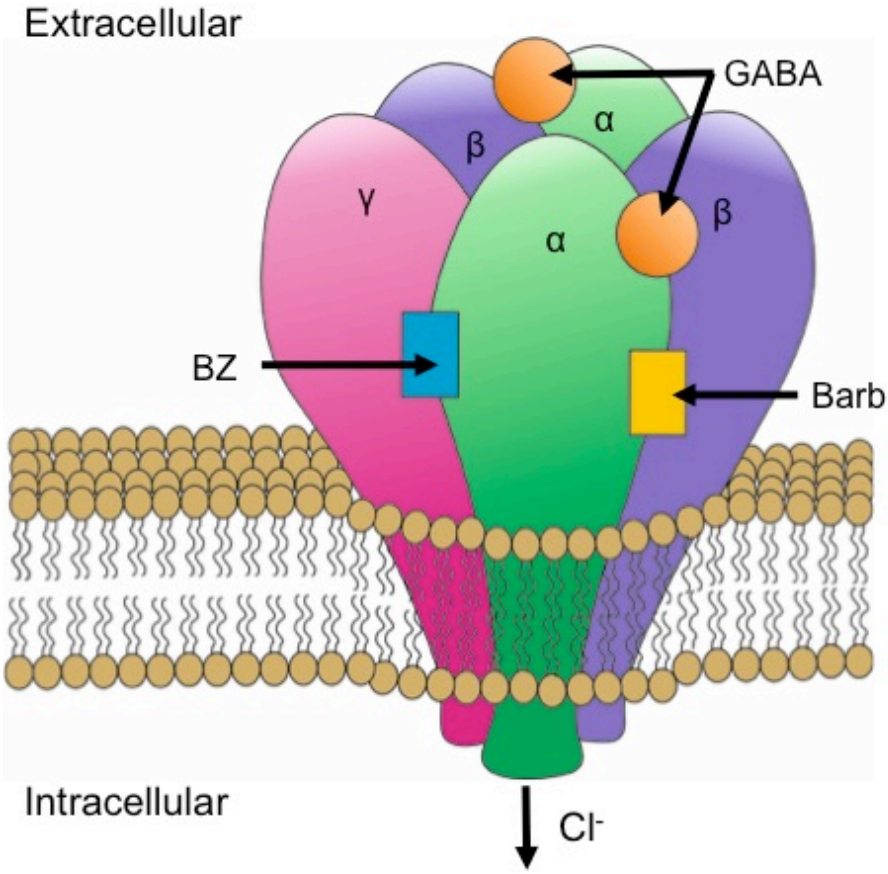

Figure 1.14 Schematic detailing the most common $GABA_AR$ subunit configuration.
The most common $GABA_AR$ conformation is composed of α, β, γ subunits in a 2:2:1 ratio (as shown). Two GABA molecules binding at their extracellular site between α and β to cause a conformational change in the shape of the receptor, opening the central pore and allowing negative chloride (Cl-) ions into the neuron, hyperpolarising and inhibiting it. $GABA_AR$ is modulated by barbiturates (Barb) and benzodiazepines (BZ), with their allosteric sites located as displayed on the schematic.

$GABA_A$ receptors ($GABA_ARs$) are ionotropic, heteromeric pentamers. The combination of subunits corresponds to receptor function. The most common isoform conformation of $GABA_A$ is 2 alpha, 2 beta and 1 gamma subunit (2α, 2β, 1γ) (Farrar et al., 1999). There are slight variations in each of these subunit types, with 6α, 3β, 3γ identified plus others including delta (δ) and omega (Ω). There are currently 19 configurations of the $GABA_A$ receptor known (Sieghart et al., 2012).

$GABA_ARs$ mediate the primary function of GABA, which is to inhibit neurons through inhibitory postsynaptic potential (IPSP) generation. This is achieved by 2 GABA molecules binding to their sites, causing a conformational change to open the central pore of the receptor, allowing anion influx (usually chloride ion (Cl^-) influx), thereby lowering membrane potential and decreasing the likelihood of discharge.

$GABA_A$Rs are expressed at both synaptic and nonsynaptic (extrasynaptic) locations, which mediate phasic and tonic inhibition respectively (Banks and Pearce, 2000; Mody, 2001; Petrini et al., 2004). Phasic inhibition arises from IPSP generation, through GABA binding to $GABA_A$R. This process allows rapid, coordinated inhibition of neurons. Due to the sheer concentration of GABA released many $GABA_A$Rs open synchronously.

Alongside the GABA binding sites on $GABA_A$Rs, a host of allosteric sites are also present, dependent on the specific subunit composition of that receptor. Taking the most common conformation of $GABA_A$Rs (2α, 2β, 1γ), barbiturate and benzodiazepine binding sites are present. The binding of either of these molecules, or certain neurosteroids, endogenous steroid ligands capable of binding $GABA_A$R, are able to potentiate or modulate $GABA_A$R response (Lambert et al., 2003).

Extrasynaptic $GABA_A$RS are located outside of the postsynaptic density, providing tonic inhibition to the neurons (Mann and Mody, 2010). Extrasynaptic $GABA_A$Rs have different configurations of subunits and, usually, though not essentially, possess a delta subunit (Belelli et al., 2009). They bind “spill over” from synaptic transmission to provide tonic inhibition to a separate dendrite. Spill over is GABA molecules that have escaped from the synaptic cleft of another pair of neurons and may bind to adjacent pre- or postsynaptic receptors. Extrasynaptic $GABA_A$Rs activate at much lower concentrations of GABA to produce tonic inhibition of neurons, also known as GABAergic tone (Stagg et al., 2011). It is thought that the delta subunit found in many recombinant extrasynaptic $GABA_A$Rs provides the machinery for this decreased GABA requirement, as well as the decreased desensitisation of the receptors (Saxena and Macdonald, 1994; Haas and Macdonald, 1999; Bianchi and Macdonald, 2002; Brown et al., 2002). Tonic inhibition is also provided by low concentrations of GABA being released into the extracellular space causing persistent activation of $GABA_A$Rs (Farrant & Nusser, 2005).

The previously classified $GABA_C$Rs, were reclassified into $GABA_A$R (Olsen and Sieghart, 2008), and contain the subunits ρ1-3. This class are non-responsive to the $GABA_A$R antagonist bicuculline and not modulated by benzodiazepines, instead having their own selective ligands (TPMPA, CACA) (Johnston, 1996; Kirischuk et al., 2003). As with extrasynaptic $GABA_A$Rs, these receptors show a higher sensitivity to GABA, do not become desensitised to GABA and, possess longer decay times than regular $GABA_A$Rs (Johnston, 1996).

1.3.2.2 $GABA_B$ receptors

$GABA_B$Rs are G-protein coupled, 7 transmembrane domain receptors and therefore, metabotropic. There are two types of $GABA_B$R: type 1 (Kaupmann et al., 1997) and type 2 (Jones et al., 1998; Kaupmann et al., 1998). Both types of $GABA_B$R must be expressed within the cell for either to activate (Pierce et al., 2002). For functional $GABA_B$R formation and

activation, heterodimerisation is required. Interaction between the intracellular C-terminals of each type forms a coiled-coil, which helps ensure heterodimerisation of the receptor complex, but is nonessential for this process (Pagano et al., 2001).

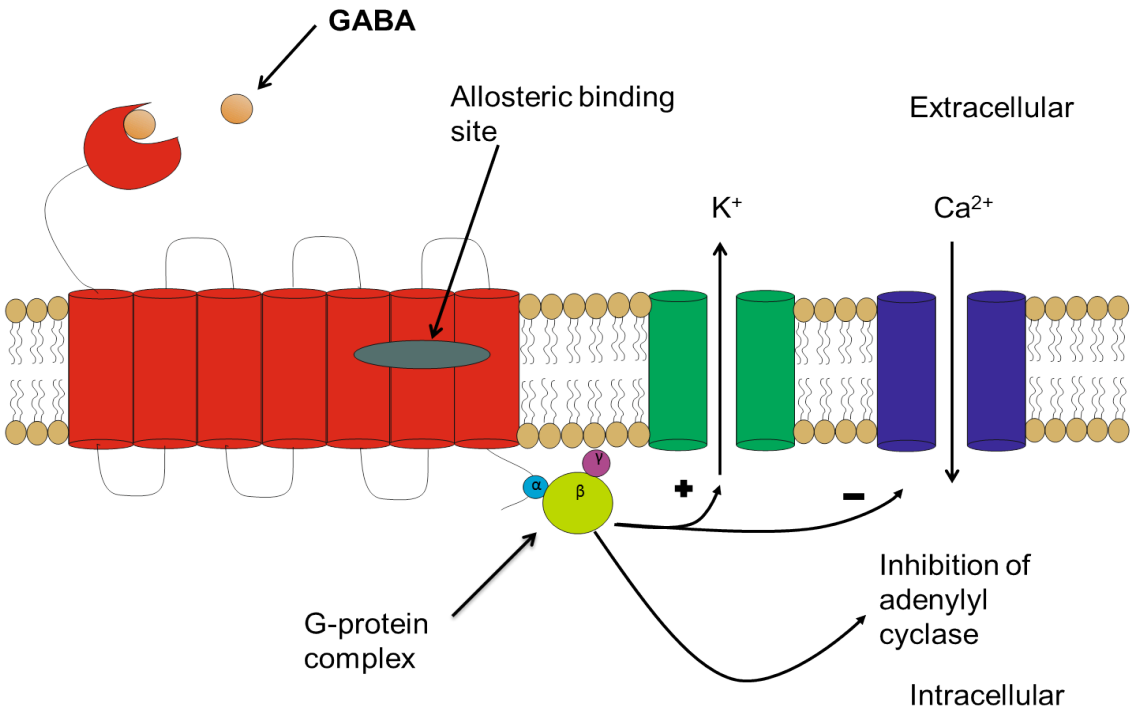

Figure 1.15 A simplified, monomeric structure of a post-synaptic $GABA_B$ receptor. The coupled G-protein and ion channels are shown. GABA binds to the "Venus fly-trap module" binding site, which is purported to close around the agonist, hence the name. Binding activates the G-protein complex, which then moves to activate the K^+ channel, allowing K^+ out, hyperpolarising the membrane. Ca^{2+} influx or adenylyl cyclase can also be inhibited. Successful dimerisation of $GABA_BR$ is prerequisite to their activation. $GABA_BRs$ are associated with slow or tonic inhibition of neurons.

The GABA binding site is dubbed the "Venus fly-trap" module, due to its structure and ligand binding mechanism, as well as this, it is active only on type 1 $GABA_BRs$. Postsynaptic $GABA_BRs$ are activated through GABA binding activating the coupled G-protein complex and causing K^+ channels to open. This allows K^+ to exit the intracellular membrane, hyperpolarising the neuron in a controlled and slow manner (Dutar and Nicoll, 1988; Lüscher et al., 1997). This action brings the neuron closer to K^+ equilibrium potential. Besides this, $GABA_BRs$ inhibit Ca^{2+} channel opening, decreasing Ca^{2+} conductance and Ca^{2+} spikes in the membrane (Mintz and Bean, 1993), and can inhibit adenylyl cyclase. In the presynaptic terminal, $GABA_BRs$ have been shown to inhibit neurotransmitter release in both inhibitory and excitatory synapses (Bowery et al., 1980). This is most likely achieved through inhibition of Ca^{2+} channels in inhibitory neurons (Takahashi et al., 1998). $GABA_BRs$ are identified through their sensitivity to the selective antagonist baclofen (Bowery et al., 1980). Defects in the $GABA_BR$ can lead to various neurological disorders including epilepsy and spasticity (Bowery et al., 2002; Bettler et al., 2004; Froestl, 2010).

1.4 Neuronal Network Oscillations

Neural oscillations are rhythmic waves of activity, produced through intracellular or extracellular mechanisms, from individual neurons or interactions between many neurons as part of neural ensembles. Brain rhythms represent the extracellular voltage changes produced by these mechanisms (Buzsaki, 2006). Neural oscillations operate across large frequency ranges; from very low to very high (0.05Hz to 600+Hz).

The first electrical activity from brains was recorded by Richard Caton in 1875. With the invention of the electroencephalogram (EEG), Berger recorded the same electrical signals from human brains some 50 years later. In 1929, Berger coined the terms alpha (α) and beta (β) waves (8-13; 12-25 Hertz/Hz) in his published work (Berger, 1929; Tudor et al., 2005).

The study of oscillations encompasses both *in vivo* and *in vitro* approaches, with magnetoencephalography (MEG) and electroencephalography (EEG) being examples of *in vivo* whole brain techniques. MEG is a neuroimaging technique that provides a functional way to study electrical currents through the magnetic fields they produce. *In vitro* examples include the recording of brain slices through local field potentials (LFP), an electrophysiological technique that allows measurement of extracellular potentials and voltage changes. The evolution of brain slicing techniques over time has enabled living tissue to be better preserved, allowing more time for longer LFP recordings.

Persistent oscillations can be induced via various agents in slices including, mGluR agonists (Whittington et al., 1995), kainate receptor agonists (Cunningham et al., 2003; Fisahn et al., 2004), cholinergic agonists (Fisahn *et al.*, 1998) and by tetanic electrical stimulation. Such persistent oscillations have been induced in many major areas of the brain such as, the CA1 and CA3 regions of the hippocampus and, the entorhinal and motor cortices (Fisahn et al., 1998; Gillies et al., 2002; Cunningham et al., 2003; Yamawaki et al., 2008).

1.4.1 Mechanism of oscillatory events

The current sources and sinks model (**Figure 1.16**) helps explain the rise of extracellular field potentials. That is to say, extracellular field potentials are generated through the summation of neural current loops across a large area. Sources and sinks arise from the requirement of neurons to remain electroneutral. An illustration of this is when an excitatory postsynaptic potential (EPSP) arises, for instance when an excitatory AMPAR is activated on postsynaptic distal dendrites. Activation of this receptor allows influx of extracellular Na^+ ions into the dendrite, generating an active intracellular sink. To counter this and achieve electroneutrality, a passive return current sink arises. The sink is formed upstream, in the axon or perisomatically, by the efflux of positive potassium ions, moving from intracellular to extracellular space. The flow of charge across the membrane results in the formation of a

dipole. A closed microcircuit is produced between net influx and efflux of positive ion movement. The circuit always summates to zero across the neuron, therefore, achieving electroneutrality. As the EPSP current moves down the dendrite toward the soma/axon, so too does the active sink. To counterbalance this, the passive return current source moves in the opposing direction, in this case towards the dendrite, thus maintaining the dipole and electroneutrality.

The same principle holds true for IPSPs but in reverse. If a $GABA_AR$ is activated it allows for a net influx of anions. This generates an intracellular active source and therefore requires a passive current return to be established. An extracellular sink is achieved through the efflux of upstream chloride ions, providing current return. Again, electroneutrality is initiated through dipole generation. Determination of whether sources and sinks are active or passive mechanisms is difficult to uncover, unless the location and type of synapse are known (Buzsaki et al., 2003).

Actions potentials (AP) have little to no role in LFP recordings, due to the rapid decay time, short attenuation distance and the lack of synchrony between AP firing. Also, the extracellular fluid that surrounds the neurons acts as a filter, negating the effect of APs. In contrast to postsynaptic potentials (PSPs), APs decay rapidly in both temporal and spatial dimensions, but have a larger effect on transmembrane potential. The LFP signal is largely achieved by PSPs, resulting from synaptic activity. Ca^{2+} spikes, electrical gap junctions and afterhyperpolarisations from APs, however, can all contribute as well (Buzsaki, 2006; Buzsaki et al., 2012).

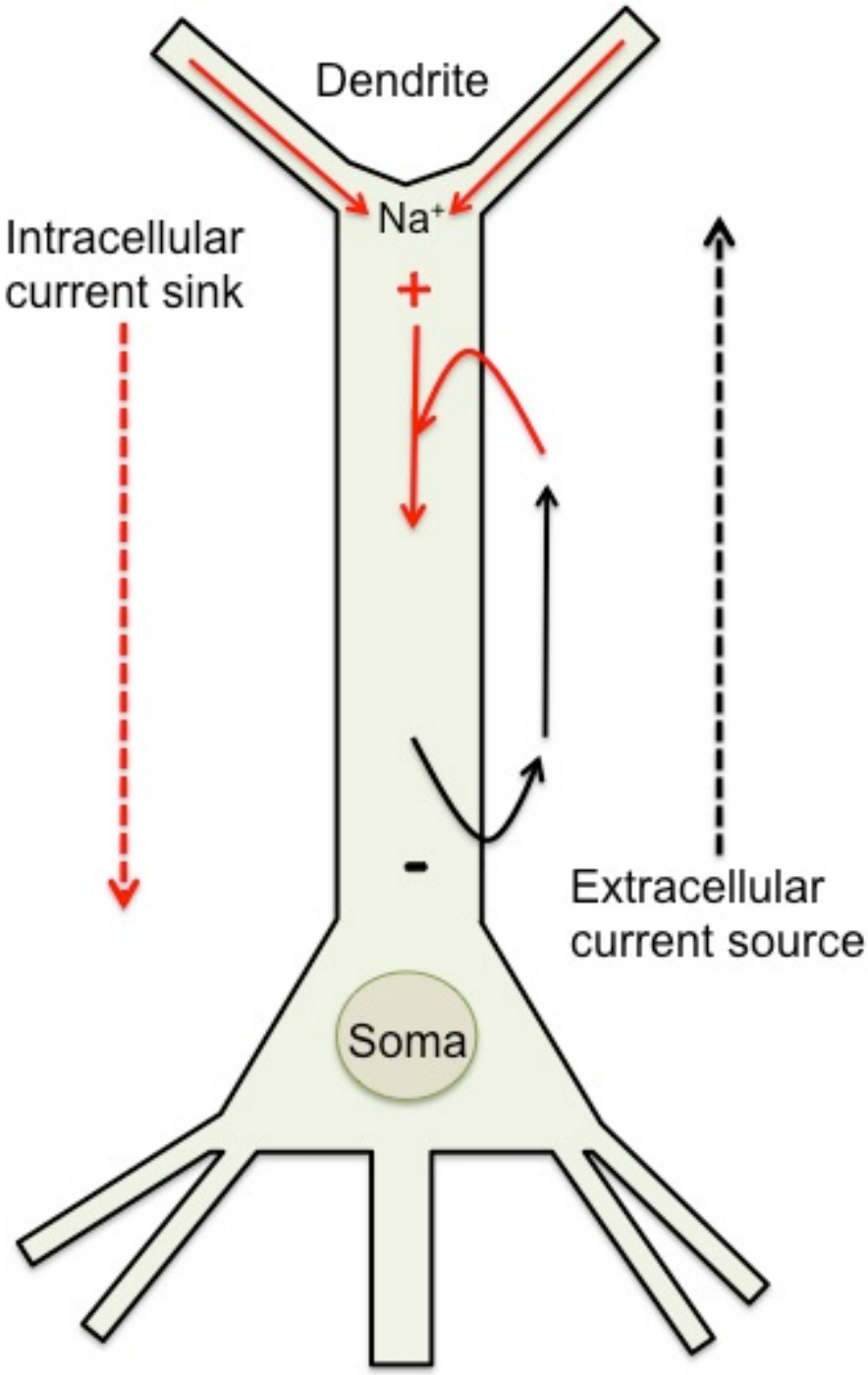

Figure 1.16 Schematic of the current source and sinks model.
As cations rush into the dendrites of a neuron, through an activated ion channels, a current sink is formed. To counterbalance this a source needs to be generated, extracellularly toward the soma. Ions flow out of the membrane causing equilibrium. In this example positive sodium ions are rushing in causing a net increase in charge intracellularly and a net decrease extracellularly, rectified by sodium leaving the cell. As the sinks progresses toward the soma the source will move upward towards the dendrites.

1.4.2 Oscillatory frequency bands

Specific frequency bands have been associated with different activities, for instance the delta frequency is associated with deep non-rapid eye movement (NREM) sleep phases, whereas gamma with attention and memory (Fell et al., 2001; Fries et al., 2001). Overlap between

bands occurs through, diversity in the brain region the frequency emanates from, the presumed mechanisms and, behavioural states.

The table below (**Table 1.1.**) shows the most commonly studied and accepted bands. Perhaps the most widely investigated frequency band type *in vitro* is the gamma oscillation, which I shall briefly review here.

Name	Frequency (Hz)
Very Slow Oscillations (VSO)	<1
Delta	1-4
Theta	4-9
Alpha	9-13
Beta	10-30
Gamma	30-70
Very Fast Oscillations (VFO)	>70

Table 1.1 Oscillation frequency table.

1.4.3 Gamma oscillations

The term “gamma oscillation” emerged in the 1980’s and is generally accepted to cover the frequency band ranging from 30-70Hz (Bressler and Freeman, 1980).

The CA3 region of the hippocampus is a popular target of study *in vitro*, due to its laminar organisation, presence of spontaneous gamma oscillations, ease of induction and visibility of pharmacological persistent gamma and, the similarity of profile to *in vivo* EEG waves. Cortical gamma oscillations are routinely studied, as they are believed to play a role in the processes of consciousness (Llinas et al., 1998; Varela et al., 2001), sensory binding (Singer, 1993; Gray, 1994), memory (Fell et al., 2001) and attention (Fries et al., 2001).

Gamma oscillations are ubiquitous occurrences throughout brain architecture, across a range of species, with each location producing kinetically similar rhythms. Gamma rhythm capable regions include: the hippocampus (Buzsaki et al., 1983; Whittington et al., 1995), the entorhinal cortex (Chrobak and Buzsaki, 1998), the amygdala (Halgren et al., 1977) and the thalamus (Pinault and Deschenes, 1992), along with many regions of the neocortex. Due to profile similarity amongst all these areas, details of what is required and what hinders gamma

oscillation generation have been detected. Three requirements are deemed necessary to produce network gamma, these include: connected networks of inhibitory interneurons linked through electrical gap junctions, $GABA_A$Rs to provide a time constant and, sufficient excitatory drive to cause interneuronal network firing (Wang and Rinzel, 1992; Whittington et al., 1995; Traub et al., 1996b).

1.4.3.1 Models of gamma

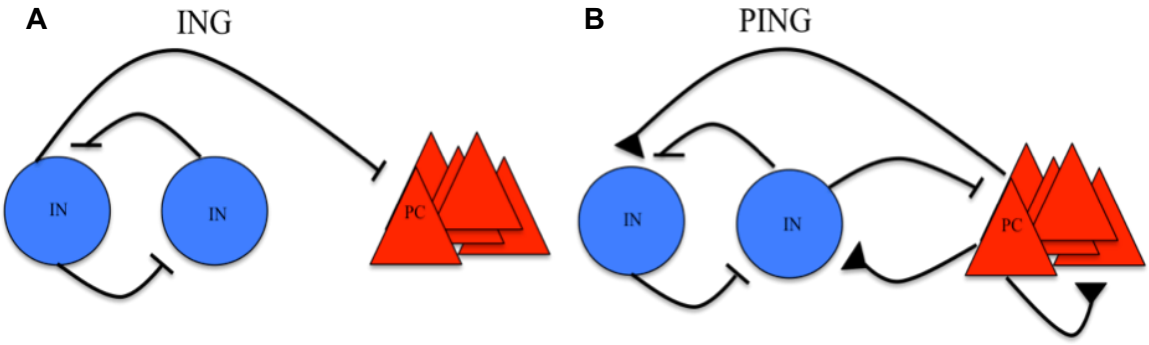

Figure 1.17 ING and PING models of gamma oscillations *in vitro*.
A) ING, the drive behind the gamma oscillations is coming from interconnected inhibitory interneurons setting the rhythm through narrow time windows through the firing of IPSPs onto themselves and pyramidal cells. Pyramidal cells respond by discharging in the intervals after decay of $GABA_A$R inhibition, producing oscillations. B) PING, drive comes from excitatory pyramid cells, which stimulate the basket cell interneurons through EPSPs, which then in turn modulate pyramid cell firing to achieve gamma wave oscillations through IPSP discharge.

Two relatively well-defined models of *in vivo* and *in vitro* gamma oscillation generation exist. One relies on inhibitory interneurons (ING/I-I), the other, excitatory pyramidal cells (PING/E-I).

1.4.3.1.1 *ING model of gamma oscillations*

The ING model (**Figure 1.17.A**) is predominantly seen *in vitro* and is unlikely to be applicable to *in vivo* conditions, though provides a useful tool for study of interneuron contribution to gamma (Traub et al., 1996b; Whittington et al., 2000). ING is capable of producing gamma oscillations through either tonic or stochastic input drives, as phasic excitation is lacking. Tonic inputs result in neurons firing at distinct intervals. Stochastic inputs cause irregular neuronal firing until sufficient synaptic interaction results in oscillation emergence. In either case, synchrony arises due to subsections of interneurons discharging concurrently, generating synchronous IPSPs in linked neurons. Inhibited neurons respond by spiking, once the $GABA_A$R-mediated hyperpolarisation has decayed. This cycle will continually repeat to produce oscillations.

The rate at which synchronous IPSPs fire is linked to IPSP kinetics and cell refractory periods (Whittington et al., 1995; Wang and Buzsaki, 1996). The duration of inhibitory postsynaptic

currents (IPSCs) depends on $GABA_AR$ subunit types (Farrant and Nusser, 2005). Experiments that cause an increase in the time decay of $GABA_AR$ hyperpolarisation period have shown a decrease in oscillation frequency (Traub et al., 1996a). Further evidence of the ING model supporting gamma oscillations *in vitro* is shown by pharmacological agents increasing coupled interneuron firing such as: mGluR agonists (Whittington et al., 1995), KAR agonists (Fisahn et al., 2004; Hajos and Paulsen, 2009) and muscarinic-cholinergic agonists (Fisahn et al., 1998).

1.4.3.1.2 *PING model of gamma oscillations*

Interconnected areas of excitatory pyramidal cells and inhibitory interneurons are the oldest models of gamma oscillation formation (Wilson and Cowan, 1972; Leung, 1982). In contrast to the relative simplicity of ING, PING (**Figure 1.17.B**) is a more complex model. The addition of excitatory pyramidal cells to the ING model enables neural networks to become phase locked to gamma rhythms (Buzsaki et al., 2012). Fast spiking PV+ basket interneurons project to pyramidal cell somas from the hippocampus to generate the gamma oscillation rhythm (Penttonen et al., 1998; Csicsvari et al., 2003). Basket cells have high mutual interconnectivity via gap junctions and GABAergic synapses (Peinado et al., 1993; Tamas et al., 2000; Deans et al., 2001; Galarreta and Hestrin, 2001; Szabadics et al., 2001; Meyer et al., 2002), a perisomatic location and, phase-locked firing of one action potential per gamma cycle (Sik et al., 1995; Gloveli et al., 2005). Excitatory pyramidal cells in the hippocampus are thought to be important in encoding, storing and processing information (Hajos et al., 2004). Inhibitory interneurons are thought to be involved in synaptic plasticity, network oscillations and spike timing (Buzsáki and Chrobak, 1995; Paulsen and Moser, 1998; Whittington and Traub, 2003).

Basket cells impose IPSP rhythms onto pyramidal cells, orchestrating discrete time windows in which they may fire. The basket cells are indirectly stimulated through low frequency, rhythmic EPSP discharge from pyramidal cells. EPSP discharging onto the basket cells causes synchronous, fast frequency firing between individual interneurons; in turn generating IPSP discharge in both the interneuron and pyramidal populations, mediated through $GABA_AR$ (Cobb et al., 1995; Traub et al., 1996a).

Gamma rhythm synchrony between interneuron-selective interneurons and basket cells discharge is due to mutual interconnectivity of synapses and electrical gap junctions (Cobb et al., 1997). Electrical gap junctions are not thought to be prerequisite to gamma but act to enhance coherence, as cells connected by gap junctions are able to pass ions much more rapidly (Bartos et al., 2002; Kopell and Ermentrout, 2004). Gap junctions selectively contribute to gamma oscillations, being able to affect amplitude, as demonstrated in connexin-36 knockout mice studies (Buhl et al., 2003).

Investigations into phase-locked gamma oscillations, using the PING model, have yielded interesting results. Intracellular studies show pyramidal cells spike at low frequencies (~3Hz) when phase-locked, while interneurons fire at a higher rate, albeit with a slight delay when phase-locked (Fisahn et al., 1998; Hajos et al., 2004). The sparse firing of pyramidal cells shown here indicates that individual hippocampal pyramidal cells are not required to fire every cycle. Phase-coupled perisomatic interneurons fire at ~18Hz with a slight delay that demonstrates strong phase coupling. Dendritic interneurons were shown to fire at ~8Hz with a more significant time delay, suggesting weaker phase coupling (Hajos et al., 2004). Further to these studies, assays aiming to clarify whether low frequency discharge pyramidal cells could support gamma oscillations generation were attempted. The data generated supports the recurrent synaptic feedback mechanism, pyramidal excitation and then interneuron inhibition, of PING as a credible explanation of network synchronisation (Hajos et al., 2004; Mann et al., 2005).

1.4.3.2 Slow wave modulation of brain-wide gamma oscillations

Gamma oscillations are usually local in nature, with a low number of neurons participating in discharge windows, at a high frequency (Kopell et al., 2000). This contrasts with slower oscillatory events such as theta, alpha and beta, which have a larger population of neurons participating, at a lower frequency that can be used for information processing over a wider area (Kopell et al., 2000). The reasons for this are mainly due to the relevant time windows each rhythm has to fire in for instance, gamma is a fast oscillatory event with a time window of only 10-30ms per discharge. Theta is slower and therefore is accompanied by a longer time window (50-100ms) allowing integration of more neuronal discharges. However, local patches of gamma oscillations within the brain have been documented as being able to interact and synchronise with one another, begging the question, how does this synchrony arise?

Cross-frequency phase coupling occurs when transient gamma oscillations are interlinked with slower oscillations. The basic premise behind this is that gamma oscillations are modulated or regulated by a slower oscillation. There are several aspects to cross-frequency phase coupling including, phase-phase, phase-amplitude and amplitude-amplitude coupling (Buzsaki and Wang, 2012). These indicate how the two rhythms are coupled in terms of wave dynamics and are measured by coherence. The most documented instance of this is by theta in a cross-frequency phase-amplitude relationship with gamma frequencies from both local and distant brain regions (Buzsaki et al., 1983; Chrobak and Buzsaki, 1998).

In the hippocampus, gamma activity is usually superimposed on theta rhythms, with nested theta-gamma waves being common. Nested theta-gamma rhythms occur when gamma fires within the peak of theta waves, and are thought to be essential for information processing within the brain (Lisman and Jensen, 2013). Data has shown that theta waves can modulate

the amplitude of gamma, and that frequency/amplitude changes between the two are positively correlated (Bragin et al., 1995). Phase coupled theta-gamma oscillations between the entorhinal and hippocampus are thought to provide an effective method of communication between the two regions of the brain. The exact mechanisms of theta generation in the hippocampus are as yet unknown, though it has been suggested that the signal is generated within the hippocampus (Orban et al., 2001).

Other frequencies are also linked to gamma modulation including alpha (Cohen et al., 2009) and delta (Lakatos et al., 2005).

1.4.3.3 Glutamate receptors in gamma oscillations

Ionotropic AMPA receptors are the prominent driver of gamma oscillations, being the main transducer of all fast, excitatory neurotransmission. The excitatory drive provided to interneurons by pyramidal cells in PING occurs through fast glutamatergic synapses generating rhythmic EPSPs. Postsynaptic binding of AMPAR agonists such as glutamate, generate most EPSPs. This binding causes the ionic pore to open allowing cations, such as K^+ or Na^+, to enter and depolarise the postsynaptic terminal.

The importance of AMPAR has been demonstrated through genetic reductions of AMPA current and by use of AMPAR antagonists (Fisahn et al., 1998; Hajos et al., 2004). Gamma oscillations have been induced in both hippocampus and medial entorhinal cortex *in vitro* in response to application of kainic acid. Kainic acid is a direct agonist of kainate receptors (KAR) (Cunningham et al., 2003) and agonist of AMPAR.

Mounting evidence suggests that AMPARs are key players in oscillatory events. Carbachol (CCh)-induced, high frequency gamma events, performed in the CA3, showed AMPARs to be involved in network synchrony (Mann et al., 2005). Further to this, the selective blocking of AMPARs by antagonists such as GYKI 53655 in the presence of CCh and NMDA, showed that high frequency gamma oscillations, EPSPs and, rhythmicity in IPSP bursts are lost (Mann and Mody, 2010). Taken together these data suggest that AMPA-mediated currents are crucially important, providing the phasic drive for interneuron networks, but do not directly ensure synchrony of the gamma network.

The addition of NMDAR selective antagonist D-AP5 to CCh induced oscillations produced no significant visible effects (Mann et al., 2005). This suggests that NMDARs do not have a critical role in gamma oscillation generation. Interestingly, however, application of NMDA agonists has been shown to increase interneuron firing speed *in vitro*, though this was possible to be counteracted by the introduction of tonic $GABA_AR$ inhibition (Mann and Mody, 2010). KARs are implicated in evoked gamma oscillations in the CA1/3, following low dose applications of

agonists such as kainic acid. At high concentrations however, KARs are thought to stimulate depression of gamma oscillations in the hippocampus. Both KARs and NMDARs are thought to be regulatory in gamma oscillation generation, whereas AMPA-mediated currents are vital for oscillogenesis.

1.4.3.4 GABA receptors in gamma oscillations

GABA is imperative for gamma oscillations, without its presence gamma oscillations would be impossible to achieve (Gray, 1994; Whittington et al., 2000; Laurent, 2002; Traub et al., 2002; Bartos et al., 2007, Tiesinga & Sejnowski, 2009; Wang, 2010; Buzsaki & Wang, 2012). It acts as the inhibitory neurotransmitter required for the basket cell interneurons to orchestrate synchrony of pyramidal EPSP discharge (Mann and Mody, 2010).

$GABA_A$Rs mediate the primary function of GABA, which is to inhibit neurons through IPSP generation. IPSP generation is critical to the production of gamma oscillations, as their decay provides the discrete time windows for pyramidal cells to fire in (Johnston & Wu, 1994).

$GABA_B$Rs act too slowly to directly influence proceedings. Their lingering effects, however, have proved capable of modulating the amplitude of gamma and other fast oscillations, by generating network activity. Blockade of $GABA_B$Rs showed prolonged induced gamma oscillations in hippocampal slices (Whittington et al., 1995), also additionally shown in a later kainate model of gamma oscillations (Brown et al., 2007). They also act to enhance the effectiveness of extrasynaptic $GABA_A$R function, i.e. tonic inhibition (Tao et al., 2013). Collectively this work strongly suggests a modulatory role for $GABA_B$ in gamma oscillation and in $GABA_A$R function.

1.4.3.5 Physiological gamma oscillations

In vivo gamma oscillations are most commonly observed in states of attentiveness, such as language perception, object recognition, sensory binding and, in learning and memory steps (Singer, 1993; Gray, 1994; Llinas et al., 1998; Fell et al., 2001; Fries et al., 2001; Varela et al., 2001). It is also thought that due to their frequent occurrence in the hippocampus, they play a role in hippocampal input selection. This is due to their ability to quickly coordinate and select neuron firing groups – important for processes such as memory storage and retrieval (Headley and Paré, 2017) and, meaning that every hippocampal pyramidal cell is not required to fire every cycle. *In vivo* studies in the hippocampus have identified two independent hippocampal gamma oscillation generators, one in the DG, the other in CA3 propagating to the CA1 (Leung, 1982; Buzsaki et al., 1983; Bragin et al., 1995; Charpak et al., 1995; Penttonen et al., 1998). Taken as a whole, gamma oscillations are seen during integration processes in the brain. As of yet, the full scale of gamma function in normal brain physiology is unknown.

1.4.3.6 Pathophysiological gamma oscillations

Abnormalities in brain rhythms are usually allied to lack of synchrony in discharges and have also been associated with various neurological disorders including schizophrenia, Parkinson's disease and autism (Buzsaki, 2006; Bernier et al., 2007; Traub and Whittington, 2010). Aberrant beta and gamma rhythms have been noted in schizophrenia, with it being thought that the loss of long-range synchronisation may be at the crux of the impairment found in cognitive function (Andreasen, 2000; Lisman, 2012; Pittman-Polletta et al., 2015; Uhlhaas and Singer, 2015). The reasons behind this loss in synchronisation are thought to be due to abnormalities in GABAergic neurotransmission and NMDAR dysfunction (Cohen et al., 2015). In addition to this, in Alzheimer's disease, lack of long-range synchronisation paired with the neuronal cell loss may explain the deterioration in cognitive function (Uhlhaas and Singer, 2006).

In contrast to these neurological disorders, epilepsy is thought to be a disorder centred on hypersynchronous discharges of networks (Uhlhaas and Singer, 2006). High frequency gamma oscillations have been noted to arise prior, and upon, the onset of ictal or seizure-like events, as too, have very fast oscillations (VFOs) (Traub et al., 2001). VFOs are observed in both *in vitro* and *in vivo* models of epilepsy and, have been attributed as biomarkers of epilepsy (Zijlmans et al., 2012).

1.5 Epilepsy

The World Health Organisation (WHO) defines epilepsy as "*a chronic disorder of the brain… characterised by recurrent unprovoked seizures as a result of excess electrical discharge in a group of brain cells*" (WHO, 2015). Epilepsy is stated as one of the oldest recorded diseases in human history, with records dating back to 4000 B.C (Mechoulam, 1986).

Epilepsy has the highest abundance for neurological disease, with an incidence rate of roughly 1% of global population (Leonardi and Ustun, 2002). The chance of developing epilepsy is highest among young children and the elderly, especially within the developing world (Bell and Sander, 2001). In developed nations it is estimated that ~70% of epilepsy cases can be successfully controlled with current anti-epileptic drugs (AEDs). Despite this fact, many of the mechanisms for seizure generation are still relatively unclear.

1.5.1 Seizures

The symptoms of epilepsy are uncontrollable seizures, of varying scale dependent on the type of epilepsy involved. Seizures are described by the International League Against Epilepsy (ILAE) as *"a transient occurrence of signs and/or symptoms due to abnormal excess or excess synchronous neuronal activity in the brain*" (Fisher et al., 2005). The nature of neuronal activity while in seizures can be readily segregated into categories: inter-ictal, pre- and post-ictal and ictal. Each of these are relatively easy to identify, though there is some natural overlap between them (Fisher et al., 2014). The basic mechanisms underlying seizure generation hinges on hyperexcitability of neurons. A hyperexcitable state can arise due to increased excitatory synaptic neurotransmission, a decrease in inhibitory neurotransmission, alterations to voltage-gated ion channels or changes in ion concentrations either intracellularly or extracellularly that favour depolarisation.

The ILAE recently updated seizure classification terminology (Fisher et al., 2017). Broadly speaking "focal" seizures are those limited to a specific region or area of the brain, while "generalised" seizures are widespread and are often bilateral.

Figure 1.18 Raw data of a seizure-like event.
Recorded using *in vitro* local field potential (LFP) and a magnesium free aCSF bath solution. Scale bar: 500pA by 10 seconds.

1.5.2 Current Anti-Epileptic Drugs (AEDs)

Current AEDs are diverse in their mechanisms of action (MOA), and though are not generally classified by MOA clinically, due to off target and unknown MOAs, can be split into target based groups; such as ionic voltage gated sodium channels, voltage gated calcium channels and, synaptic transmission either by inhibiting synaptic excitation or increasing synaptic inhibition (GABA uptake, etc.) (Rogawski and Loscher, 2004; Margineanu, 2012).

AEDs are also split between first and second generations, with second generation AEDs generally having less frequent side effects, fewer unwanted pharmacokinetic interactions, therefore, generally being more tolerable in patients. Despite this there are no real differences in the efficacy of seizure cessation between first and second-generation AEDs. The AED(s) selected for use in patients is wholly dependent on the type of epilepsy, age of patient and seizure class demonstrated. Initially, monotherapy with a single AED is trialled, but often more AED are added if monotherapy is unsuccessful.

1.5.3 Drug Resistant Epilepsy

A patient is said to have drug resistant epilepsy (DRE) when they are unable to become seizure free after adequate trials of two AEDs, as defined by the ILAE (Kwan et al., 2010). ~70% of worldwide epilepsy cases can sufficiently be treated by current AEDs, the remaining 30% are unable to be treated and are said to have refractory, intractable or drug resistant epilepsy (DRE) (Rogawski and Loscher, 2004). Further to this, another third of those initially responsive to AEDs will transition to DRE over the course of their treatment. Refractory epilepsy rates are higher in less economically well-developed countries, usually due to the substandard healthcare provisions available in these countries.

Underlying mechanisms of DRE are difficult to establish, though have been linked to a failure of drugs hitting their targets, for instance having efficacy at more than one target or differences in bioavailibity from patient to patient or, due to differences in the sensitivity of patients to specific drugs, such as carbamazepine (Bourgeois, 2008). Patients can be labelled as DRE due to inappropriate diagnosis or treatment of their epilepsy type, which can lead to incorrect AED selection, vastly increasing the odds of those patients being progressed into DRE status (Kwan et al., 2011). Current treatments of refractory epilepsy involve neurosurgery to resect the seizure susceptible foci of the brain, as determined through a myriad of testing including, but not limited to, MRI, MEG and electrocorticography (ECoG). Resection depends on a risk-reward basis, with placement of the foci in the brain a large factor in whether surgery is performed or not. Furthermore, the seizures must be focal in nature (affect one side of the brain only) for surgery to be considered. This treatment is used as a last resort due to the

invasive and higher risk nature of surgery. The numbers affected by DRE are substantial and demand a large and, as of yet, unmet medical response.

1.5.4 Temporal Lobe Epilepsy

Temporal Lobe Epilepsy (TLE) is one of the most frequently diagnosed epilepsy conditions, accounting for around 41% of all cases (Curia et al., 2014). TLE seizures are a form of focal onset seizures, able to arise through a variety of aetiologies, such as trauma, tumours, infection, cortical dysplasia or mesial temporal sclerosis (Camacho and Castillo, 2007; Pascual, 2007). Accordingly, TLE seizures arise in the temporal regions of the brain; though have the ability to generalise across the brain (Noebels and Jasper, 2012).

Following the initial insult is a period of no seizures, otherwise termed the latent period. The length of the latent period is highly variable and thought to be dependent on a multitude of factors including age and severity of insult (French et al., 1993; Mathern et al., 1995; Annegers et al., 1998). During the latent period the molecular, cellular and, network properties of the brain are remodelled, becoming seizure susceptible, in a process named epileptogenesis (Wong, 2009). The changes are observed mainly in the hippocampus and include; increased mossy fibre sprouting in the CA3, a loss of granular cell organisation in the DG and hippocampal sclerosis in the CA1 and subiculum (Babb et al., 1991; Lim et al., 1997; Buckmaster et al., 2002; Nadler, 2003; Dudek and Shao, 2004; Freiman et al., 2011). Upon conclusion of the latent period spontaneous recurrent seizures (SRS) appear (Turski et al., 1983a, 1983b).

1.5.5 The EC and TLE

Much focus of TLE research has been centred around the hippocampus, though there is now increasing attention on the EC, with evidence from both basic and clinical studies suggesting the clinical importance of the EC in TLE, alongside many other neurological disorders (Rutecki et al., 1989; Lothman et al., 1990; Du and Schwarcz, 1992; Du et al., 1993, 1995; Bertram and Cornett, 1994; Spencer and Spencer, 1994; Bernasconi et al., 1999, 2000; Wennberg et al., 2002). The EC has been linked with epileptogenesis, with a loss in the volume of layer III neurons and, demonstrable hyper-excitability in layer II of chronically epileptic rats observed (Du et al., 1993; Kumar and Buckmaster, 2006). Rat brain *in vitro* experiments have demonstrated EC susceptibility to induced acute epileptiform events, with pharmacologically induced seizures initiating in the EC and propagating outward to the hippocampus and other adjacent cortical regions (Walther et al., 1986; Jones and Lambert, 1990a, 1990b; Rafiq et al., 1993; Avoli et al., 1996; Iijima et al., 1996; Jones, 1996; Buchheim et al., 2000; Weissinger et al., 2000; D'Arcangelo et al., 2001). The deeper layers are seemingly more vulnerable to pharmacologically induced seizure events ("seizure susceptible") than the superficial layers ("seizure resistant"). Similar seizure activity differences have been found across the laminar

organisation of the neocortex (Hoffman and Prince, 1995; Yang and Benardo, 2002). The majority of epileptiform events originate in deeper layers and, are highly suggestive of potential pathological synchronisation being able to occur within the deep layers (Jones and Lambert, 1990a, 1990b; Jones, 1988, 1994; Avoli et al., 1996; D'Arcangelo et al., 2001).

1.5.6 Focal Cortical Dysplasia

Focal cortical dysplasia (FCD) is defined as a congenital abnormality of cortical laminar structure and presents as one of three types (Type I-III) (Blumcke et al., 2011). Type I is the least severe form of FCD, with seizures usually manifesting in early adulthood. Type II generally manifests seizures during childhood, while type III cases usually present type I/II symptoms alongside another epileptic lesion (Palmini et al., 2004; Fauser et al., 2006; Blumcke et al., 2011; Kabat and Krol, 2012).

FCD is more commonly diagnosed today in part due to vast improvements in imaging equipment. FCD is currently the highest operated on type of DRE in paediatric patients (Harvey et al., 2008), though was once thought of as rare (Taylor et al., 1971). Up to 75% of patients operated on are seizure-free a year after surgery, with the presented type of FCD being the most critical factor and indicator of success (Tassi et al., 2002; Colombo et al., 2003).

1.5.7 Models of temporal lobe epilepsy

Animal models of human disease are a vital area for medical research as they allow researchers to look intricately at both the progression and the mechanisms of diseases. By developing and studying animal models, researchers are better equipped to identify pharmacologically relevant targets.

For temporal lobe epilepsy there are currently three commonly accepted models: the kindling model (Goddard, 1967), the kainic acid model (Nadler et al., 1978) and, the pilocarpine model (Turski et al., 1983a). Each is a model of acquired TLE, where an insult is applied to the brain causing a progression from initial seizures to epileptogenesis (latent period brain remodelling) and finally recurrent seizures to occur. Acquired models of epilepsy are normally used, instead of genetic, to study epileptogenesis and recurrent seizures development.

1.5.7.1 Kindling

The kindling model involves repeated electrical stimulation of certain brain regions. Devised by Goddard et al, (1969), repetitive electrical stimulation (60-100Hz) of the hippocampus over the course of a week eventually resulted in afterdischarges (ADs), abnormal behaviour (that normally corresponds to the Racine scale (Racine, 1972). Currently spontaneous recurrent seizures (SRS) can be obtained if an overkindling model is used (McIntyre et al., 1982; Milgram et al., 1995). The amount of stimulus and intensity of the seizures seemingly corresponds to

the brain region that is kindled (McIntyre and Gilby, 2006). Kindling models result in subtle neuronal loss and cellular alterations of brain circuits, which eventually manifest as seizures and seizure-like events (Morimoto et al., 2004). The time constraints and laborious nature of kindling models mean they are not widely used, also as there is no set protocol many labs have taken to creating their own. This has led to vast differences in many aspects of the protocol such as stimulus duration and strength, brain region kindled, interstimulus intervals and AD thresholds (McIntyre and Gilby, 2006). The kindling model's strength is in studying the progression of epileptogenesis and response to AEDs but has drawbacks, through the time required and the lack of consistency across laboratories. As the classical kindling model does not produce SRS, which are characteristic of TLE models, it is therefore unsuitable for its study.

1.5.7.2 Kainic Acid

Kainic acid is an L-glutamate analogue, which when delivered either systemically or focally can induce seizures and neuronal depolarisations, culminating in SE, preferentially targeting the hippocampus (Nadler et al., 1978). Systemic application of KA results in generalised brain injuries, whereas intracerebral injections to the hippocampus provide a more focused lesion in the hippocampal region (Ben-Ari et al., 1980; Lancaster and Wheal, 1982; Drexel et al., 2012). KA is widely used as a model of TLE, as it mirrors human TLE closely, especially with focused hippocampal injections, whereby inducing SE (or initial insult to generate first seizure events) is followed by a latent or silent period where no seizures are observed, before finally progressing into SRS or chronic seizures (Dudek et al., 2005; Levesque and Avoli, 2013).

Seizure generation in the KA model is thought to arise via several mechanisms, though notably via activation of GluK2 subunit containing KARs in the CA3 post-synapse of DG mossy fibres (Ben-Ari and Cossart, 2000). The morbidity rate of KA can be low, with some animals making a recovery from SRS, which has been ascribed to the use of certain anaesthesia. Without anaesthesia the morbidity rate does increase, but so too does the mortality rate (Cavalheiro et al., 1982; Behrens et al., 2005).

1.5.7.3 Pilocarpine

Pilocarpine is another chemoconvulsant used to generate a model of TLE. Pilocarpine is a non-selective acetylcholine agonist acting upon muscarinic M1 receptors that mediates the transition into SE (Clifford et al., 1987; Hamilton et al., 1997). The pilocarpine model itself is the third most commonly used model of TLE (Turski et al., 1983a, 1983b). High doses of pilocarpine are administered to the rats (~300-400mg/kg) to induce intense epileptic seizures that can last for up to 3 hours. Due to high mortality rates associated with the pilocarpine model, researchers have sought a way to increase the efficiency of the protocol while decreasing mortality. This lead to the reduced intensity status epilepticus (RISE) utilised by the host lab and used throughout the present work (Modebadze et al., 2016).

1.5.7.3.1 *RISE*

The model of RISE TLE is a continuation of the pilocarpine model. Lithium chloride (LiCl) is applied 24 hours pre-pilocarpine dose, it is thought that lithium acts to potentiate the cholinergic response without acting as a proconvulsant alone (Ormandy et al., 1991).

As the name suggests, the RISE model aims to decrease both the severity of seizure and the mortality rate of the protocol, without losing any of its effectiveness. Instead of using large doses (300-400mg/kg) to induce SE, smaller doses (20-30mg/kg) are used in combination with LiCl. SE is a stage defined by two or more stage 4 as defined by the modified Racine scale (**Table 2.1**) seizures, a stage where mortality is common in the normal pilocarpine model. In the RISE model SE has a much lower mortality rate (~5%), in part due to the lower pilocarpine load applied.

Once in SE, xylazine, a potent muscle relaxant and agonist of α_2 adrenergic receptors is applied, helping to limit seizure severity and decrease mortality rates (Glien et al., 2001; Curia et al., 2008). The rats are relieved from SE one hour later by use of a 'stop' solution, containing MPEP, MK801, diazepam; a mGluR5 antagonist, NMDAR antagonist and $GABA_AR$ agonist respectively (Tang et al., 2007). Rats are then monitored to mark progression through the epileptogenic stages before being used for experiments.

The use of lithium chloride, xylazine and the STOP solution, as well as the lower dose of pilocarpine used, are the main differentiators between the standard pilocarpine model and the RISE model we have used in this project.

1.6 Cannabinoids

Cannabinoids are the main constituents of *Cannabis Sativa* plant, usually termed exocannabinoids or phytocannabinoids. Presently over 100 phytocannabinoids have been isolated from the *Cannabis sativa* plant (El-Alfy et al., 2010), each with their own distinct pharmacological profile and structure. Tetrahydrocannabinol delta 9 (Δ^9-THC) and cannabidiol (CBD) are the most prominent and abundantly used of these (Gaoni and Mechoulam, 1964).

1.6.1 The history of cannabis and cannabinoids

Cannabis Sativa has long been used both medicinally and recreationally, with some publications suggesting at least 5000 years of recorded medicinal use (Mechoulam, 1986). The earliest recorded usage of marijuana comes from 2727BC Chinese documents, written by Emperor Shen Nung, who experimented with botanical products on himself to discover if there were any medicinal benefits (Abel, 1980). The Chinese were also the first to record recreational use of cannabis (Abel, 1980). Cannabis is first noted in medicine in 1839, where it was marketed as a highly flexible drug, with purported effects including: sedation, analgesia, anti-inflammation, anti-spasticity and anti-convulsant. Many of these effects have been recently demonstrated in preclinical models.

Investigations into the active ingredients present in cannabis were conducted, fruitlessly, for over 100 years (for review see Mechoulam and Hanus, 2000). In 1896, the first real breakthrough into cannabinoids was made, with an Oxford group managing to distil a crystalline structure, later identified as cannabinol (CBN), from Indian *charas* (Wood et al., 1897). In the 1930's the chemical structure of CBN was elucidated, moreover, so too the first isolation of cannabidiol (CBD) (Mechoulam et al., 2014). Further investigation into CBN determined that it was not the primary active ingredient of cannabis. It wasn't until the 1960's, with the advent of modern chromatography techniques, that Δ^9-tetrahydrocannabinol (THC) was elucidated and identified as the active component in cannabis (Gaoni and Mechoulam, 1964). The discovery of dedicated cannabinoid receptors (CBRs) was due to their action as the primary mediators of THC (Devane et al., 1988; Matsuda et al., 1990; Munro et al., 1993). CBR existence was confirmed through complementary molecular biological assays. Application of exocannabinoids to neuroblastoma cells resulted in decreased cyclic adenosine monophosphate (cAMP) production, which implied G-protein coupled receptor signal transduction (specifically $G_{i/o}$ protein) (Howlett and Fleming, 1984; Howlett et al., 1986; Howlett, 1987). Radioligand binding studies, using the synthetic cannabinoid analogue of THC CP55950 in rats, confirmed CBR as being present in mammalian brains (Devane et al., 1988), with later genetic analysis confirming CB1R existence in rat brain and, subsequently, in humans (Matsuda et al., 1990; Gerard et al., 1991; Chakrabarti et al., 1995).

1.6.2 The endocannabinoid system

As previously discussed, cannabinoid receptors (CBRs) are a small family of presynaptic G-protein coupled receptors (GPCRs), with only CB1R and CB2R having been formally characterised as CBRs. Genetic analysis indicates that a third CBR is unlikely (Pertwee et al., 2010). Recent evidence is suggestive of other receptors sensitive to cannabinoids, with the orphan GPCRs GPR55 (Pertwee, 2007; Ryberg et al., 2007; Lauckner et al., 2008; Kapur et al., 2009) and GPR18 (Alexander, 2012; McHugh et al., 2012a, 2012b) activated by certain cannabinoid ligands, leading to discussion as to whether these should also be included as CBRs (Moriconi et al., 2010; Pertwee et al., 2010; Alexander, 2012).

CB1Rs and CB2Rs are sometimes classified as “neuronal” and “non-neuronal” respectively, though this is not strictly correct, as CB1Rs are commonly found throughout the nervous system, whereas CB2Rs are most generally associated with the immune system (but see Morgan et al, (2009) for evidence to the contrary).

1.6.2.1 Endocannabinoids

With the advent of CBR discovery and THC as a lipid molecule, it was assumed that any endogenous ligands would also be lipids. A candidate was extracted from pig brain tissue and was subsequently identified as a CB1R partial agonist, classified as anandamide (AEA), Sanskrit for “bliss” (Devane et al., 1992; Howlett et al., 2002). AEA was classified as an endogenous cannabinoid (eCB) as it was able to inhibit electrically evoked contractions of mouse *vas deferens*, while being insensitive to naloxone, a potent opioid receptor antagonist (Devane et al., 1992). This step was crucial as opioid receptor agonists were also able to inhibit electrically evoked contractions in the *vas deferens*. Further bioassays confirmed the classification of AEA to be correct through use of synthetic cannabinoid receptor antagonist such as SR141716A, which acts to inhibit action of AEA at CB1Rs. Further bioassays confirmed the classification of AEA to be correct through use of synthetic cannabinoid receptor (Rinaldi-Carmona et al., 1994).

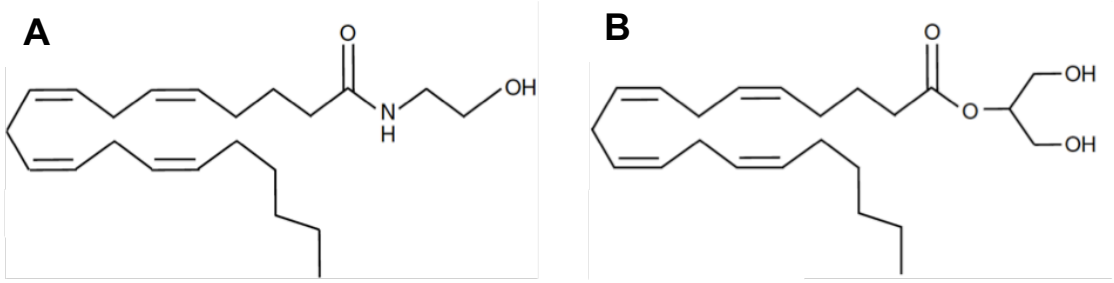

Figure 1.19 Skeletal chemical structure of AEA (A) and 2-AG (B).

Following the discovery and classification of AEA, reports arose claiming that other fatty acid derived compounds also acted as CBR sensitive cannabinoids (Di Marzo et al., 2005). The

CB1R agonist, 2-Arachidonoyl glycerol (2AG) was identified soon after (Mechoulam et al., 1995).

eCBs are eicosanoids-like lipophilic molecules, synthesised on-demand via the breakdown of acrachidonic acid (AA) phospholipid derivatives (Wang and Ueda, 2009; Luchicchi and Pistis, 2012). AEA synthesis is mediated by the conversion of N-arachidonoyl-phosphatidyl-ethanolamine (NArPE) catalysed by Ca^{2+}-sensitive N-acyltransferases (NATs) and phospholipase D (PLD). 2-AG synthesis is dependent on the hydrolysis of diacylgylcerols (DAGs) by DAG lipases (DAGLα/β), modulated by phospholipase Cβ (PLCβ) (Mechoulam et al., 1995; Köfalvi, 2008; Marinelli et al., 2008). AEA and 2AG are the most commonly investigated eCBs, though other eCBs have since been illuminated, mainly CBR agonists (Pertwee, 2006), though recently a CB1R inverse agonist was identified in virodhamine (Pertwee, 2005). The discovery of eCBs marked the existence of the once unknown endocannabinoid system. eCBs possess powerful regulatory powers on GABA neurotransmission, as shown by decreasing both IPSPs and IPSCs (Szabo et al., 1998; Hajos et al., 2000).

eCBs are retrograde messengers, diffusing backward across the synaptic cleft to bind receptors on the presynaptic membrane, or within the neuronal matrix (Kreitzer and Regehr, 2001; Ohno-Shosaku et al., 2001; Wilson and Nicoll, 2001). Following cellular reuptake processes, eCBs are metabolised by fatty acid amine hydrolysis (FAAH) in the case of anandamide or by monoacylglycerol lipase (MAGL) for 2AG (**Figure 1.20**; Di Marzo et al., 2005).

Figure 1.20 Schematic demonstrating both the catabolic and anabolic pathways of eCBs at the synapse.
AEA is synthesised from glycerophosplipid and phosphatidylethanolamine precursors, with the biosynthetic enzymes responsible for its synthesis NArPE, N-acyltransferases (NATs) and PLD all located on postsynaptic intracellular locations, though the exact location is currently unknown. Alongside this, enzymes required for the inactivation of AEA are also located in the postsynapse, with fatty acid amine hydrolyse (FAAH) mediating the conversion of AEA to ethanol amine and arachidonic acid. Conversely, 2-AG is inactivated within the presynapse by monoacylglcerol lipase (MAGL). The synthesis of 2-AG also occurs within the postsynapse, catalysed by membrane bound PLC and diacylgylcerol lipases (DAGL), localised on the post-synaptic plasma membrane from a glycerophosopholid precursor. Release of 2-AG into the synaptic cleft is facilitated by an as of yet unknown eCB membrane transporter (EMT). Taken from (Di Marzo et al., 2004).

1.6.3 CB1 Receptors

As mentioned, CB1Rs are observed throughout the CNS, and are also present at various sites in the peripheral nervous system (PNS) (Howlett et al., 2002). Aside from this, CB1Rs have also been detected in a number of organs and tissues: heart, liver pancreas and adipose tissues; as well as throughout the cardiovascular, gastrointestinal and reproductive systems (Croci et al., 1998; Szabo et al., 1998; Pertwee, 2001a, 2001b; Wagner et al., 2001; Kunos et al., 2009). CB1Rs are involved in a vast range of physiological functions including: nociception, appetite, learning and memory and neurite outgrowth (Pertwee, 2009; Katona and Freund, 2012).

CB1Rs are abundantly expressed GPCRs in the rodent brain, with particular emphasis in the cerebellum, hippocampus, cortex, amygdala and basal ganglia (Howlett, 1998; Pettit et al., 1998; Tsou et al., 1998). Of these the highest areas of CB1R expression, using autoradiography studies, were found at the cerebrum, hippocampus and entorhinal cortex (Herkenham et al., 1990, 1991; Glass et al., 1997). In addition, CB1Rs are commonly found clustered in the plasma membrane of the axonal perisynapse of both GABAergic and glutamatergic neurons (Katona et al., 1999, 2006; Kawamura et al., 2006). Further to their surface axonal presence, intracellular vesicles of CB1Rs have been exposed in both soma and dendrites from whole cell immunostaining experiments (Irving et al., 2000; Coutts et al., 2001).

Activation of CB1R-coupled G_i proteins, the most predominant G protein coupled to CB1R, inhibits production of cAMP through inhibition of adenylate cyclase and subsequently, protein kinase A (PKA) phosphorylation pathways (Howlett, 2002, 2004, 2005). Further signal cascades that modulate various kinases activation have been described as occurring at this step (Glass et al., 1997; Lauckner et al., 2005), however the classical effect of CB1R is the inhibition of N-, P- and Q-type voltage gated Ca^{2+} channels through interaction with the G_i βγ-subunit and, activation of G_i coupled inwardly rectifying potassium channels (K_{ir}/GIRK). CB1R activation, therefore, results in decreased Ca^{2+} and increased K^+ conductance, and as such, a decrease in neurotransmission from the presynaptic terminal. This has been described as depolarisation-induced suppression of excitation (DSE) or inhibition (DSI) depending on the neuron type (GABA-/glutamatergic) (Llano et al., 1991; Pitler and Alger, 1992, 1994; Kreitzer and Regehr, 2001; Ohno-Shosaku et al., 2001; Wilson and Nicoll, 2001; Diana and Marty, 2004).

CB1Rs are often described as being “promiscuous” due to their ability to interact with various members of the G protein family, commonly with G_i α subtypes as mentioned, but also with

G_o, G_q and G_s. These interactions allow CB1Rs to have differing responses, which have been related to the cell type or compartment location, hetrodimerisation of the receptor and, off-target agonist effects (Howlett, 2004; Pertwee, 2009). Responses to interactions with different G proteins allow CB1R to effect PLC and Ca^{2+} intracellular signalling pathways (Netzeband et al., 1999; Lauckner et al., 2005; De Petrocellis et al., 2007). In the hippocampal formation, CB1R activation depresses presynaptic GABA release (Hajos et al., 2001; Wilson and Nicoll, 2001). CB1R agonists, both endo-/exogenous, reduce amplitude and frequency of GABAergic spontaneous inhibitory postsynaptic currents (sIPSCs), but not the amplitude of action-potential-independent miniature inhibitory postsynaptic currents (mIPSCs) (Inada et al., 2010; Kovacs et al., 2012). Other studies indicate that CB1R activation enhances network oscillatory activity in the hippocampus (Bragin et al., 1995). In the parahippocampal region, CB1R activation is able to modulate both GABA release and neuronal network oscillations (Morgan et al., 2009).

1.6.3.1 CB1R pharmacology and ligands

CB1Rs have a complex pharmacology, in part due to the ligands commonly being small lipophilic molecules, able to cross the lipid bilayer effectively, with inhibitors usually being inverse agonists not neutral antagonists (Pertwee, 2005; Pertwee et al., 2010). Inverse agonists block the receptors constitutive activity and stabilise the receptor in its inactive conformation. As a consequence of the lipophilic nature of its ligands, CB1Rs are not required to be embedded in the membrane to be activated, demonstrated using the non-permeable peptide hemopressin, which allowed intracellular CBRs to be investigated (Rozenfeld and Devi, 2008; Gomes et al., 2009; Benard et al., 2012) – the results raised the suggestion of subtly distinct physiological roles between intracellular and membrane CBR populations.

Currently, the majority of CB1R pharmaceuticals of use in the clinic are synthetic derivatives of THC including: Sativex® (GW pharmaceuticals), dronabinol (Marinol®; Solvay Parmacuetiucals) and nabilone (Cesamet® Eli Lilly), prescribed for their analgesic properties or as anti-emetics and appetite stimulants for patients with cancer and acquired immunodeficiency syndrome (AIDs) (Di Marzo et al., 2004). CBR inhibitors include the well-known ligand SR141716A or 'rimonabant' (Acomplia®; Sanofi-Avent), an inverse agonist of CB1R, marketed in Europe in 2006 as an effective anti-obesity treatment, but withdrawn in 2008 due to unwanted side-effects, such as depression and contemplation of suicide (Wong et al., 2012). Several endocannabinoid-manipulating drugs, which can indirectly modulate cannabinoid receptor activity, through activation or inhibition of the endocannabinoids, have already been developed and are either on the market or undergoing clinical trials (Piomelli, 2003; Di Marzo et al., 2004), including the FAAH inhibitor URB597, developed for the treatment of neuropathic pain, anxiety and depression (Di Marzo, 2008).

Interestingly, THC only possesses partial agonist activity at CB1Rs, which is thought to account for the increasing dependency observed in habitual users of *Marajuana* (Howlett et al., 2004). CBD is a very low affinity antagonist at CB1Rs, so much so, that specific binding is uncommon.

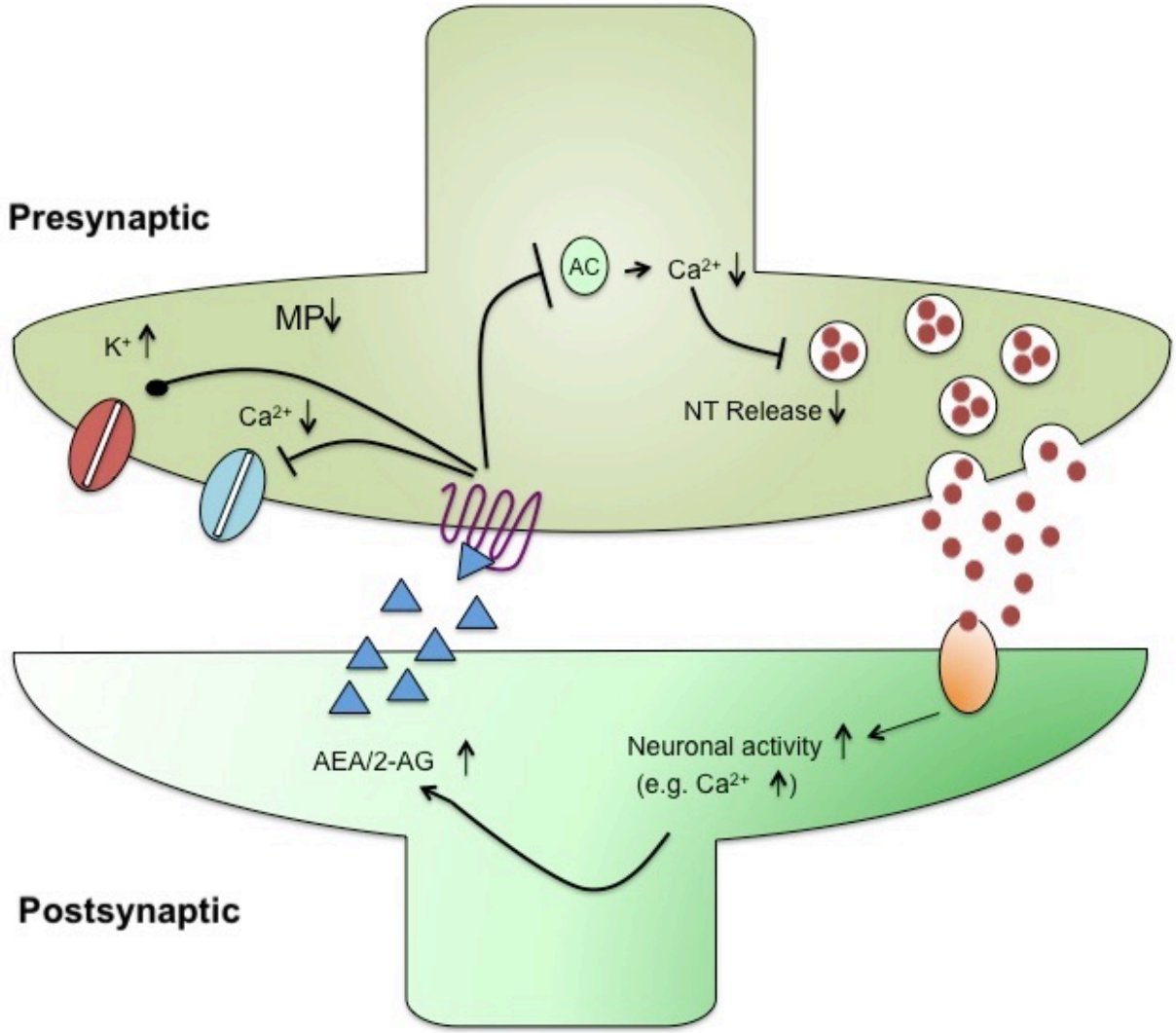

Figure 1.21 Schematic for the mechanism of action of endocannabinoids at CB1Rs. Neurotransmitters (NT) bind to postsynaptic receptors (glutamatergic or GABAergic triggering an increase in neuronal activity (example given increase in Ca^{2+} influx as seen with glutamatergic receptor activation). Increased neuronal activity results in upregulation of AEA/2-AG synthesis. The eCBs are then released from postsynaptic terminal where they bind to presynaptic CB1R. CB1R activation causes adenylyl cyclase (AC) and Ca^{2+} channels to become inhibited (while K+ channels activated). As a result, neurotransmission is decreased due to the lowering of Ca^{2+} concentration and hyperpolarisation of the membrane (MP = membrane potential).

1.6.4 CB2 Receptors

CB2Rs share 44% amino acid sequence homology with CB1Rs and were initially identified in rat spleen and cloned HL-60 cells (Munro et al., 1993). Historical immunohistological evidence associates CB2R with the immune system, glia and peripheral tissues only (such as mast cells, β-lymphocytes etc) (Galiegue et al., 1995; Schatz et al., 1997; Carayon et al., 1998; Bouaboula et al., 1999), new work however indicates a role and function in the CNS. A steady stream of immunohistological work has been published demonstrating the presence of CB2Rs in CNS

areas such as human and cultured sensory nerves (Ross et al., 2001; Stander et al., 2005), rodent brain stem (Van Sickle et al., 2005), with CB2R mRNA present in human spinal nerves (Beltramo et al., 2006). Gong et al., (2006) identified CB2R mRNA in rodent spinal cord and CB2R protein throughout rodent brains (Gong et al., 2006). Published work from the host lab added to this, with CB2Rs discovered to be have significant functional roles in neurons across the layers of the EC, being able to modulate action potential dependent GABA release (Morgan et al., 2009).

1.6.5 Cannabinoids as novel antiepileptic agents

THC is the most prominent exocannabinoid, in part due to its psychoactive nature imbuing the feel of a "high" when inhaled as cannabis smoke for instance. THC has shown some promise as an anticonvulsant itself, however, its unwanted psychoactive effects as a therapeutic agent ensure it is not an eligible candidate for medicinal use in children and many adults (Hill *et al.*, 2012). Indeed, in some animal models THC has proven to be a proconvulsant at low doses, though this was inhibited through the use of matching doses of CBD (Boggan et al., 1973). CBD and its propyl analogue cannabidivarin (CBDV) have both recently shown promise as anti-epileptics (Jones et al., 2010, 2012; Hill et al., 2012). Neither displays psychoactive properties, making them prime candidates for further research.

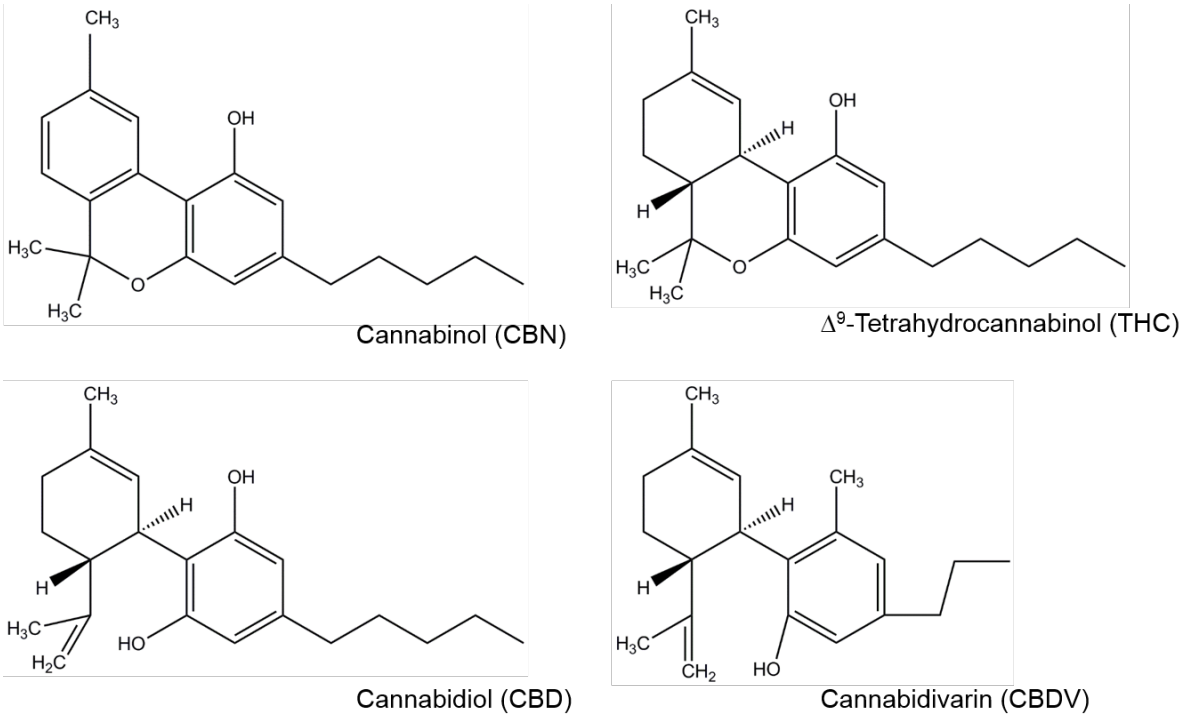

Figure 1.22 Skeletal chemical structures of prominent cannabinoids.
CBN was the first cannabinoid to be isolated and have its chemical structure elucidated, THC is the most prominent of all phytocannabinoids, whereas CBD is purported to have the highest number of medical applications. CBDV is a propyl analogue of CBD linked to possessing anticonvulsant effects.

1.6.6 CBD

CBD is a water insoluble crystalline solid at room temperature, though is soluble in organic solvents, such as DMSO. It is synthesised in the cannabis plant initially from cannabigerolic-acid (CBGA), which is converted to CBA-caroxylic acid (CBDA) by CBDA synthase. Decarboxylation of CBDA then occurs to produce CBD. THC synthesis utilises them same precursor, CBGA, with THCA synthase substituting in for CBDA synthase to produce tetrahydrocannabinol acid (THCA) which is then decarboxylised to produce THC (**Figure 1.23**; Marks et al., 2009).

CBD is a low affinity allosteric antagonist at both CB1R and CB2Rs (Pertwee, 2008) and acts as an antagonist at GPR55 (Pertwee, 2008). It acts as a partial antagonist at 5-HT1A receptors, which may be how it exerts its purported anti-depressant, neuroprotective and anxiolytic effects (Mishima et al., 2005; Russo et al., 2005; Hayakawa et al., 2007; Campos and Guimaraes, 2008; Resstel et al., 2009; Zanelati et al., 2010). CBD has also been shown to an allosteric modulator at both and delta and mu (δ, μ) opioid receptors (Kathmann et al., 2006). Alongside these effects CBD has also displayed inhibitory effects on fatty acid amide hydrolysis enzyme (FAAH), which may be responsible for increased AEA levels in the presence of CBD (Bisogno et al., 2001; Massi et al., 2008; De Petrocellis et al., 2011; Ibeas Bih et al., 2015). Recent work has also shown that CBD has a benzodiazepine-like effect on $GABA_AR$ though does not bind to the classical benzodiazepine site to exert this effect (Bakas et al., 2017).

As well as potential in epilepsy, CBD has shown much promise in other disease states including: cancer, neuroprotection, anxiety, analgesia and Type-1 diabetes (Bakas et al., 2017). In the UK, Sativex (GW Pharmaceuticals), a combination of 50% THC and 50% CBD, has been granted a licence for treatment of spasticity in patients afflicted with multiple sclerosis. Sativex is also licensed for pain relief in cancer patients undergoing chemotherapy in Canada.

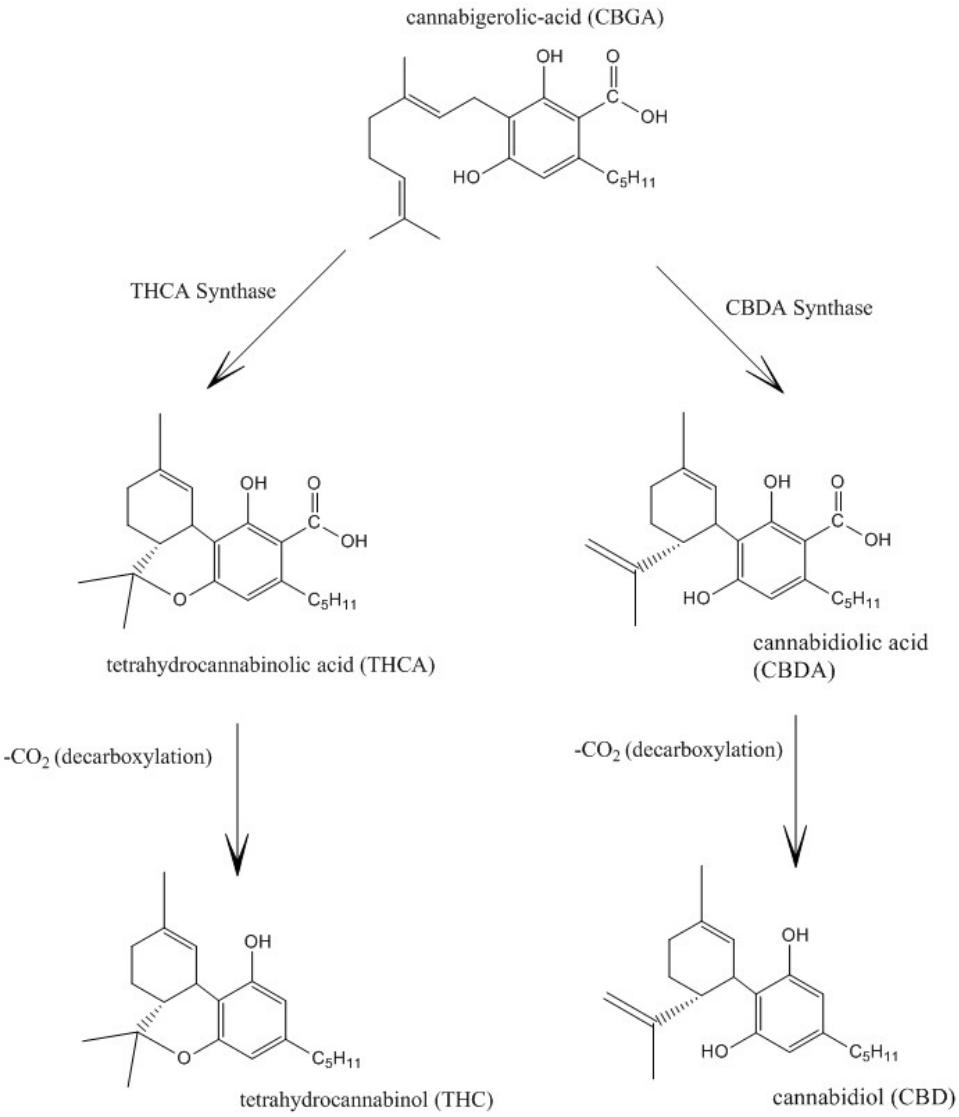

Figure 1.23 Schematic of the precursor molecules for THC and CBD.
The synthesis of both THC and CBD from precursor molecules and the enzymes required for their synthesis depicted by their skeletal chemical structures. Taken from (Taura et al., 2007).

1.6.6.1 CBD as an anticonvulsant

Several *in vivo* animal models of epilepsy studies have shown CBD has a propensity to reduce seizure occurrence and intensity (Consroe et al., 1982; Wallace et al., 2001; Jones et al., 2010, 2012). Limited historical studies have shown similar in humans (Cunha et al., 1980). Recent studies utilising CBDV have also shown similar results *in vivo* (Hill et al., 2012, 2013). Mediation of the responses to CBDV has been shown to be independent of CB_1R (Hill et al., 2013). Elucidation of the MOA of these cannabinoids is difficult as they act promiscuously, with varying effects and affinities across a wide range of receptors (Ibeas Bih et al., 2015). Current thinking of receptor targets includes GPR55, $5\text{-}HT_{1A}$ and $5\text{-}HT_{2A}$ as potentially playing a role in the anti-epileptic effects of both CBD and CBDV (Russo et al., 2005; Mechoulam et al., 2007; Devinsky et al., 2014)

.

In vitro studies of CBD and CBDV are a less common, though some research has corroborated the *in vivo* work in the case of CBD. In completed *in vitro* studies CBD has been shown to have a powerful effect on DRE models, using the magnesium free (Mg^{2+} free) models (Jones et al., 2010).

Trials of CBD efficacy are, and have, been conducted on human patients with epileptic encephelopathies including Lennox Gastaut and Dravet Syndromes using Epidiolex (a proprietary oral solution of pure plant–derived CBD produced by GW Pharmaceuticals). The investigator-initiated open label study, reported in Rosenberg et al, (2015), spans 10 epilepsy centres in the USA, collecting data on 213 patients with DRE (Rosenberg et al., 2015). The mean age of this population is 10.8, with a range of 2.0-26.0. Epidiolex/CBD was added supplementary to the patients existing AED treatment plans, with an average of three concomitant AEDs. Average total seizure frequency per month was 60, while the average for convulsive seizures was 30. In total, 137 patients followed the program for 12+ weeks and were included in the efficacy study. The results of which showed an average decrease in seizures of 54% at week 12. In that sample were 23 Dravet syndrome patients who showed an average decrease in seizures of 55%, while 16% reached complete cessation of seizures by week 12. Patients afflicted with Lennox Gastaut syndromes (n=10) showed a median decrease of 52% in seizures by week 12. Investigators concluded CBD is a generally well tolerated and effective means of seizure reduction, with mild adverse effects including somnolence, fatigue, decreased appetite and diahorrea. 9% of the sample curtailed their involvement in the study due to adverse effects.

A further clinical trial, reported by Devinsky et al, (2016), produced a similar conclusion to the previous. 214 patients with DRE enrolled in the trial, with an age range of 1.0 to 30.0. Adverse effects were higher this time, with reports from 128 (79%). Serious adverse effects were high, with 48 (30%) patients reporting. There was also one unseen death in the study, though this was ruled not to be associated with CBD usage, with cause of death *status epilepticus* (SE). The most common serious adverse effect was status epilepticus (SE) with 9 reports (6%). The median monthly motor seizures were 30.0 (11.0-96.0) baseline and 15.8 (5.6-57.6) after 12 weeks, with a median decrease of 36.5%. The authors came to a similar conclusion as the previous, that CBD might be tolerable and generally effective at decreasing seizure frequency in children and young adults (Devinsky et al., 2016).

Chapter 2

Materials and Methods

2.1 Animal and Ethical Approval

All procedures carried out were performed in accordance with the Animals (Scientific Procedures) Act 1986 UK, European Communities Council Directive 1986 and Aston University ethical review documents.

2.2 RISE model of temporal lobe epilepsy

Lithium chloride (LiCl) (127mg/kg) was administered, subcutaneously (S/C) 24-hours prior to induction, to male Wistar rats (0-1 day post-weaning/18-19 days postnatal; ≤55g). (-) scopolamine methyl bromide (1mg/kg, S/C) was delivered 30 minutes before administration of pilocarpine (25mg/kg, S/C). The rats were continually observed for the onset of status epilepticus (SE) – defined as two stage 4 or above seizures using a modified Racine scale (**Table 2.1.**). Stage 4 seizures include rearing, sitting back onto hind limbs with both forelimbs shaking. Stage 5 seizures are identical, but rats fall either backward or sideways. If any rats had not entered SE after 45-60 minutes another dose of pilocarpine (25mg/kg was then administered (up to a maximum of 3 doses total). Once rats had entered a second stage 4 event, they were dosed with xylazine (2.5mg/kg) intramuscularly (I/M). Extra (-) scopolamine methyl bromide could also be administered at this point if rats displayed foaming at the mouth. After one hour in SE 0.05ml "STOP" solution was delivered, containing (in mg/kg): 2.5 diazepam, 0.1 MK801 and 20 MPEP, dissolved in ethanol. Post-op, the rats were allowed to recover on a heat pad at 33°C, under constant observation and were rehydrated once every two hours for 10 hours with the administration of 0.5ml 0.9%/5% NaCl saline solution (S/C) until fully recovered. Furthermore, rats were fed with high calorie food to try and mitigate weight loss (e.g. milkshakes, peanut butter etc).

Stage	Symptoms
1	Oroalimentary movements
2	Head nodding
3	Anterior limb clonus
4	Forelimb clonus, dorsal extension (rearing)
5	Falling, loss of balance whilst rearing

Table 2.1 Modified Racine scale (Cordeiro et al., 2009)

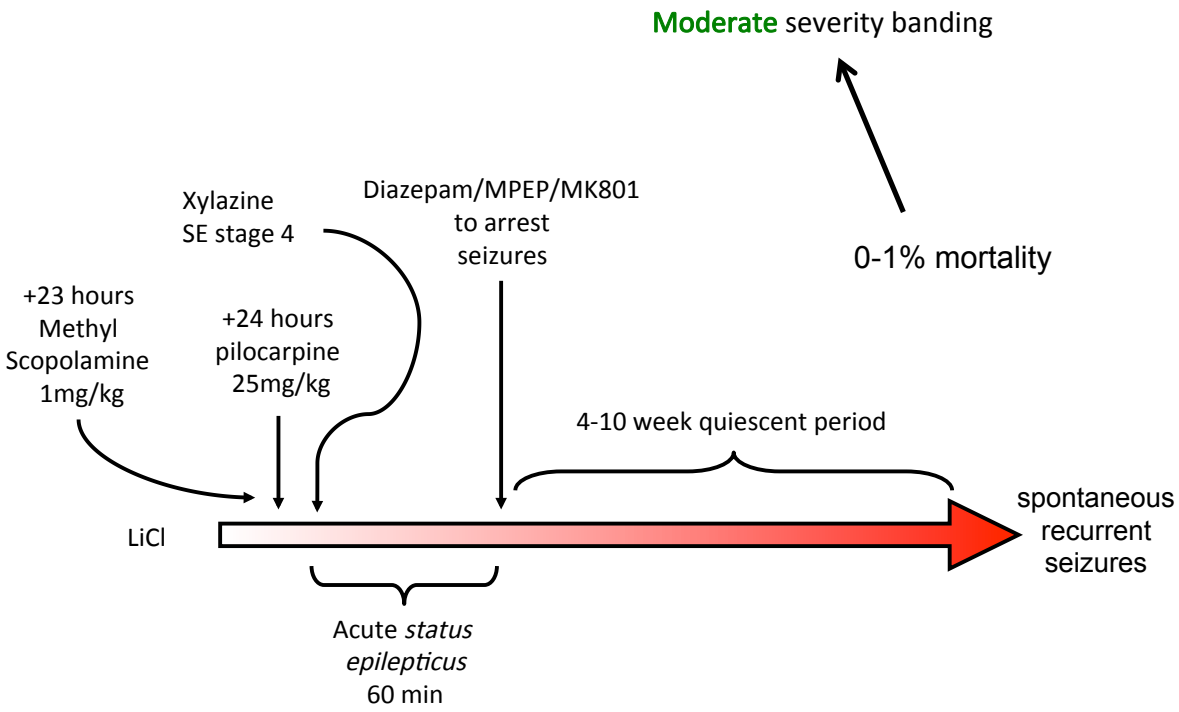

Figure 2.1 Flow chart representative of the RISE epilepsy induction model.
Detailing drugs administered, and rough estimates of time taken to reach spontaneous recurrent seizures (SRS). Figure courtesy of R. Jones (University of Bath).

Drug	Concentration Used; Solvent	Supplier
(-)-scopolamine methyl bromide	1mg/kg; Water	Sigma
Diazepam	2.5mg/kg; Ethanol	Hameln
Lithium Sulphate	127mg/kg; Water	Sigma
MK801	0.1mg/kg; Water	Abcam
MPEP hydrochloride	20mg/kg; Ethanol	Sigma
Pilocarpine	25mg/kg; Water	Sigma
Xylazine	0.1mg/kg; Water	Bayer

Table 2.2 Drugs administered in RISE model of epilepsy.
The concentrations used (mg/kg), solvent and, suppliers are all listed

2.2.1 Post-Seizure Behavioural Battery (PSBB)

Rats were tested for the onset of chronic epilepsy using a modified version of the PSBB. This involved touching the posterior of the rat with a blunt object (e.g. pen) and scoring its response against a predefined list of expected behaviours (listed in **Table 2.3 touch column**). Rats were then gripped around their forelimbs and their responses were scored (listed in **Table 2.3 pick up column**). The scores were multiplied together to give a final total score. If this score was over 10 for 4 sessions in a row the rat was deemed to be chronically epileptic or spontaneous recurrent seizures (SRS). PSSB sessions were performed twice weekly with rotating examiners each session to limit bias.

Score	Touch	Pick Up
1	No reaction	Very easy pick up
2	Rat turns toward instrument	Easy pick up
3	Rat moves away from instrument	Some difficulty in pick up (rat rears and faces hand)
4	Rat freezes	Rat freezes
5	Rat turns toward touch	Difficult pick up (rat moves away from hand)
6	Rat turns away from touch	Very difficult pick up (rat behaves defensively or attacks hand)
7	Rat jumps (with or without vocalisation)	

Table 2.3 The scoring table used for PSBB.
The tests used and the definitions for each score are listed.

2.2.1.1 Rodent “Big Brother” System

8 rats were individually filmed following confirmation of chronic epilepsy by PSBB to ensure independent confirmation of behavioural seizures. All rats were housed separately and recorded 24 hours a day using high-resolution infrared video cameras and infrared light provided by the rodent big brother system (AstraZeneca, UK). The recordings were saved to individual computer systems. This system is currently under development by AstraZeneca to enable automatic detection of seizures. As this system is currently being developed lab members and AstraZeneca employees watched the videos and marked seizure events when they arose, which they eventually did in all rats. Once a seizure had been observed the rat was categorically defined as chronically epileptic and, a new rat was introduced to the enclosure, up to the eighth and final rat, with three enclosures recording simultaneously. Upon conclusion of the observations, the equipment was returned to AstraZeneca for further development.

2.3 Extracellular experiments

2.3.1 Brain slice preparation and storage

Rats were anaesthetised using isoflurane. After loss of consciousness, deep anesthesia was induced using pentobarbital (60mg/kg, S/C) and co-application of ketamine/xylazine (100/10mg/kg respectively, I/M). Upon loss of pedal reflex, transcardial perfusion was performed using carbogen (95%O_2/5%CO_2) bubbled ice-cold saCSF. After perfusion sufficient to fully decolourise the nares, paws and ears, rats were decapitated, and the brain quickly resected and placed into cold saCSF.

The cerebellum was dissected away, as too, was a small section of the frontal lobe allowing for easier orientation. The brain was then hemisected, and the dorsal surface cut away in a parallel plane to the base of the brain. The cut surface was then glued to a steel platform, using cyanoacrylate glue (Loctite 480, USA). The brain was sliced using a ceramic blade (Campden, UK) until the ventral portion of the hippocampus and the rhinal fissure were observable; both used as indicators that slices will contain the parahippocampal regions of interest (i.e. mEC). Combined hippocampal-entorhinal slices were then cut in the horizontal plane using a Vibrotome slicer (Campden Instruments, UK) to a nominal thickness of 450μM. Vibrotome was set to a speed of 7, with a slow manual speed of cutting used.

The best slices were immediately placed onto the recording chamber (**Figure 2.2**) on small sections of lens tissue, while the rest of the slices were placed in an interface holding chamber, both containing normal aCSF again bubbled with carbogen. A Parafilm (Chicago, USA) covering was used to ensure adequate humidity and viability of slices.

2.3.1.1 Sucrose-based cutting aCSF (mM)

The recipe for the sucrose cutting solution was as follows (in mM): 180 Sucrose, 2.5 KCl, 10 $MgSO_4$, 1.25 NaH_2PO_4, 10 D-Glucose, 0.5 $CaCl_2$, 1 Absorbic Acid, pH 7.3, 300-310 osmolarity. saCSF also contained several neuroprotectants to increase slice viability (mM): 0.3 uric acid, 0.045 indomethacin, and 0.13 ketamine.

2.3.1.2 Normal aCSF (mM)

The recipe for the normal aCSF solution was as follows (in mM): 126 NaCl, 2.5 KCl, 1 $MgCl_2$, 2.5 $CaCl_2$, 26 $NaHCO_3$, 2 NaH_2PO_4, 10 D-Glucose, pH 7.3, osmolarity 280-290. aCSF was used in both the holding chamber and the LFP rigs. aCSF in the holding chamber had added (in mM): 0.045 indomethacin and 0.3 uric acid to prolong viability of slices.

2.3.2 Local Field Potential (LFP) recordings

Microelectrodes were pulled from borosilicate glass (1.2mm diameter) with a resistance of 1-5 MΩ using a Flaming-Brown microelectrode puller (P-2000, Sutter Instruments, CA, USA). Electrodes were filled with normal aCSF and placed in holders connected to EXT-02F headstages (NPI, Germany). After one-hour recovery and acclimatisation at 30-32°C in the interface recording chamber (BSC-1, SSD, Canada), with a flow rate of ~2ml/min, microelectrodes were placed into Layer II of the mEC of 2-4 separate slices.

An Olympus SZ51 field microscope (Olympus, UK) was used to locate Layer II and ensure contact between electrodes and slice. Signals were amplified x100 initially by EXT-02F amplifiers and then further amplified x10 by LHBF-48X amplifiers (NPI, Germany), with Bessel filters set at 700Hz low pass, 0.3Hz high pass, with a sampling rate of 8.3KHz. 50Hz noise was removed via a Humbug (Quest Scientific, Canada). Analogue signals were then digitised using a Digidata 1440a (Axon CNS, Molecular Devices, USA). Each of these components is shown in **Figure 2.3**.

Persistent gamma oscillations were induced in rats using 400nM KA, applied as two separate 200nM doses roughly 10 minutes apart, as anecdotal experience by this researcher had found this to be the most effective method for inducing stable gamma oscillations consistently.

Recordings were made using Clampex 10.3 and saved to the local hard drive. Backups were made externally upon completion of the experiments. Subsequent analyses were made using Clampfit 10.3, Spike2 7.3, Microsoft Excel and GraphPad Prism 7 (further details in **Section 2.11.1.**).

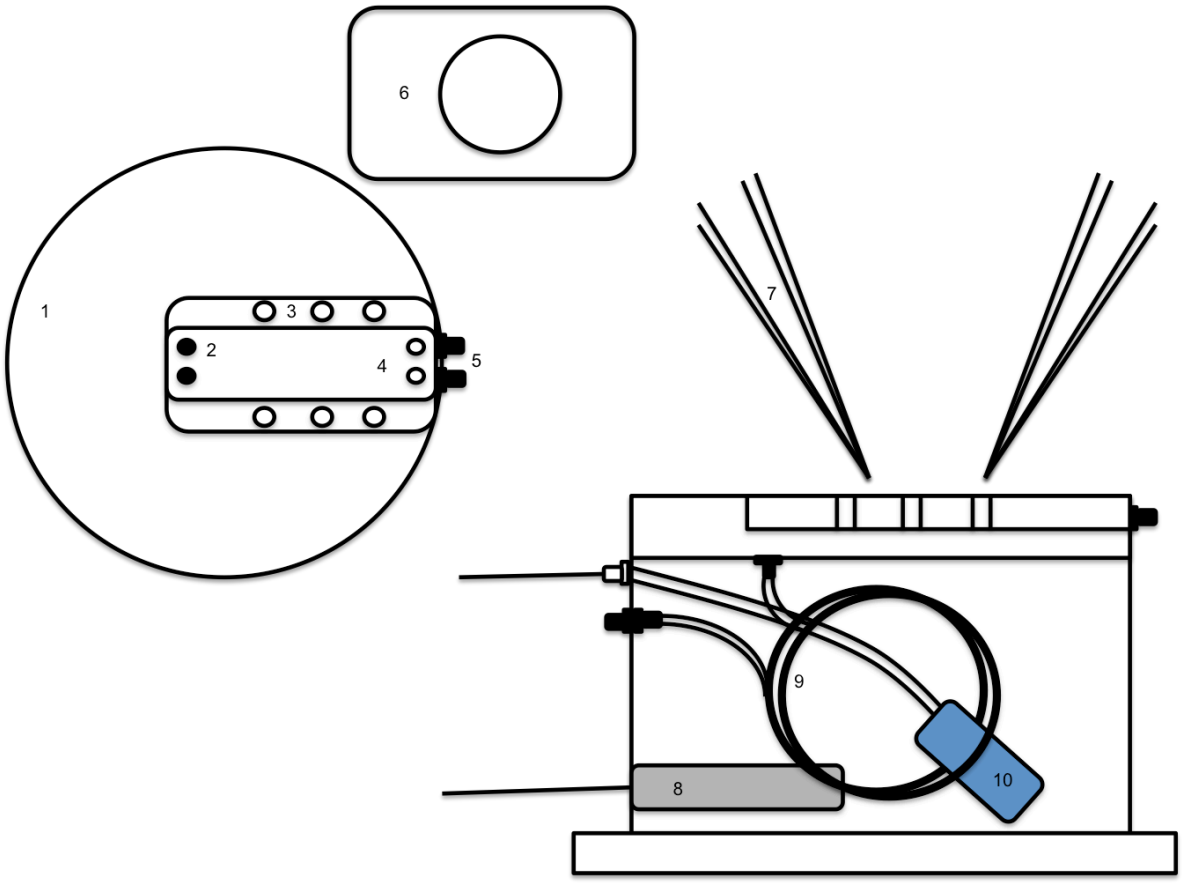

Figure 2.2 Schematic of LFP interface chamber.
Numbers highlight distinct sections of the rig and are listed as follows: (1) Upper lid of chamber (2) Wells for liquid dispersal onto netting (3) Air holes to allow oxygen to pass from across surface (4) Wells allowing aCSF out of platform to be wicked away ready to be recycled (5) Wicking exit, would be lined with filter paper to ensure proper wicking (6) PVC plastic covering ensuring even distribution of oxygen, with hole to allow electrode entry (7) Electode filled with aCSF (8) Heating element, heats water to ensure correct temperature and humidity in chamber (9) Tubing connecting to liquid wells at rear of platform and rear of chamber providing the aCSF (10) Air stone providing carbogen.

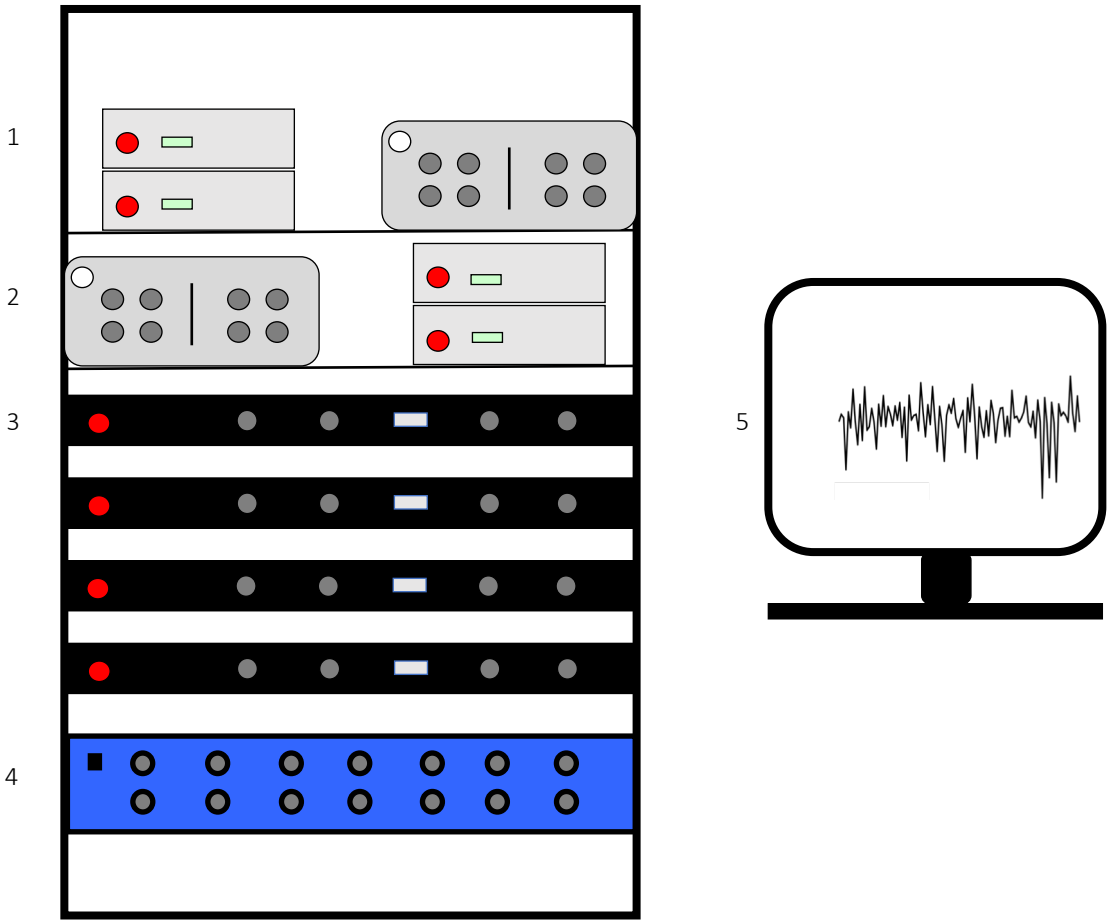

Figure 2.3 Electrical component set up LFP rig.
(1) 50Hz Humbugs (Quest Scientific, Canada) for removal of 50Hz noise (2) EXT-02F amplifier x100 amplification of 2 headstages (NPI, Germany) (3) LHBF-48X amplifiers x10 amplification of individual headstage signal (NPI, Germany) (4) Digidata 1440A for conversion of analogue signal to digital (Axon CNS, Molecular Devices, USA) (5) Computer running Clampex software (Axon CNS, Molecular Devices, USA).

All drugs used in LFP experiments are detailed in **Table 2.4**. Drugs were applied for 30 minutes, in LFP experiments (with the exception of kainic acid which was used to induce persistent oscillations in LFP).

Drug	Stock Concentration; Solvent	Concentration Used	Supplier
CBD	60mM; DMSO	0.3-30μM	GW Pharma
CBDV	60mM; DMSO	0.3-30μM	GW Pharma
DL-AP5	25mM; Water	50μM	Abcam
Flumazenil	10mM; DMSO	500nM	Abcam
Kainic Acid	1mM; Water	200-400nM	Abcam
MK801	20mM; Water	100nM	Abcam

Table 2.4 Drugs used in LFP experiments.
Listed with suppliers, concentration used at and solvent type.

2.4 Whole cell voltage-clamp experiments

Whole cell patch clamp experiments were implemented to allow for the CBD/V effect on single mEC layer II principal cells to be observed. Postsynaptic principal neurons were investigated using voltage-clamp techniques as this allowed for the visualisation of presynaptic neurotransmitter (NT) release as well as observing the corresponding postsynaptic current alterations, through the observation of spontaneous inhibitory/excitatory postsynaptic currents (sI/EPSCs). This method provides some advantages over intracellular recordings (sharps recordings), those being an increased resolution as well as providing control to alter the internal cellular environment to the experimenter. The drawbacks are the reverse, with artificial manipulation of the internal environment difficult in sharps recordings.

2.4.1 Brain preparation and slicing

Patching slices were prepared in the same way as the LFP preparation previously described, though were cut to a thickness of 350µm. The slices were submerged in a holding chamber (**Figure 2.4**) containing bubbled aCSF and allowed to recover for a minimum of one hour at room temperature.

Patching slice storage involved the assembly of a custom storage facility. This required the use of a 5ml syringe being cut into 1cm circular sections. 6 sections were then orientated around a central section to provide 7 slice storage units and glued together. Fine netting was then glued to the base of this collection and allowed to dry overnight making up the chamber, where the slices were stored. A chimney portion was fashioned using a cut 10ml syringe, which was then wrapped in Parafilm (Chicago, USA) laboratory film until an appropriate width was achieved which would allow the chamber section to be suspended when both were placed into a 250ml beaker together. The chimney acted to allow an air stone to be placed into the beaker without overtly disturbing the slices placed in the chamber but still allowing circulation of the aCSF by providing a path for the air bubbles (see **Figure 2.4** below for an accurate representation).

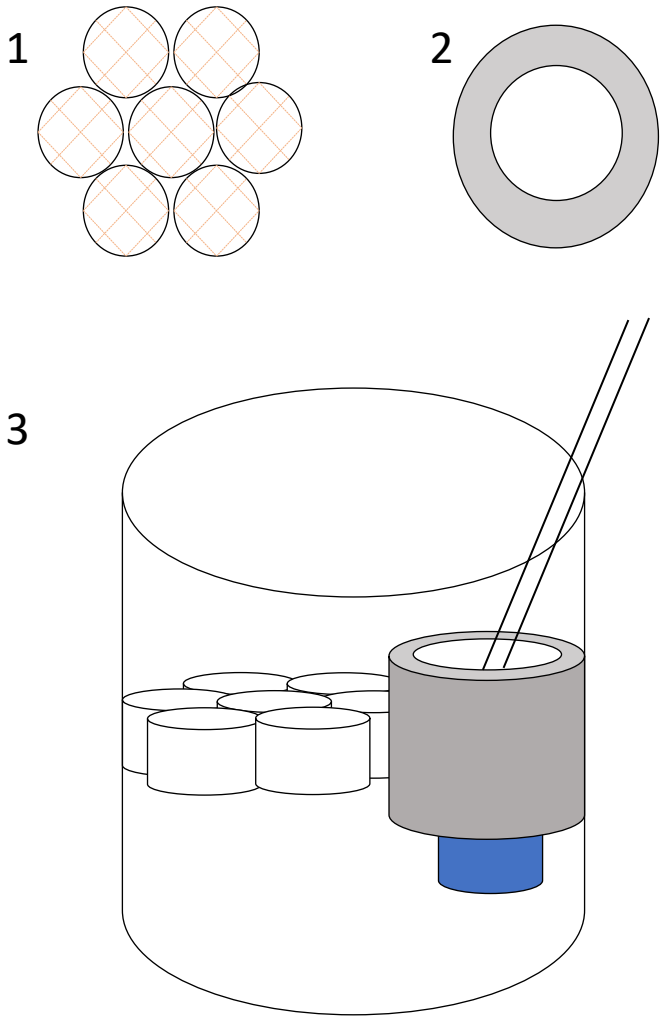

Figure 2.4 Storage facility for patching slices.
Numbered portions show different parts and, are as follows: (1) 1cm circular netted syringe pieces used to hold slices. Slices laid flat on top on netting and left for 1-hour recovery. (2) 10ml syringe section wrapped with Parafilm to create chimney for air stone. (3) Assembled storage facility in 250ml beaker, complete with air stone.

2.4.2 Whole cell voltage-clamp visualisation

After an hour recovery time, a single slice was transferred to a submerged recording chamber mounted on the stage of an Olympus U-CAMD3 microscope (Olympus, Japan). Once submerged, the slice was allowed to recover in the chamber for 5-10 mins. The chamber was continuously perfused with aCSF at 30°C with a flow rate of ~2ml/min. Cells were viewed using a x40 water immersion objective and visualised using DIC optics and an infrared camera.

Cells were chosen based on a number of factors including their depth within the slice, size and morphology. Cells in layer II were generally large, nominally principal in shape and just below the surface, as these generally provided the best results.

2.4.3 Whole cell voltage-clamp recording

Microelectrodes were pulled from borosilicate glass (Harvard Apparatus, UK) with a tip resistance between 3-6MΩ (open tip diameter ~1µm), using a Flaming-Brown puller (P-2000, Sutter, USA) and filled with IPSC or EPSC solution (**Section 2.9.1/2**). When patching onto cells the seal between the membrane and the electrode was allowed to reach a resistance of at least 1GΩ (gigaOhm) before breaking through. This allowed for a more stable baseline and consistent access resistance to be achieved. Upon breaking through, the seal test was applied for a minimum of 10 minutes to facilitate filling with the internal solution and ensure adequate space-clamp.

Cells were held at -64mV for sIPSCs/sEPSCs to be recorded and, once broken through, gain was altered from 1 to 5. A mutliclamp 700A amplifier (Axon Instruments, USA) was used for recordings, with a low-pass Bessel filter at 5KHz engaged, and a sampling rate of 10KHz. **Figure 2.5** shows the patching set up used for recording.

All drugs were prepared according to their safety and information profiles and, stored for suitable amounts of time (approximately 3-6 months depending on the drug). All drugs were bath applied and allowed to perfuse for 15 minutes (solvents and concentrations used listed in **Table 2.4**). Due to the highly lipophilic nature of the two cannabinoids that are the focus of this project, washing out of the drugs from the slices was found to be impossible. This was found to be true for each of the experimental set ups used, therefore it was decided to not perform wash steps in these experiments.

Recordings were deemed adequate for analysis if the access resistance (series resistance) did not alter by 25% of the original access resistance. The reason for this is large changes to the access resistance can cause alterations to the amplitude and kinetics of events, distorting the validity of recordings. For instance, a decrease in access resistance can lead to a decrease in the amplitude of events which, if in a drug treatment, can be misconstrued as a drug effect. Monitoring the access resistance, therefore, is critical to maintaining reliability of experimental data. This policy resulted in discarding roughly 30% of all recordings. Access resistance was measured roughly every 10 minutes of recording time and measured using the dedicated access resistance (seal test) switch on the Axoclamp amplifier (for at least 10 seconds at a time). Clampex 10.3 was again used for live recording, with MiniAnalysis, Microsoft Excel and GraphPad Prism used for data analysis (**Section 2.6**).

Drug	Stock Concentration; Solvent	Concentration Used	Supplier
17-PA	1mM; DMSO	1μM	Bio-Techne
AM251	25mM; Water	1μM	Bio-Techne
AM630	66mM; Water	50nM	Bio-Techne
CBD	60mM; DMSO	30μM	GW Pharma
CBDV	60mM; DMSO	30μM	GW Pharma
Clobazam	10mM; DMSO	1μM	Sigma
D-AP5	25mM; Water	50μM	Abcam
Flumazenil	10mM; DMSO	500nM	Abcam
Ifenprodil	20mM; Water	10μM	Bio-Techne
MK801	20mM; Water	100nM	Abcam
PEA-QX	10mM; Water	1μM	Bio-Techne
Pentobarbital	100mM; Water	40μM	Sigma
URB597	2mM; DMSO	1μM	Bio-Techne
Zolpidem	10mM; Ethanol	100nM/1μM	Bio-Techne
β-Carboline-3-carboxylic acid N-methylamide	100mM; Water	5μM	Sigma

Table 2.5 All drugs, concentrations and suppliers used in patch experiments.

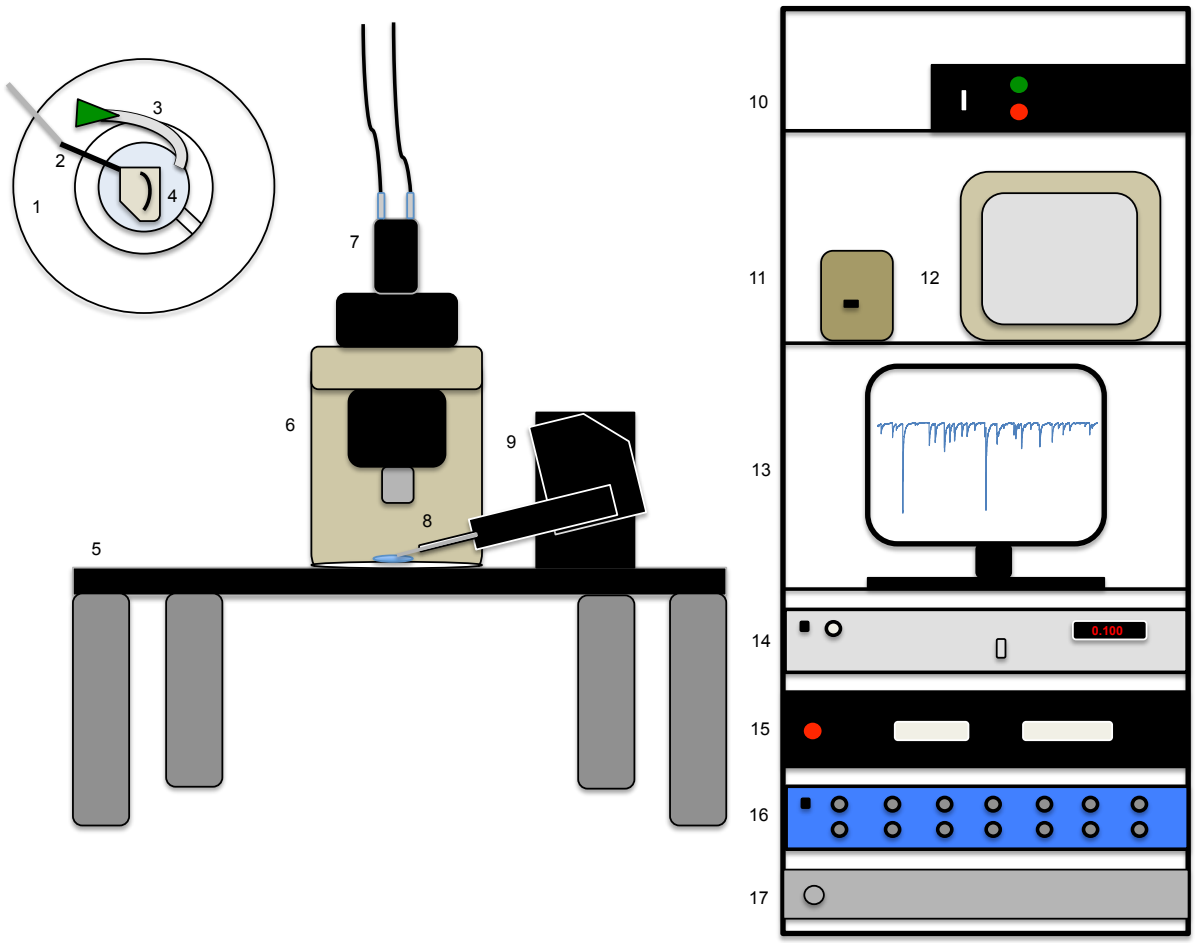

Figure 2.5 Schematic of patching rig set-up.
(1) Chamber and coverslip holder (2) Heater thermometer (3) Liquid aspirator (4) Coverslip and submerged chamber (example of slice placement (5) Patch rig table (6) Olympus microscope (7) Infrared camera (8) Electrode and electrode holder (9) Micromanipulator PatchStar (NPI, Germany) (10) Camera controller (11) Light controller for microscope (12) Television for visualisation (13) Computer running Clampex software (Axon CNS, Molecular Devices, USA) (14) Multiclamp 700A amplifier (Axon Instruments, USA) (15) Heater (16) Digidata 1440A for conversion of analogue signal to digital (Axon CNS, Molecular Devices, USA) (17) Micromanipulator control box

2.4.3.1 IPSC solution (mM)

IPSC solution recipe was as follows (mM): 90 CsCl, 33 HEPES, 5 QX-314, 0.6 EGTA, 5 $MgCl_2$, 10 TEA-Cl, 7 phosphocreatine, 4 ATP, 0.4 GTP, 1 IEM. Osmolarity 275mOsmol and pH 7.3. CsCl and TEA-Cl block potassium channels and were included to decrease the loss of current caused by propagation to the soma from the dendrites, partially unavoidable due to inherent space-clamp issues. As we were utilising a single electrode method of voltage-clamp, the more distal regions of the cell to the electrode were less influenced by its presence.

IEM 1460 was included to block AMPA and NMDA receptors internally, dispelling the need to apply dedicated blockers via the bath and thus allowing network effects to be studied.

2.4.3.2 EPSC solution (mM)

EPSC solution recipe used was as follows (mM): 100 D-Gluconate, 40 HEPES, 1 QX-314, 0.6 EGTA, 2 NaCl, 5 Mg-Gluconate, 5 TEA-Cl, 10 Phospohocreatine, 4 ATP-Na, 0.3 GTP-Na. Osmolarity 25mOsmol and pH 7.3.

2.5 Human Tissue

Human tissue samples were collected from the Birmingham Children's Hospital, one of four UK centres for epilepsy surgery services (CESS) that perform neurosurgery to resect epileptic foci in children with chronic drug resistant epilepsy. The age range for patients was 18 months to 17 years. Note the human tissue samples were not entorhinal cortex tissue, instead were from disparate brain areas and separate patients.

The removed tissue was immediately placed into bubbled choline solution (see **Section 2.5.1.1**) for transport to the lab, where samples were sliced in the choline solution and tested under identical conditions as the rodent tissue voltage-clamp recording experiments.

2.5.1.1 Choline solution (mM)

Choline solution recipe used was as follows (mM): 26 Choline Chloride, 10 $NaHO_3$, 10 D-glucose, 11.5 Ascorbic acid, 7 $MgCl_2$, 3.1 Sodium Pyruvate, 2.5 KCl, 1.25 $NaHPO_4$, 0.5 CaCl2. To increase slice viability 0.3 Uric Acid, 0.045 Indomethacin were added). Choline solution was preferred to standard saCSF to standardise HT protocols across other HT epilepsy research institutes in the UK.

2.6 Data Analysis

2.6.1 LFP Data Analysis

Clampex 10.3 was the recording software for LFP experiments, with recordings being made directly to the computer hard-drive. Offline external back ups were made upon completion of experiment. LFP oscillation data was then transferred to Spike2 7.1 for further offline analysis, including Fast-Fourier Transforms (FFT) measurements (see **Section 2.6.1.1.**) at each drug time point. Data from Spike2 7.1 was transferred to Microsoft Excel for storage. All statistical analysis for LFP experiments was performed in Prism 7.0, with either student's t-test or Friedman's test with Dunn's multiple comparisons post-hoc test used to assess statistical significance of results depending on the number of groups being analysed (*<0.05, **<0.01, ***<0.001, ****<0.0001).

2.6.1.1 FFT Algorithms

Fast-Fourier Transforms (FFTs) are a widely used method of decomposing a signal into its frequency components. The purpose of this type of analysis is to uncover information not readily observable in the time domain representation of the signal. FFTs are centred on the basis that non-periodic signals are considered integrals of non-harmonically related sinusoids. Unlike a digital signal, which is sampled in the time domain, FFTs sample in the frequency domain, producing a set of spectral coefficients, representing the underlying continuous spectral function. FFTs are so widely used throughout many areas largely due to the speed at which they can be performed.

The in-built FFT algorithm of Clampfit 10.3 was used to build FFTs to test the stability of the oscillations during the experiments. On completion of experiments and in analysis the FFT function of Spike was used, which allowed data to be copy and pasted into Prism 7.0 and pooled FFT figures to be made.

2.6.1.2 Peak Gamma

Peak Gamma was found from collating and normalising the n numbers for each weight category to form a normalised FFT. The highest value power (shown by the normalised area under the curve (nAUC) from within the gamma frequency (30-60Hz) was extracted from this. The power at the selected frequency was found for each slice recording performed and subsequently pooled together resulting in an overall peak gamma output for each age/condition.

2.6.2 Patch Data Analysis

Patch data were analysed in MiniAnalysis (Synaptosoft, USA), though were recorded in Clampex 10.3. Again, external hard-drive back-ups were made upon completion of

experiments. Experimental files were converted to ABF 1.8 Integer files in Clampfit 10.3, allowing them to be opened in MiniAnalysis.

Minianalysis allows for detection parameters to be set individually for each experiment, to define which deflections from the baseline were to be considered genuine events and to allow for variation across the population. This was done by first manually selecting a number of events and then entering their characteristics as the parameters for peak detection. The parameters available were: amplitude, threshold for peak, area, minimum and maximum periods for rise and decay times and, direction of event. In this case IPSCs and EPSCs were both being downward deflections. IPSCs/EPSCs required 200 events for each condition.

Analysis provided detailed information on: amplitude (pA; in patch), inter-event intervals (IEI; ms), rise time (ms), decay time (ms), area, baseline as well as variations upon these.

Statistical analyses were mainly performed in Prism 7.0. Again, most of these data were nonparametric, tested using D'Agostino-Pearson omnibus K2 normality test, the recommended normality test suggested by the in-built statistical analysis compatibilities present in Prism 7.0. This normality test computes both skewness and kurtosis first, which quantifies how far from Gaussian the data is in terms of shape and asymmetry. These values are then used to calculate distance to expected Gaussian values, with a single P value provided to show distance. In most cases, unless otherwise specified, mean median values for each drug treatment have been calculated for each dataset. The normality tests were then performed on the pooled mean median values for each experiment.

Due to the nonparametric nature of much of the data, paired Wilcox matched pairs signed-rank test was used for data with two experimental conditions, whereas one-way ANOVA, Friedman's test with Dunn's multiple comparisons test post-hoc was employed for data with three or more parameters. As with the normality tests, statistical analysis was performed on pooled mean median values, unless otherwise stated.

2.6.2.1 Normalised Inhibitory Charge Transfer (NICT)

Inhibitory charge transfer (ICT; ms*pA) is a method of measuring the amount of charge that has crossed the membrane, which in turn is a representation of the level of neurotransmitter that has been released. It may be calculated by measuring the area under the curve of each event (Hollrigel and Soltesz, 1997), which is proportional to the decay time (ms) of a single event multiplied by its amplitude (pA). The advantages of this method of analysis include an indication of drug effect on NT release.

Normalised inhibitory charge transfer (NICT), used here, was formulated from summing the area parameter values, a multiplication of amplitude (pA) and decay time (ms) for each set of 200 events. This calculation provided the raw overall value of inhibitory charge passing across the membrane for the duration of 200 events. This number was then divided by the time taken to reach 200 events (final event time (ms) minus initial event time (ms) and multiplied by 1000, to provide a value of cumulative charge transfer per second (coulombs per s or, NICT).

2.6.2.2 Principal Component Analysis (PCA)

Principal component analysis (PCA) was performed to assess which parameters of IPSC kinetics were the source of the largest variance and therefore, most affected by the application of CBD. We postulated that once we had been determined we could theorise hypotheses for the mechanism of action of CBD and select appropriate drugs to target possible interaction/binding partners of CBD.

PCA measurements possess certain advantages over normal x-y data, as principal components allow elucidation of the factors causing the largest amount of variance within the results. Principal components can be described as the data's underlying structure and the means of variation across the data, for instance, in this report decay time is a principal component. Every dataset is able to be deconstructed into a set of eigenvalues and eigenvectors, with the two existing as pairs, every eigenvector corresponds to an eigenvalue.

Eigenvectors are directional, indicating an axis of some description and its direction (horizontal, vertical, or angled), while eigenvalues are a number value that correspond to the variation produced in the dataset for that eigenvector. The eigenvector with the largest eigenvalue becomes the first principal component, as it represents the largest amount of variance, the second largest becomes the second principal component, and so on. Eigenvalues, therefore, indicate the spread of the data and the parameter responsible for the largest variation between the values. For data to be eligible for use in PCA, it must first be transformed orthogonally, ensuring the principal components are perpendicular, allowing the axes to represent the spread of data and the variation across it effectively. The number of eigenvectors & eigenvalues determines the number of dimensions the dataset possesses. Here, 5 variables have been utilised (amplitude (pA), interevent interval (IEI; ms), rise time (ms), decay time (ms) and, area (amplitude * decay time)) meaning our PCA is a 5-D dataset, with 5 pairs of eigenvectors and eigenvalues.

All PCA calculations were performed in R, with the RCommander and ggbiplot2 repositories installed. The visual output of the PCA calculations was as concentric rings, each representing a different drug condition, with the size and position of the ring alongside the arrow size and

direction indicating the largest source of variance within the dataset. A sample of the exact code used for the PCA computation is included in **Appendix 1**.

Chapter 3

Further verification of the RISE model

3.1 Introduction

3.1.1 RISE as an effective model of TLE

In this study, the RISE model of TLE was utilised, described by this lab in Modebadze et al, (2016). The RISE model features low mortality and high morbidity, with mortality reduced to ~1%, while high epileptogenicity and spontaneous recurrent seizure development (SRS) are retained. The RISE model promotes lower levels of global neuronal damage, in particular in terms of neuronal network function in the CA3 region of the hippocampus. At 1%, RISE shows much lower mortality in comparison to previous models (~10-50% in the low-dose lithium-pilocarpine models (Glien et al., 2001; Curia et al., 2008) and ~50-80% in high dose pilocarpine models (Moser et al., 1988).

Due to the lower levels of brain damage presented, the RISE model allows for the detection of subtle changes occurring during epileptogenesis. The low mortality rate of this model is also in line with the 3R principles of animal use in scientific procedures.

Figure 3.1 Average PSBB scores for AMC (n = 12) and SE (n = 36) rats.
Taken from (Pennifold, 2016).

Validation of SRS in the RISE model has been performed using a modified Post-Seizure Behavioural Battery test (PSBB – described in the Materials and Methods chapter (**Chapter 2, Section 2.3**). Analysis of this work is presented in **Figure 3.1,** showing an average of 20.3 ± 0.86 weeks for SRS to develop. SRS is defined as scores remaining over 10, when multiplied together, over 4 sessions.

Comparisons between network and cellular changes between the RISE afflicted and AMC rats have been observed as a by-product of other work performed in this thesis. Here they are presented as they demonstrate further validation of the RISE model as an alternative to the most commonly used epilepsy models.

3.2 Results

To verify the effectiveness of our RISE epilepsy model, baseline (400nM KA only) responses have been compared between the AMC and SE rats. These comparisons have been performed in various experimental scenarios including: LFP, where all ages have been compared, and in voltage-clamp recordings of both IPSCs and EPSCs (p18-26).

3.2.1 LFP data

Commencing with the LFP data (**Figure 3.2**), we have compared all ages of rats used later in this body of work to determine the differences between the AMC and SE rats in LFP responses in baseline conditions. We have utilised 3 analysis parameters to observe differences between the two disease conditions, which are, peak frequency, peak power and, peak gamma measurements, the procurement of which has been described previously (**Chapter 2**).

Peak frequency was found by taking the frequency with the highest power at baseline conditions from a normalised FFT, while peak power took the power from this frequency. Peak gamma took the highest power from only the gamma range (30-60Hz) from the normalised FFT (explained further in **Chapter 4**) .

The n numbers used for this section are as follows for the AMC population: 24-hours: n =13, animal n = 4; 1-week: n = 13, animal n = 7; 3-month: n = 15, animal n = 7. For the SE population the n numbers were: 24-hours: n = 13, animal n = 4; 1-week: n = 17, animal n = 8; 3-months: n = 16, animal n = 6.

Comparing the 24-hour age groups (P18-19) a highly significant difference between the two peak frequencies was visible (**Figure 3.2.Aii**), with the AMC population possessing a peak frequency of ~42Hz, while the SE population had a peak value of ~36Hz. The box and whisker plot show the minimum to maximum values with the bars, with 95% confidence limits making up the box. The line across represents the mean value. No significance was observed in either the peak power or peak gamma measures (**Aiii** – **Aiv**).

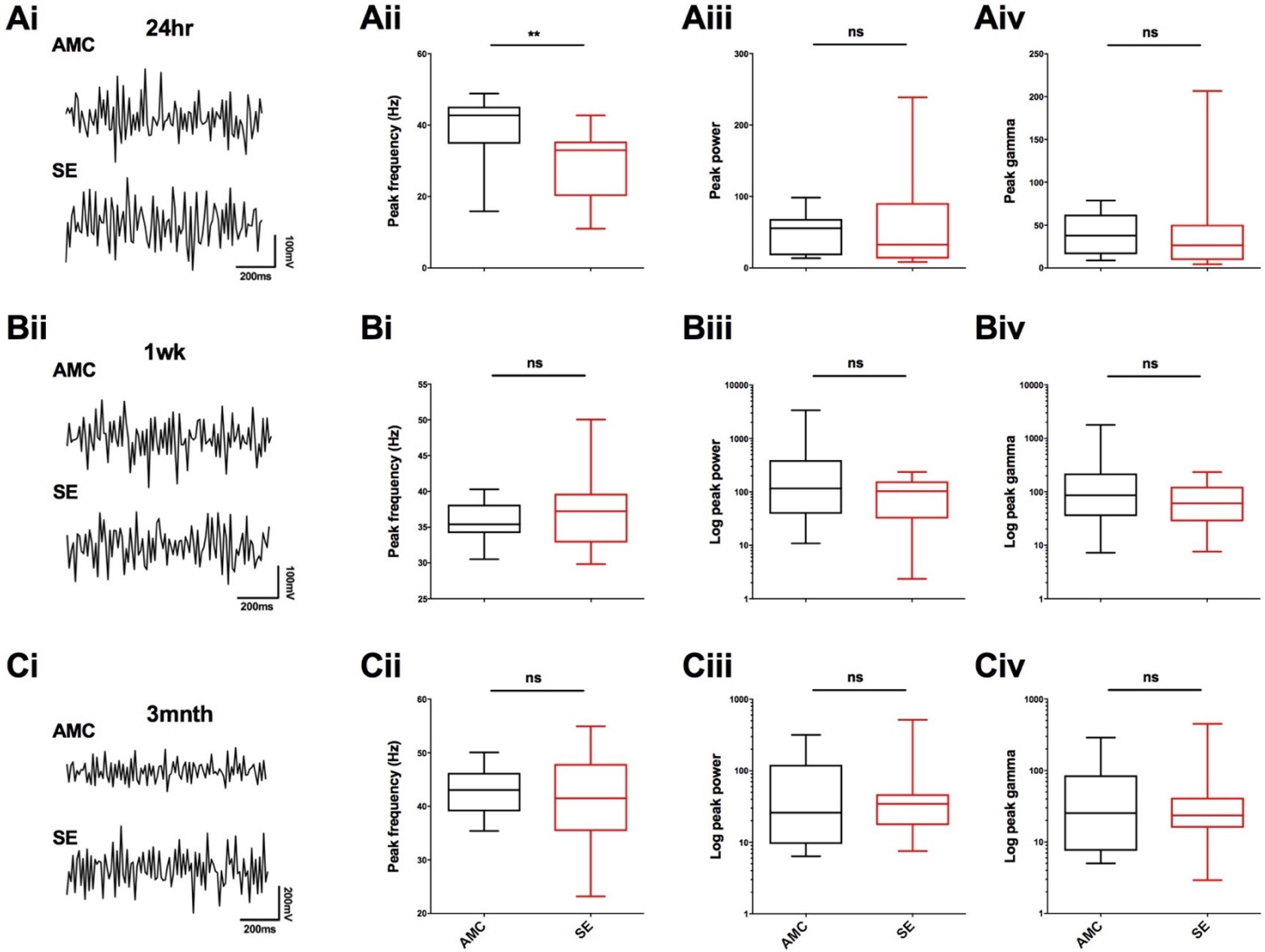

Figure 3.2 Comparison between baseline AMC and SE LFP data.
Raw LFP data from each age and disease state, indicated by age range and, AMC or SE tags, with scale bars (A-Ci). Box and whisker plots (black AMC; red SE) from left to right: peak frequency analysis (Hz; A-Cii), peak power analysis (A-Ciii) and peak gamma responses (A-Civ). ** $p < 0.01$.

The 1-week post-induction populations (P26; **Bi-Biv**), showed no significant differences across any of the measures. Interestingly the mean peak frequency of the AMC population decreased to ~35.5Hz, very similar to that of the SE population. The SE peak frequency did not shift greatly from what was observed in the 24-hour post-induction animals previously. The peak power and peak gamma figures both showed an obvious outlier as the maximum value, though despite this there was no significance between the values of the two populations in either measure.

The chronic or 3-month time point, represented in the final row (**Ci-Civ**), again showed no significant differences in any measure. Both population peak frequencies increased to a similar value (~41Hz). The peak power values showed little differences in the mean value or 95% confidence limits, though the SE population did have a large maximum value. This was repeated in the peak gamma where no significant differences were observed, though differences were present in the size of the respective box and whiskers, with the SE population having a smaller box but a larger range, suggestive of high clustering in the majority of the responses but with several outliers.

3.2.2 Whole-cell voltage-clamp data

Alongside the LFP results previously discussed, whole-cell voltage-clamp experiments were also performed on both control and SE tissue (P18-26). Spontaneous inhibitory post-synaptic currents (sIPSCs) and spontaneous excitatory post-synaptic currents (sEPSCs) were recorded. The results are graphed in Figure **3.2.Ai-Biv**, with **A** showing sIPSCs and **B** showing sEPSCs.

In sIPSC conditions, AMC: n = 12, animal n = 9; SE: n = 26, animal n = 19. In sEPSC conditions, AMC: n = 5, animal n = 4; SE: n = 6, animal n = 5.

Aii showed the mean median inter-event intervals, which relates to the frequency of currents by showing the time between each event in milliseconds (ms). As can be observed, no significant difference was present between the two populations, though differences in the size and shape of the box and whisker plots were observed, with a trending decrease noted (AMC: 86.8ms; SE: 67.5ms; p = 0.07). **Aiii** highlights the mean median amplitude of each event, again no significance was observed between the two populations, though differences were observed in the size/shape of the box and whisker plots again, with the AMC data showing a slightly lower mean median value but a larger range than the SE data (AMC: 21.1pA; SE: 23.22pA; p=0.29). **Aiv** represents a measure of inhibitory charge transfer (ICT), which was produced from the sum area of 200 events divided by the time taken to achieve 200 events (final event time minus initial event time). This number was then multiplied by 1000 to give a charge transfer per second value (femtocoulombs (fC)). Again, no significant difference between the

two populations were noted (AMC: 2202fC; SE: 3016fC; p = 0.20), though the size and shapes of the box plots themselves were somewhat different, with the SE ICT displaying a smaller range but larger box than that of the AMC.

The sEPSC data follows the same order as that of the sIPSC data just discussed. Again, in the mean median IEI (**Bii**) no significant differences were noted (AMC: 296ms; SE: 136ms; p = 0.09). Moving onto the amplitude results (**Biii**), significant differences were observed ($p < 0.01$), with the SE population presenting both a larger mean median value (SE: 23pA; AMC: 9pA), larger box plot as well as a larger range in responses. **Biv** shows excitatory charge transfer, which is found using the same formula used for ICT. Once more, significance was observed between the two populations here (AMC: 151fC; SE: 561fC; $p < 0.01$), with the SE population showing a larger mean median value, box plot and range than that of the AMC population.

Kolmogorov-Smirnov tests were performed on pooled data for both IPSC and EPSC parameters (IEIs and amplitudes; **Figure 3.4**) to observe if the distributions show any significant changes. The cumulative frequencies have been shown as a percentage and, here, significant differences were noted in both the EPSCs, as the mean median analysis of **Figure 6.3** showed, but also in the IPSC analysis, with every KS test showing a p value of $p < 0.0001$ (****). The KS-D, the vertical deviation between the two curves, was different for each however, with **Ai** showing a value of 0.12, **Aii** = 0.14, **Aiii** = 0.19 and, **Aiv** = 0.64. Indeed, here the EPSC data still showed the largest effect, especially with regards to amplitude, suggesting more profound changes occurring to the excitatory mechanisms in the SE animals.

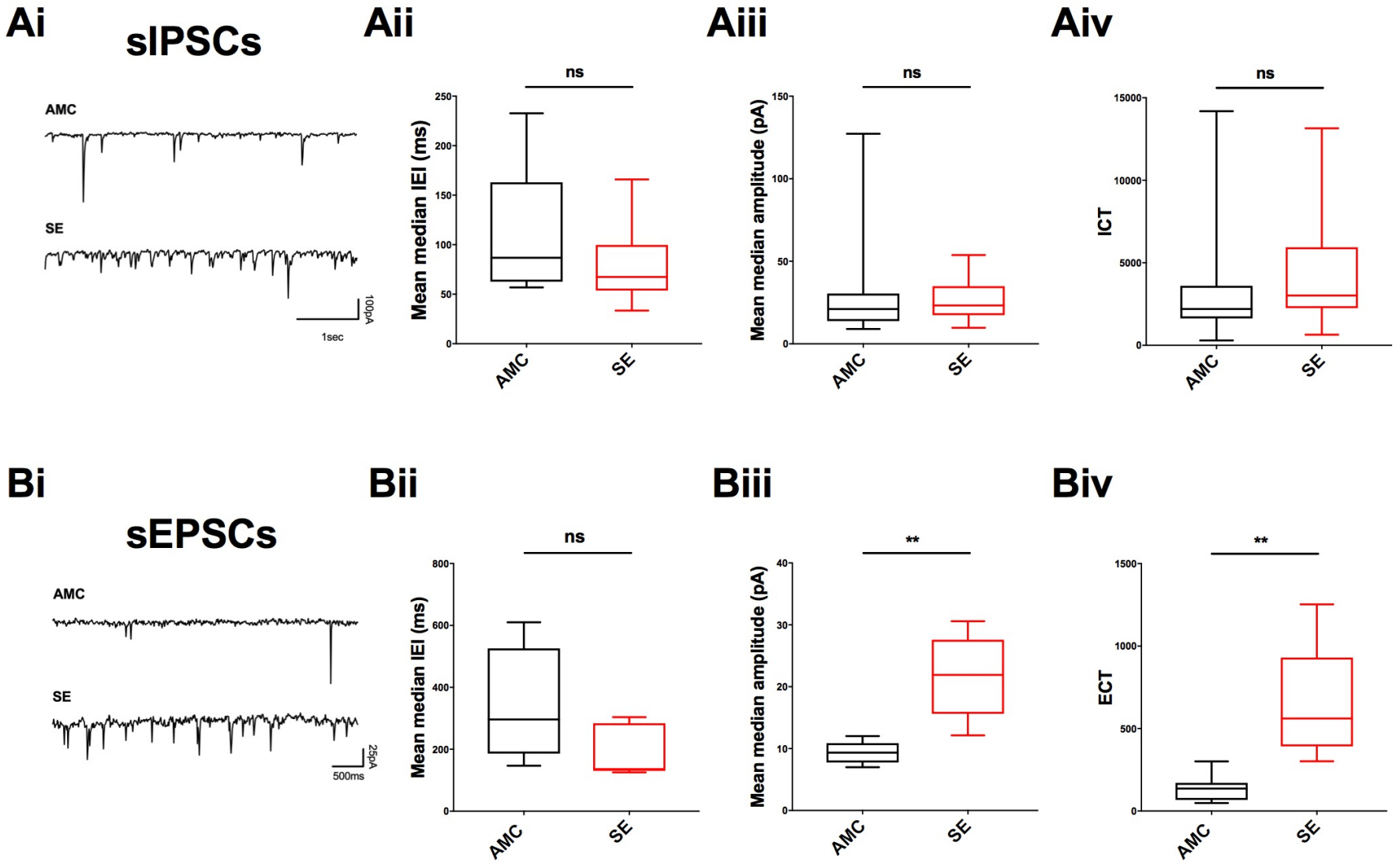

Figure 3.3 Comparison between baseline AMC and SE sIPSC/sEPSC data.
Raw data taken from sIPSC (Ai) and sEPSCs (Aii) in both AMC and SE rats (labelled). Box and whisker plots detailing any differences between AMC (black) or SE (red) rats in: mean median IEI (Aii), mean mean amplitudes (Aiii) and inhibitory/excitatory charge transfer (I/ECT; Aiv). ** $p < 0.01$.

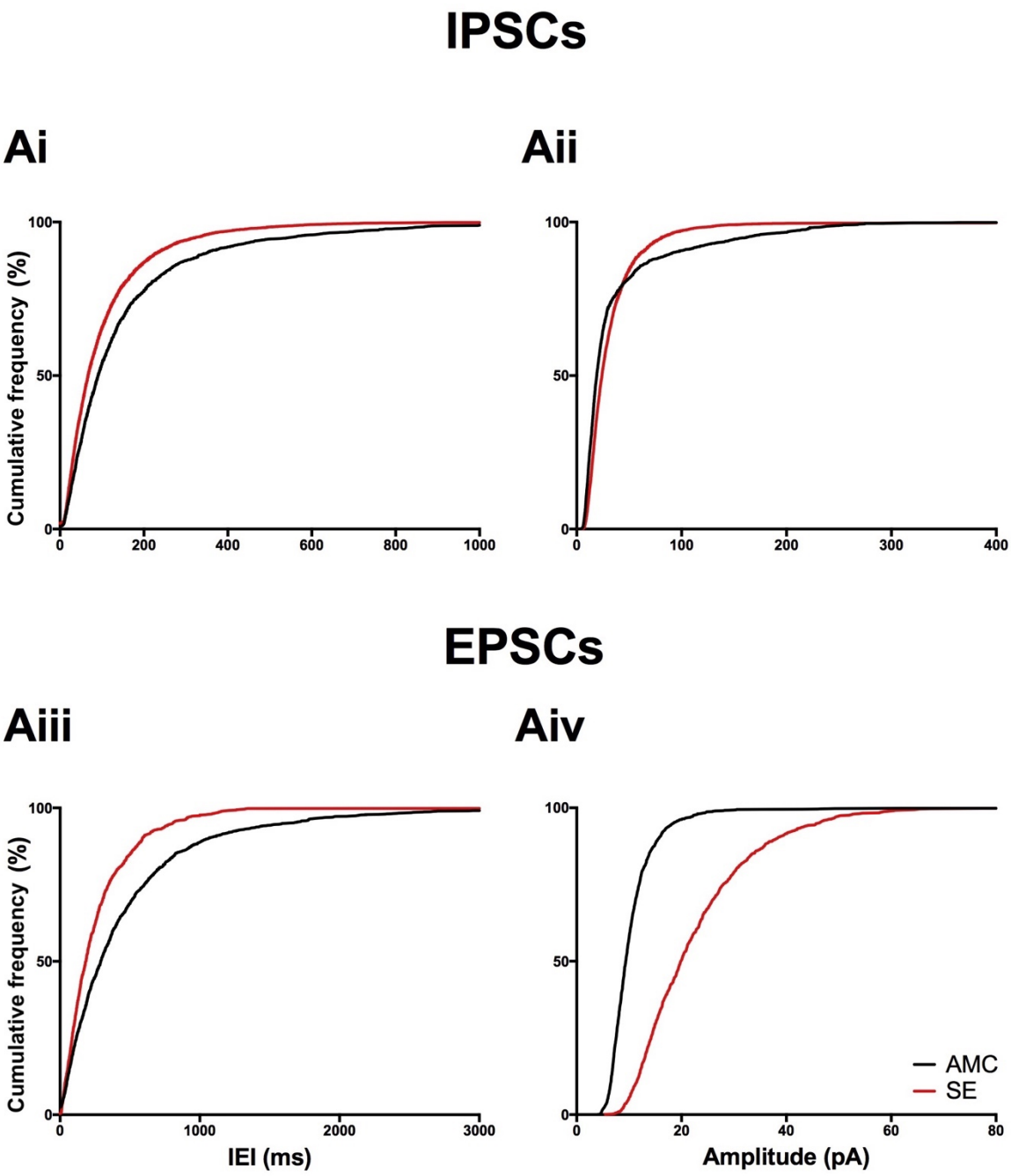

Figure 3.4 Cumulative frequency of IPSC and EPSC parameters
Cumulative frequency for pooled IPSCs (Ai-ii) & EPSCs (Aiii-iv) events including both IEIs (Ai & Aiii) and amplitudes (Aii & iv). All events collected were pooled together for AMC (black line) and SE (red line) conditions for each analysis.

3.3 Discussion

3.3.1 Differences in frequency apparent at early time points are lost with development

The data presented in **Figure 3.2.Aii** shows a significant difference between the two juvenile rat populations, with the AMC population showing a higher peak frequency value than the SE population. This is highly suggestive of a change to neuronal firing and synchronicity in Layer II mEC neurons early post-SE induction. This is indicative of RISE-induced changes to neuronal receptor composition in the mEC, suggested by the collaborative protein expression studies and also by various previous studies (Chapman, 1998; Meldrum and Rogawski, 2007). Another possibility is due to damage caused through the induction process itself, though this may not be plausible due to the lack of change to both peak power and peak gamma measures, which are suggestive of normal neuronal function. Significant changes between the two populations are lost with development, though differences/trends can be observed with the size and shape of the box + whisker plots, suggestive of possible slight changes, though obviously due to the lack of significance no conclusions can be drawn about this. This recovery in peak frequency with maturation of the SE rat population highlights the plasticity and recoverability of neuronal networks, being able to endure a traumatic event (i.e. *status epilepticus*) and recover with time.

Interestingly, the peak frequency data shows a slowing in adolescence of the AMC population from 43Hz in the juvenile rats to 35Hz in adolescence, a pattern not observed in the SE population. This may suggest that the AMC animals are undergoing neuronal rewiring associated with adolescence, which is blunted in the SE animals, which have most likely undergone neuronal rewiring in response to the RISE induction process. No significant changes were observed at any of the age range when peak power and gamma were analysed.

3.3.2 No significant effects on inhibition

As can be observed in **Figure 3.3.Ai-iv** no significant effects were observed between AMC and SE populations when investing sIPSCs from Layer II mEC pyramidal cells from p18-26 rats. Non-significant differences are visible between the size and shapes of the box and whisker plots across the parameters. In **Aii**, the SE data shows a tighter clustering and lower mean median value and range compared to the AMC data, with a trending decrease noted here. This is contrasted in the mean median amplitude data presented in **Figure 3.3.Aiii**, where the SE population displays a higher mean median value than the AMC data, though as previously the AMC population possesses the higher range. The final comparison between the two populations is the ICT measure (**Aiv**), where both populations have visually similar size/shapes, though again the AMC data has a slightly higher range, while the SE data shows

a higher ICT value and a larger box plot. The lack of significance in each of these analyses suggests that the overall inhibition of Layer II mEC cells is relatively unperturbed by the SE protocol.

Significant changes in the distribution of the responses are noted in **Figure 3.4**, with changes in both IEI and amplitudes noted, with a highly significant p value, suggesting alterations are present in the distribution of event values, though these do not present themselves in the mean median comparisons of **Figure 3.3**.

3.3.3 Significant alterations observed on excitation

Data presented in **Figure 3.3.Bi-iv** shows the analysis of sEPSCs performed in the same area as the sIPSCs just discussed. **Bii** displays the two populations mean median IEIs, which show no significant changes, though a visible change is seen in the box and whisker plots – with the SE population demonstrating a tighter clustering and smaller range and mean median value than the AMC population. As this data is non-significant, no definitive conclusions can be borne out of it. This is in contrast to the adjacent figure (**Biii**), which displays mean median amplitude values, and possesses a significant difference between the two groups, with the SE population demonstrating a significantly higher amplitude value than the AMC population. These changes are further cemented when looking at the data presented in **Figure 3.3.Biv** which shows excitatory charge transfer (ECT), where once more the SE population displays a significantly higher value when compared to the AMC. Furthermore, **Figure 3.4** displays the KS tests results for sEPSCs, showing highly significant differences between the AMC and SE populations, with profound changes noted in the amplitude distributions especially. Both parameters display large amounts of significance, backing the mean median findings of **Figure 3.3**. These results strongly suggest that fundamental changes occur to excitatory transmission in the RISE model.

It is difficult to state whether one test takes precedent over another when comparing the mean median analysis and changes to distributions. KS tests are prone to giving overly positive results due to taking each event as a separate n number, while it is probable that the mean median analyses have less of a connection physiologically to network function than analyses of amplitudes and IEIs distribution. Here, however, the EPSC results obtained show both the variance box plots and cumulative probability are significantly altered in the RISE model, while the IPSC parameters show significant differences only in distributions. This is highly suggestive that excitation is the key element of change in the RISE model, with significance achieved in both analysis methods. Of course, no single test is a better description than another and so here we have tried to provide a holistic overview of all changes for comparison.

When allied with the protein expression work discussed in the previous chapters (**Chapter 4**), rises in the expression of the NMDAR subunit GluN1 are noted in the TLE in the immediate 24-hours following RISE induction, which is the same time point these rats are taken from (**Appendix 2**). It may be this apparent rise in NMDAR expression that is responsible for the increased excitation noted here. A significantly increased GluN1 subunit expression suggests a greater number of NMDARs present at both the pre- and postsynaptic membranes, and as such, a greater density of NMDARs is suggestive of an increased response to glutamatergic transmission.

3.4 General discussion and future experiments

Epilepsy is widely regarded as a neurological disease caused by an imbalance in excitation-inhibition balance, with excitation dominating inhibition. The data presented in this chapter suggest that the RISE induction protocol is successfully able to mimic this imbalance, supporting RISE as a valid model of TLE. Here, little or no difference between AMC and SE baselines in sIPSC or LFP experiments have been demonstrated, suggestive of no changes to inhibitory balance upon initial insult, whereas sEPSC experiments have noted significant differences in both the mean median amplitudes and excitatory charge transfer (ECT; femtocoulombs (fC)). Further electrophysiological experiments would most likely concentrate on increasing the n number of sEPSCs recordings, to increase statistical significance and further validate the findings.

When combined with the preliminary protein expression work (**Appendix 2**), increases to the NMDAR subunit GluN1 are noted early after SE induction, which could explain the increased excitatory charge crossing the postsynaptic membrane. Further experiments here could include, recording miniature postsynaptic currents to investigate if this effect noted in the SE population is action potential independent and, therefore, whether it is presynaptic in nature. Further to this, a broader range, and higher n number, of proteins could be screened for including, GluN2, mutations of which have been strongly implicated in seizure generation and epilepsy (Bledsoe et al., 2017), CB1Rs, mGluRs and GABA receptors, each of which is noted for their ability to establish or maintain seizure events.

Chapter 4

Dose-response of CBD and CBDV on mEC Layer II using LFP recordings in SE and AMC rats.

4.1 Introduction

Neural network oscillations have been observed in humans in vivo since 1929, expanded with the invention of the electroencephalogram (EEG) by Hans Berger in 1939 (Berger, 1929; Tudor et al., 2005). This work was expanded to allow investigation of neuronal activity in vitro, while the development of brain slicing techniques over time has enabled living tissue to be well preserved, allowing oscillations to be recorded from *in vitro* preparation to be taken using LFP (Aghajanian and Rasmussen, 1989). Tetanic electrical stimulation experiments produced the first *in vitro* oscillations observed in 1995 (Whittington et al., 1995, 1997, Traub et al., 1996, 1999). This discovery allowed a new field of investigation to be opened; *in vitro* rhythmogenesis and its mechanistic study.

Persistent oscillations are inducible via various agents in i*n vitro* slices by: mGluR agonists (Whittington et al., 1995), kainate receptor agonists (Cunningham et al., 2003; Fisahn et al., 2004), cholinergic agonists (Fisahn et al., 1998) and by tetanic electrical stimulation. Persistent oscillations have been induced in many major regions of the brain such as, the CA1 and CA3 regions of the hippocampus and the entorhinal and motor cortices (Fisahn et al., 1998; Gillies et al., 2002; Cunningham et al., 2003; Yamawaki et al., 2008).

The study of neural oscillations provides a good source of information about how neuronal networks perform their natural function. As such, neural oscillations have been chosen to observe the effects of CBD(V) at a network level. Our interest in epilepsy, specifically temporal lobe epilepsy, lead us to investigate the mEC, an important area for both oscillations and epilepsy, with epilepsy being a disease of pathological network oscillation.

The work in this chapter has been collected using LFP recordings in layer II of the mEC of AMC and SE rats. The aim of this work was to investigate the effect of CBD and CBDV on pharmacologically induced gamma oscillations, as a prelude to similar investigations of the pathological oscillations seen in epilepsy, and to find the most effective working concentration for subsequent investigations. Hence, dose-response investigations were performed, with increasing phytocannabinoid dose over the course of the experiments, using a half-log unit cumulative regime: 0.3μM, 1μM, 3μM, 10μM, 30μM. Each dose was bath applied for a 30-minute period and, was added upon stabilisation of network oscillations. Oscillation stabilisation was judged by performing FFTs every ten minutes, with a less than 10% overall change in the power of the gamma oscillations adjudged to confirm stable oscillations. KA was added at least an hour before addition of first cannabinoid doses, dependent on the presence of stable gamma oscillations. 1-minute epochs of data were used for analysis of gamma using FFTs.

Exclusion criteria was commonly related to unstable gamma oscillations, observed using FFTs, with usually one or two slices out of four displayed a lack of stability, as such the results from those slices were excluded. Other datasets were excluded if large outliers were observed in more than one dose (e.g. a four-fold increase in power at 0.3μM with another large increase in 1μM, while little change was noted in the other slices – though again this was usually related to oscillatory instability).

As no experimental work had been done on our model of epilepsy and cannabinoids, we used animals from different time points along the epileptogenesis pathway, those being – 24-hours post induction (p19-20), 1-week post induction (p26-27), and chronically epileptic (usually around 3-months post induction – confirmed with PSBB (**Section 2.3**)) – with age-matched controls (AMCs) taken from comparable time points. This selection allowed us to cover a multidimensional space of epilepsy progression and the effectiveness of CBD(V) at these points in comparison to AMC responses.

Specific protocols, materials and analysis techniques utilised are detailed in **Chapter 2**.

4.2 Results

4.2.1 Effects of CBD on pharmacologically induced persistent gamma on 24-hour (~P19) AMC and SE rats

As stated, we used rats from the 24-hour post induction time point (24hr SE), and similarly-aged control rats (AMC) to test CBD effect on epileptic and physiological neural oscillations. A total of 2 animals were used for each of the AMC and SE experiments, both with an n of 6 overall, with each n referring to the results of a single slice.

4.2.1.1 FFTs and split frequency histogram analysis

Our data analysis efforts first concentrated on the effects of CBD on three broadly-defined oscillatory ranges (0-29Hz, 30-60Hz and >60Hz), as we hypothesised that CBD might cause a reduction in gamma power (30-60Hz), perhaps with the power shifting from gamma down to slower bands such as beta or alpha.

FFT were produced for individual slice responses, examples of which can be observed in **Figure 4.1.Aii-Bii**, which show the maximal effect of 30μM CBD against the cannabinoid free KA induced gamma oscillations. Here no real effects were observed in the AMC slice response (**Aii**), while the SE showed a shift leftward, indicating a decrease in gamma frequency, as well as a decrease in power (**Bii**). To gauge the FFT responses from each population, each slice response in that population was pooled, normalised and compiled into average FFTs.

A similar FFT to that presented in **Aii-Bii**, is shown in **Aiii-Biii**, though this highlights the effect of the maximal CBD addition on pooled population gamma oscillations of both AMC and SE rats, with the SEMs depicted as the slightly transparent fill area on either side of the respective lines**.** These FFTs continued to show little to no effect on either the size or shape of the FFT line at the maximal CBD dose in the AMC animals (**Aiii**), similar to the individual slice response observed in **Aii**. In contrast, the SE population (**Biii**) showed an active effect of CBD, with the power and frequency of the FFT peak decreasing substantially at the maximal CBD dose, showing an average effect comparable to that observed in the single slice (**Bii**). The full drug dose addition responses and their effects on the FFT are shown in **Aiv-Biv** for the AMC and SE populations respectively, with each dose representing a different coloured line (clarified in the legend). Due to the large number of doses performed clear trends on the shape and sizes of the FFTs are hard to observe, however clear decreases can be observed upon subsequent doses in the SE animals (**Biv**), while little change is noted in the AMC population (**Aiv**).

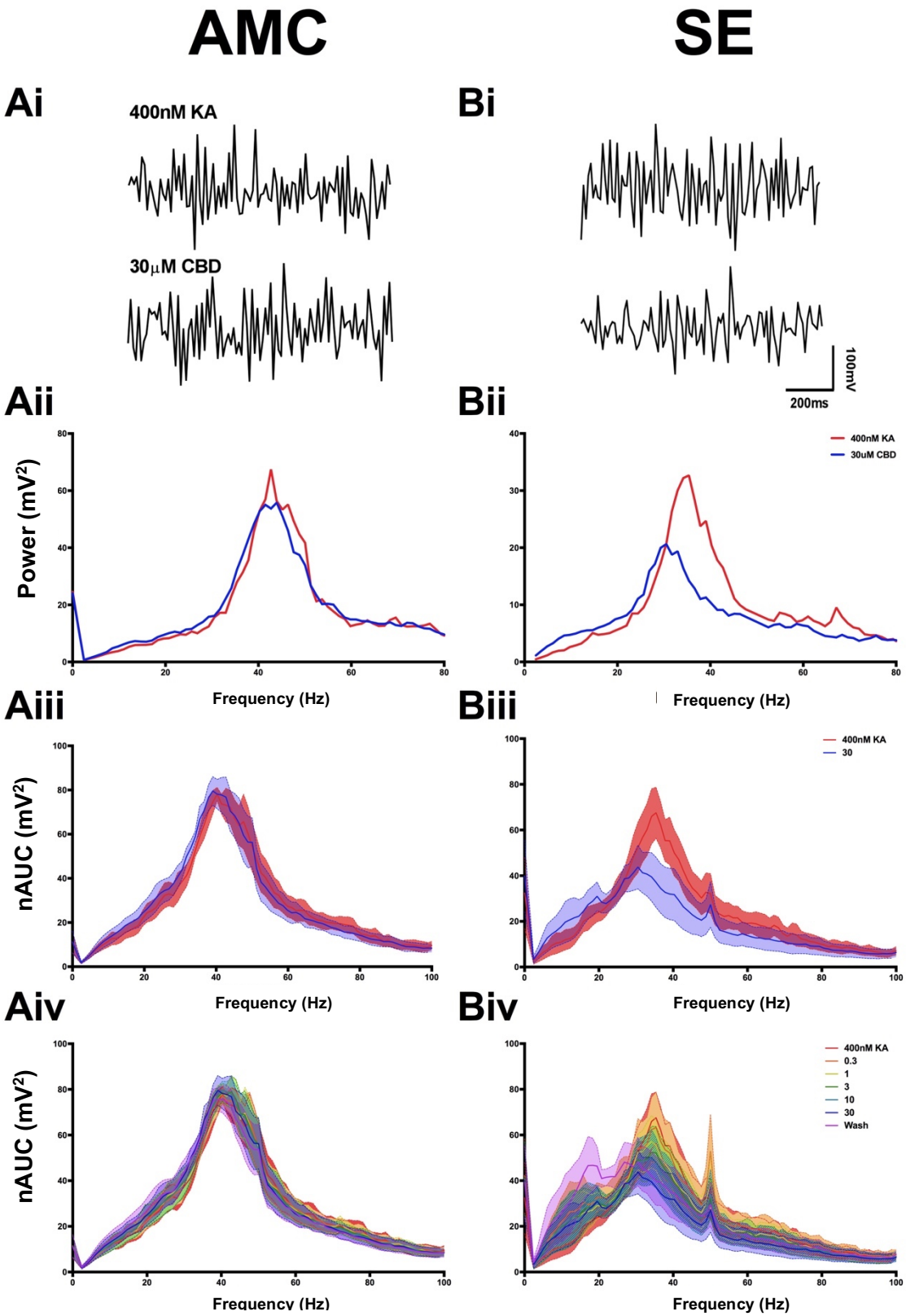

Figure 4.1 Raw traces and FFTs for CBD 24-hour post-induction.
Ai-Bi Representative raw traces of pharmacologically induced gamma oscillations in both AMC (left) and SE (right) rats at 400nM KA and the maximal 30μM CBD. Aii-Bii A single slice response to the maximal 30μM CBD addition, for both the AMC (left) and SE (right) rats. Aiii-Biii Normalised FFT displaying the normalised area under the curve (nAUC) for both the 400nM KA and maximal 30μM CBD for the AMC (left) and SE right) data set, SEM is represented by the coloured fill area flanking the line. Aiv-Biv Normalised FFT data for all CBD doses applied in AMC (left) and SE (right). Coloured lines and fill refer to: red (400nM KA), orange (0.3μM CBD), yellow (1μM), dark green (3μM), light green (10μM), blue (30μM), purple (wash).

To clarify if these effects were significant, FFT data for the area under the curve in each of the defined frequency bands (0-29Hz, 30-60Hz, 60+Hz; the spectral power for that band) was calculated and pooled to produce a split frequency histogram (**Figure 4.2**). The control portion translates to the cannabinoid free (baseline) 400nM KA only segment of the experiments – this control section was then normalised to 100 across ranges. The specified CBD concentrations were then added, and differences calculated. Where mean values have been shown, the standard error has also been shown (with ± used for this).

As can be seen in **Figure 4.2.Ai**, there were no real differences observed across any of the frequency bands at low doses of CBD in the AMC animals. Significant, though slight, increases were observable in the low frequencies at both 30μM CBD ($p < 0.01$) and in the wash step ($p < 0.0001$), though the 30-60Hz and 60+Hz frequencies remained unaffected. The mean of the low frequencies (0-29Hz) at 30μM CBD was 112.13 ± 3.60 (range: 100.5-124.5), and 116.57 ± 3.12 (101.7-123.6) in the wash.

In the 24hr SE rats (**Figure 4.2.Aii**), no significant evidence of gamma suppression was noted as dose of CBD increases. At the maximal 30μM dose, no significance was observed, despite the decrease previously observed in the normalised FFT. The only significance observed in this analysis method was an increase in the final wash step (when compared to 400nM KA) to the slow frequencies (0-29Hz), with a mean of 158.24 ± 24.01 (106.28-256.11). The mean value of both the gamma and fast frequencies (60+Hz) slightly decreased from the 30μM doses in the wash, at 68.87 ± 2.60 (24.32-91.01) and 133.51 ± 37.12 (60.11-288.45) respectively, though neither is significant.

This analysis method seemed to be at odds with the seemingly obvious effect noted in the raw SE FFTs presented previously, where a clear shift leftward and down was noted at high CBD doses. The lack of similarity between what was observed in the FFTs and what was found in the split frequency histograms suggests this particular analysis method was not providing an accurate representation of CBD effect. As such, different analysis methods were utilised to try and represent the data, including both peak frequency and peak power comparisons, the results of which are detailed in the next section.

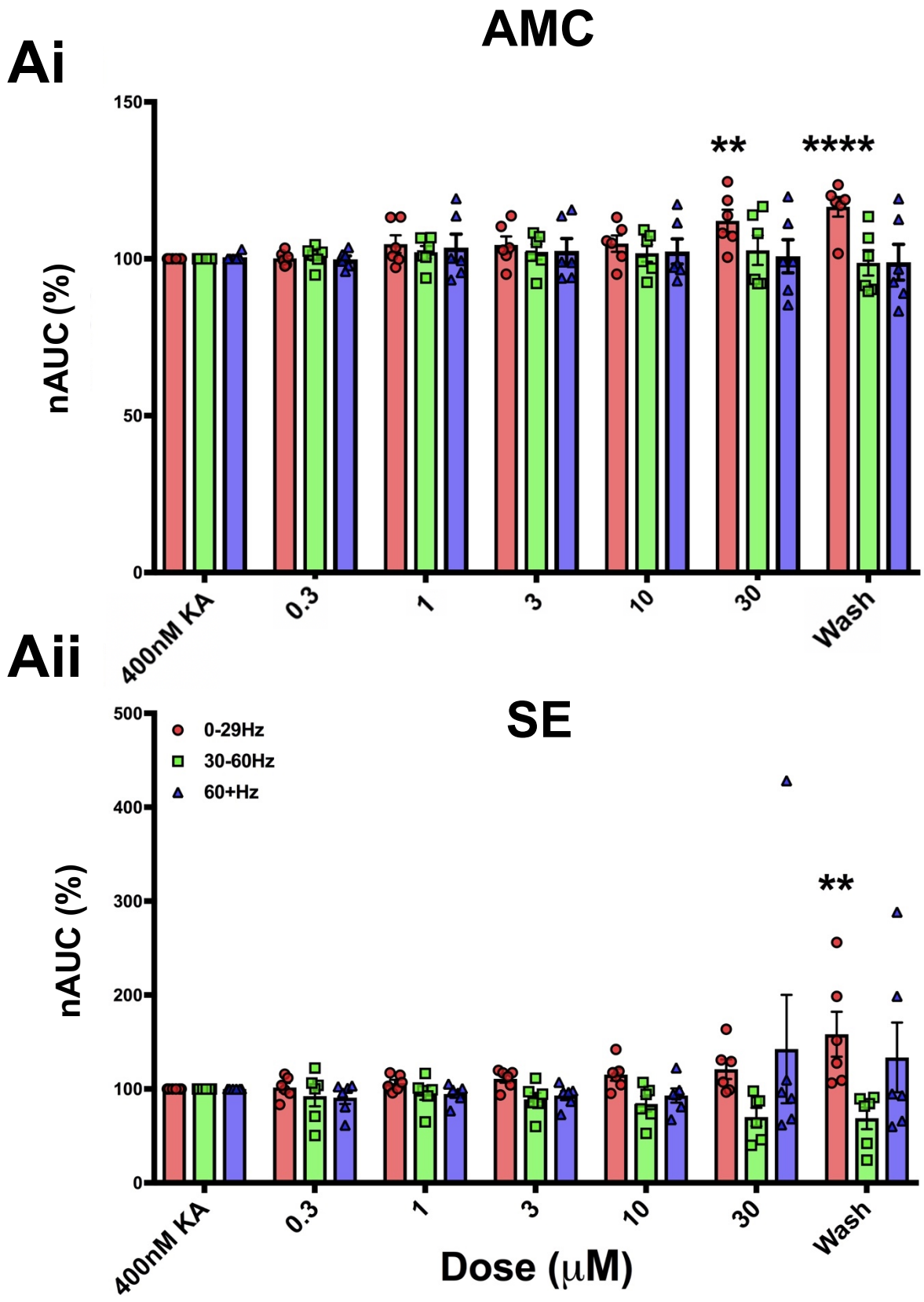

Figure 4.2 Split frequency histograms for CBD 24-hour post-induction.
Ai showing the band specific nAUC response to increasing doses of CBD plus wash in the AMC condition, with population responses included. Data was normalised, with the 400nM KA response set to 100%. Aii Same histogram data shown for the SE dataset, with population responses included. Legend: low frequency (0-29Hz) - red bars; gamma (30-60Hz) - green bars; high frequency (60-1000Hz) - blue bars. Black capped bars show standard error. ** $p < 0.01$, **** $p < 0.0001$.

4.2.1.2 Peak frequency and power comparisons

As the analysis did not seem to represent the data well in the previous analytical method, we investigated the effect of CBD on peak frequencies for each experiment within the population. We hypothesised from the initial normalised FFT figures (**Figure 4.1**) that we would see a decrease in the frequency in the SE rats – as there is a leftward trend that is seemingly dose dependent – and no effect in the AMC population.

For peak frequency analysis we took the frequency displaying the highest power (largest AUC in our datasets) at each drug dose condition for each n within the two populations. These data were then entered into GraphPad Prism 7 and averaged at each drug condition. The resulting data from both disease conditions were plotted onto a mean line graph with the individual responses, to display the differences between both the conditions and the drug dose, shown in **Figure 4.3**.

As shown, there was quite a large disparity between the two peak frequencies of the AMC and SE rats, with AMC having an initial peak frequency of 43.74Hz ± 1.62 and SE of 34.59Hz ± 1.66. Statistical analyses (Mann-Whitney test) were performed on this difference and returned a significant p value ($p < 0.0043$). No discernible effect of CBD on AMC peak frequency at any dose was observed, with a low variability present (depicted by population responses). The SE animals displayed a significance decrease only in the maximal 30μM CBD dose, with a final frequency of 29.09Hz ± 2.30 ($p < 0.05$). The wash step produced a frequency of 24.41Hz ± 2.82 ($p < 0.01$). This analysis method seemingly fits with what was observed previously in the FFT data regarding the frequency decrease noted with higher applications of CBD.

As we had investigated the peak frequency of both sets of data, we also decided to look at the peak power of each of the conditions. This was performed in a way similar to peak frequency measurements, though instead of taking the frequency value the power was instead taken. Peak power calculations were performed with highest AUC value being taken, regardless of the frequency, for each cannabinoid dose, for every slice. The results were then normalised to their initial 400nM KA (baseline) peak in each slice (set to a value of 100). Once a full set was achieved the data was averaged to produce an overall, normalised mean value for each condition, complete with population responses. Both conditions were then charted on a combined line graph for comparison (**Figure 4.3.Aii**).

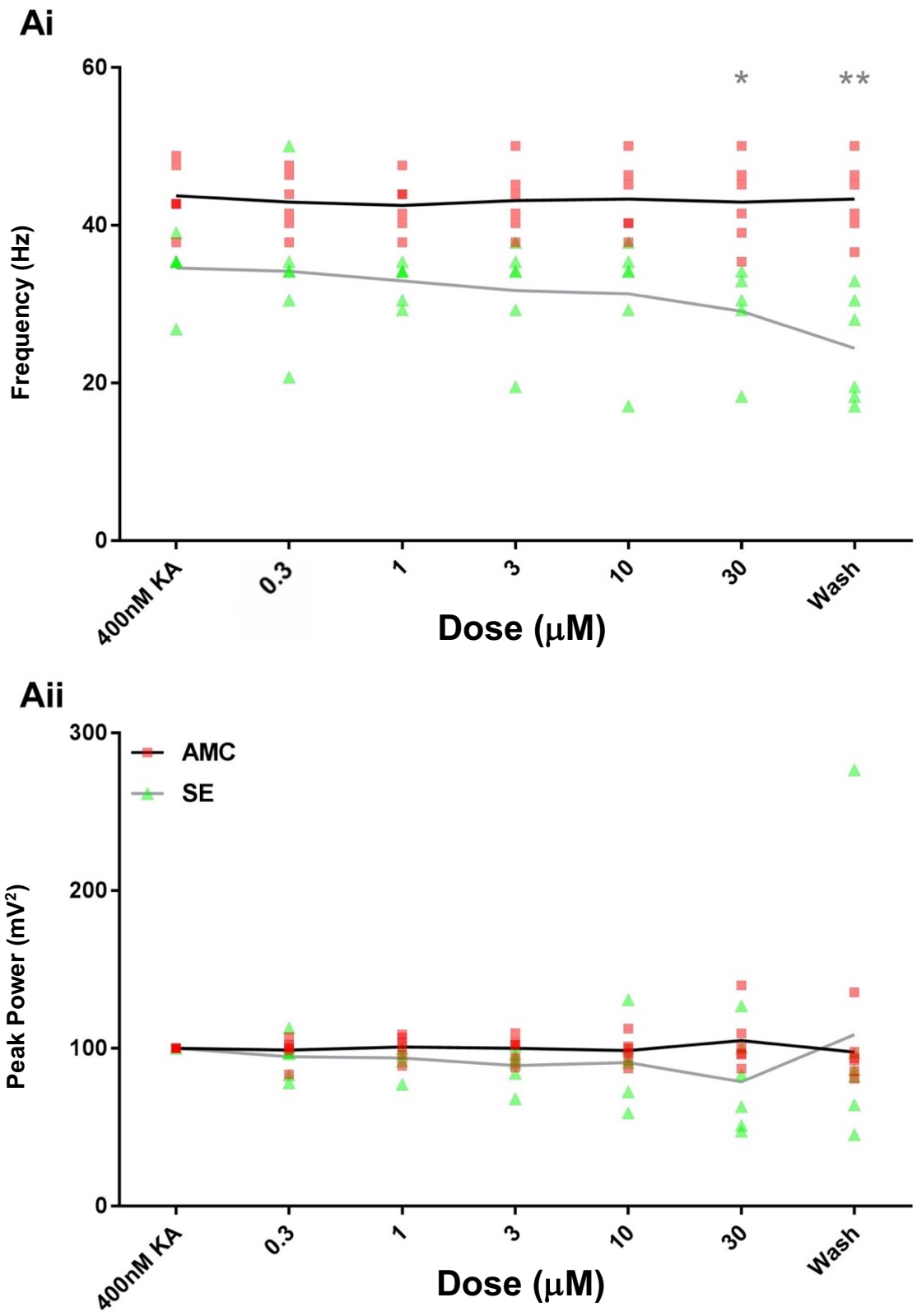

Figure 4.3 Mean peak frequency and power line graphs for CBD 24-hour post-induction. Ai Mean peak frequency line graph with AMC (black line) and SE (grey line) averages. AMC (red squares) and SE (green triangles) population frequencies are also plotted. Aii Normalised peak power responses across the CBD doses for both the AMC (black line) and SE (grey line). Again, population responses are also plotted (AMC: red squares; SE: green triangles). * $p < 0.05$, ** $p < 0.01$, with grey asterisks referring to SE significance.

As with the peak frequency, normalised FFTs and, histograms presented previously, the AMC data showed remarkable stability across all drug doses, with no changes and a lowest value of 97.67 ± 7.97 returned in the wash step. No significance was noted in any of the drug dose additions. The SE data also showed no significant change to peak power upon the addition of CBD, once more in contrast to the observable effect noted in the raw FFT analysis (**Figure 4.1**).

As this analysis compared peak power regardless of its frequency, another method of analysis was formulated to look specifically at only the power loss within gamma range.

4.2.1.3 Peak gamma measurements

The measuring of peak power across doses showed a more promising approach to assessing CBD responses but included the whole range of frequencies present. As we were specifically interested in gamma oscillations in the mEC we decided to limit the range of frequencies to just those that fall within our defined gamma range (30-60Hz).

We applied a modified approach to finding the peak frequency across datasets, with the gamma frequency being taken from the normalised FFT work previously presented (**Figure 4.1**). Therefore, the highest pooled, normalised power in 400nM KA was taken from the FFT. To be able to perform rigorous statistical analyses on the data it was decided that the nAUC would be taken from the specified frequency in each individual slice, that is, the frequency that showed the largest nAUC measurement. The frequencies found were 40.2Hz in the AMC, and 35.4Hz in the SE, similar to the peak frequencies found previously.

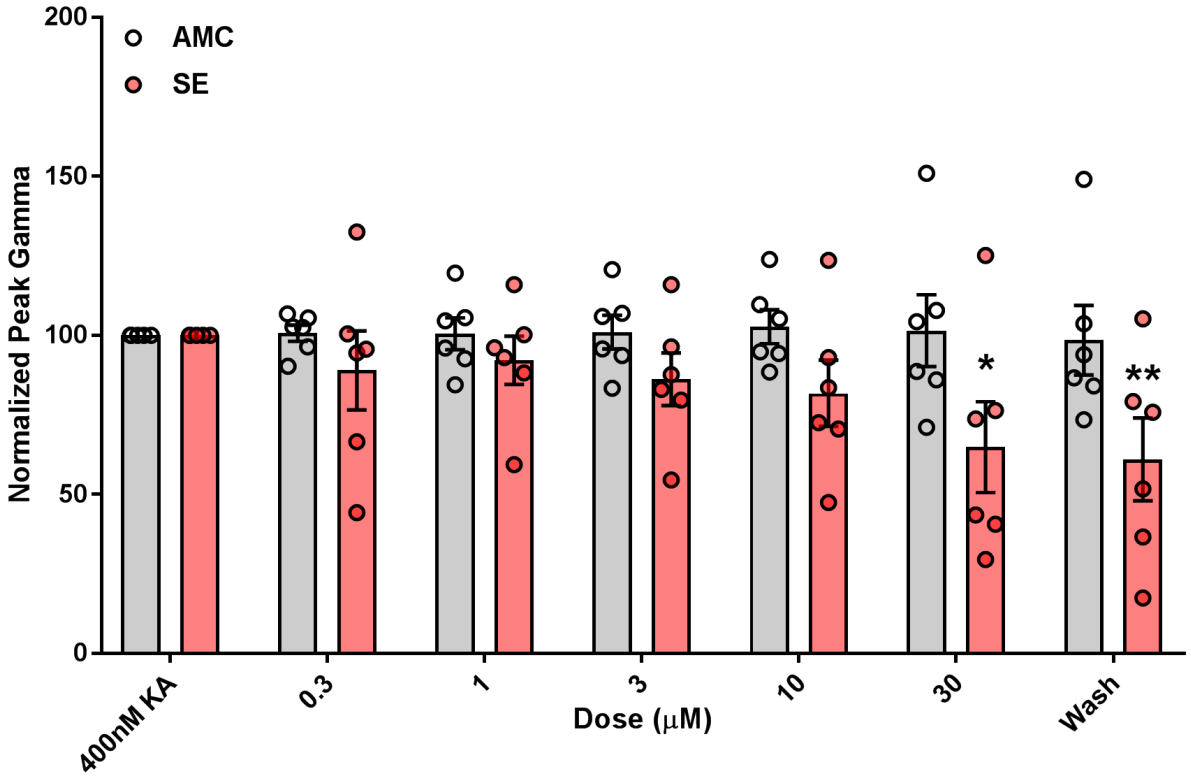

Figure 4.4 Mean normalised peak gamma response to CBD 24-hour post-induction.
Each condition is plotted on the same dose point, with AMC in grey and SE in red, with population responses also plotted. Black capped bars show standard error. * $p < 0.05$, ** $p < 0.01$.

These data were then plotted into a joint histogram displaying the mean, SEM and population responses of both conditions at each dose (**Figure 4.4**). This measure showed the differences between the two disease populations, with a relative amount of stability across all drug doses in the AMC animals.

A gradual fall in power in the SE animals was observed. The differences are most pronounced, and significant, at 30μM CBD (64.80 ± 14.30; range: 29.53-125.1; $p < 0.05$) and wash steps (60.97 ± 13.01; range: 17.45-105.2; $p < 0.01$) in the SE animals.

This analysis method showed the most comparability with the FFT produced for each dataset and, as such, was determined to be the best way of comparing cannabinoid effectiveness on gamma oscillations.

4.2.2 Effects of CBD on pharmacologically induced persistent gamma on 1-week old (~P26) AMC and SE rats

We were interested in the processes of epileptogenesis and the effect this process may have on the responses and effect of CBD. As such, we used a time point of 1-week post-induction to assess CBD effectiveness in the "latent period", the point where no seizures are observed within animals or humans (Modebadze et al., 2016; further confirmed in the PSBB data performed in this project).

The AMC population is comprised of 4 animals in total, providing an n of 7, while the SE population is composed of 5 animals in total to give an n of 10 (though the "wash" step was only performed in 8 of these). The experiments are analogous as those conducted in the initial section of this chapter (**Section 4.2**) and will be presented in the same manner.

4.2.2.1 FFTs and split frequency histogram analysis

As with the 24-hour SE rats and AMCs, we conducted initial analysis focusing on producing FFTs and normalised split frequency histograms. FFT were produced for individual slice responses, examples of which can be observed in **Figure 4.5.Aii-Bii**, which show the maximal effect of 30μM CBD against the cannabinoid free baseline gamma oscillations. Here, effects were observed in both the AMC slice response (**Aii**), and SE response (**Bii**) with a shift leftward, indicating a decrease in gamma frequency, as well as a decrease in power. Interestingly this effect appeared more prominent in the AMC dataset than the SE population.

Again, to gauge the FFT responses from each population, each slice response in that population was pooled, normalised and compiled into average FFTs. As can be seen in **Figure 4.5.Aiii**, the normalised FFT of the AMC condition at control and 30μM CBD, the shift in both power and frequency endures – indicative of a slowing of the rhythm and less neuronal excitability within the network. This trend was also notable in the full dose FFT (**Aiv**), where what appeared to be a dose-dependent decrease in both power and frequency was observable. In contrast, **Figure 4.5.Biii** shows CBD effect on the SE condition, which though present, was clearly lesser than that seen in the AMC data. Alongside this, in the 30μM dose it appears that the peak becomes broader, suggestive of less synchronous neuronal firing producing a wider spread of frequencies. Despite this, a trend towards a decrease in power, though not frequency, was observed at high doses of CBD when compared to the lower doses (**Biv**).

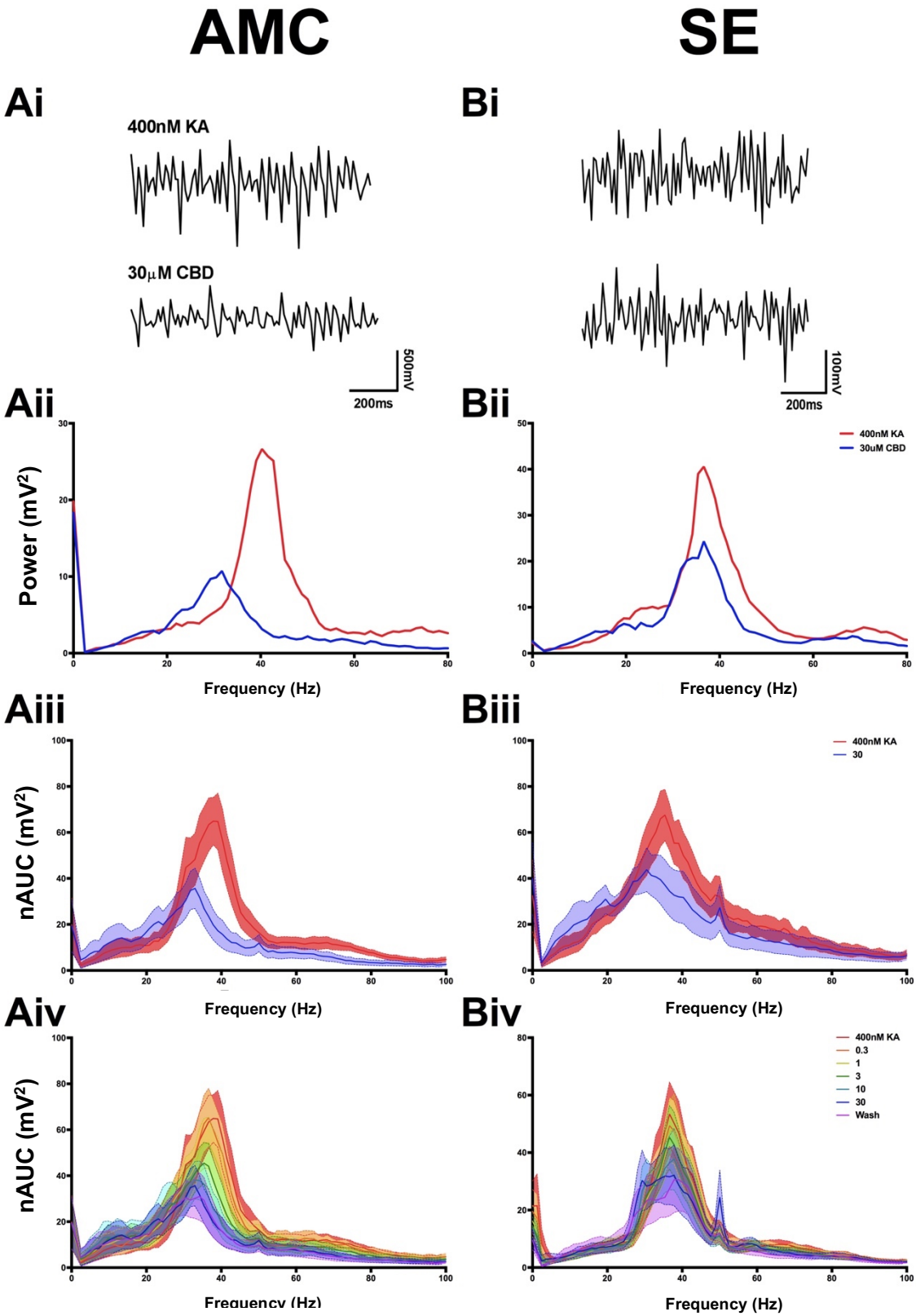

Figure 4.5 Raw traces and FFTs for CBD 1-week post-induction.
Ai-Bi Representative raw traces of pharmacologically induced gamma oscillations in both AMC (left) and SE (right) rats at 400nM KA and the maximal 30μM CBD. Aii-Bii A single slice response to the maximal 30μM CBD addition, for both the AMC (left) and SE (right) rats. Aiii-Biii Normalised FFT displaying the normalised area under the curve (nAUC) for both the 400nM KA and maximal 30μM CBD for the AMC (left) and SE right) data set, SEM is represented by the coloured fill area flanking the line. Aiv-Biv Normalised FFT data for all CBD doses applied in AMC (left) and SE (right). Coloured lines and fill refer to: red (400nM KA), orange (0.3μM CBD), yellow (1μM), dark green (3μM), light green (10μM), blue (30μM), purple (wash).

The split frequency histograms are displayed in **Figures 4.6.Ai-Aii**. These data were intriguing, as it clearly followed the previous FFTs and, showed CBD had a far larger effect on the AMC animals than on the SE rats. In the AMC animals (**Figure 4.6.Ai)** it is clear the drug dose significantly decreased the gamma and above frequencies (60+Hz; green and blue bars), while the slower frequencies (0-29Hz; red) trended toward increase, though are not significant. Comparing the mean increase in the slow frequencies (a high of 138.2 ± 26.97) to that of the decrease in the higher frequencies (60+Hz) (low of 41.93 ± 7.83 at 30μM; 51.73 ± 8.59 in 60+Hz) it is possible to state that the increase observed was not proportional to the decrease of the fast frequencies.

In contrast, the SE rats (**Figure 4.6.Aii**) show no significance at any dose of CBD in any frequency, though high significance in the wash for both, gamma (60.97 ± 12.07; $p < 0.01$) and, 60+Hz frequency bands (70.3 ± 11.48; $p < 0.0001$) were observed.

When these histograms are compared to those observed from the 24-hour time point the differences are quite stark, with a tangible effect observed in the AMC animals, and a relatively smaller effect in the SE animals, contrasted to no effect in the AMC animals and a relatively large effect in the SE population at 24-hours post induction.

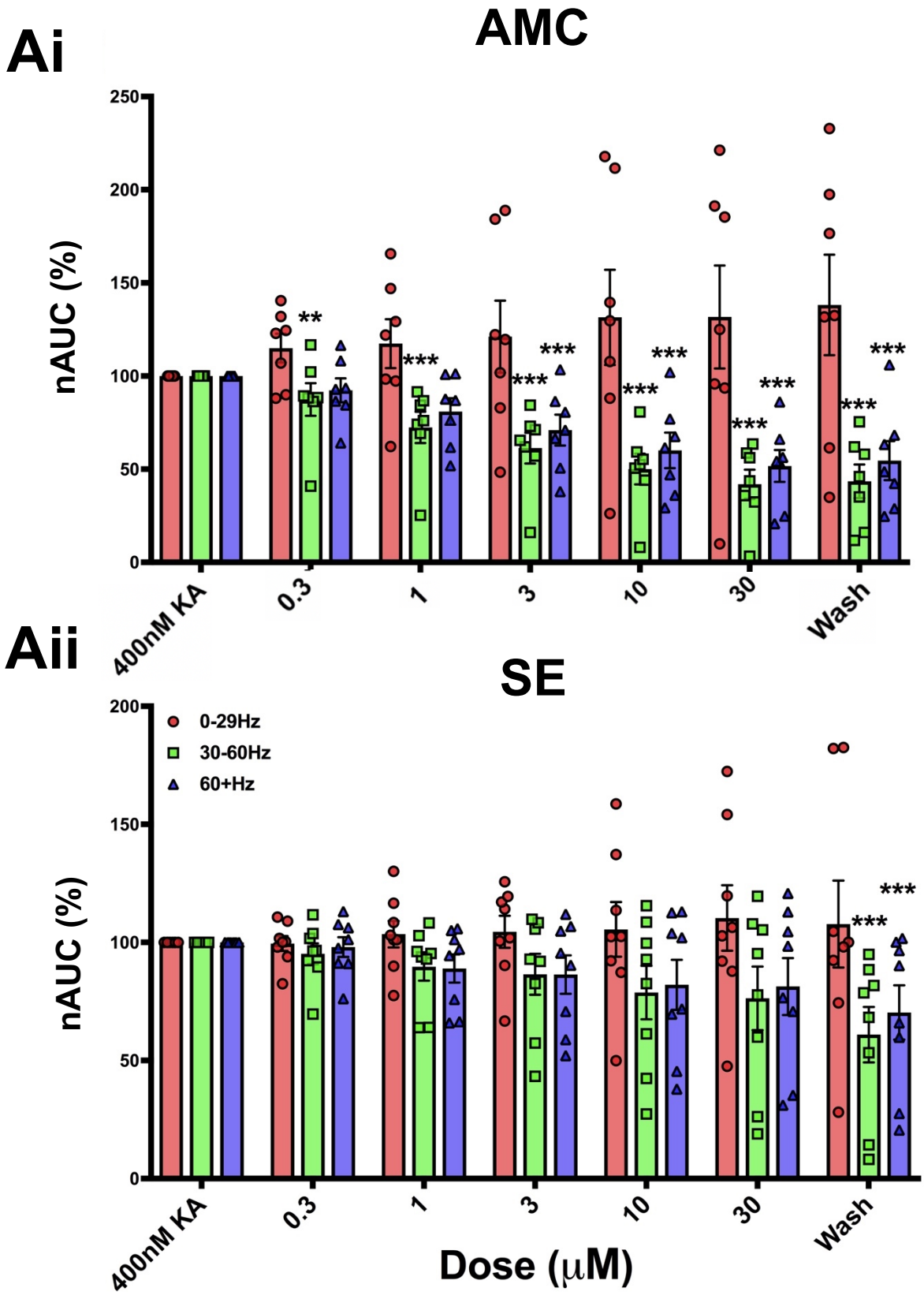

Figure 4.6 Split frequency histograms for CBD 1-week post-induction.
Ai showing the band specific nAUC response to increasing doses of CBD plus wash in the AMC condition, with population responses included. Data was normalised, with the 400nM KA response set to 100%. Aii Same histogram data shown for the SE dataset, with population responses included. Legend: low frequency (0-29Hz) - red bars; gamma (30-60Hz) - green bars; high frequency (60-1000Hz) - blue bars. Black capped bars show standard error. ** $p < 0.01$, *** $p < 0.001$, **** $p < 0.0001$.

4.2.2.2 Peak frequencies and peak power comparisons

Figure 4.7.Ai visualises the peak frequencies for both the AMC and SE populations. Surprisingly both populations initially had very similar starting peak frequencies (Hz) (36.79 ± 1.34 compared to 37.0 ± 1.0, AMC to SE). Differences became apparent upon the first dose of CBD however, with the frequency dropping to 34.5Hz ± 1.61 in AMC but remaining stable in the SE population. This trend continued, with further drops in peak frequency occurring in the AMC animals, and significance arising at 10μM CBD ($p < 0.01$), falling to a low of 25.30Hz ± 3.45 at 30μM CBD ($p < 0.0001$), before recovering somewhat to 30.0Hz ± 1.60 in the wash ($p < 0.01$). The SE peak frequency however remained remarkably consistent, in contrast to both the AMC data and, also, the data for the 24-hour SE peak frequency (**Figure 4.3.Ai**). In the 24-hour SE frequency comparison, major differences were observed between both the AMC and SE initial peak frequencies (43.74Hz ± 1.62 – 34.6Hz ± 1.66, AMC to SE) and, in the drops of these frequencies, with stability remaining in the AMC, while the SE showed falls in this frequency, particularly at 30μM and in the wash, in contrast to what was observed here.

Analogous to peak frequency measures, peak powers for both AMC and SE populations were also analysed (**Figure 4.7.Aii**). As indicated by the presented histograms and normalised FFT, the AMC population showed a gradual dose dependent decrease in peak power as CBD dose was increased. Significance arose at 10μM CBD ($p < 0.05$), while peak power fell further, to 44.58 ± 8.16, at 30μM CBD ($p < 0.001$). The wash step again saw a fall in peak power to 41.60 ± 9.94, though the significance was slightly lower ($p < 0.01$), Similarly, the SE data showed a gradual decrease upon higher doses of CBD, with significance achieved at 10μM CBD (79.70 ± 12.50; $p < 0.05$), and 30μM CBD (74.11 ± 17.51; $p < 0.05$) was found. The wash appeared to decrease this peak further to 62.35 ± 13.66, though significance was unable to be calculated due to the lower n number provided.

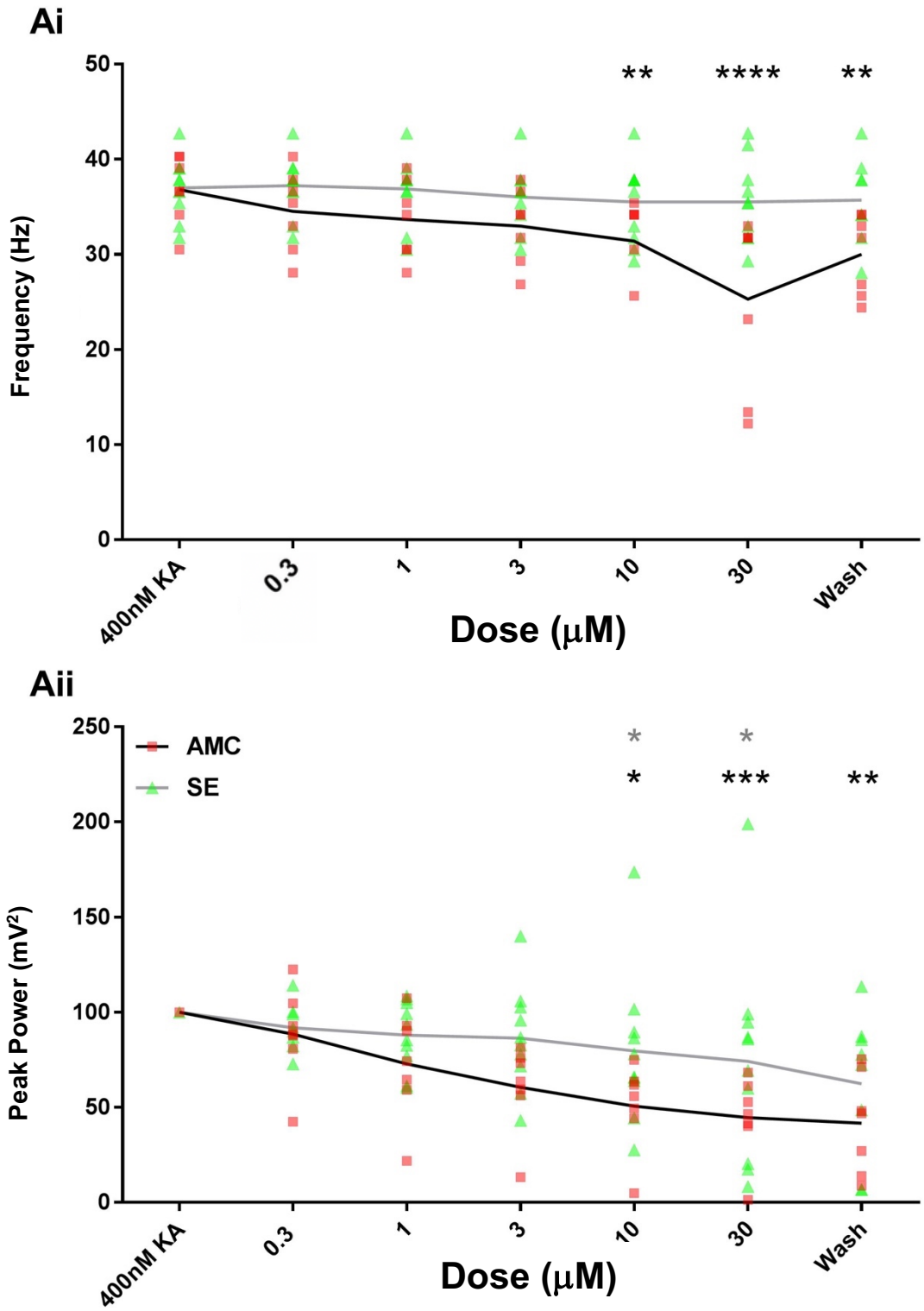

Figure 4.7 Mean peak frequency and power line graphs for CBD 1-week post induction. Ai. Normalised peak frequency line graph, AMC (black line) and SE (grey line). AMC (red squares) and SE (green triangles) population frequencies are also plotted onto a line graph. Aii Normalised peak power responses across the CBD doses for both the AMC (black line) and SE (grey line). Again, population responses are also plotted (AMC: red squares; SE: green triangles). Significance denoted by black (AMC) or grey (SE) asterisks, * $p < 0.05$, ** $p < 0.01$, *** $p < 0.001$, **** $p < 0.0001$, black asterisks for AMC, grey for SE.

4.2.2.3 Peak gamma measurements

The peak gamma measurements produced 37.8Hz for the AMC peak gamma frequency and 36.6Hz as the SE, again very similar to the peak frequencies yielded in the peak frequency section previous.

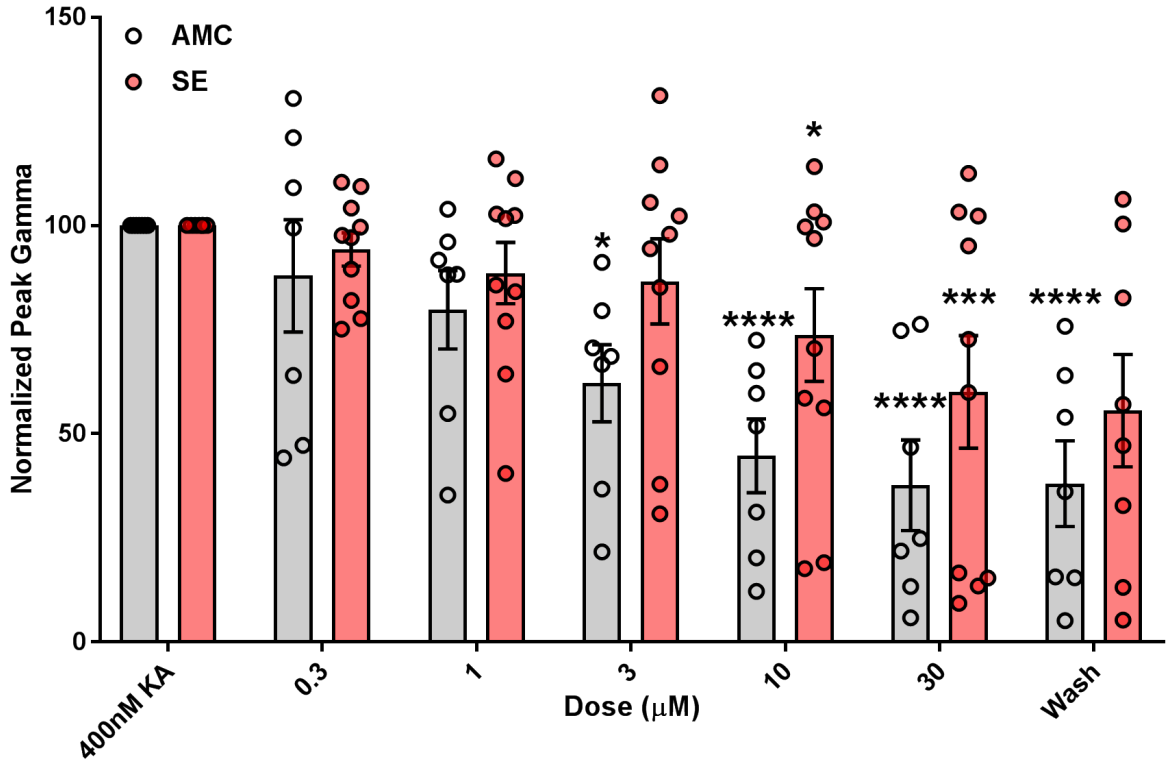

Figure 4.8 Mean normalised peak gamma response to CBD 1-week post-induction.
Each condition is plotted on the same dose point, with AMC in grey and SE in red, with population responses also plotted. Black capped bars show standard error. * $p < 0.05$, *** $p < 0.001$, **** $p < 0.0001$.

The histogram displays a clear dose-dependent drop caused by CBD in the AMC population (**Figure 4.8**), with significant decreases in peak gamma produced by 3μM CBD ($p < 0.05$), which decreased further at both 10μM and 30μM CBD to remain highly significant through to the wash ($p < 0.0001$).

The analogous SE data showed a wider variety in individual responses; certain slices displayed no change, while some increased in peak gamma, while furthermore, a cluster of slices decreased in peak gamma very effectively. Statistical analyses were performed, and indications of significance are depicted on the histogram, with the highest significance reached at the maximal 30μM CBD ($p < 0.001$). It must be noted that the wash step had not been performed in one set of experiments for the SE animals, resulting in the exclusion of the wash step in the analyses of this data (as repeated measure ANOVAs require equal numbers in each group).

4.2.3 Effects of CBD on pharmacologically induced persistent gamma on 3-month(+) old AMC and chronically SE rats

As our model provides an effective transition into SRS or chronic epilepsy, we also looked at the effect of CBD in this time point. As stated in the Materials and Methods section (**Chapter 2**), we tested SE animals in our experiments once they had been confirmed to be in SRS, using the modified PSBB tests (**Section 2.3**). AMC animals were also used for comparison. The data here is in accordance with the other data presented within this chapter.

A total of 4 animals were used for the AMC population, with an overall n of 9, though differences in software and equipment resulted in different frequency ranges being used. This meant that only an n of 6 could be used for the analysis after the split frequency ranges and scatter plots (**Figure 4.10-11-12**). 3 animals were used for the SE population producing an overall n of 9.

4.2.3.1 FFTs and split frequency histogram analysis

As with the previous sections, single slice FFT responses are presented in **Figure 4.9.Aii-Bii**, where seemingly smaller effects of CBD are observed, though they appeared similar for both the AMC and SE populations. An interesting observation here was that in the AMC population (**Aii**) showed a slight shift leftward in frequency alongside a small decrease in power at the maximal CBD dose. Meanwhile, the SE population suggest a shift to the right in frequency with a decrease in power, suggesting an increase in the peak frequency upon 30μM CBD application. Normalised FFTs for both conditions were again produced (**Figure 4.9.Aiii-Biv**). For reference, the AMC n number in this graph is now 6, not 9.

Figure 4.9.Aiii highlights the effect 30μM CBD has on population gamma oscillations, where a decrease in power, though not frequency, was observed (**Figure 4.5.Aiii-iv**). The overlap of error bars, suggests there may not be a significant difference between the two. The full dose FFT (**Aiv**) appeared to show a dose-dependent decrease in power, not frequency, with increasing additions of CBD. This was comparable to what appears to again be a dose-dependent decrease in the SE data, observed in both **Biii** and **Biv**. The pooled normalised 400nM KA line shows a high amount of variability, especially so at frequencies below 35Hz, resulting in a high standard error fill area, obvious in **Biii**. Despite this, a gamma peak was notable, as too was a decrease in the power of this peak at 30μM CBD, alongside a complete loss in the low frequency variation (as indicated by the now narrow standard error area around the 30μM CBD line). The full dose FFT (**Biv**) suggests once more a dose-dependent decrease of gamma by increasing CBD doses.

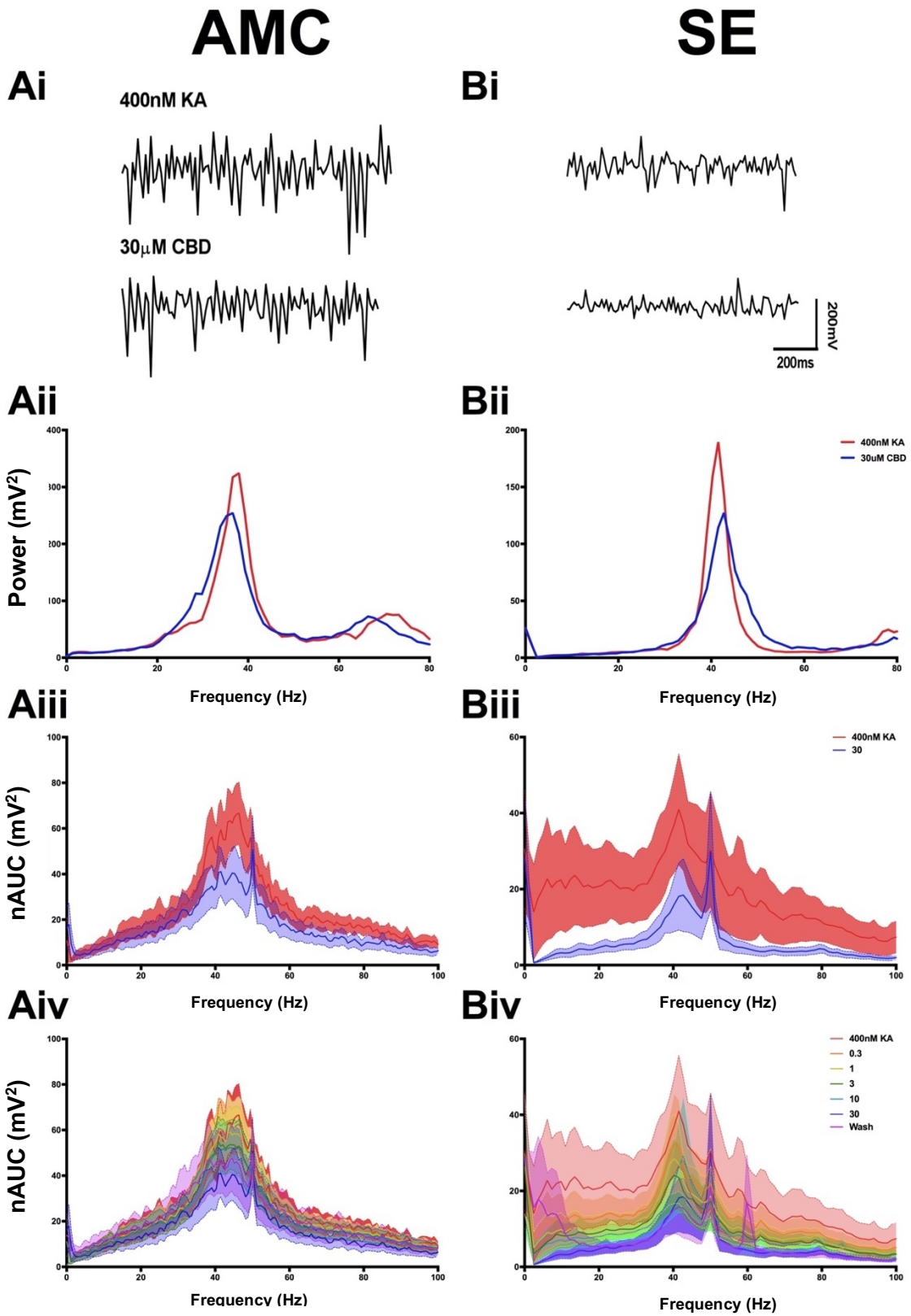

Figure 4.9 Raw traces and FFTs for CBD 3-months post-induction.
Ai-Bi Representative raw traces of pharmacologically induced gamma oscillations in both AMC (left) and SE (right) rats at 400nM KA and the maximal 30μM CBD. Aii-Bii A single slice response to the maximal 30μM CBD addition, for both the AMC (left) and SE (right) rats. Aiii-Biii Normalised FFT displaying the normalised area under the curve (nAUC) for both the 400nM KA and maximal 30μM CBD for the AMC (left) and SE right) data set, SEM is represented by the coloured fill area flanking the line. Aiv-Biv Normalised FFT data for all CBD doses applied in AMC (left) and SE (right). Coloured lines and fill refer to: red (400nM KA), orange (0.3μM CBD), yellow (1μM), dark green (3μM), light green (10μM), blue (30μM), purple (wash).

The AMC data is presented as a normalised split frequency histogram in **Figure 4.10.Ai**, and as with the 24-hour time point AMC animals, there was no significant effect on any of the frequency bands. When compared to the FFT of **Figure 4.9.Aiii**, this analysis seems not to represent the decrease observable at 30μM CBD.

Similarly, **Figure 4.10.Aii** displays little significant changes to any of the frequency bands in the SE condition, until the wash step where a dramatic, and significant, rise in the low frequencies was visible ($p < 0.01$) due mostly to the rise of 2 population responses. Disregarding the large responses in the wash step, there was visual similarity between the histograms of **Figure 4.10.Ai-Aii**, though neither represents the normalised FFT data presented in **Figure 4.9.Aiii-Biii**, which was suggestive of a comparable suppressive effect of CBD in both conditions.

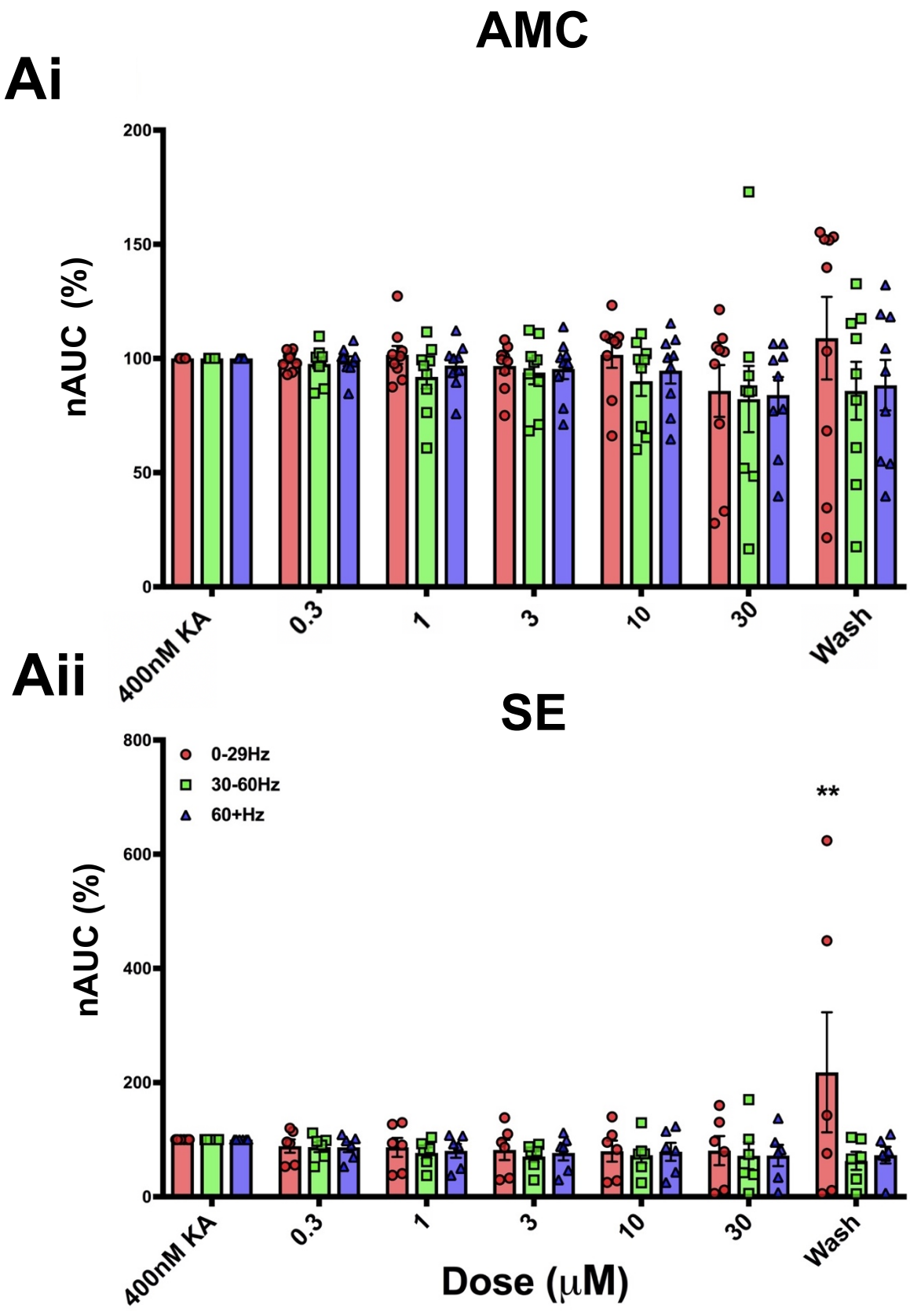

Figure 4.10 Split frequency histograms for CBD 3-months post-induction.
Ai Split frequency histograms, showing the band specific nAUC response to increasing doses of CBD plus wash in the AMC condition, with population responses included. Data was normalised, with the 400nM KA response set to 100%. Aii Same histogram data shown for the SE dataset, with population responses included. Legend: low frequency (0-29Hz) - red bars; gamma (30-60Hz) - green bars; high frequency (60-1000Hz) - blue bars. Black capped bars show standard error. ** $p < 0.01$.

4.2.3.2 Peak frequency and peak power comparisons

Again, the peak frequency and powers were analysed, with the results presented in **Figure 3.11**.

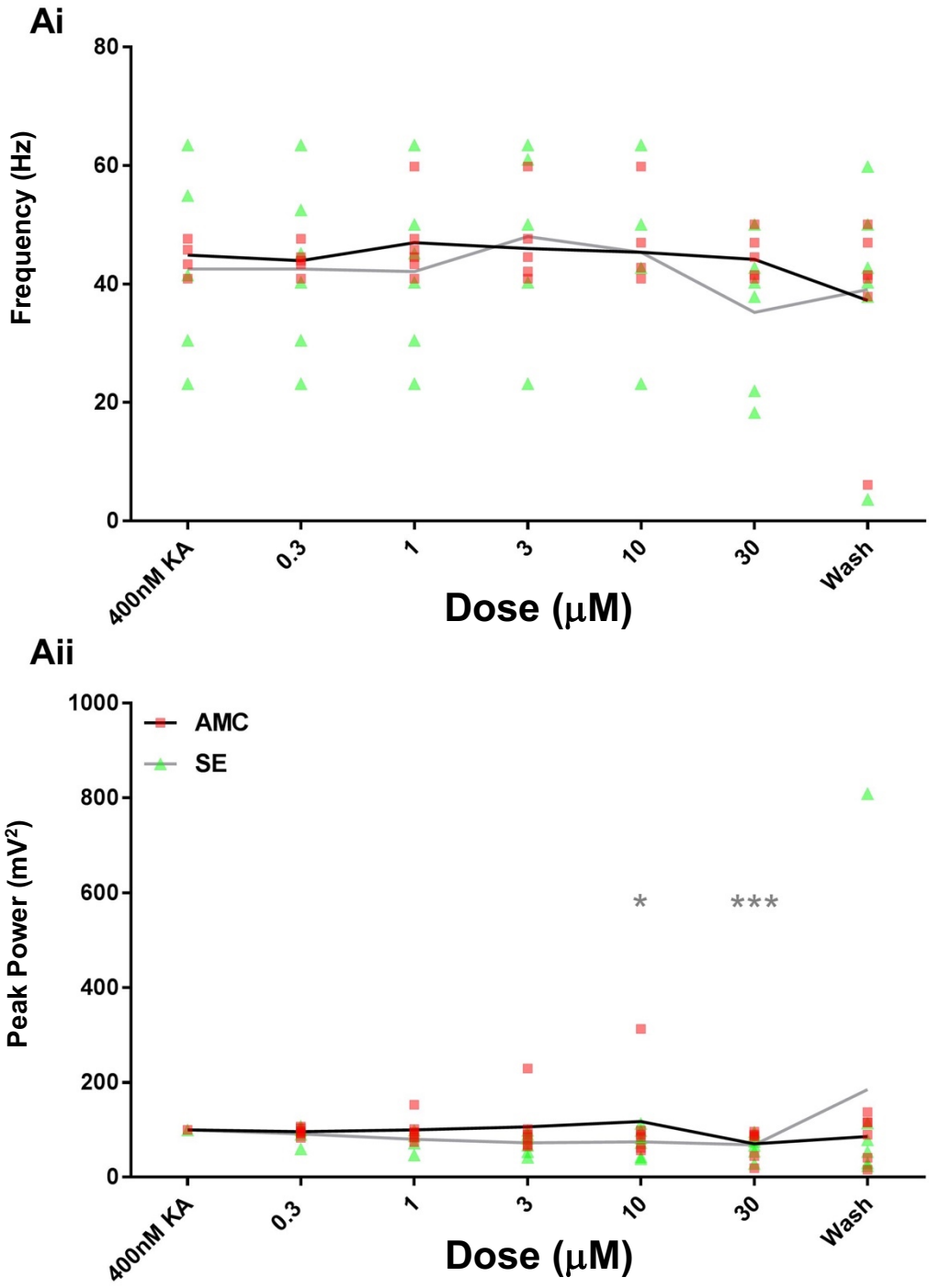

Figure 4.11 Mean peak frequency and power line graphs for CBD 3-months post induction. Ai Mean peak frequencies for both the AMC (black line) and SE (grey line). AMC (red squares) and SE (green triangles) population frequencies are also plotted onto a line graph. Aii Normalised peak power responses across the CBD doses for both the AMC (black line) and SE (grey line). Again, population responses are also plotted (AMC: red squares; SE: green triangles). Significance denoted by black (AMC) or grey (SE) asterisks. * $p < 0.05$, *** $p < 0.001$, grey asterisks denote SE significance.

The AMC data shows relative stability in peak frequency (44.9Hz ± 0.97), with no significant changes observed. Similarly, the SE data (41.5Hz ± 0.84) shows a seesaw distribution through the doses, but no significance observed. When both of these results are compared to the normalised FFT data presented in **Figure 4.9** this outcome is not surprising.

Similarly, the peak power comparisons between the two conditions (**Aii**) show the AMC peak power not to significantly change across the drug additions. The SE data however, showed a prolonged decrease in normalised power, which may be dose-dependent, though significance only first occured at 10μM ($p < 0.05$), while a value of 56.3 ± 10.37 was found at 30μM ($p < 0.001$). The wash step saw a large increase to 213.0 ± 102.7 (with SEM greatly increased) with a corresponding loss of significance.

4.2.3.3 Peak gamma measures

As previously, peak gamma was our final method of analysis. The AMC data had a peak gamma frequency of 46.3Hz, while the SE, 41.5Hz.

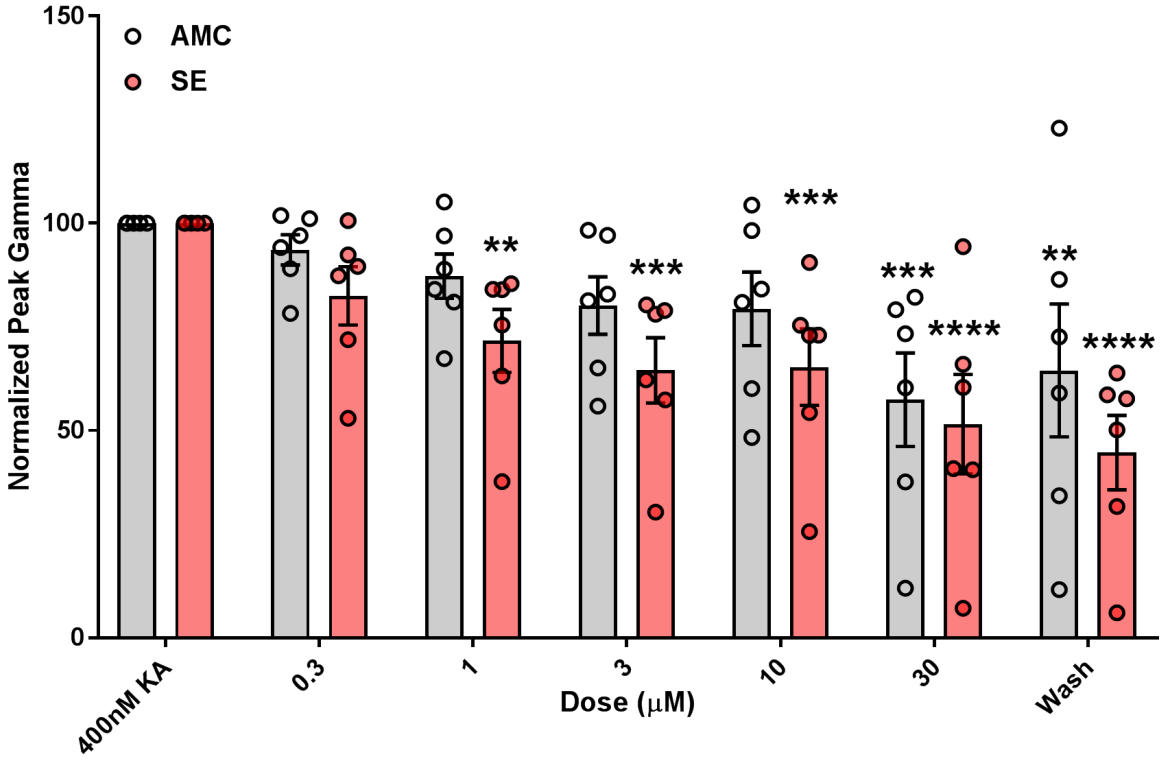

Figure 4.12 Mean normalised peak gamma response to CBD 3-months post-induction. Each condition is plotted on the same dose point, with AMC in grey and SE in red, with population responses also plotted. Black capped bars show standard error. ** $p < 0.01$, *** $p < 0.001$, **** $p < 0.0001$.

The AMC population only displayed a significant response to CBD at 30μM, though the response was extremely significant ($p < 0.001$). Conversely, the SE population displays significance at 1μM CBD ($p < 0.01$), which continued to become more significant as the doses increased ($p < 0.0001$ in 30μM CBD and wash).

Although the AMC population responses show what appeared to be a dose-dependent decrease at increasing CBD levels, this was not matched in the statistical analysis, which suggested that only the maximal CBD dose was effective. A higher level of sensitivity to CBD appeared to be present in the SE data**,** with apparent and significant decreases in peak gamma occurring at much lower dose of CBD. This is suggestive of a higher sensitivity or affinity for CBD in the mature SE brains, though this is still present in AMC brains to a lower extent.

4.2.3.4 Summary of CBD effects of gamma oscillations

Table 4.1 below shows the overall effects noted on induced gamma oscillations at each of the ages used here, for both AMC and SE animals, when cumulative doses of CBD were applied. As can be noted, 1-week AMC showed the highest sensitivity to CBD from the AMC animals, while 3-months SE showed the highest sensitivity from the SE population, and indeed overall.

Age	CBD Dose (µM)				
	0.3	1	3	10	30
24-hr AMC	-	-	-	-	-
24-hr SE	-	-	-	-	↓
1-week AMC	-	-	↓	↓↓↓↓	↓↓↓↓
1-week SE	-		-	↓	↓↓↓
3-month AMC	-	-	-	-	↓↓↓
3-month SE	-	↓↓	↓↓↓	↓↓↓	↓↓↓↓

Table 4.1 Summary of CBD dose effects on the rats used in this section.
Ages and condition of animals are noted on the left, with the increasing CBD doses noted horizontally across the top. The arrows have been used to show the level of significance achieved at that dose (1 arrow = 0.05, 2 = 0.01, 3 = 0.001, 4 = 0.0001), with the direction of the arrow also representing the direction of change in gamma.

4.2.4 Effects of CBDV on pharmacologically induced persistent gamma in 24-hour (~P19) AMC and SE rats

In parallel to the CBD LFP experiments just described, CBDV, a CBD analogue that has also previously shown promise as an anti-epileptic (see **Section 1.7.3** for further information) was also tested at the same time points, in the same manner.

In the first time point (~p19), a total of 2 AMC animals were used to provide an n number of 7. A total of 3 SE animals were used to produce an n of 7, though the wash step was only performed in 3 of these therefore the wash step is not included in any statistical analysis.

4.2.4.1 FFTs and split frequency histogram analysis

Single slice FFTs are presented in **Figure 4.13.Aii-Bii**, where drops in both the power and frequency are noted in the AMC slice (**Aii**), however, the decrease in power especially was slight. There was also a drop presented in the SE slice (**Bii**), though a more broadband trace was visible in the 30μM CBDV dose.

Once again, a normalised FFT was produced for both epilepsy conditions between the baseline and 30μM CBDV dose (Figure **4.13.Aiii-Biii**). The AMC FFT (**Aiii**) showed a large overlap of standard errors between the 400nM KA baseline and 30μM CBDV, suggesting that the drop observed may not be significant. Assessment of the normalised peak suggests multiple peaks occurring in the gamma range. The full dose FFT (**Aiv**) suggests that as dose increased the power decreased, but interestingly, the peak shifts to the right, thereby indicating an increase in frequency. This is viewed more easily in **Figure 4.3.13.Aiii**, showing only the 400nM KA and 30μM CBDV doses.

The broad range of frequencies observed in the AMC data was even more pronounced in the SE population (**Biii**), with close to parity in power across a very wide spectrum of frequencies (~10-50Hz). Again, this was highly suggestive of multiple peaks being produced in the individual experiments at a wide range of frequencies, therefore, upon normalisation each of these is given equal weighting producing what is observable in the figure. A decrease in power can be identified between 400nM KA and 30μM, easily seen in **Biii**, though a dose-dependent decrease was not observable, with many of the traces remaining equal with the initial 400nM KA trace, visible in the full dose FFT (**Biv**).

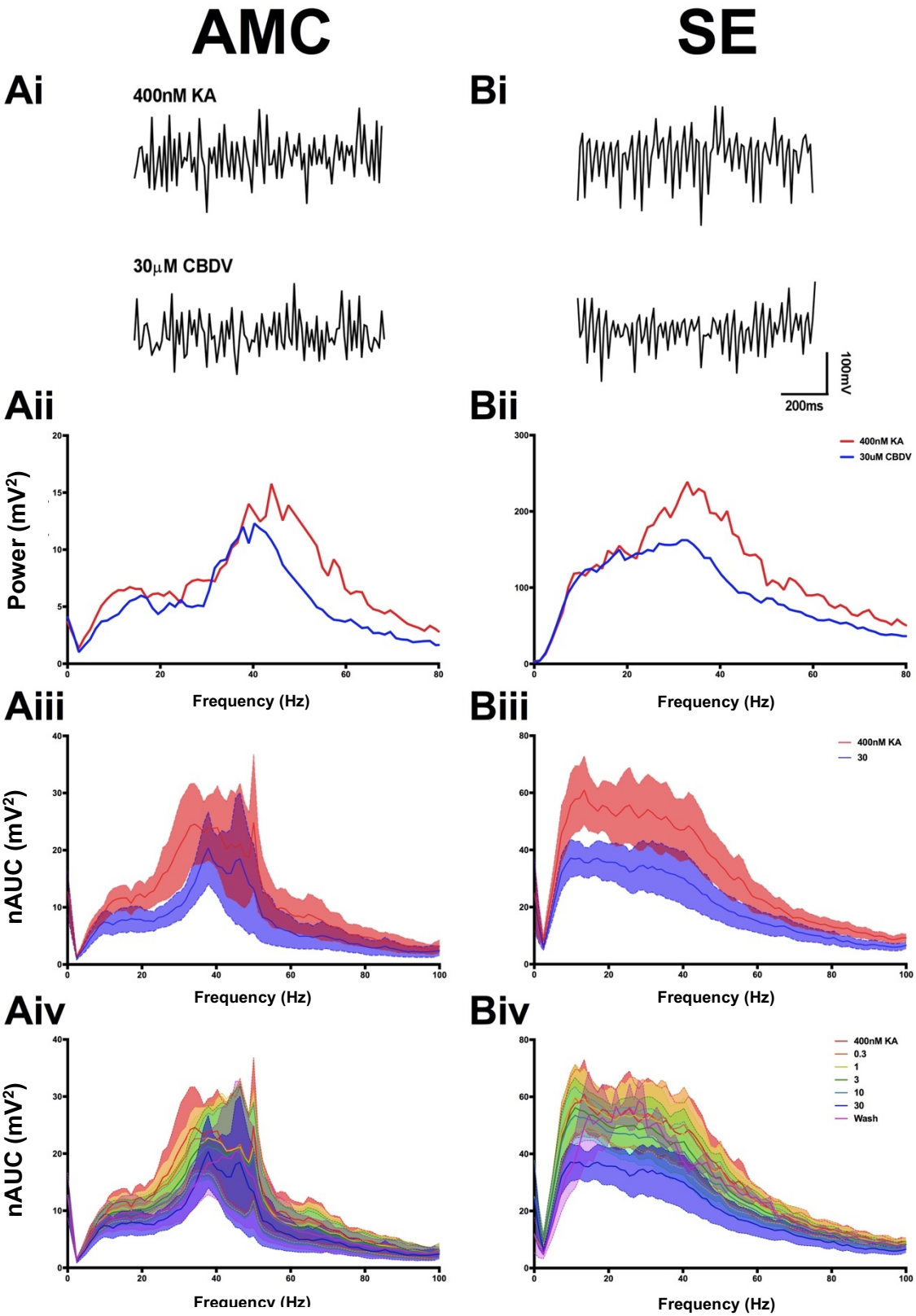

Figure 4.13 Raw traces/FFTs for CBDV 24-hour post-induction.
Ai-Bi Representative raw traces of pharmacologically induced gamma oscillations in both AMC (left) and SE (right) rats at 400nM KA and the maximal 30μM CBDV. Aii-Bii A single slice response to the maximal 30μM CBDV addition, for both the AMC (left) and SE (right) rats. Aiii-Biii Normalised FFT displaying the normalised area under the curve (nAUC) for both the 400nM KA and maximal 30μM CBDV for the AMC (left) and SE right) data set, SEM is represented by the coloured fill area flanking the line. Aiv-Biv Normalised FFT data for all CBDV doses applied in AMC (left) and SE (right). Coloured lines and fill refer to: red (400nM KA), orange (0.3μM CBDV), yellow (1μM), dark green (3μM), light green (10μM), blue (30μM), purple (wash).

The AMC data here presented a general trend toward decrease across all the doses in all of the frequency bands (**Figure 4.14.Ai**). Significance was only achieved in the 30μM CBDV dose at all frequency bands, something not seen in the CBD data (**Figure 4.2.Ai**). As can be observed, varying levels of significance at 30μM were produced, with the low frequency (0-30Hz) and gamma range both showing high levels of significance ($p < 0.01$) (low: 69.91 ± 12.28; gamma: 65.29 ± 14.39) and the high frequency range displaying extreme levels of significance ($p < 0.001$) (high: 77.37 ± 4.79). At all frequencies the mean increased into the wash, though both the gamma and high frequencies retained significance ($p < 0.05$) (gamma: 68.91 ± 16.56; high: 83.53 ± 7.38).

In contrast, the SE responses (**Figure 4.14.Aii**) showed significance earlier in the gamma frequency bands (3μM: $p < 0.05$). Alongside this, there was a clear trend toward decrease in the high frequencies, which achieved significance at 30μM (80.25 ± 6.19; $p < 0.001$). The low frequency band showed no significant changes at any dose of CBDV. The data showed a dose-dependent decrease in the gamma band (3μM: 87.29 ± 3.69; 10μM: 81.37 ± 3.44; 30μM: 58.38 ± 6.78). There was a large increase in the low frequency in the wash step, but as this condition only had an n of 3 the results here were not entered into the statistical analysis and will not be discussed here.

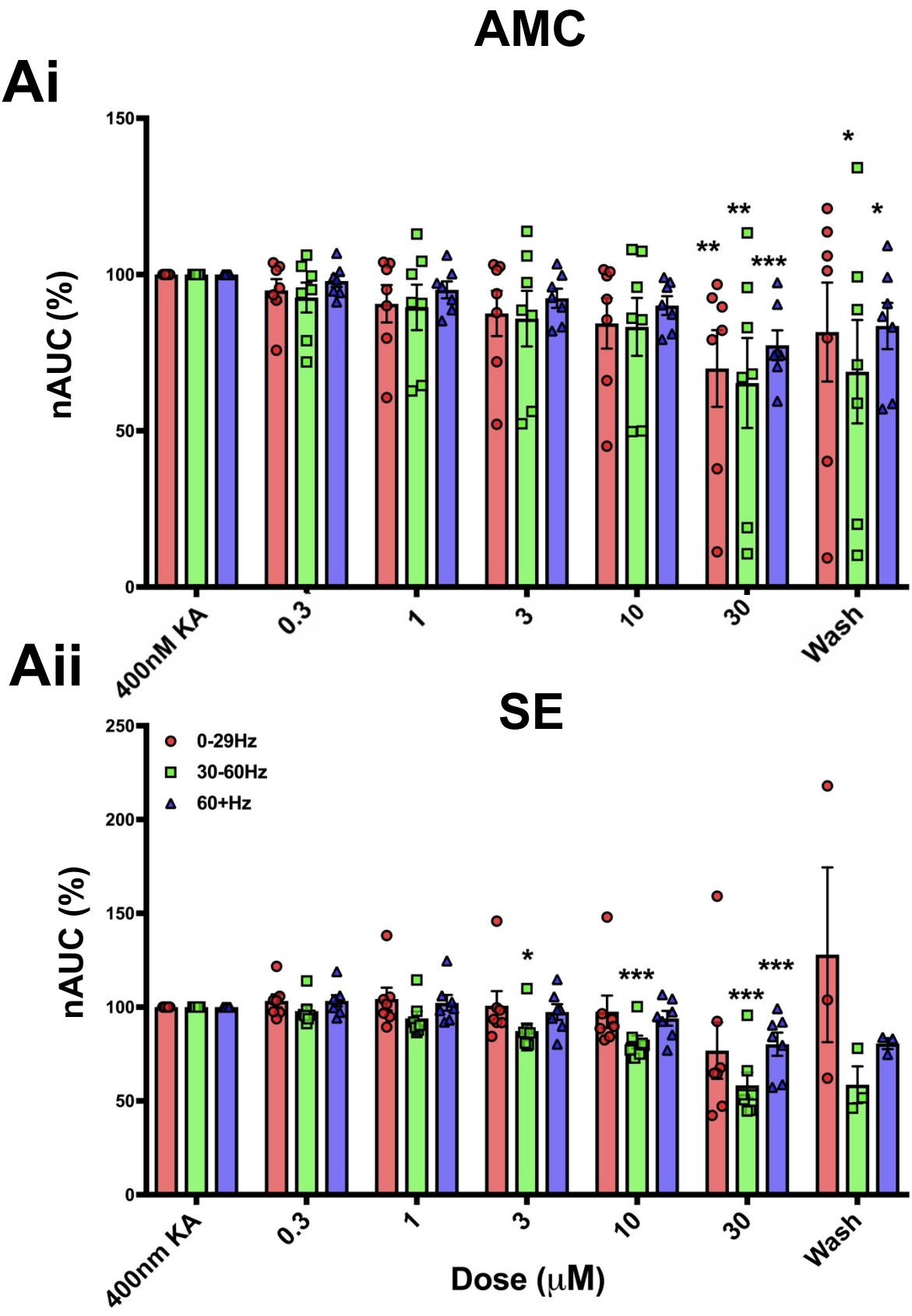

Figure 4.14 Split frequency histograms for CBDV 24-hour post-induction.
Ai Split frequency histograms, showing the band specific nAUC response to increasing doses of CBDV plus wash in the AMC condition, with population responses included. Data was normalised, with the 400nM KA response set to 100%. Aii Same histogram data shown for the SE dataset, with population responses included. Legend: low frequency (0-29Hz) - red bars; gamma (30-60Hz) - green bars; high frequency (60-1000Hz) - blue bars. Black capped bars show standard error. * $p < 0.05$, ** $p < 0.01$, *** $p < 0.001$.

4.2.4.2 Peak frequencies and peak power

The peak frequencies of both the AMC and SE populations are represented on **Figure 4.15.Ai**. As with the 24hr CBD peak frequencies (**Figure 4.3.Ai**) there was a clear difference between the two populations at the 400nM KA (AMC: 34.35Hz ± 4.17; SE: 23.72Hz ± 4.26). Again, a Mann-Whitney test was performed returning a p value < 0.0001, once more suggesting that the epilepsy model itself has an effect on networks in the mEC providing the persistent oscillations.

The AMC population showed no significant differences when any dose of CBDV was applied. In contrast, the SE line remained relatively stable, until a significant decrease was observed at 30μM (21.28Hz ± 4.42; $p < 0.05$).

The normalised peak power data are plotted as a line graph on **Figure 4.15.Aii** containing both AMC and SE data. Initial effects of CBDV are very similar in both populations, with no significance observed in either. At 10μM the two diverge, with the AMC peak power remaining non-significant, while the SE showed a significant decrease ($p < 0.05$), before falling further to a low at 30μM of 61.87 ± 6.56 ($p < 0.001$). No significance was noted at any dose of CBDV in the AMC data.

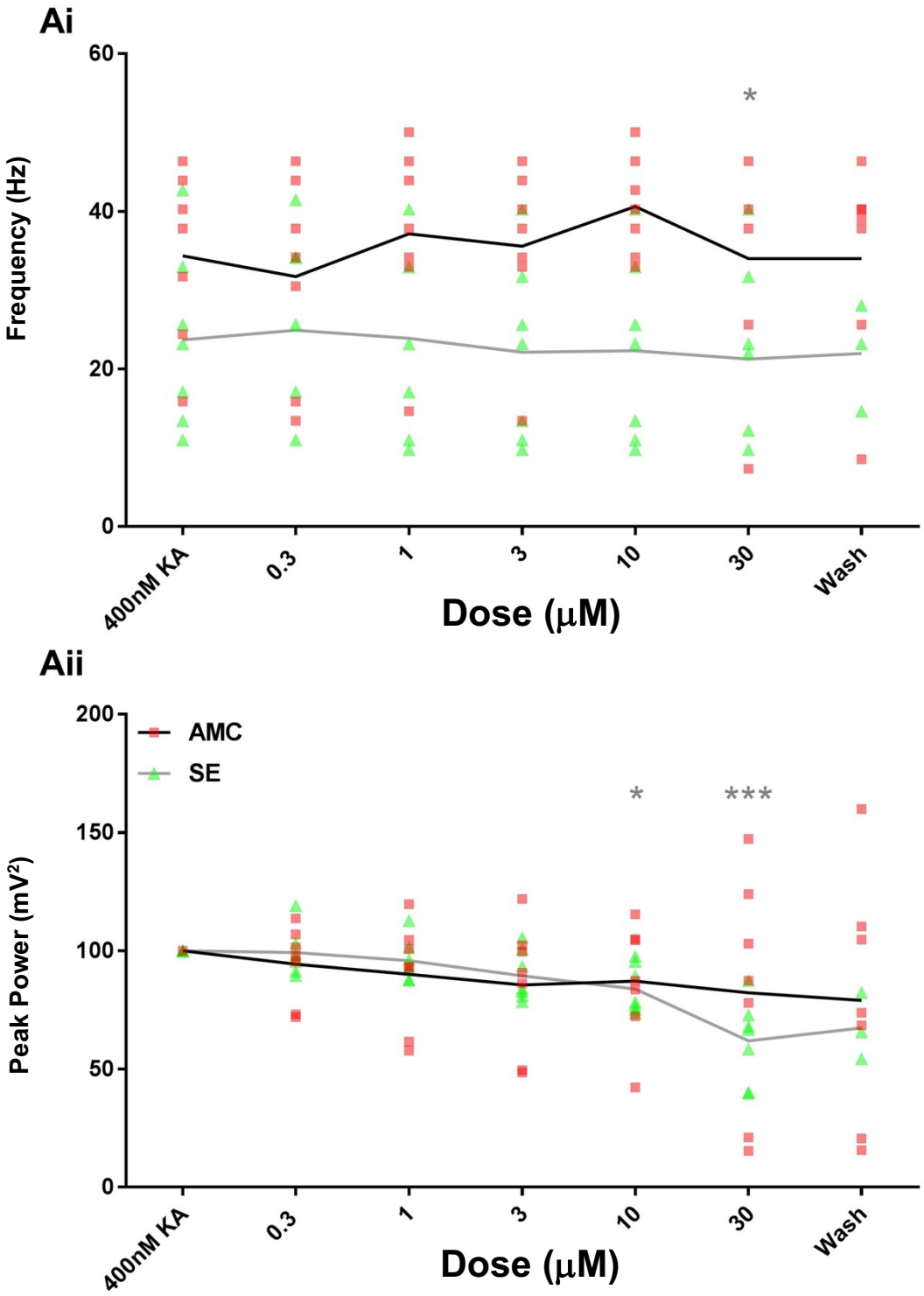

Figure 4.15 Mean peak frequency and power to CBDV 24-hour post induction.
Ai. Mean peak frequencies for both the AMC (black line) and SE (grey line). AMC (red squares) and SE (green triangles) population frequencies are also plotted onto a line graph. Aii. Normalised peak power responses across the CBDV doses for both the AMC (black line) and SE (grey line). Again, population responses are also plotted (AMC: red squares; SE: green triangles). Significance denoted by black (AMC) or grey (SE) asterisks, * $p < 0.05$, *** $p < 0.001$, grey asterisks denote SE significance.

4.2.4.3 Peak gamma measurements

As with the CBD measures, peak gamma was determined to be the most effective way to assess CBDV effect on network responses. The AMC data had a peak gamma frequency of 34.17Hz, while the SE data had a peak frequency of 30.51Hz. The histogram produced from these responses are shown in **Figure 4.16**. where both the AMC and SE mean responses, SEMs and, population responses are plotted.

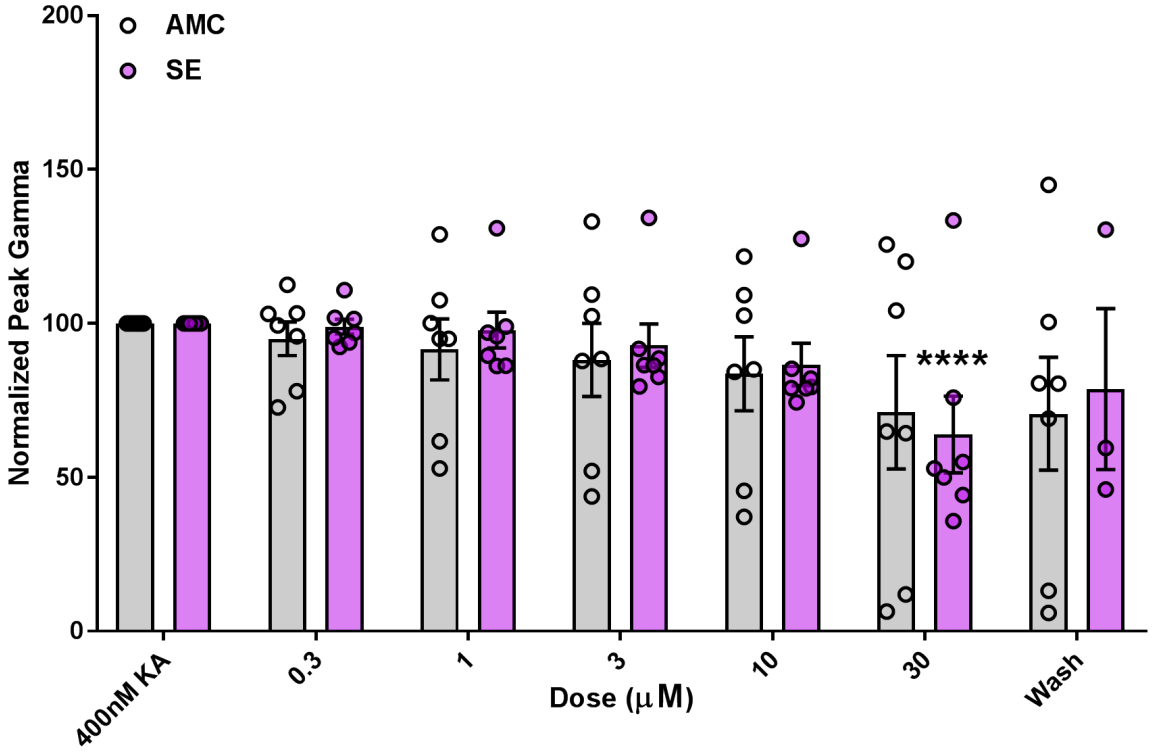

Figure 4.16 Mean normalised peak gamma response to CBDV 1-week post-induction. Each condition is plotted on the same dose point, with AMC in grey and SE in red, with population responses also plotted. Black capped bars show standard error. **** $p < 0.0001$.

Surprisingly, none of the AMC peak gamma decreases are significant, with the lowest value, at 30μM CBDV, possessing a mean of 71.09 ± 18.41. In the SE data, only the 30μM CBDV showed any significance, with $p < 0.0001$ (63.9 ± 12.49), which is surprising as both peak power and normalised split frequencies showed significance at 10μM for the SE dataset ($p < 0.01$).

4.2.5 Effects of CBDV on pharmacologically induced persistent gamma on 1-week old (~P26) AMC and SE rats

This next section will provide the data collected from the effect of CBDV on the latent period aged rats (~p26). The total number of animals used for the AMC data was 3 giving a total n of 6, while the SE data came from a total of 3 animals to give an n of 7. As has been described in previous animals, the wash step was only performed in 5 of these slices, and as such the wash has been disregarded for statistical analysis and some of the figures presented here, with those figures labelled to reflect this.

4.2.5.1 FFTs and split frequency histogram analysis

Once more, single slice FFTs are presented (**Figure 4.17.Aii-Bii**) for both AMC (**Aii**) and SE (**Bii**). In both, a decrease in power was visible, though it appeared as though no shift in frequency was present in either. Pooled normalised FFTs are presented next, with 400nM KA and 30μM CBDV only shown first. In the AMC data (**Aiii**), a clearly defined peak in the 400nM KA dose at a frequency of 35.4Hz was visible. The decrease noted in the single slice FFT was preserved in the pooled dataset and, once again, no frequency change was noted. A dose dependent decrease appeared to be present when the full dose FFT is observed (**Aiv**)

Dose-dependent decreases to the largest gamma frequency power appeared to be present in the SE population (**Bii**), though these were not as well-defined as those observed in the AMC data. A secondary, lower frequency peak was visible, showing the higher frequency variance produced in this population. A possible slight slowing in frequency and decrease in power is observed in the 400nM KA vs. 30μM CBDV figure (**Biii**), though there was substantial overlap between the two doses, suggestive of a lack of significance. The large overlap in both the average line and standard error fill area which make assessment of the cumulative CBDV effect difficult to visualise fully (**Biv**).

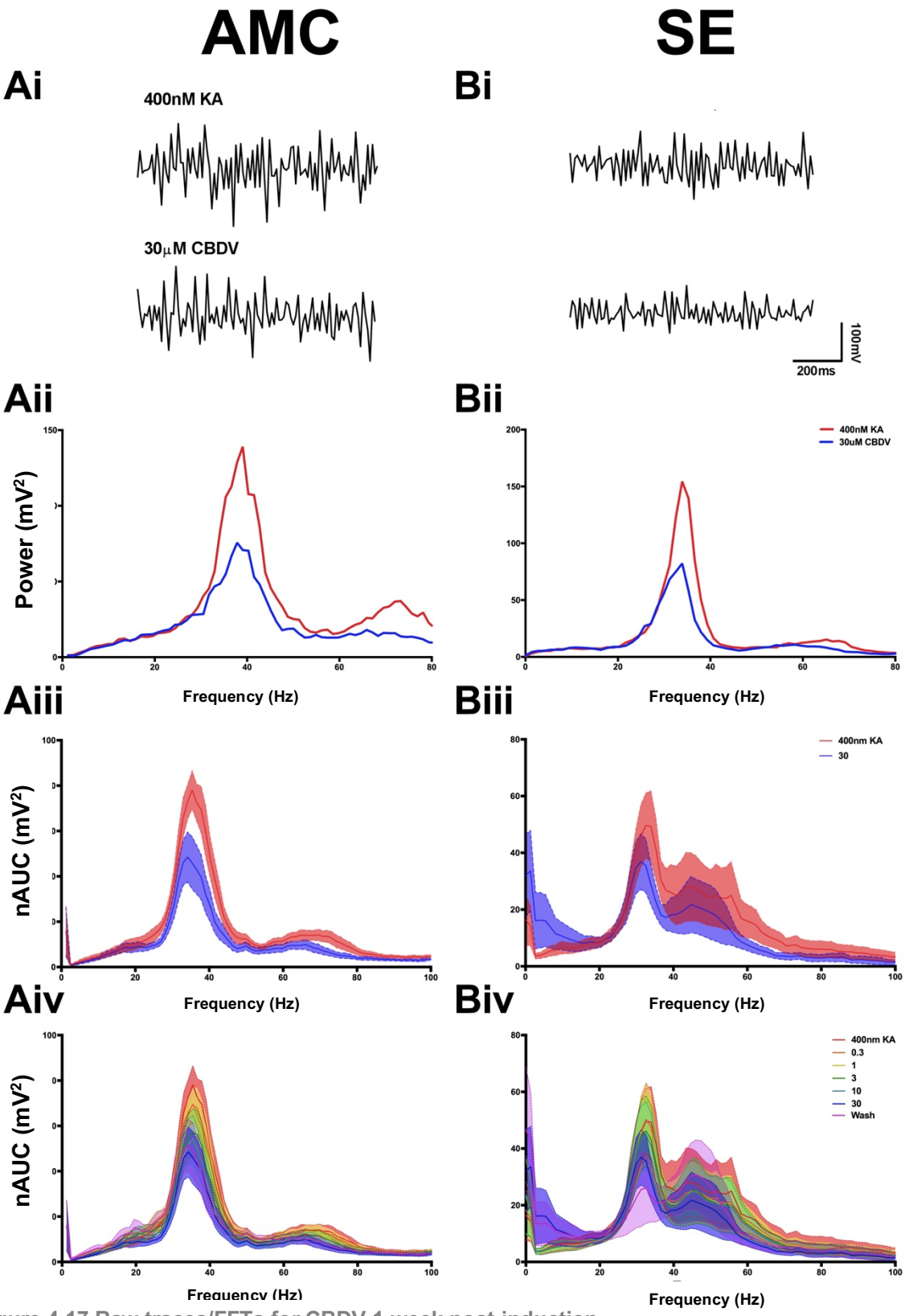

Figure 4.17 Raw traces/FFTs for CBDV 1-week post-induction.
Ai-Bi Representative raw traces of pharmacologically induced gamma oscillations in both AMC (left) and SE (right) rats at 400nM KA and the maximal 30μM CBDV. Aii-Bii A single slice response to the maximal 30μM CBDV addition, for both the AMC (left) and SE (right) rats. Aiii-Biii Normalised FFT displaying the normalised area under the curve (nAUC) for both the 400nM KA and maximal 30μM CBDV for the AMC (left) and SE right) data set, SEM is represented by the coloured fill area flanking the line. Aiv-Biv Normalised FFT data for all CBDV doses applied in AMC (left) and SE (right). Coloured lines and fill refer to: red (400nM KA), orange (0.3μM CBDV), yellow (1μM), dark green (3μM), light green (10μM), blue (30μM), purple (wash).

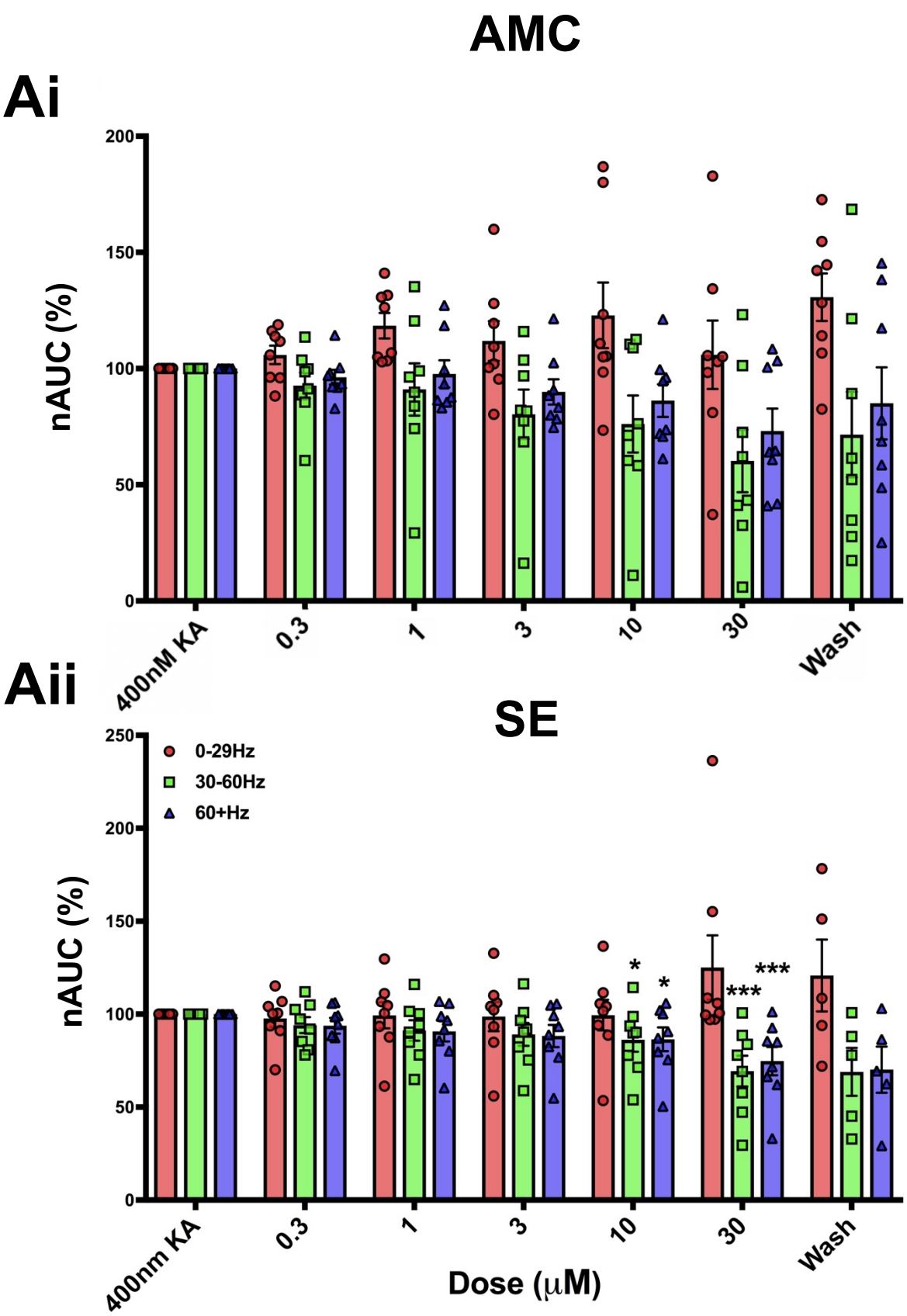

Figure 4.18 Split frequency histograms for CBDV 1-week post-induction.
Ai Split frequency histograms, showing the band specific nAUC response to increasing doses of CBDV plus wash in the AMC condition, with population responses included. Data was normalised, with the 400nM KA response set to 100%. Aii Same histogram data shown for the SE dataset, with population responses included. Legend: low frequency (0-29Hz) - red bars; gamma (30-60Hz) - green bars; high frequency (60-1000Hz) - blue bars. Black capped bars show standard error. *** $p < 0.001$.

The split frequency histogram for the AMC population dataset is displayed in **Figure 4.18.Ai**. Visually there appears to be a trend toward decrease in the higher frequency bands (gamma and 60+ Hz), while there was also a trend toward increase in the low bands as the cannabinoid dose increase. Despite this, there was no significant difference between any of these doses and baseline (400nM KA).

A similar sequence occurs in the SE data (**Aii**), with increasing low frequencies (though no significance was shown) and decreasing gamma and high frequencies corresponding to increasing doses of CBDV. Significance was achieved in both the gamma and high (60+Hz) frequency ranges, at 10μM and 30μM, with a mean of 86.26 ± 6.49 ($p < 0.05$) and 69.34 ± 8.28 ($p < 0.001$) respectively.

With regards to wash step, all bands had a lower mean value, but as there was not an equal number of n in this data repeated measures ANOVAs were unable to be performed.

4.2.5.2 Peak frequency and peak power comparisons

The peak frequency analysis (**Figure 4.19.Ai**) shows the SE population had a higher baseline frequency (37.43Hz ± 2.26) compared to the AMC data (34.88Hz ± 0.70), though this was not significant, it is interesting, as it was similar to the 1-week CBD peak frequency (**Section 4.2.2.2**).

Increasing CBDV doses had little effect of the AMC peak frequency, which remained relatively stable throughout. Indeed, no significance was noted upon any of the drug doses. The SE data was also remarkably stable across all doses, and once more, no significant changes were produced at any CBDV dose.

The peak powers (**Figure 4.19.Aii**) of both conditions trend downward, with the both conditions reaching significance at 30μM. In the AMC data there was relative stability, until a low of 59.36 at 30μM ($p < 0.05$). The SE data reach a value of 73.72 ± 9.89 ($p < 0.001$) at the same dose. The wash step caused an increase in both mean and SEM though again this was only an n of 5 and as such, no statistical analyses were performed due to this lack of n.

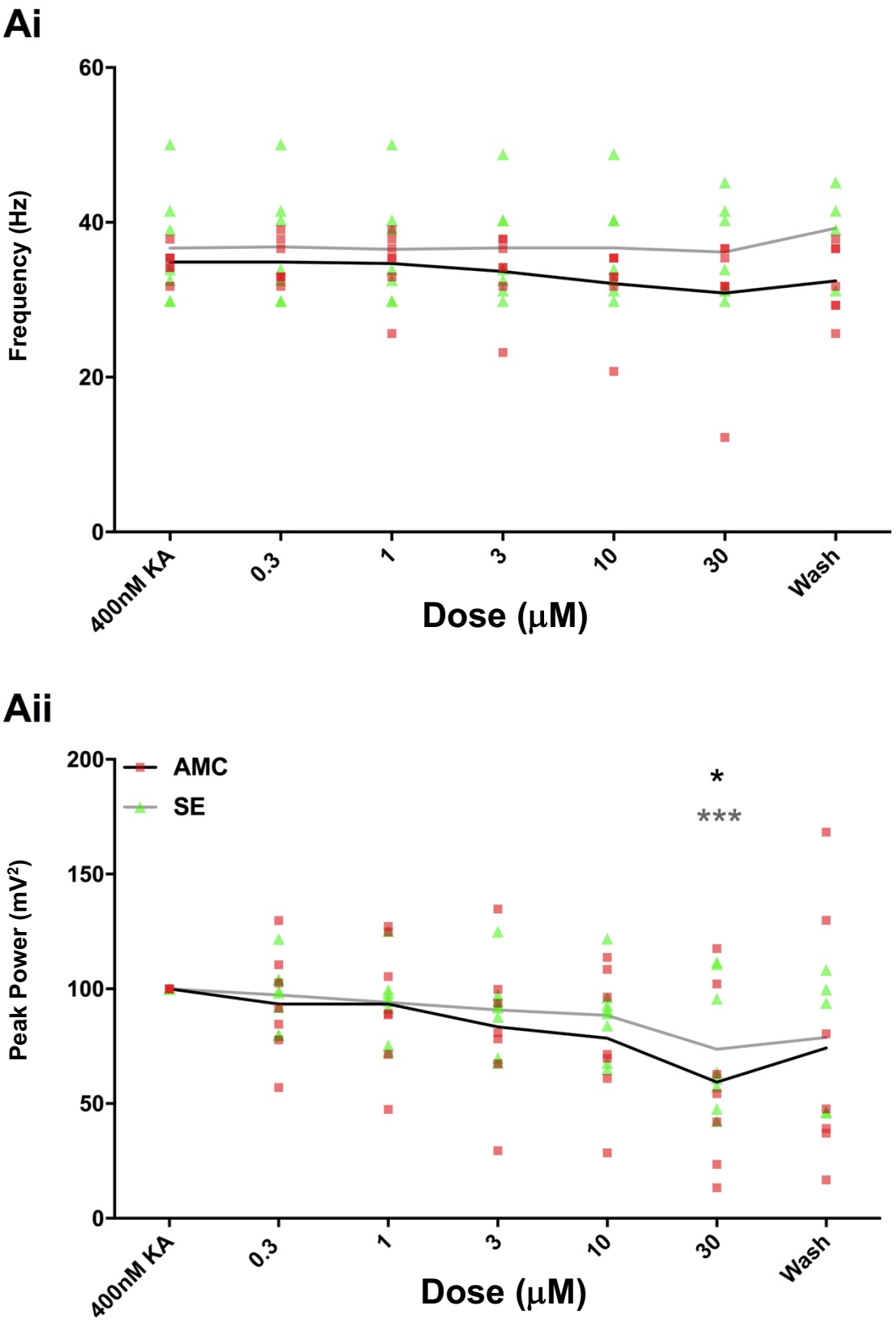

Figure 4.19 Mean peak frequency and power line graphs to CBDV 1-week post induction. Mean peak frequencies for both the AMC (black line) and SE (grey line). AMC (red squares) and SE (green triangles) population frequencies are also plotted onto a line graph. Aii. Normalised peak power responses across the CBDV doses for both the AMC (black line) and SE (grey line). Again, population responses are also plotted (AMC: red squares; SE: green triangles). Significance denoted by black (AMC) or grey (SE) asterisks, * $p < 0.05$, *** $p < 0.001$, black and grey asterisks denote significance (AMC, SE respectively).

4.2.5.3 Peak gamma measurements

The AMC population was determined to have a peak gamma frequency of 35.4Hz, while the SE data was found to be 32.5Hz.

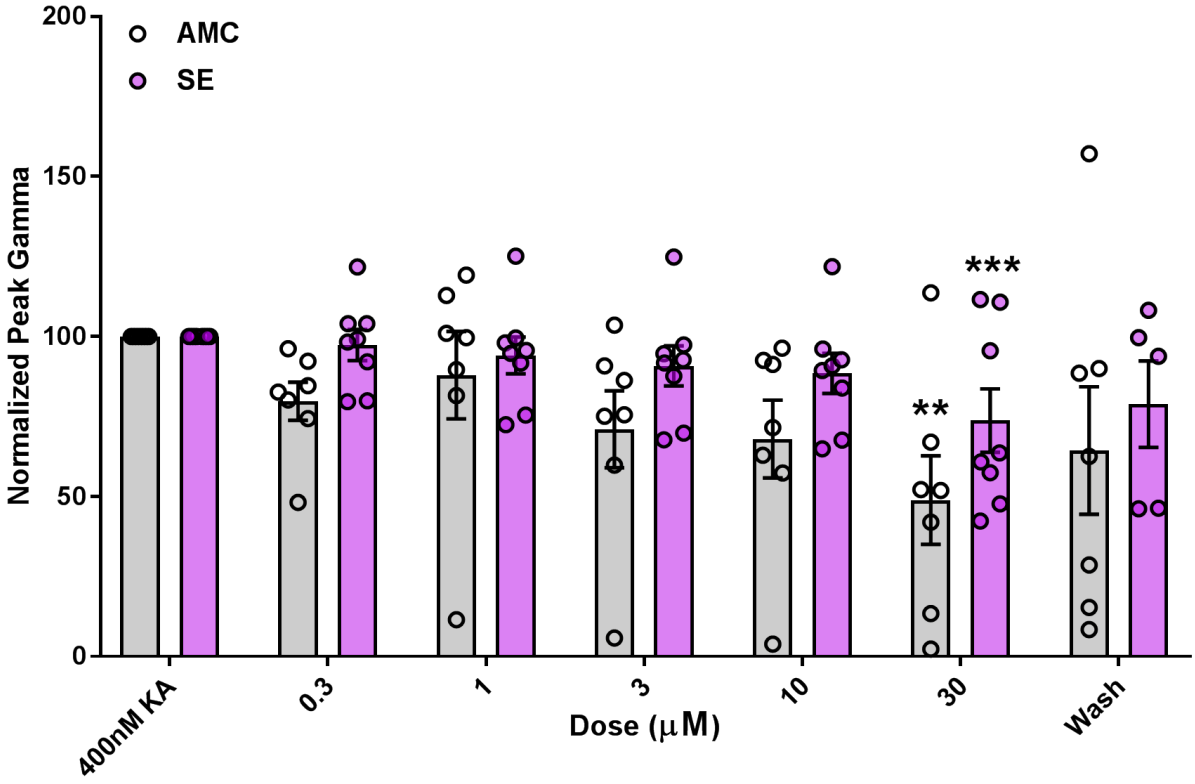

Figure 4.20 Mean normalised peak gamma response to CBDV 1-week post-induction. Each condition is plotted on the same dose point, with AMC in grey and SE in red, with population responses also plotted. Black capped bars show standard error. ** $p < 0.01$, *** $p < 0.001$.

The combined histogram of the peak gamma for both the AMC and SE data is presented in **Figure 4.20**. As can be noted, both AMC and SE populations only showed significant decreases at 30μM CBDV (AMC: $p < 0.01$; SE: $p < 0.001$).

4.2.6 Effects of CBDV on pharmacologically induced persistent gamma on 3-month(+) old AMC and chronically SE rats

As with the CBD results, we were interested in the effect of CBDV on SRS animals, which had a general age of around 3 months. Both AMC and SE populations consisted of 2 animals each, with total n numbers being 8 and 7 respectively (AMC wash step n = 6).

4.2.6.1 FFTs and split frequency histogram analysis

Figure 4.21.Aii-Bii shows single slice response FFTs, the AMC (**Aii**) and the SE (**Bii**) slices both showed a drop in both frequency and power upon maximal CBDV dose application. **Figure 4.21.Aiii** shows the AMC average responses to 30μM CBDV as a normalised FFT. As with the single FFT previously, a decrease in power was evident, though the decrease in frequency does not appear to have endured. The peak frequency (41.5Hz) appeared to be consistent across the doses until the wash step where, alongside an increase in frequency (46.4Hz), the power of the peak was also mostly recovered (mean – 57.29). The full dose FFT (**Aiv**) appeared to show the decrease as dose-dependent.

In contrast to the clear peak observed in the AMC population (**Figure 4.21.Aiii**), the SE data (**Figure 4.21.Biii**) showed another broadband oscillation, again highly suggestive of multiple competitive peaks within the population. The peak occurs at 50.04Hz and, as there was a gradual increase and decrease in the power before and after the peak, it was determined to not be electrical noise. The averaged responses of the SE 400nM KA baseline to 30μM CBDV are displayed in **Figure 4.21.Biii**, where a large decrease in power was observable. Any decrease in frequency was hard to clarify due to the broadband nature of the peak. A dose-dependent decrease was very visible in the full dose FFT (**Biv**), with a gradual decrease in nAUC observed from 0.3μM to 10μM. A larger decrease was noted at 30μM, with a further subsequent decrease shown in the wash.

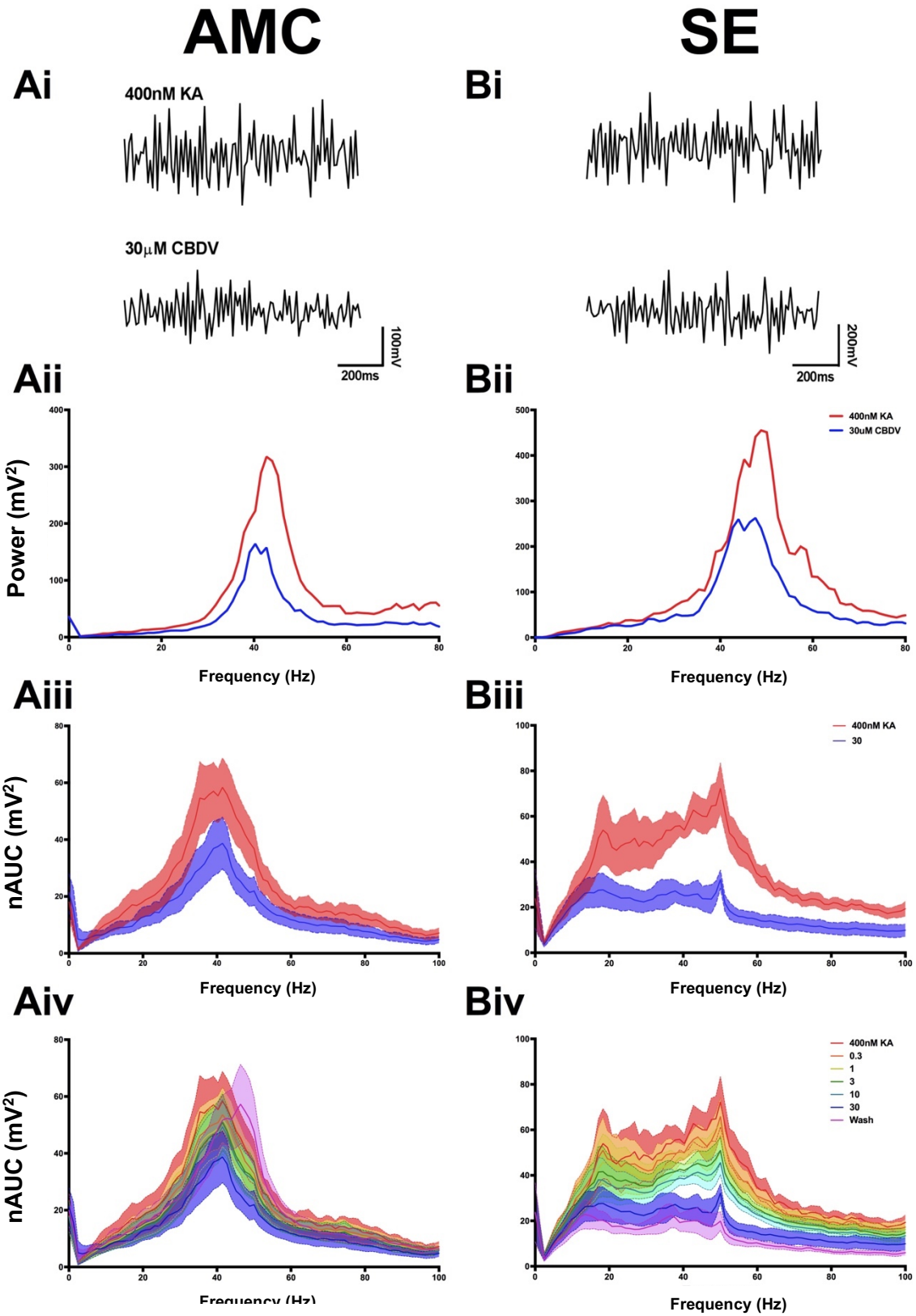

Figure 4.21 Raw traces and FFTs for 3-month conditions.
Ai-Bi Representative raw traces of pharmacologically induced gamma oscillations in both the AMC (left) and SE (right) rats at 400nM KA and the maximal 30μM CBDV. Aii-Bii A single slice response to the maximal 30μM CBDV addition, for both the AMC (left) and SE (right) rats. Aiii-Biii. Normalised FFT displaying the normalised area under the curve (nAUC) for both the 400nM KA and maximal 30μM CBDV for the AMC (left) and SE (right) data set, SEM is represented by the coloured fill area flanking the line. Aiv-Biv. Normalised FFT data for all CBDV doses applied in AMC (left) and SE (right).

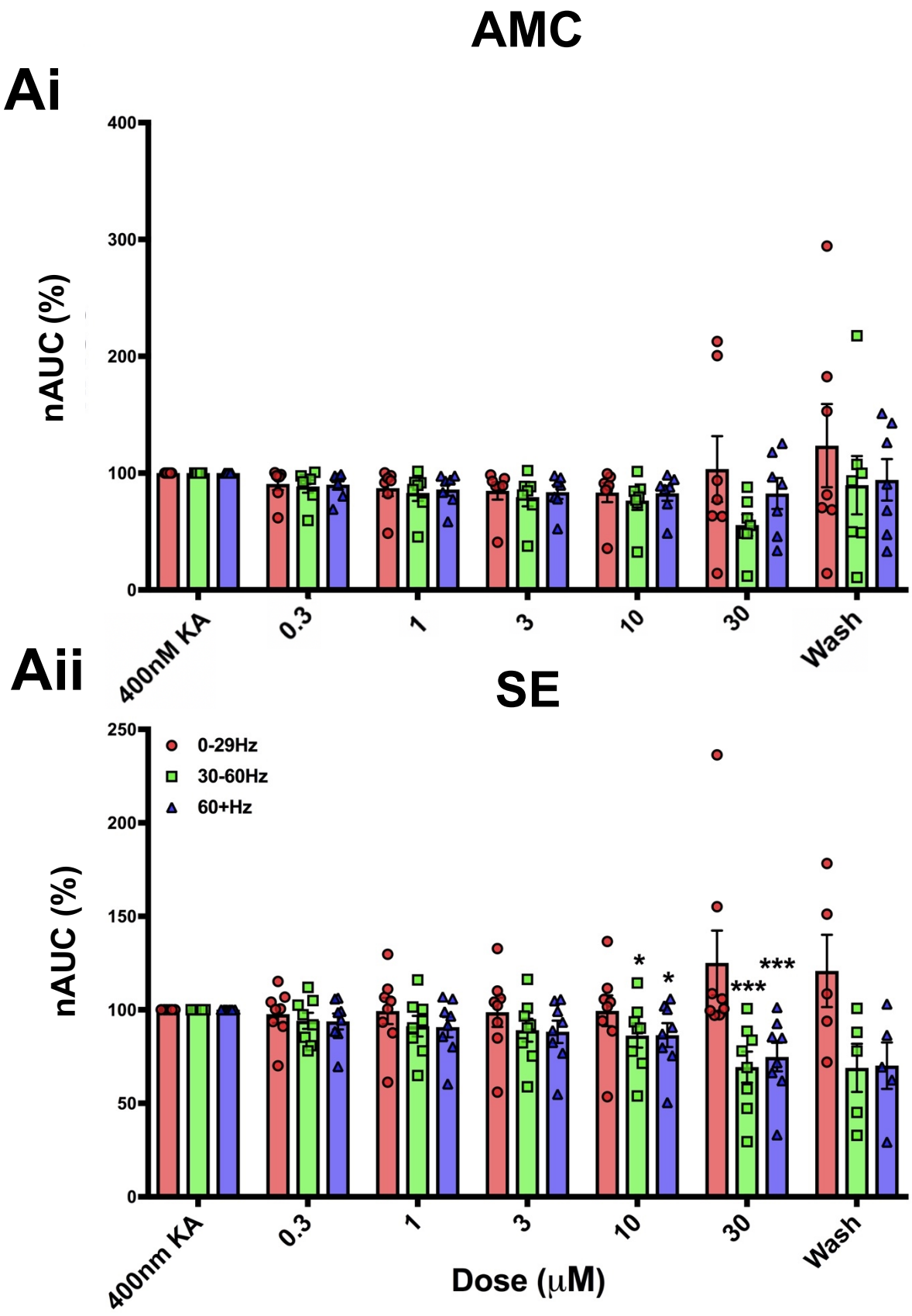

Figure 4.22 Split frequency histograms for 3-month post-induction rats.
Ai. Split frequency histograms, showing the band specific nAUC response to increasing doses of CBDV plus wash in the AMC condition, with population responses included. Data was normalised, with the 400nM KA response set to 100%. Aii Same histogram data shown for the SE dataset, with population responses included. Legend: low frequency (0-29Hz) - red bars; gamma (30-60Hz) - green bars; high frequency (60-1000Hz) - blue bars. Black capped bars show standard error. * $p < 0.05$, *** $p < 0.001$.

Once more histograms splitting the frequencies into designated bands showing the area under the curve (AUC) data after normalisation (nAUC) were produced. The results for the AMC population are presented in **Figure 4.22.Ai**, while the SE in **Aii**. The AMC data showed no significant changes upon the application of increasing doses of CBDV, in contrast to the FFTs previously presented.

This data was remarkably different to that observed in the SE data, where significance was achieved in the gamma oscillatory band at 10μM ($p < 0.05$), with extremely significant decreases at 30μM ($p < 0.001$). The high (60+Hz) band also showed significance at 10μM ($p < 0.05$), enduring into the 30μM CBD ($p < 0.001$). The low frequency band (0-29Hz), meanwhile, displayed no significance at any dose.

4.2.6.2 Peak frequency and power comparisons

The peak frequencies of both conditions are presented in **Figure 4.23.Ai,** which showed the similarity in starting peak frequency between both populations. The AMC animals produced a peak frequency of 41.4Hz ± 2.08, while the SE 38.36Hz ± 3.08, with no significance between the baseline conditions. The appearances of the two lines followed similar trends, with general stability across all doses, the AMC population showed a peak frequency of 39.38Hz ± 1.84 at 30μM CBDV, while the SE had a peak of 35.40Hz ± 4.01. No significance at any of the CBDV additions were observed in either population.

The dose-dependent decrease noted in the SE data is an obvious stand out from the peak power line graph (**Figure 4.23.Aii**), with significant differences noted at 0.3μM ($p < 0.01$), reduced further at 1μM through to the wash ($p < 0.0001$). This trend was not observed in the AMC data, where no significance was noted at the early doses. A large and significant decrease, however, was observed in 30μM CBDV ($p < 0.01$) in the AMC dataset. The wash step plateaus, though due to the loss of n, no statistical analysis could be performed.

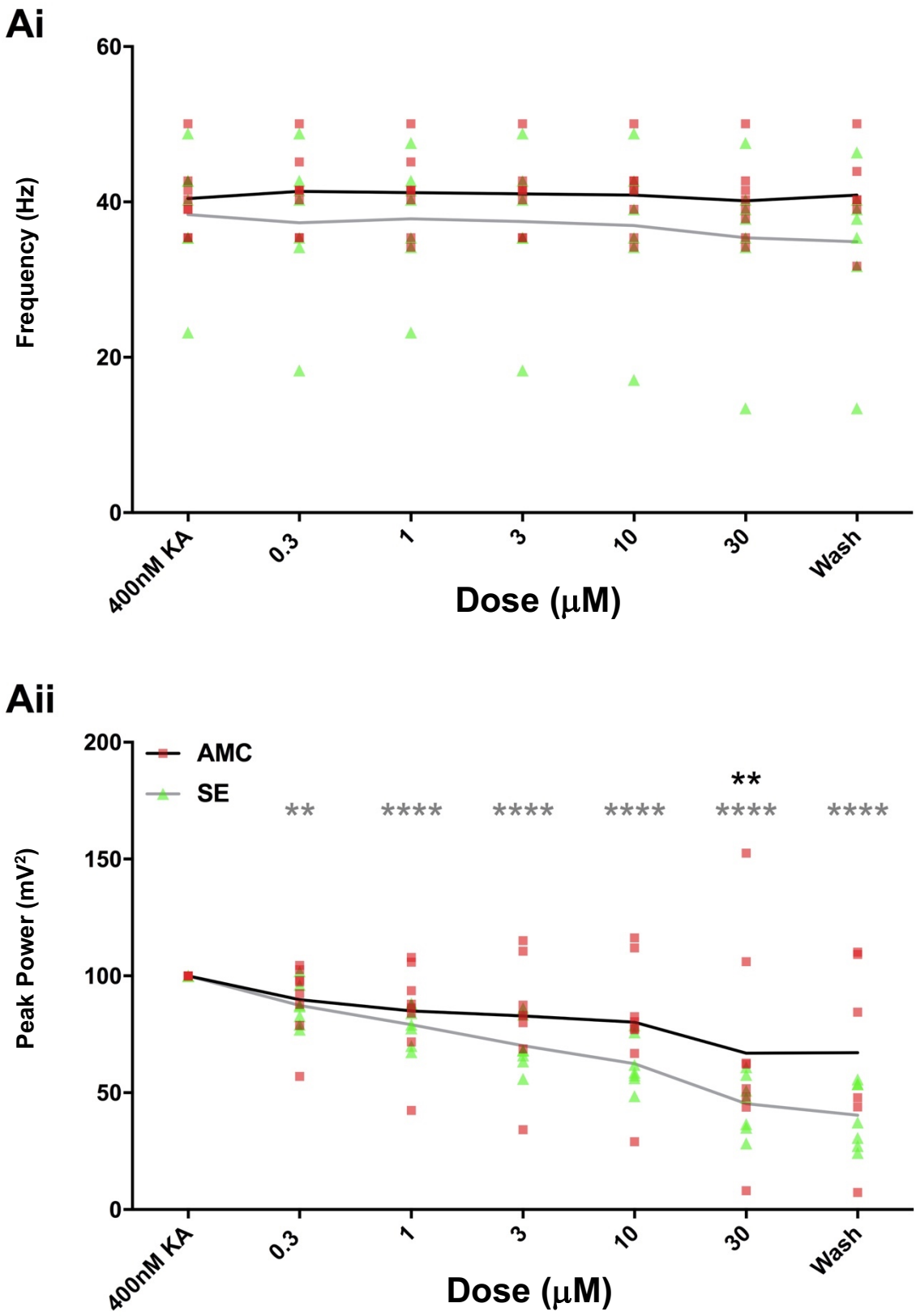

Figure 4.23 Mean peak frequency and power line graphs for CBDV 3-month post induction. Ai Mean peak frequencies for both the AMC (black line) and SE (grey line). AMC (red squares) and SE (green triangles) population frequencies are also plotted onto a line graph. Aii Normalised peak power responses across the CBDV doses for both the AMC (black line) and SE (grey line). Again, population responses are also plotted (AMC: red squares; SE: green triangles). Significance denoted by black (AMC) or grey (SE) asterisks, ** $p < 0.01$, **** $p < 0.0001$, black and grey asterisks denote significance (AMC, SE respectively).

4.2.6.3 Peak gamma measurements

The AMC population was determined to have a peak gamma frequency of 41.5Hz, while the SE data was found to be 50Hz.

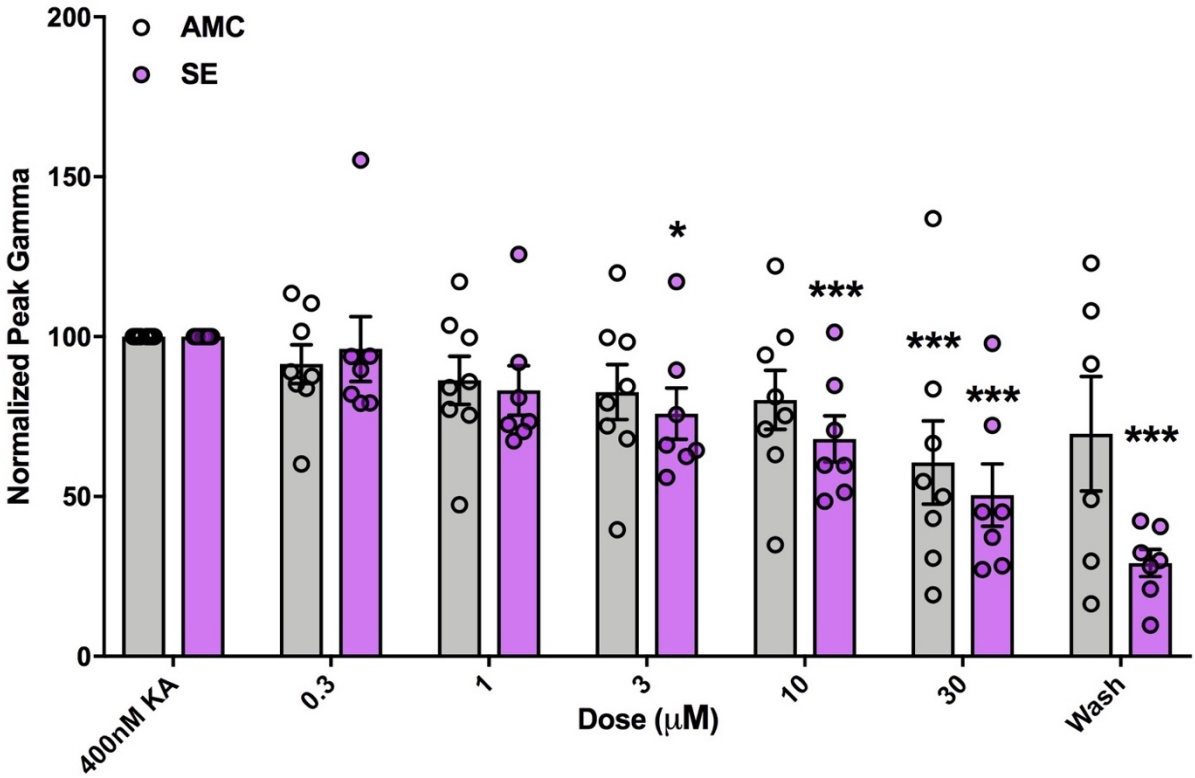

Figure 4.24 Mean normalised peak gamma response to CBDV 3-months post-induction. Each condition is plotted on the same dose point, with AMC in grey and SE in red, with population responses also plotted. Black capped bars show standard error. * $p < 0.05$, *** $p < 0.001$, **** $p < 0.0001$.

The joint peak gamma histogram (**Figure 4.24**) shows the mean, SEM and population response data from both conditions, effectively highlighting the dose-dependent decrease CBDV had on the slices, especially in regards to the SE population. Significance was reached at 3μM ($p < 0.05$), with higher levels of significance achieved at 10μM ($p < 0.001$) which endured through to the wash. In contrast, the AMC data showed significance only at 30μM CBDV ($p < 0.001$).

4.2.6.4 Summary of CBDV effects on gamma oscillations

Table 4.2 shows the overall effects noted on induced gamma oscillations at each of the ages used here, for both AMC and SE animals, when cumulative doses of CBDV were applied. As can be noted, 3-month AMC showed the highest sensitivity to CBDV from the AMC animals, while 3-months SE also showed the highest sensitivity from the SE population, and indeed overall.

Age	CBDV Dose (µM)				
	0.3	1	3	10	30
24-hr AMC	-	-	-	-	-
24-hr SE	-	-	-	-	↓↓↓↓
1-week AMC	-	-	-	-	↓↓
1-week SE	-		-	-	↓↓↓
3-month AMC	-	-	-	-	↓↓↓
3-month SE	-	-	↓	↓↓↓	↓↓↓

Table 4.2 Summary of effects of increasing CBDV doses on the rat used in this section. Ages and condition of animals are noted on the left, with the increasing CBDV doses noted horizontally across the top. The arrows have been used to show the level of significance achieved at that dose (1 arrow = 0.05, 2 = 0.01, 3 = 0.001, 4 = 0.0001), with the direction of the arrow also representing the direction of change in gamma.

4.2.7 Maximal doses of CBD and CBDV effects in similarly aged AMC and SE rats

Once a completed dataset for each age group, condition and, phytocannabinoid used was obtained, comparisons between the two cannabinoids and their comparative effectiveness were made. As such, the responses from the most effective dose, 30μM in the case of both CBD and CBDV, were plotted together in histograms along with a normalised control (baseline) set to 100. This was performed for each age group and each condition (AMC v SE) separately, so drug performance within comparable parameters were plotted together. The histograms produced from these analyses are presented in **Figure 4.25**.

As can be observed in the 24-hour AMC data, neither CBD or CBDV had any significant effect (CBD – 101.4 ± 11.28; n = 6; CBDV – 71.09 ± 18.41; n = 7, respectively). In contrast, both exocannabinoids had significant effects in the SE population, with negligible differences between the two means, though CBDV achieves a higher level of significance (CBD: 64.80 ± 14.30; n = 6; $p < 0.05$; CBDV: 63.90 ± 12.49; n = 7; $p < 0.0001$).

In the 1-week age range, the AMC populations show extreme changes to the addition of either exocannabinoid. CBD caused a highly significant decrease to 37.67 ± 10.89 (n = 7; $p < 0.0001$), while CBDV did also, to 48.92 ± 13.82 (n = 7; $p < 0.01$). In the 1-week SE population, significant decreases were again observed by both cannabinoids, with a CBD induced decrease to 60.06 ± 13.51 (n = 10; $p < 0.001$) and CBDV to 67.74 ± 9.77 (n = 8; $p < 0.001$).

As observed in the 1-week category, both cannabinoids induced extremely significant decreases in the chronic (~3-month old) animals, at 30μM. Both induced highly similar decreases. CBD in the AMC animals caused a drop to 57.44 ± 11.26 (n = 6; $p < 0.001$) and CBDV to 58.78 ± 9.16 (n = 8; $p < 0.001$). Meanwhile, in the SE dataset CBD perpetuated a drop to 45.64 ± 7.85 (n = 9; $p < 0.0001$), while CBDV a similar drop to 50.45 ± 9.75 (n = 7; $p < 0.0001$).

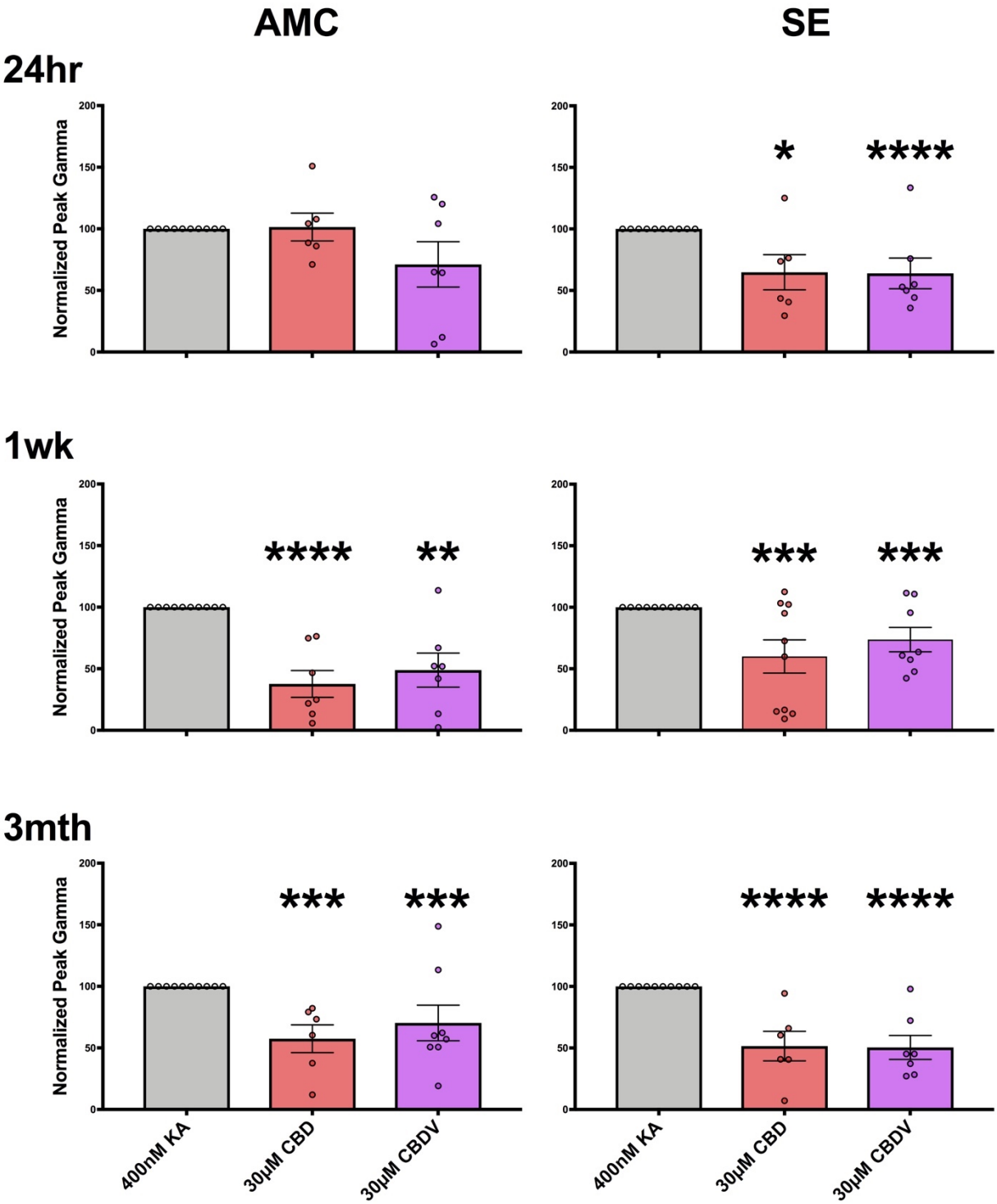

Figure 4.25 Normalised peak gamma responses to maximal 30μM doses of CBD and CBDV. Maximal CBD (red) and CBDV (purple) response shown at each epilepsy condition (AMC left; SE right) and age group (vertically 24-hour, 1-week, 3-months). * $p < 0.05$, ** $p < 0.01$, *** $p < 0.001$, **** $p < 0.0001$.

4.2.8 Comparison of peak gamma power deltas across disease and age populations

To understand whether the differences in sensitivity to phytocannabinoid application across the disease conditions and between the different time points were significant, the peak gamma power deltas for each slice were calculated (the amount of change caused by CBD(V) to the initial value). These were then pooled and statistically analysed using unpaired Mann-Whitney or, Kruskal-Wallis tests, depending on number of variables (Mann-Whitney for comparisons between the two epilepsy conditions, Kruskal-Wallis for comparisons across age range).

Comparing the peak gamma power deltas between the AMC and SE responses to CBD at 3-months, no significant differences were present ($p = 0.82$). This was also true for comparisons at 1-week ($p = 0.36$) and, 24-hours though a trending difference was noted here ($p = 0.07$), unsurprising given the lack of effect noted in the 24-hour AMC population.

In addition, the peak gamma deltas were compared between each of time points, using a Kruskal-Wallis test (unpaired non-parametric test). Here, significance was noted between the AMC responses ($p = 0.0034$), but not between the SE dataset ($p = 0.74$). Again, unsurprising given the lack of effect at 24-hours AMC and then subsequent effectiveness at both 1-week and 3-month time points.

Mann-Whitney tests were again performed for each of the peak gamma power deltas for the CBDV datasets; with the 24-hour AMC and SE comparison showing no significance ($p = 0.71$), as neither did the 1-week ($p = 0.23$) nor 3-month comparison ($p = 0.32$). Comparing the peak gamma power deltas between all of the time points of each population to CBDV, using a Krusal-Wallis test, no significance was returned in either the AMC dataset ($p = 0.47$) or the SE dataset ($p = 0.18$).

4.2.9 Dose-response curves based on peak gamma responses

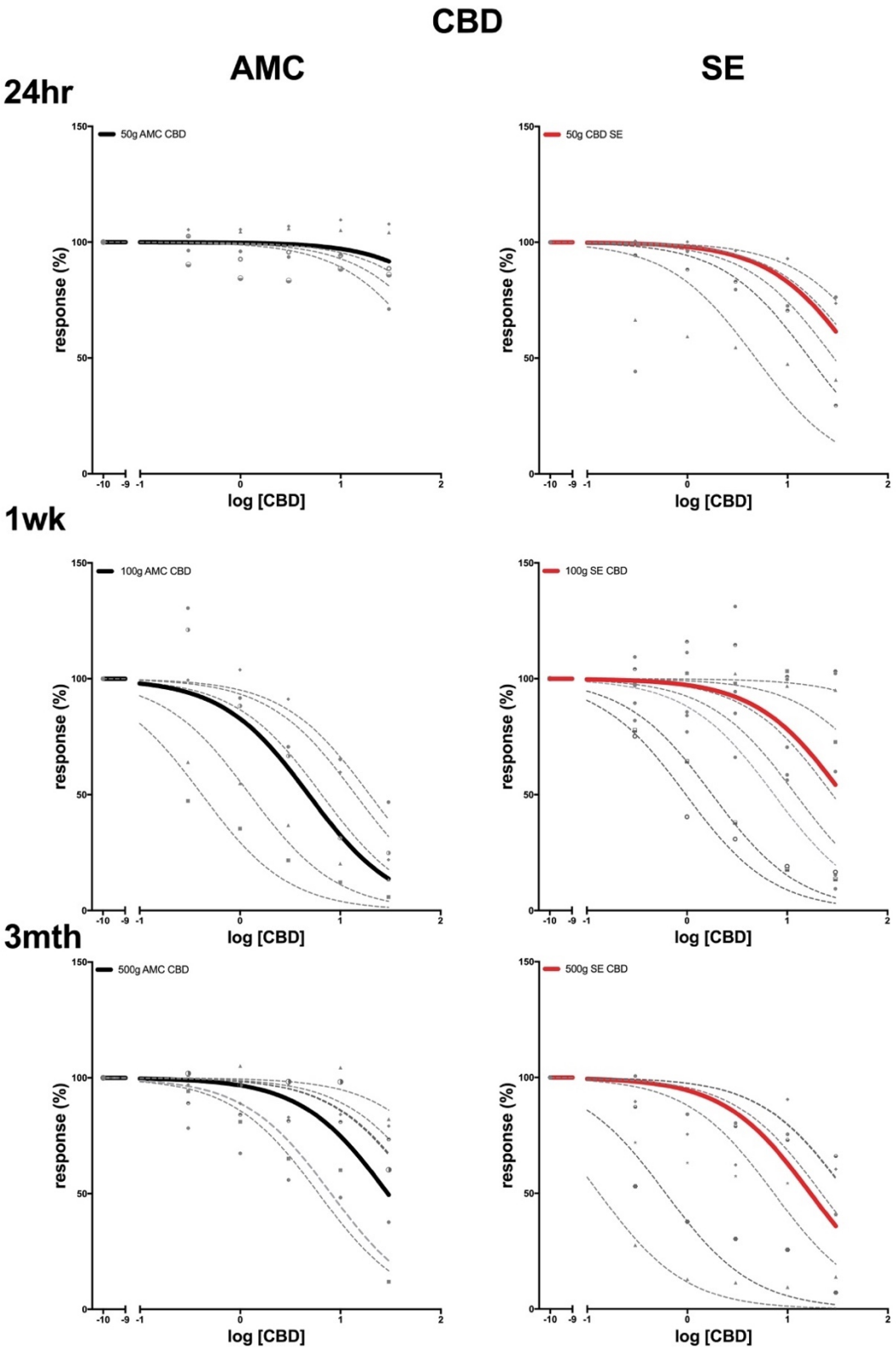

Figure 4.26 Dose-response curves (DRC) of CBD using peak gamma measurements. Responses were only taken from experiments where CBD showed a decrease to peak gamma over the doses. Graphs display individual responses at each dose (symbols; with each symbol type representing a different n) with individual non-linear regression curves for each (grey dashed lines). The overall mean non-linear regression response is represented by either a solid black (AMC) or red line (SE). The n numbers for each are as follows: AMC: 24hrs (5), 1wk (5), 3mnth (6); SE: 24hrs (5), 1wk (9), 3mnths (4).

Figure 4.26 shows the responses to CBD over the dose range for each disease and time condition. This figure shows that both developmental and disease related changes influence the response to CBD. Illustrating this, looking solely at the AMC data no effect was observed at the 24hr age, while large, significant effects were observed in the 1wk time point, indeed the most dramatic response observed. These effects were then diminished at the 3mth/chronic time point, though some sensitivity to CBD remained at the high doses. In contrast, the SE data showed an increasing sensitivity to CBD with development, especially into adulthood (3+ months), as well as effects being initially observed at the 24hr time point.

Comparable analysis was also performed for the CBDV data (**Figure 4.27**), which showed more consistent responses to CBDV in both the AMC and SE data across development. The largest response is in the chronic (3 month) SE population, though all age and disease populations demonstrate similar responses to CBDV.

Data have been omitted from these dose-response curve figures, with any responses that lead to a prolonged increase in gamma oscillations being excluded. This was done so that pertinent information about the suppressant effects of both phytocannabinoids could be extracted. Obviously, the exclusion of data results in an incomplete representation of the cannabinoid effect, which seemed to be somewhat variable from slice to slice.

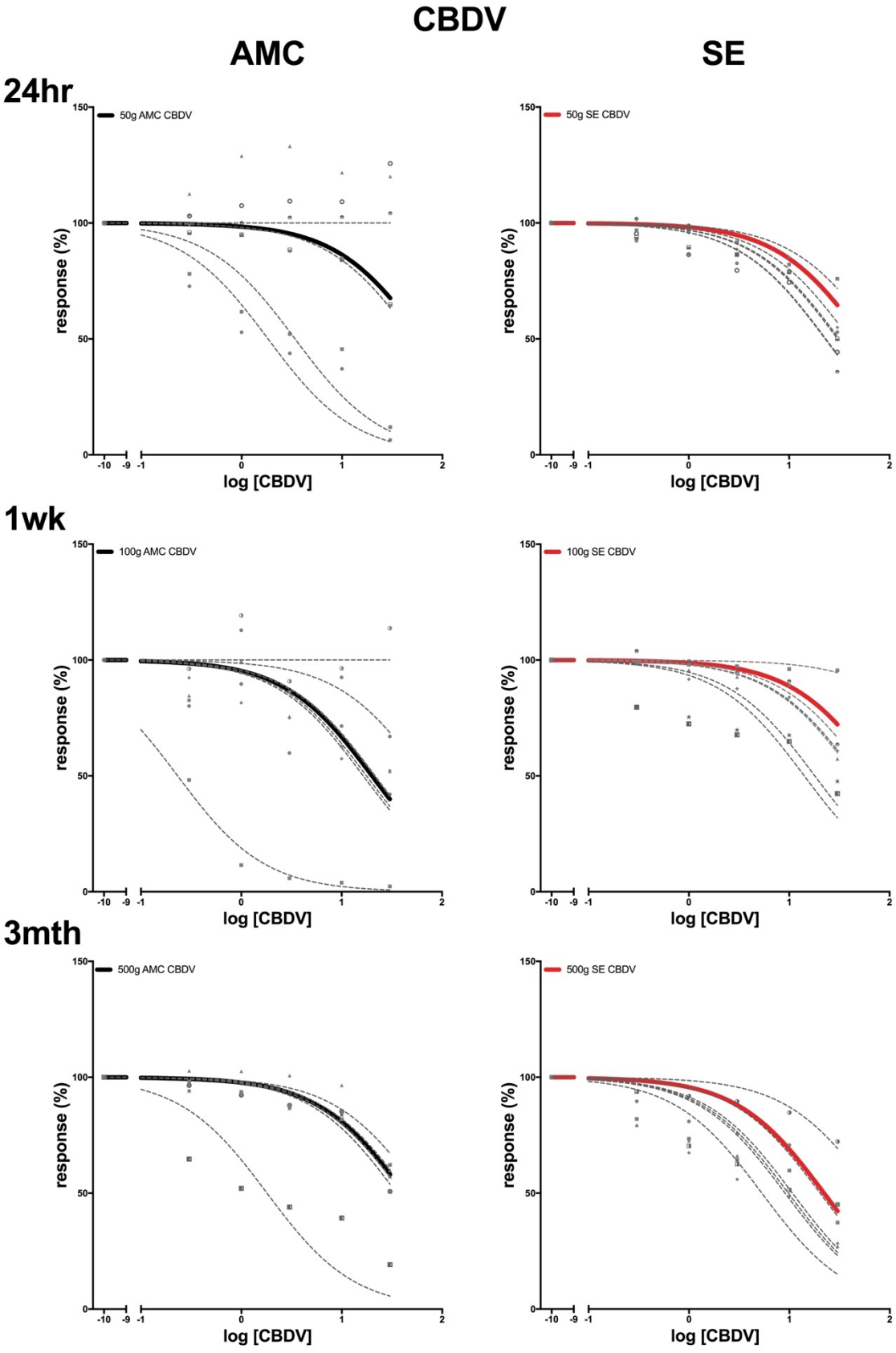

Figure 4.27 Dose-response curves (DRC) of CBDV on peak gamma measurements for both AMC and SE populations.
AMC data is shown with a black solid line indicating the mean non-linear regression response, with the SE as a red solid line. AMC n numbers: 24hr (7), 1wk (7), 3mnth (6); SE: 24hr (6), 1wk (6), 3mnth (6).

4.3 Discussion

Looking at the results presented in the previous chapter as a whole, it is easy to see that both CBD and CBDV have an effect on *in vitro* oscillations in Layer II mEC networks. In this next section some points of key observations are highlighted and discussed.

4.3.1 Benefits of using peak gamma to measure phytocannabinoid effects

The decision to utilise "peak gamma" as a reference of network activity and then as a marker for the effect of exocannabinoids was taken as the previous measures had proven to not display particularly robust results. As mentioned previously, the peak gamma data were as composed of normalised area under the curve (nAUC) readings for the highest frequency point within the 30-60Hz range at 400nM KA (baseline) and then followed at each step in these experiments for each individual slice.

The peak gamma could be interpreted in two ways, either by identifying the highest frequency in the 30-60Hz range for each slice and collating those to give a peak gamma power change at disparate frequencies within the 30-60Hz range or; by collating all the nAUC for each n into a normalised dataset (as had already been performed for the normalised FFT figures) and finding the normalised peak frequency for each age and population. Once identified, the peak frequency nAUC was collected from each separate n and normalised to 100 for the 400nM KA (baseline) result. Changes from baseline across the cannabinoid doses were normalised to this, providing a percentage of 100 for each dose. Once all the data for each separate n, age and condition was amassed, they were averaged within these variables to provide the averages, SEMs and ranges. Statistical analysis was then also performed.

This method was employed as the initial method of splitting the bands into frequency ranges provides an idea of changes across whole frequency sections but lacked the specificity to display changes in the gamma region. Relatively high frequency oscillations, such as gamma, are most effective at synchronising local networks when a defined peak is present, while broadband oscillations are unable to synchronise activity in local networks effectively (Sedley and Cunningham, 2013). Broadband oscillations were observed here in only the SE juvenile mEC networks used for CBD (**Figure 4.1.Biii-iv**). In the CBDV experiments both juvenile networks showed some broadband oscillations in the normalised FFT (**Figure 4.13**), while both the SE adolescent and mature networks did also (**Figure 4.17.Biii-iv**, **4.21.Biii-iv**). As such the peak gamma measurement used here is a useful tool, as it dilutes the effect of these broadband oscillations on CBD(V) effectiveness. By using the peak gamma measure we are able to see discrete and clear effects of CBD(V) in the induced oscillatory band in the mEC.

4.3.2 Ability of CBD(V) to alter the frequency of gamma oscillations

The peak frequency analysis was performed as several of the normalised FFTs showed changes in the frequency alongside a suppression of the power of gamma oscillations. As described the peak frequency (that is, the frequency with the largest power) was collected from each individual slice for each of the cannabinoid doses and then averaged to produce a collective “peak frequency” for each age and disease population.

Notable occasions where a slowing in oscillation frequency occurred included the 24-hour SE (**Figure 4.3.Ai**) and 1-week AMC (**Figure 4.7.Ai**) when CBD was applied. The 24-hour SE showed a slowing in oscillation frequency at the maximal 30μM CBD dose, which remained in the wash step. The 1-week AMC showed a slowing at 10μM CBD enduring through to the wash. CBDV application caused a slowing only in the 24-hour SE condition (**Figure 4.15.Ai**) when 30μM CBDV was applied. Upon each of these occasions, a significant decrease peak gamma power was noted, suggestive of a link between gamma power suppression and peak frequency decrease. This is a fallible conclusion however, as only three of twelve disease/age conditions showed a significant alteration to peak frequency, whereas ten of twelve conditions showed a significant decrease in peak gamma at the maximal 30μM cannabinoid dose. Interestingly, both post-induction 24-hour SE populations show a decrease in frequency upon the maximal dose of CBD(V), which may be linked to changes by the RISE induction.

4.3.3 Possible changes to rat neuronal networks immediately after RISE induction and confirmation of RISE as an epilepsy model

The most interesting results produced by this series of experiments arises when comparing the peak gamma responses in the 24-hour time points (**Figure 4.4** & **4.16**).

Assessing first the peak gamma CBD data (**Figure 4.4**), no effects are present in the AMC data, while a significant decrease was found in the 30μM CBD and the wash steps of the SE population, with a general trend towards dose-dependent decreases observable across the earlier doses too. This is highly suggestive of an effect of the RISE induction process stimulating a change in the expression of potential drug targets of at least the EC, if not more areas of the rodent brain. The differences between the two populations were also clearly visible in

Figure 4.1. These clear differences are perhaps analogous to the human condition of acquired TLE, where initial insults to the head and brain induce seizures or seizure-like events (as the RISE model does in rats) (Modebadze et al., 2016).

CBDV showed no significant changes to the 24-hour AMC rats, similar to the data observed for CBD. CBDV did, however, produce a significant decrease in peak gamma in the SE data.

This result suggests similar effects of CBDV and CBD are present in the recent SE induced rats.

Current collaborative investigations between the host lab and the Henley lab at the University of Bristol are being undertaken to assess protein expression levels at the epileptogenesis time points used here (24-hours, 1-week and, 3-months post-induction) compared to the corresponding AMC expression levels. Preliminary data has suggested significantly altered expression levels of GluN1 in the temporal lobe 24 hours post-induction, with a clear 1.5-fold increase noted in comparison to the corresponding AMC data ($p < 0.05$). Significant decreases of AMPAR subunits GluA1 (40%; $p < 0.01$) and GluA2 (25%; $p < 0.05$), as well as the KAR subunit GluK2 (35%; $p < 0.0001$) are also noted in the hippocampus after 24-hours (unpublished work; see **Appendix 2**). When paired with the peak gamma data from the 24-hour SE animals, this indicates a possible role of GluN1 for the action of CBD(V) in suppression of mEC gamma oscillations.

4.3.4 Age dependent effects of CBD(V)

Further to the last section discussed, obvious changes in CBD and CBDV sensitivity were notable from the first 24-hour time point to the 1-week time point, especially in the AMC data.

As stated the 24-hour AMC data showed no effect of CBD addition, in stark contrast to 1-week AMC data where dose-dependent CBD effects are visible, indeed the most notable of all populations tested here (**Figure 4.5**, **Figure 4.8**, **Figure 4.26**). This distinction lends support to the idea that there are neuronal changes and development between these two time points. Indeed, the brain is still developing at this point, with a recent study suggesting an increase in brain size of 25% from P12 to P24 (Ray et al., 2016).

Specific developmental alterations are noted across a plethora of receptor expressions with excitatory AMPARs, NMDARs, KARs and, mGluRs all shown to differ dependent on developmental time point. For instance, AMPA receptors switch from mainly GluA2-independent compositions to mainly GluA2-containing in rat by the second postnatal week (p14), imbuing an inability to pass Ca^{2+} onto the majority of AMPARs, with all AMPAR expressing synapses noted to express GluA2 by this time point (in rat) (Monyer et al., 1991; Pellegrini-Giampietro et al., 1992). Further changes are noted after this, with a decline in the number of GluA1-containing AMPARs, replaced by GluA3-containing AMPARs occurring by p21, the arrival of which most likely causes the increase duration in AMPAR response and postsynaptic excitability, as GluA3-containing AMPARs are noted for displaying decreased deactivation and desensitisation (Suzuki et al., 2008; Blair et al., 2013). KARs have also been shown to change depending on the maturity of the brain, with for instance, the Q/R editing of KARs shown to be dependent on developmental regulation (Chittajallu et al., 1999). Further to

this, there is also evidence of stunted excitatory mechanisms in general across juvenile brains (Kleckner and Dingledine, 1991).

These instances are but a small fraction of the known changes in receptor expression with maturity in the specific time point we are looking at and, as such, complex biochemical experiments would be required to locate the target of CBD(V) here. By assessing known interactions CBD(V) have with any of these receptor systems, however, we are able to narrow down possible targets. Indeed, later in this report, we demonstrate CBD interactions at NMDARs. A multitude of alterations in NMDAR expression and function are noted during development, for instance, overexpression of NMDARs in the hippocampus, overexpression of recurrent collateral excitatory synaptic connections and, increased contribution of NMDARs to postsynaptic responses in the neocortex have all been found in juvenile animals (Hamon and Heinemann, 1988; Tremblay et al., 1988; Jones and Heinemann, 1989; Burgard et al., 1990; Luhmann and Prince, 1990; Swann et al., 1993). Furthermore, there is evidence that juvenile NMDARs may display a lower Mg^{2+} sensitivity then that of adult animals (Bowe and Nadler, 1990; Kleckner and Dingledine, 1991). In addition, there is a noted switch in NMDA subunit composition with development, from NR2B to NR2A, thought to be indicative of synaptic maturity, related to neuronal activity and experience (Monyer et al., 1994; Sheng et al., 1994; Sans et al., 2000). This switch in subunit composition is linked to the mechanisms of synaptic plasticity, though the exact nature of this relationship remains controversial (Liu et al., 2004; Bartlett et al., 2007; Morishita et al., 2007; Xu et al., 2009). It is possible that any of these changes in NMDA expression may contribute to the age-dependent effects of CBD(V) observed here. Possible links may occur indirectly through interactions between cannabinoid receptors (CBRs) and NMDARs (Sánchez-Blázquez et al., 2013; Rodríguez-Muñoz et al., 2016), or via direct binding at the NMDARs, though there is currently no concrete evidence for this. These possible CBR-NMDAR interactions, when combined with recent research postulating that CBD may act as a high affinity negative allosteric modulator (NAM) at CB1R, may help explain the actions of CBD(V) as either or both of these exocannabinoids could be interacting at NMDARs, directly or indirectly, to modulate excitatory or inhibitory synaptic transmission (Xue et al., 2011; Laprairie et al., 2015).

Aside from the clear and obvious differences within the AMC data, the SE data showed only a slight change (with 10μM CBD now enough to elicit a significant decrease in oscillatory power) from 24-hour to 1-week (**Figure 4.8**). The differences between the two populations were also interesting, as stated there was a slight increase in the CBD sensitivity in the SE data, while the AMC showed a large increase in sensitivity. This again lends support to the neuronal rewiring through epilepsy induction, as if the networks have been altered via the RISE induction, they have remained that way through to one week (or are continuously developing) and, as such, the dramatic dose-dependent decrease seen in the AMC data was not observed

in the SE data, with only a slight increase of the 24-hour effect observed. The 3-month populations showed, again, apparent heightened sensitivity to CBD in the SE data, with significant decreases to oscillatory power observed at 1μM, while the AMC data does show a trending dose-dependent decrease, though significance was only displayed at 30μM (+ wash). These changes in response may correspond to alterations in benzodiazepine (BZ) site expression and function early after SE induction, as $GABA_A$Rs are noted as displaying large changes after SE induction. Indeed, a decrease in BZ efficacy has been noted in some forms of TLE and is commonly observed in DRE. Causes for this are namely thought to be a loss of BZ sites, with previous studies in humans showing the loss in BZ sites was greater than the loss of neurons in sclerotic area (Savic et al., 1988; Hand et al., 1997; Koepp et al., 1997). Furthermore, other publications have demonstrated BZ sites that display decreased affinity, with PET studies showing areas with BZ site deficient $GABA_A$Rs as an indicator for epileptic foci (Ryvlin et al., 1998; Bouvard et al., 2005).

In pilocarpine induced SE rodents, 24 hours post-SE isolated DG cells displayed decreases in mRNA expression levels for $GABA_A$ subunits α1 and β1, while the α4, δ, and ε subunit mRNA levels were increased, with these changes remaining apparent through to chronic stages (defined as 1-4 months here), with reductions in zolpidem efficacy also noted (Brooks-Kayal et al., 1998). *In situ* hybridisation analyses of CA3 neurons were in agreement with this, showing depleted α1 mRNA subunit expression (Friedman et al., 1994). Conversely, flumazenil binding studies displayed increase binding efficacy at 24 hours post-SE across all hippocampal regions, which subsequently decreased in some areas with progression into the chronic period, though here a KA model of epilepsy was used (Vivash et al., 2011). Other reports show similar mIPSC levels at 24-48 hours and 3-5 months post-SE, with a limited sensitivity to diazepam at 24-48 hours and, a loss of diazepam sensitivity at 3-5 months in DG cells. Despite this, modulation by flumazenil remained constant in both time points, though in this model of epilepsy no seizure cessation drugs were applied (Leroy et al., 2004). Latent period studies of the BZ site in DG neurons, show an initial decrease in mIPSC amplitudes (6-8 days post-SE), which later recover, though become insensitive to zolpidem, with a trend towards decrease in γ2 expression at 4 days noted, which subsequently increases significantly at 60 days post-SE; a similar pattern is noted in α4 subunit expression also, though the rise was noted as early as 30 days here (Cohen et al., 2003; Peng et al., 2004).

Work completed later in this project (**Chapter 6**) shows a role for the BZ site in CBD effectiveness, with CBD possessing similar qualities to those of BZ site agonists. From this published work, however, it appears as though affinity of the BZ site, to BZ agonists at least, decreases as time from induction increases, whereas CBD displays the opposite effect, with its sensitivity increasing as epileptogenesis progresses, more similar to the apparent effectiveness of the BZ site inverse agonist flumazenil, suggested in Cohen et al, (2003).

Indeed, the early change in subunit expression from α1 to α4 would suggest a loss in the number of BZ sites present, which are classically located at the interface between α1γ2 subunits. CBD is not binding to the BZ site directly to deliver its effects (Bakas et al., 2017), though its blockade does have a negative effect on CBD, suggesting there is a requirement for the BZ site to be unimpeded for CBD to produce its effects.

Taken together, these results suggest a bell-shaped efficacy of CBD in AMC animals with age, where no effects are noted in juvenile animals (~p19), peak sensitivity at 1-week in AMC animals (~p26), which diminishes somewhat with maturity, though to state with certainty more n numbers would be required. The SE data meanwhile, was suggestive of increasing sensitivity to CBD with age, with limited significance observed early, increasing efficacy at 1-week post induction, and a very high sensitivity in the chronic animals. Statistical comparisons between the disease conditions using an unpaired Mann-Whitney test showed no significance in CBD sensitivity, however comparisons between all time points in the AMC population, using the unpaired non-parametric Kruskal-Wallis test, showed significance. This is indicative of a time/age dependent effect of CBD, with increased sensitivity at adolescence and in mature networks. The lack of significance in the SE dataset was unsurprising, as significant decreases were noted in the 24-hour population upon maximal CBD dose, and suggests that the initial epileptic insult was sufficient for CBD effectiveness.

Significant differences were noted in age related responses to CBDV, with what appeared to be an increase in sensitivity in the SE population from both the 24-hour and 1-week responses, to the chronic 3-month responses, most likely explained by neuronal alterations due to epileptogenesis in the SE population. The AMC data only showed response to CBDV at the maximal dose in adolescence and maturity, though albeit with a higher significance at the mature age, which was most likely due to the full maturation of the neuronal circuits. The comparisons of the peak gamma power deltas, however, showed no significant differences in either the time point comparisons or the disease comparisons for CBDV application.

Further to this, the collaborative protein expression data showed significant decreases in GluA2 ($p < 0.05$), GluK5 ($p < 0.01$) and, GluN1 ($p < 0.01$) in the temporal lobe (TL) in the 1-week time point, with significant decreases in GluA1 ($p < 0.0001$) and GluK5 ($p < 0.05$) still present in the hippocampus. At the 3-month time point a significant decrease in the TL was shown in the expression of GluA1 ($p < 0.0001$), with the significant decrease in GluA1 ($p < 0.0001$) still present in the hippocampus (unpublished work; see **Appendix 2**). This work highlights some of the effects epileptogenesis is having on neuronal networks and synaptic reorganisation within the TL and hippocampus, thought to play a pivotal role in the development of TLE (Sutula et al., 1989; Lee et al., 2007). When all time points are observed clear roles for each of the ionotropic glutamate receptors are noted. An immediate

downregulation in the expression of GluA1 is shown upon the induction of SE, while a similar downregulation in the TL is only present upon SRS, raising the possibility of the loss of GluA1 being vital for seizure initiation, onset and spread, which is in agreement with other studies, with GluA1 downregulation noted in medial TLE (Sutula et al., 1989). GluA2 is only downregulated in the latent period for the TL, while in the hippocampus SE induction causes its downregulation, here previous studies show agreement with GluA2 downregulation noted upon initial insult (Lorgen et al., 2017).

The KAR subunit GluK5 is only downregulated in the latent period in both the hippocampus and the TL, suggesting a role in seizure generation, which is also concurrent with work showing GluK5 antagonists as being anti-convulsant in pilocarpine-induced epilepsy studies (Smolders et al., 2002). GluK2 is downregulated in the hippocampus immediately upon SE induction, though may be due to neuronal or synaptic damage incurred by the insult. GluN1 downregulation is noted only in the TL and only initially after SE induction, alongside the downregulation of AMPAR and KAR subunits previously described. It may be possible that these downregulations act as a compensatory decrease in excitation following seizure initiation to induce the latent period, with an increase in excitatory receptor subunits incurring SRS generation and chronic epilepsy.

Expression levels of the pre- and postsynaptic markers, synaptophysin and postsynaptic density 95 (PSD-95), were explored at each of the time points. No changes are noted in either in the TL until a significant decrease in PSD-95 noted in the mature, chronically SE animals ($p < 0.05$). In the hippocampus immediate significant decreases in PSD-95 were noted in the juvenile brain upon SE induction ($p < 0.01$), which remained in the adolescent animals ($p < 0.05$), no changes to synaptophysin were noted in either the juvenile or adolescent ages. At the 3-month time point a reversal was noted, with a large increase in the expression of PSD-95 noted (roughly a 3-fold increase; $p < 0.05$) while a significant decrease in synaptophysin was observed ($p < 0.001$). These differences are suggestive of a large increase in the number of postsynaptic elements, but a fall in the number of presynaptic elements in the hippocampus upon chronic epilepsy establishment. No changes to the presynaptic number were noted in the TL though a significantly lower number of postsynaptic boutons is noted at the chronic stage. Both of these alterations are suggestive of RISE induced neuronal rewiring in both the hippocampus and TL. These changes could relate to the higher significance of gamma suppression noted at the chronic time points presented here.

4.3.5 Disease condition dependent effects of CBD/V

The differences between the AMC and SE populations and cannabinoid effectiveness in each disease condition, showed the largest differences occur in the early age groups (24-hour). As

mentioned the CBD data showed a clear difference between the two, with no changes at all present in AMC data due to CBD, while there was a decrease which achieves significance at 30μM in the SE data, suggesting an increase sensitivity to CBD is caused by a RISE induced change.

In the CBDV data, in the AMC data of the 24-hour group, no significance was achieved. In the SE data a significant decrease was found at 30μM, again highly suggestive of a RISE induced change in CBDV responsiveness.

4.3.6 CBD v CBDV effectiveness

Comparing the effect of maximal CBD(V) doses (**Figure 4.25**), a larger variance in CBD response was notable, whereas CBDV appeared to produce a generalised decrease. This was also highlighted when observing the DRC results produced in **Figure 4.26** & **4.27**.

Looking initially at the AMC data, the lack of significance both cannabinoids showed suggests that the drug targets responsible for the suppression of gamma noticed in later AMC time points have not yet been established. Comparing the two phytocannabinoid responses at 1-week AMC highly suggests either a differing mechanism of action or different affinities for the target, due to the disparity in gamma suppression each achieves. Both CBD and CBDV are similarly effective at gamma suppression in the mature (3-month) AMC population, indicating the target for each is fully established by this time point. The decrease in effect between CBD treatments between the 1-week and 3-month time points raises an interesting question about the nature of mEC network change between adolescence and maturity in terms of CBD binding targets.

The SE responses suggest an increasing sensitivity to CBD once more, with gamma suppression increasing as evidenced by the peak gamma responses, though comparison of the deltas contradicts this somewhat. CBDV, on the other hand, delivers a more consistent decrease in peak gamma, with the 24-hour and 1-week populations showing similar values. The 3-month SE population does provide a slightly lower peak value, and one that is similar to that provided by CBD under comparable conditions.

4.4 General conclusions and future work

Here we have successfully shown that both CBD and CBDV are able to significantly suppress gamma oscillations in mEC layer II neuronal networks in adolescent and mature AMC rats *in vitro*, though not in juvenile rats. Beyond this, we have also shown CBD and CBDV as able to suppress gamma oscillations in all age ranges of rats tested using a maximal dose of 30μM. Moreover, we have shown that CBD especially is able to act in a dose-dependent manner in adolescent and above AMC and SE rats, with striking effects observed in the SE animals.

Taken together the above data suggests an age and disease dependent mechanism of action for CBD, though maybe not CBDV.

Future experiments could involve performing receptor mRNA screening across our defined time points, further to the protein expression work already carried out, to highlight temporal protein expression profiles that match, or are similar to, the relative effectiveness of CBD(V). Particular focus could be given to both $GABA_AR$ and NMDAR subunits, due to their importance in the development and maturity of the brain and, their significance in TLE and possible role in CBD(V) MOA. In addition, double label immunocytochemistry could be performed to investigate the effect of RISE model and CBD(V) on mEC GABAergic neurons in controlling rhythmogenesis.

Chapter 5

The effect of CBD(V) on single cell currents using voltage-clamp electrophysiology

5.1 Introduction

In response to the initial LFP data, we determined to focus investigation on the age-range where the differences in the effects of CBD were most pronounced, specifically, the time between 24-hour post induction (p19) and 1-week post induction (p26).

5.1.1 Whole-cell voltage clamp

The historical gold standard technique for investigation of inhibitory synaptic function has been whole-cell voltage-clamp. Hence, alongside the LFP experiments, we also investigated the response of individual mEC Layer II principal neurons to CBD and CBDV, employing the use of both spontaneous inhibitory post-synaptic currents (sIPSCs) and spontaneous excitatory post-synaptic currents (sEPSCs). No discrimination between p19-p26 animals has been made for the experiments performed throughout the rest of this project.

As discussed in the Methods and Materials chapter (**Chapter 2**), using the voltage-clamp method of whole cell patch clamp electrophysiology allowed observation of the postsynaptic currents and any alterations made by the application of either CBD or CBDV.

5.1.2 Human tissue whole-cell voltage-clamp

As well as testing rat responses, through collaboration with Birmingham Children's Hospital, we were able to obtain and test human tissue, resected from children with severe refractory epilepsy where surgery is the only treatment option. This tissue was obtained immediately upon resection and was then processed in exactly the same manner as the rat tissue – though a choline based aSCF was used to allow standardisation of protocols across all human tissue laboratories across the UK (detailed more thoroughly in **Chapter 2**).

Usually this tissue was resected from the frontal or temporal lobes of the patients, with common epilepsy types being frontocortical dysplasia and temporal lobe epilepsies as detailed in the methods section above. In patch clamp experiments on both rat and human tissue, slices were visualised using IR-DIC optics and principal neurons with a pyramidal morphology and smooth membrane appearance were selected. All recordings were made using similar pipettes pulled from borosilicate glass and filled with a standard solution.

5.2 Results

5.2.1 Rat sIPSC responses to CBD

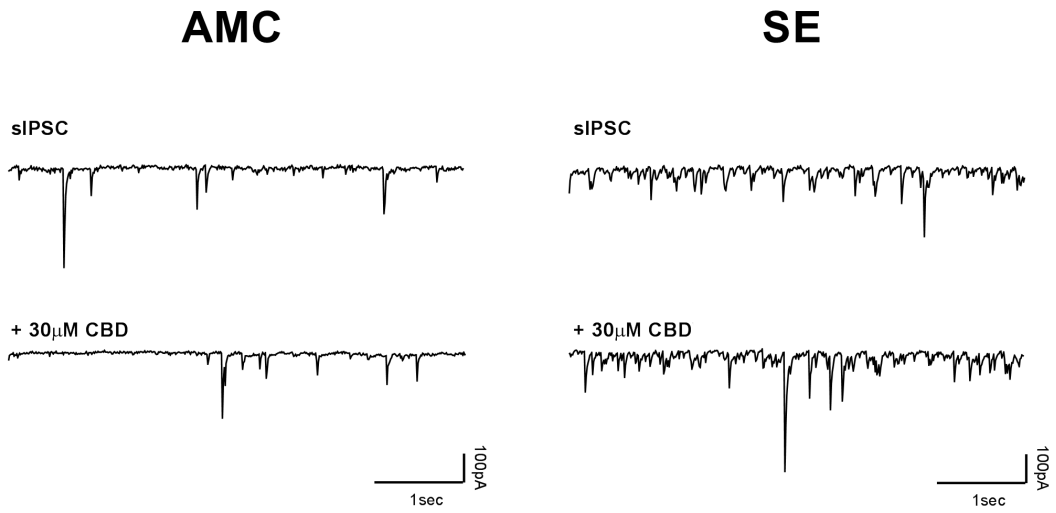

Figure 5.1 sIPSC raw traces before and after 30μM CBD addition
Representative raw traces taken from AMC (left) and SE (right) rat populations, before and after CBD addition.

Our first voltage-clamp experiments were to investigate the effect of CBD on both AMC (n = 12; animal n = 9) and SE (n = 26; animal n = 19) populations, to observe any differences in responses of mEC Layer II pyramidal cells between the two conditions in p19-26 animals.

Figure 5.1 shows two representative traces for each of the AMC and SE populations. There is visually a difference apparent between the two disease conditions in the sIPSC control condition (baseline), with a higher frequency of sIPSCs noticeable in the SE trace. Upon the addition of CBD, there is little change visually in the AMC population, though in the SE population a slight increase in IEI and amplitude looks to have occurred. As these are representative traces and not averaged traces, little information can be truly posited from these figures alone.

Further analyses of these experiments are presented in **Figure 5.2**, with each AMC histogram presented on the left, and SE correspondingly on the right. **Ai** and **Bi** highlight the mean median amplitude (pA) for each condition in the control sIPSC and 30μM CBD. Looking first at the AMC data (**Ai**), no change in mean median amplitude was observed (29.9 ± 9.28 – 34.8 ± 11.5; p = 0.11). The range for these data remained relatively consistent (9.0-126.3; 9.64-132.5). Similarly, the SE population (**Bi**) displayed no change in mean median amplitude (26.8 ± 2.29 – 29.8 ± 3.12; range: 9.74-53.8; 11.2-73.2; p = 0.12).

The next parameter presented is the mean median IEI (ms) in figures **Aii** and **Bii.** The AMC data (**Aii**), showed no change in IEI (112 ± 17.8 – 120 ± 25.1; p = 0.54; range: 56.9-233; 38.9-

262). In contrast, a significant decrease in mean median IEI was present in the SE data (77.8 ± 6.59 – 71.9 ± 5.73; 35.5-166; 32.1-146; p = 0.022).

Aiii/Biii presents the mean median decay time (ms) for each population. **Aiii** shows the AMC data, which displayed no change in decay time upon CBD addition (8.99 ± 0.97 – 9.20 ± 1.06; p = 0.39; range: 5.40-18.1; 4.5-19.1). In contrast, a significant increase was observed in the SE population decay time upon CBD addition (8.62 ± 0.5 – 9.30 ± 0.68; range: 4.0-14.9 to 4.30-19.9; p = 0.045).

Finally, the NICT values are presented in **Aiv/Biv**. In **Aiv**, the AMC data showed no change upon CBD addition, with a mean value of 115 ± 12.4 (range: 50.3-179), which produced a p value of 0.27. In contrast, the SE dataset (**Biv**) showed a significant increase in NICT upon CBD application, returning a mean value of 131 ± 11.7 (range: 31.7-727; p = 0.012). The 727 value looks to be an anomalous result, however the values it provides for each of the other parameters are within the normal range set by the other responses here. Inclusion of this result in this statistical analysis does not alter the p value drastically (0.012 when included, 0.02 without) and, therefore, it has been kept in the analysis pool.

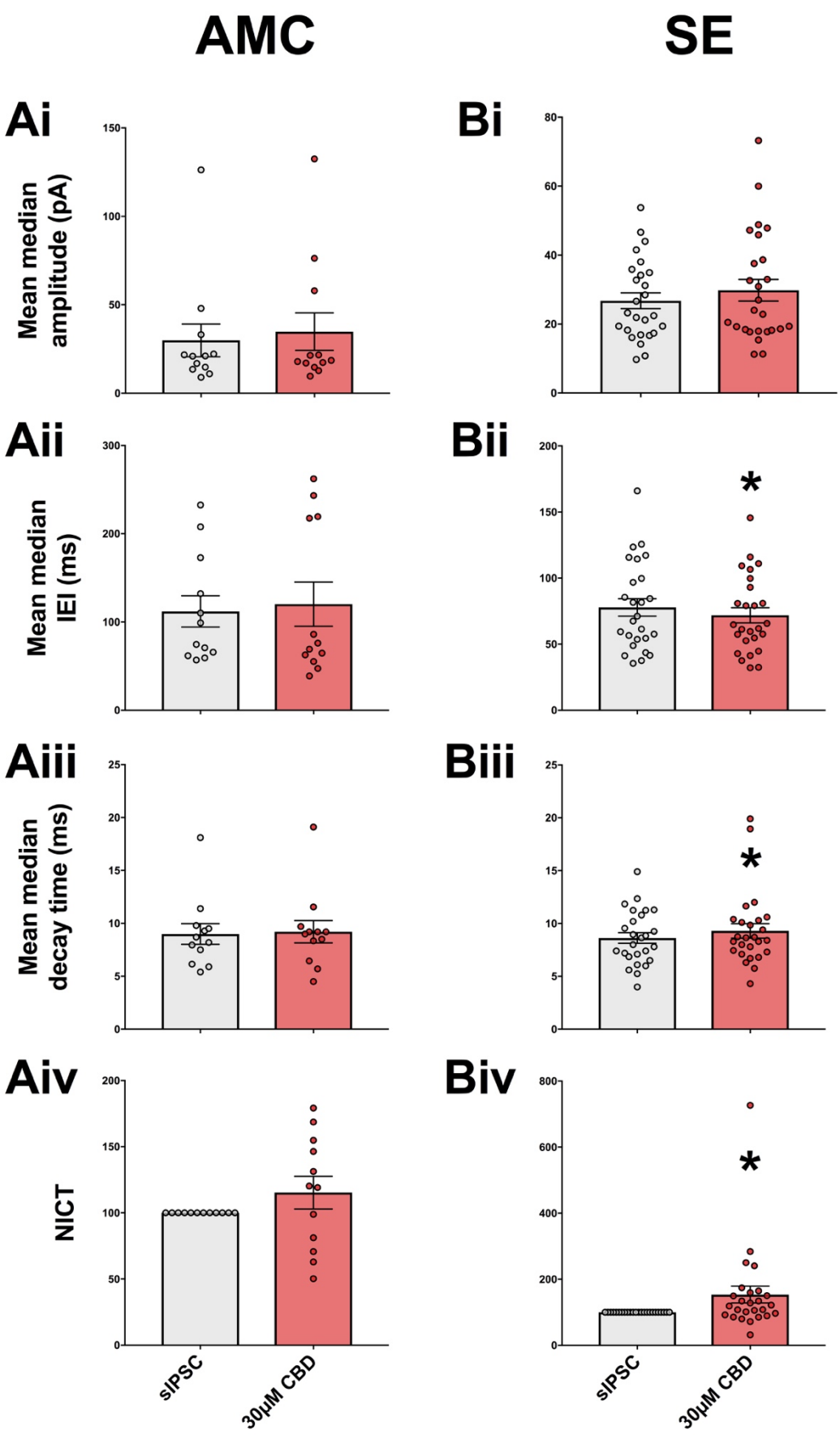

Figure 5.2 Histograms showing the effect of CBD on each of the sIPSC parameters.
Ai/Bi show mean median amplitude (pA) comparisons. Aii/Bii represent mean median IEI comparisons (ms). Aiii/Biii highlight mean median decay time comparisons (ms). Aiv/Biv show comparisons of NICT values. AMC left, SE, right. * $p < 0.05$.

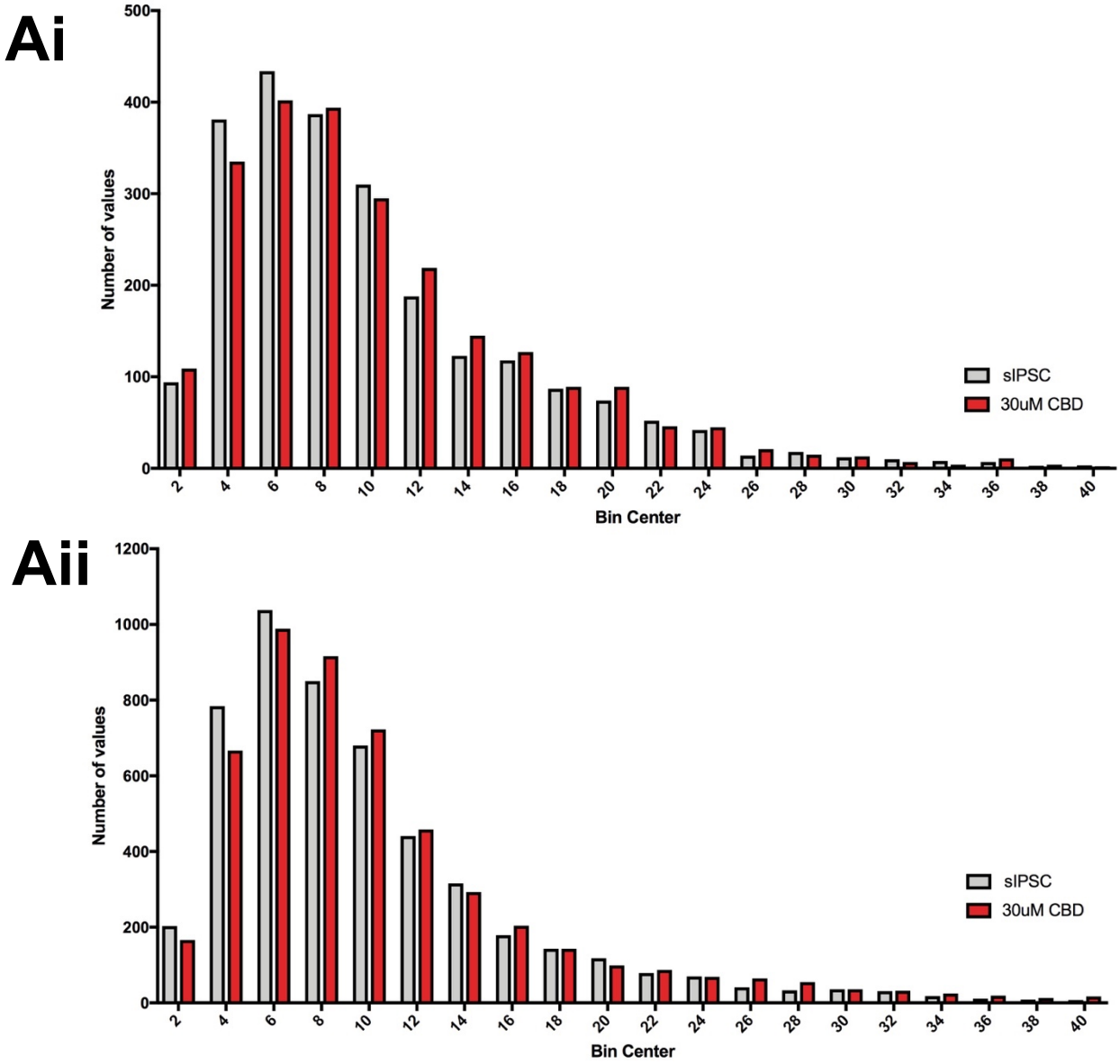

Figure 5.3 Binned decay time frequency histograms
Decay time frequency histograms showing 2ms bins for AMC (Ai) and SE (Aii) populations from 2-40ms and the number of value in each bin. Legend shows baseline/sIPSC (grey columns) and 30μM CBD (red columns).

To analyse whether all, or only certain population of cells were being affected by the increase in decay time induced by CBD addition, decay time response distributions have been observed, with 2ms bins defined and presented for all decay times analysed in the AMC and SE populations (**Figure 5.3.Ai-ii** respectively). Here decreases are noted in the fast decay time bins (<6ms) with increases noted in decay times above (>6ms) when CBD is applied in both the AMC (**Ai**) and SE (**Aii**) populations. This alteration in decay time is most noticeable upon CBD application in the SE population, where a larger number of values are observed in the >6ms bins than in baseline, though the change looks to be very slight.

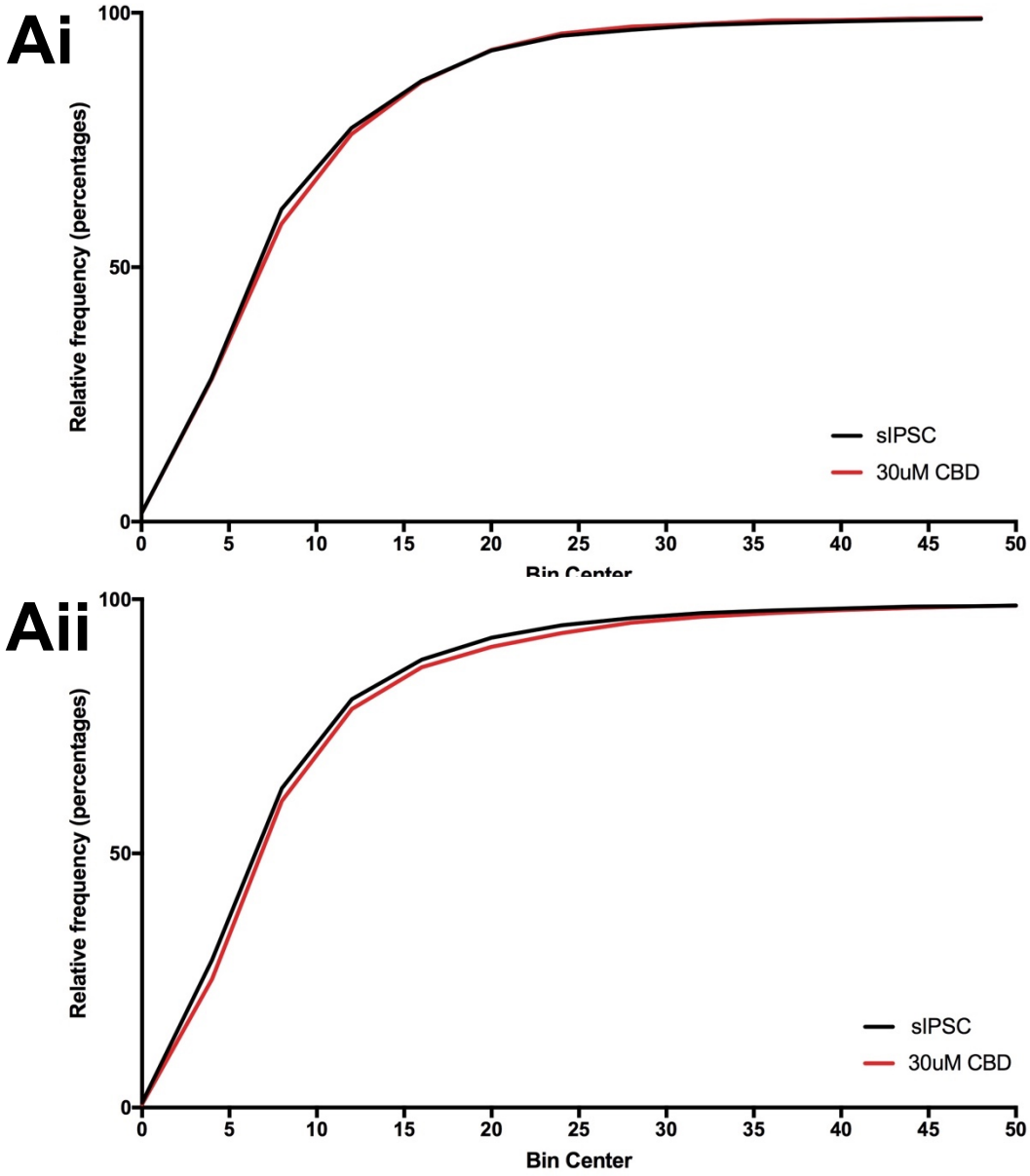

Figure 5.4 Cumulative frequency line graph for decay times.
AMC (Ai) and SE (Aii) populations. Legend shows baseline/sIPSC (black line) and 30μM CBD (red line).

The alteration of decay times is shown again as a cumulative frequency line graph (**Figure 5.4**) for both AMC (**Ai**) and SE populations (**Aii**). Here a very subtle shift to the right is noticeable in the SE population, recapitulating the data shown in **Figure 5.3**. The AMC data in contrast, does not show this, though a shift is somewhat visible between 8-10ms.

The shift to the right observable in the SE analysis is suggestive of a change in decay time of all cells synapsing onto the recorded cell, not just a specific population of cells, something supported by the binned histograms presented in **Figure 5.4.Aii**, as notable alterations in each bin are observed up to 12ms.

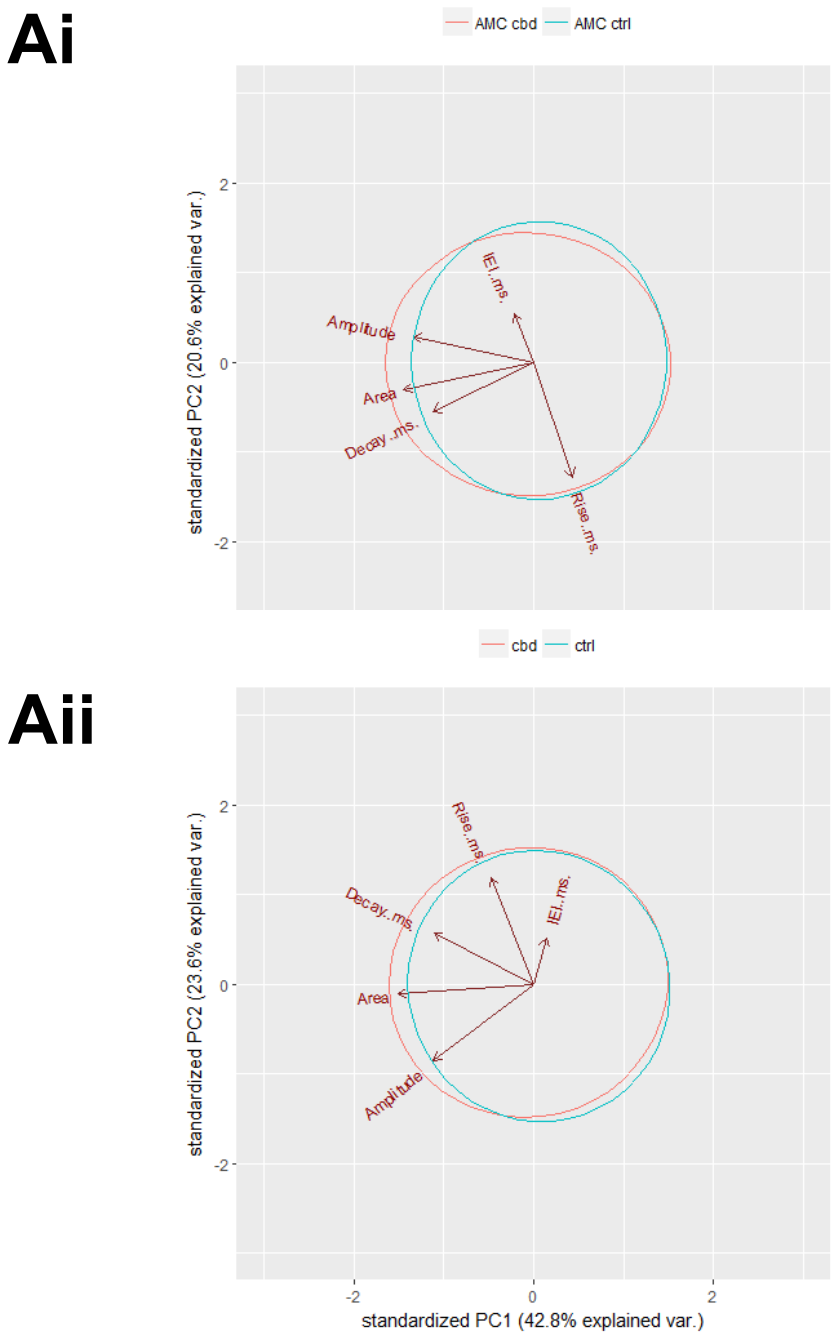

Figure 5.5 Principal component analysis (PCA) of CBD effects.
AMC (Ai) and SE (Aii) experiments. The direction and size of the arrows coupled with the movement of the ring (blue – baseline/control; red – CBD) indicates the components most responsible for the variation between the before and after drug treatment.

Figure 5.5 represents two separate PCA computations, one for AMC (**Ai**) and one SE (**Aii**). PCA was performed to allow us to gain an insight into which of the analysed parameters was most responsible for the increased inhibition observed upon CBD. In both, the main sources of variation are amplitude, decay time and area, as shown by the direction of the arrows for each of these parameters alongside the shift in the position of the circle – each of these components are integral to our NICT analysis, detailed in the Materials and Methods chapter previous (**Chapter 2**).

5.2.2 Rat sIPSC responses to CBDV

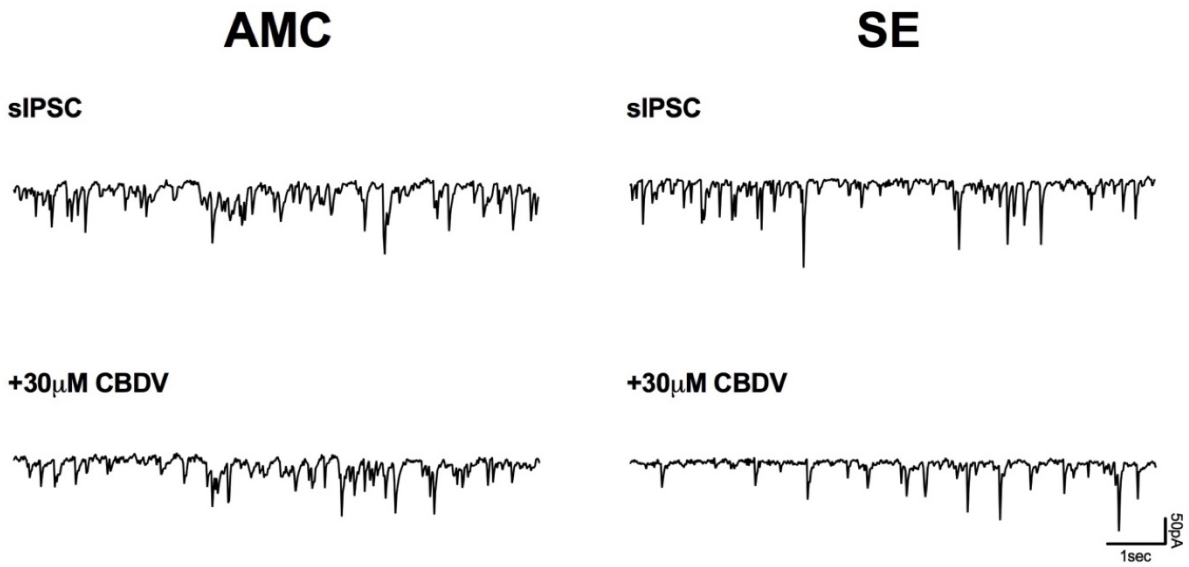

Figure 5.6 Representative sIPSC raw traces to maximal 30μM CBDV dose.
Before and after raw traces shown for the AMC (left) and SE (right) populations in response to 30uM CBDV

Figure 5.7 followed the same experimental formula, with both AMC (n = 6; animal n = 3) and SE (n = 6; animal n = 5) populations investigated, though CBDV has been applied in place of CBD. Here no significant changes, except for the SE NICT value, are observed in any of the parameters analysed, though a lower n number than that of the CBD experiments has been performed.

Figure 5.7.Ai/Bi highlight the mean median amplitude responses of both the AMC (**Ai**) and SE (**Bi**) populations. **Ai** shows no change in amplitude upon the addition of CBDV (37.6 ± 8.1 – 35.5 ± 6.2; range: 10.9-54.9; 11.0-49.4; p = 0.69). A trending decrease was observed in the SE dataset (**Aii**; 31.8 ± 5.58-27.9 ± 5.09; range: 15.5-54.0; 15.5-51.5; p = 0.063). **Aii** shows the responses of the AMC mean median IEIs, where no changes were observed upon CBDV application (83.9 ± 14.8 – 78.6 ± 17.1; range: 39.7-129; 35.2-150; p = 0.84). Again, in the SE population, no change to the mean median IEI was observed (56.1 ± 10.0 – 61.1 ± 8.96; range: 32.8-102; 34.9-101; p = 0.22).

The next parameter analysed was the mean median decay time, in **Aiii/Biii**. The AMC data (**Aiii**), showed no change when CBDV was present (10.3 ± 1.73 – 11.5 ± 2.47; range: 6.20-17.3; 4.80-21.9; p = 0.31). A similar result was observed in the SE population (**Biii**) response to CBDV, where no alterations in decay time occurred (7.39 ± 0.50 – 7.69 ± 0.25; range: 5.85-9.10; 7.20-8.90; p = 0.68). The final analysis parameter for the CBDV addition was NICT values (**Aiv/Biv**). Here the AMC dataset showed no changes in value, 119 ± 26.6, range: 50.6 – 218 (p = 0.56)**.** The SE data (**Biv**), on the other hand, presented a significant decrease in NICT value upon CBDV application (79.0 ± 8.94; range: 39.3 – 97.4; p = 0.03).

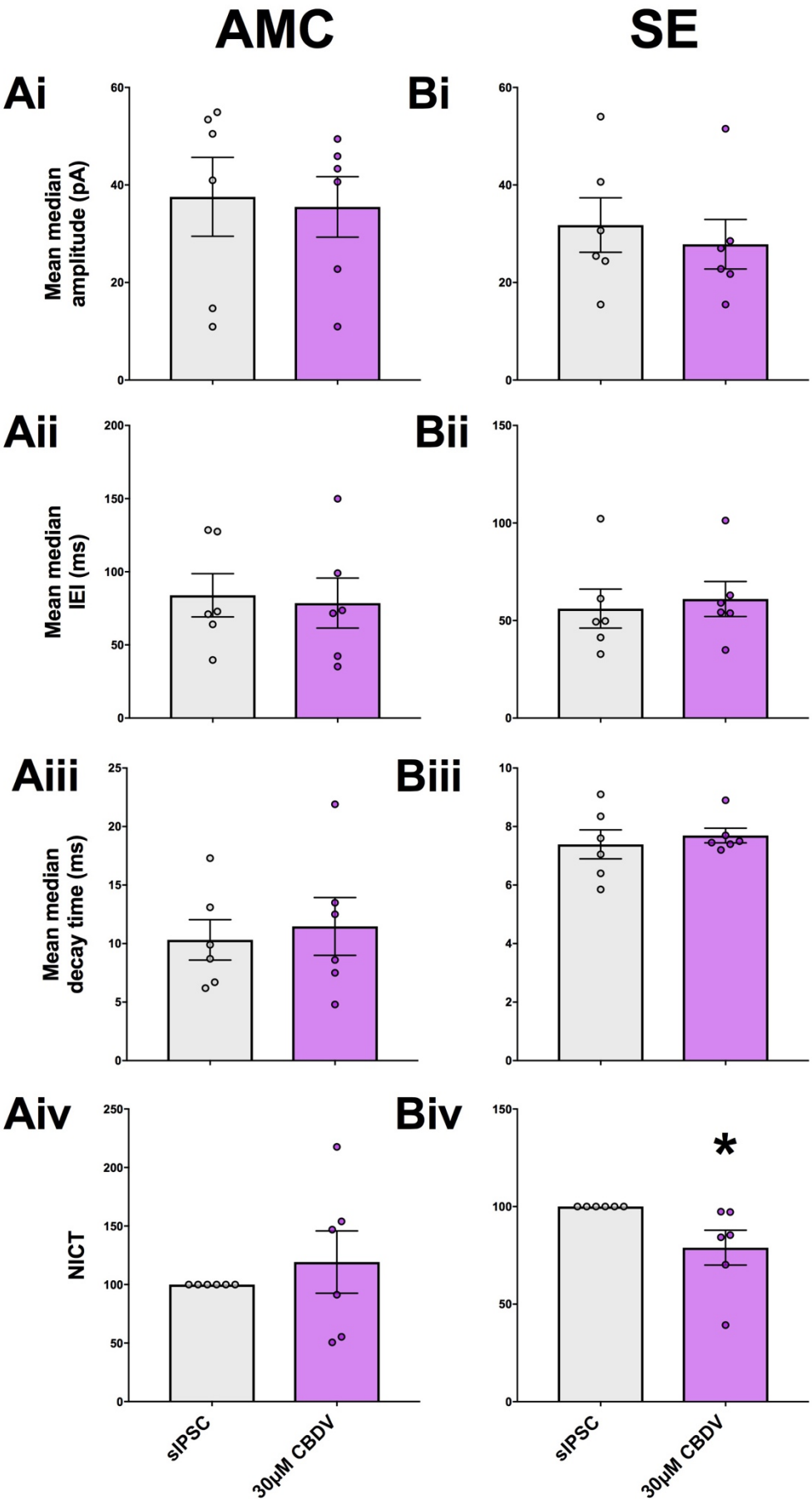

Figure 5.7 Histograms showing the effect of CBDV on sIPSCs.
AMC (left) and SE (right). Ai/Bi show mean median amplitude (pA) comparisons. Aii/Bii represent mean median IEI comparisons (ms). Aiii/Biii highlight mean median decay time comparisons (ms). Aiv/Biv show comparisons of NICT values. * $p < 0.05$.

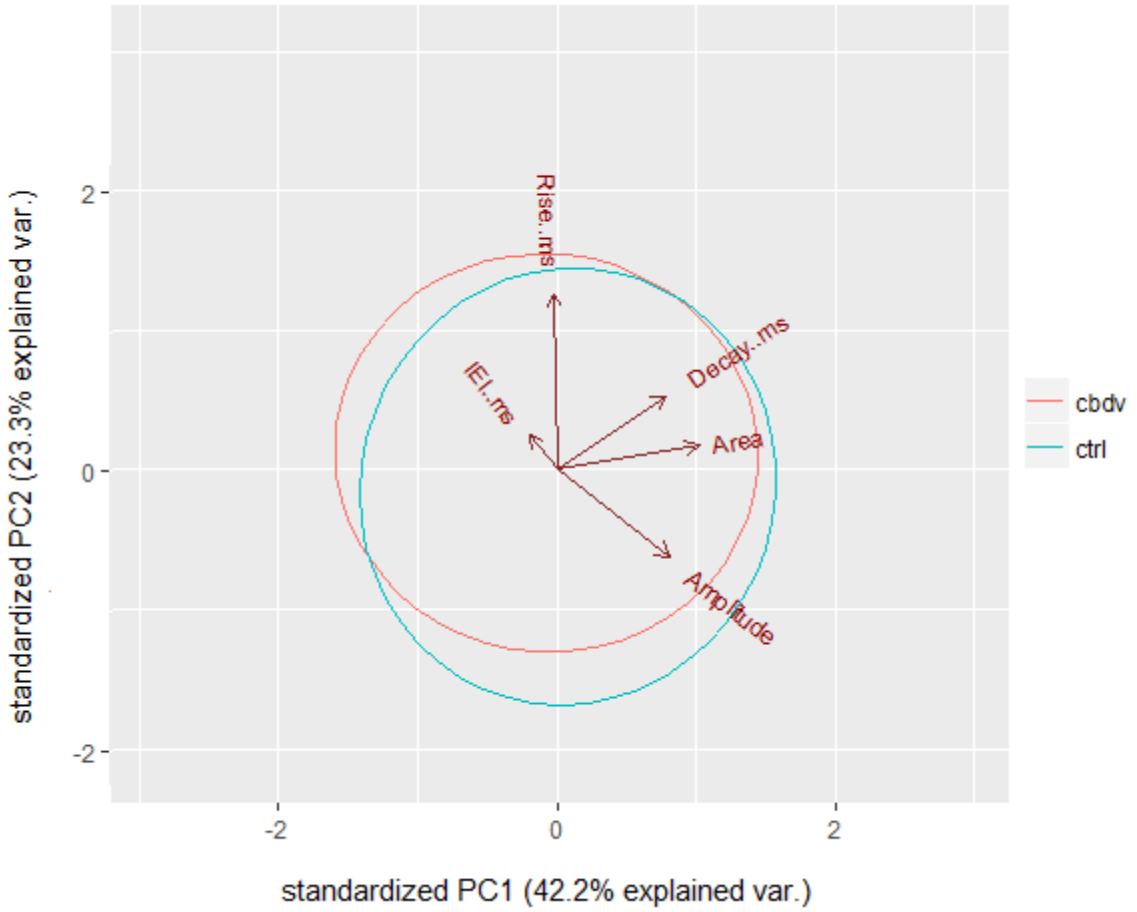

Figure 5.8 PCA for the addition of 30μM CBDV in SE rats
The direction and size of the arrows coupled with the movement of the ring (blue – baseline/control; red – CBDV) indicates the components most responsible for the variation between the before and after drug treatment.

Figure 5.8 shows the PCA for the SE dataset, which seemingly returns a different set of parameters causing the variation to that of the CBD addition. The first principal component appears to be the amplitude, with the second being rise time, in stark contrast to the CBD PCA computations. This is highly suggestive of CBDV acting via a different MOA to CBD.

5.2.3 Human tissue whole-cell voltage-clamp sIPSC responses to CBD

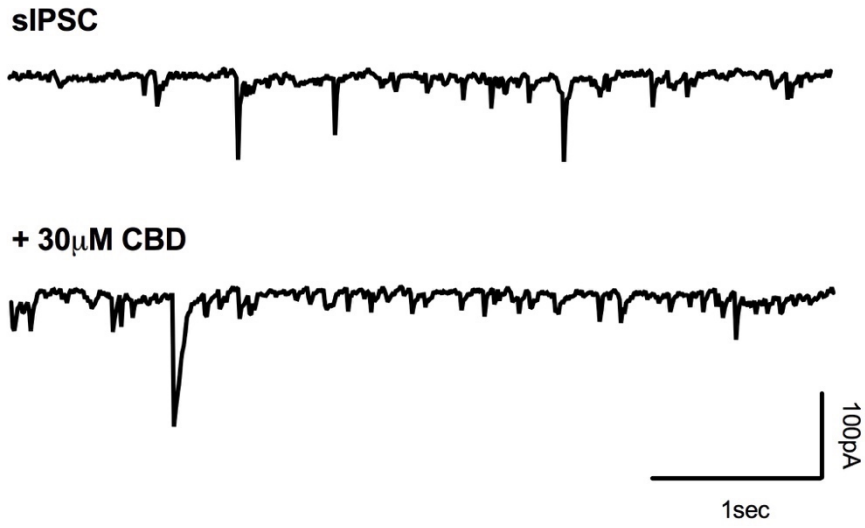

Figure 5.9 Representative sIPSC raw trace of a HT cell in response to CBD.
Raw traces before and after 30μM CBD addition in a HT pyramidal cell

Figure 5.9 shows a representative trace of HT pyramidal cells in both control sIPSC and 30μM CBD. Visually there looks to be a slight increase in amplitude and possibly frequency as well, though no valuable data can be drawn from this alone.

We therefore have analysed the human tissue (HT) data (n = 9; sample number n = 7) in the same manner as the rat CBD and CBDV data previously, displayed in **Figure 5.10.Ai-iv**.

Figure 5.10.Ai shows the responses of HT mean median amplitude (pA) upon the application of CBD. No change was noted when CBD was applied (26.7 ± 3.96 – 25.8 ± 3.49; range: 10.1-47.2; 11.3-43.1; p = 0.50). **Aii** shows the response of the mean median IEI (ms), where again no changes were present (101 ± 16.5 – 88.7 ± 8.02; range: 49.4-208; 57.5-128; p = 0.57). **Aiv** highlights the mean median decay time (ms), where a significant increase was present once CBD was added (8.08 ± 0.67 – 9.31 ± 0.95; range: 4.10-11.2; 4.45-14.5; p = 0.009). The final histogram (**Aiv**) displays the NICT values, where again a significant increase was observed upon CBD application (148 ± 25.2; range: 88.5 – 308; p = 0.039).

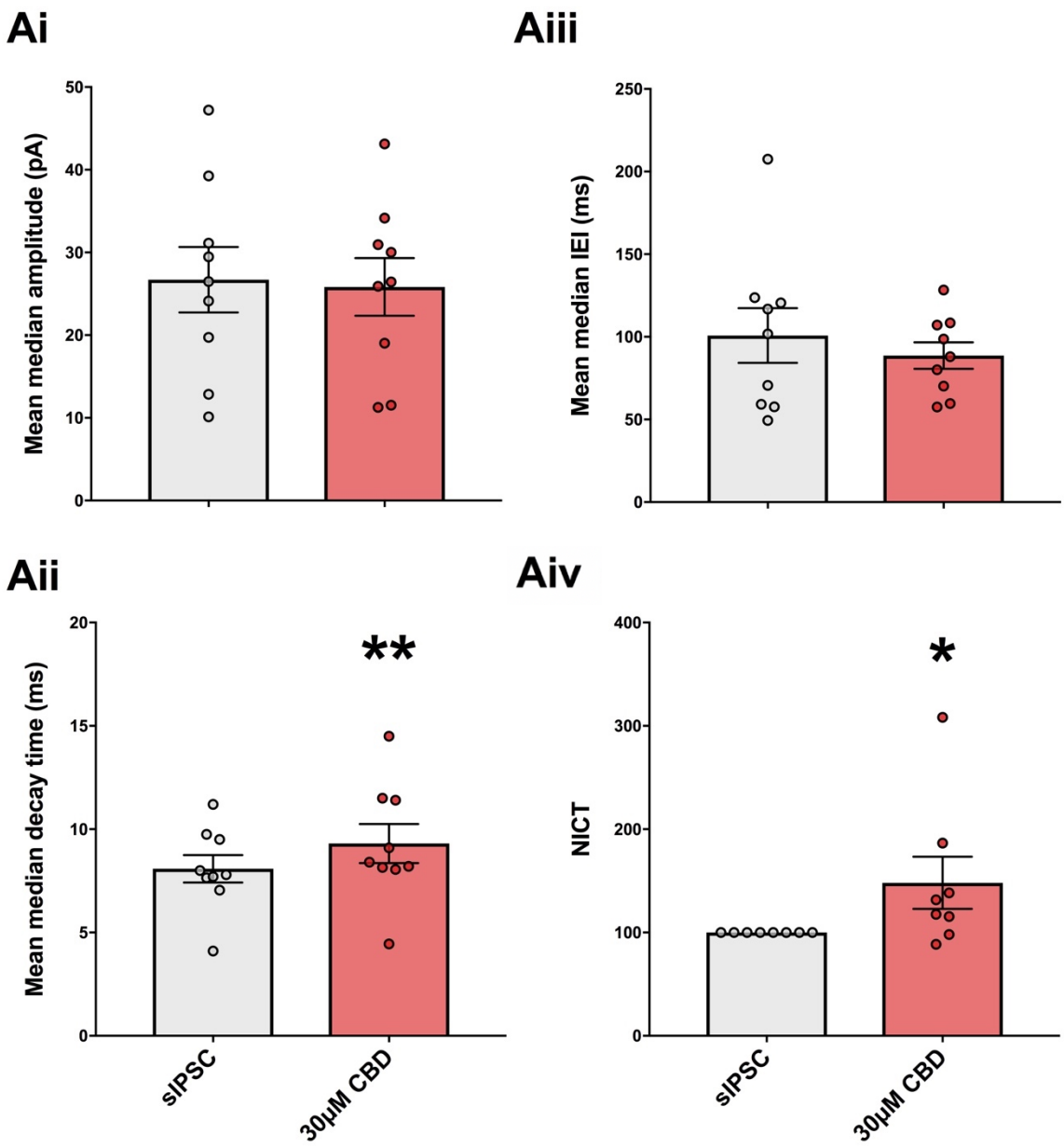

Figure 5.10 Histograms showing the responses of HT cells to CBD.
Mean median amplitude (Ai), IEI (Aii) and decay time comparisons (Aiii), as well as NICT analysis (Aiv) for HT samples all analysed. * $p < 0.05$, ** $p < 0.01$.

Figure 5.11 shows the PCA for the HT cells, showing a highly similar relationship to that observed in the SE tissue, where area and decay time show the highest variations between the baseline and CBD addition. This analysis suggests that in both the HT and SE rat conditions CBD is affecting similar responses, most likely through a similar mechanism.

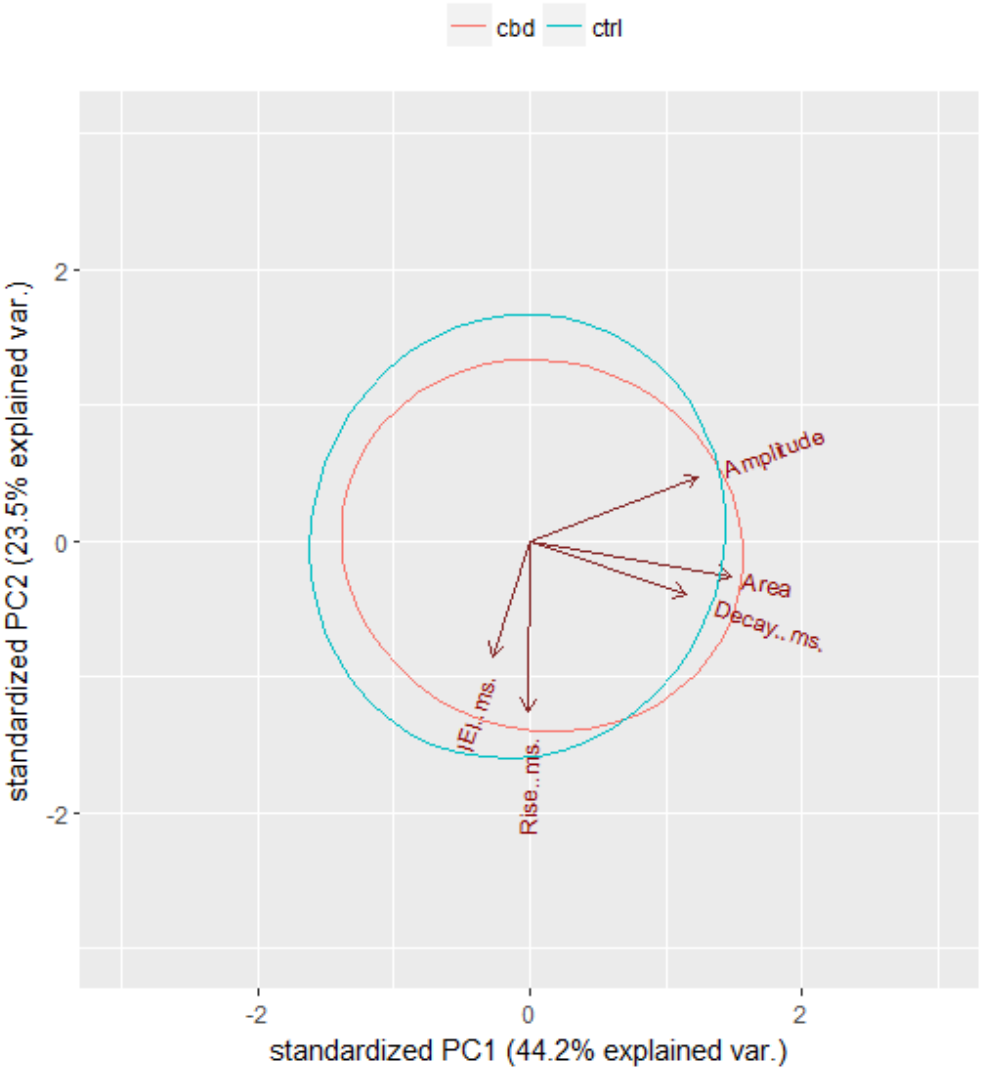

Figure 5.11 PCA of HT cells when exposed to 30μM CBD.
The direction and size of the arrows coupled with the movement of the ring (blue – baseline/control; red – CBD) indicates the components most responsible for the variation between the before and after drug treatment.

5.2.4 Rat sEPSC responses to CBD

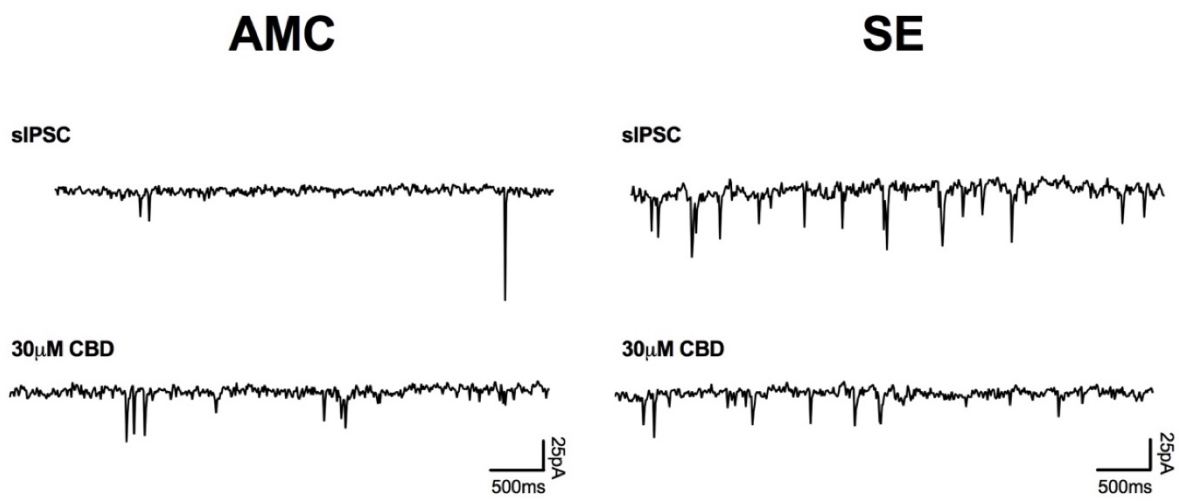

Figure 5.12 Representative raw sEPSC traces in response to 30μM CBD.
Raw traces from AMC (left) and SE (right) animals, before and after CBD addition.

Alongside the sIPSC data performed with CBD, we also observed spontaneous excitatory postsynaptic currents (sEPSCs) in both AMC and SE rat populations using whole cell voltage-clamp recordings. sEPSCs were investigated as epilepsy is a neurological disease caused through an imbalance of excitation and inhibition, usually citing a lack or dysfunction in inhibitory signalling leading to an excessive amount of neuronal excitation. As decreases in gamma oscillations have been shown, as too increasing inhibition on pyramidal cells by the application of CBD, it is plausible that CBD may act via excitatory receptors or excitatory neurotransmitter release mechanisms to exert this effect. As such, sEPSCs are a clear method of looking at the effect, if any, CBD has on neuronal excitation.

Representative traces from both the AMC (n = 8; animal n = 5) and SE population (n = 5; animal n = 4) are displayed in **Figure 5.12**, for both the sEPSC baseline period and 30μM CBD condition. There are little differences between the two traces visually when the CBD is added, though definite differences between the two disease conditions are visible in baseline, something discussed more thoroughly later (**Chapter 6**).

The same data analysis has been performed on the sEPSC data as with the sIPSC data, the results of which are presented in **Figure 5.13.Ai-iii/Bi-iii**. As before, **Ai** shows the mean median amplitude response of the AMC dataset, where no effect was observed when CBD was applied (9.40 ± 0.61 – 10.1 ± 0.95; range: 6.99-12.0; 7.32-15.8; p = 0.38). **Bi** highlights the SE dataset mean median amplitude responses, where again no effect was observed (21.7 ± 3.04 – 30.1 ± 2.15; range: 12.2-30.6; 12.8-25.3; p = 0.44).

Figure 5.13.Aii shows the mean median IEI responses for the AMC population, where no alterations were observed upon CBD addition (282 ± 75.6 – 245 ± 65.0; range 72.9-610; 28.5-550; p = 0.31). **Bii** also shows no change in SE mean median IEI upon CBD application (193 ± 37.8 – 189 ± 23.7; range: 125-304; 156-282; p = 1).

The final set of parameters analysed were the NECT values, comparable to the NICT values described previously. **Aiii** shows the NECT value for the AMC population, where no change was shown (127 ± 26.4; 78.9-308; p = 0.46). **Biii** shows the comparable data for the SE population, where there was no alteration in NECT value upon CBD addition (101 ± 21.2; 51.8-151; p = 0.81).

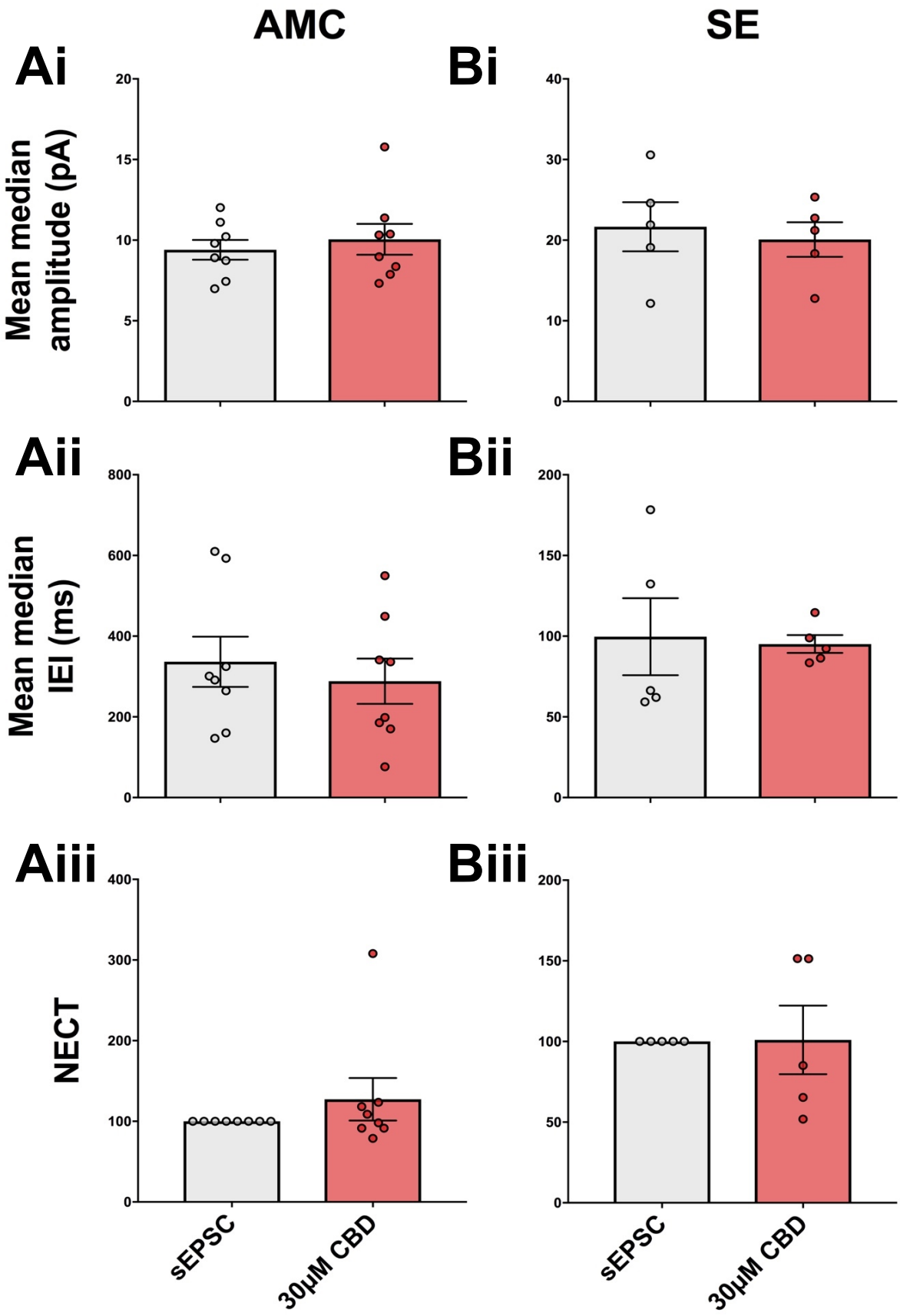

Figure 5.13 Histograms showing the responses of sEPSCs to CBD.
Mean median amplitude (**Ai/Bi**), IEI (**Aii/Bii**) and NECT analysis (**Aiii/Biii)** for AMC and SE samples, with AMC (left) and SE (right).

5.3 Discussion

5.3.1 Rat sIPSC show increased decay time and inhibitory charge transfer in response to CBD

The results presented from the CBD sIPSCs (**Figure 5.2**) show no significant change to any of the parameters in the AMC dataset (**Ai-iv**), though there are arguably trending increases in the amplitude and NICT values upon the application of CBD, though as there is already quite a substantial number of ns performed for this dataset which would make this difficult to argue (n =12; animal n = 9). As these data correspond to the 24-hour post-induction LFP data, this is perhaps not surprising as there was no effect of CBD in this age group. When viewed in conjunction with the PCA presented in **Figure 5.5**, however, both AMC and SE PCA tests show similar variation caused by CBD addition, especially in regard to the area, amplitude and decay time components, so the lack of any significant effect is somewhat interesting.

In contrast, the SE data (**Figure 5.2.Bi-iv**) shows significant changes in three of the four parameters, with only the mean median amplitude showing no effect. The mean median IEI significant decrease is suggestive of an increased frequency in post-synaptic currents upon the addition of 30μM CBD. Whether this decrease is a physiologically relevant decrease is debatable, with a drop of only 5.8ms presented. There is also a subtle, yet significant, increase in the mean median decay time, suggestive of a prolonged receptor opening time, something symptomatic of benzodiazepines and benzodiazepine-like compounds. These changes are recapitulated in the NICT values, where again a significant increase is noted. There is an overall average increase in NICT upon CBD addition, which is representative of higher inhibition levels. This increase may be due to increased pre-synaptic GABA release, higher GABA uptake or increased $GABA_AR$ opening time – suggested by the noted increase in decay time in the SE population.

The decay time differences were explored further in **Figure 5.3**, where decay times from the AMC and SE populations were binned at 2ms intervals, with number of events plotted on the y-axis. Here fast decay times (>6ms) seem to decrease in the SE dataset, while slower decay times (<6ms) seem to increase, suggestive of an increased $GABA_AR$ open time caused by the application of CBD in the SE animals. This is recapitulated in the next figure (**Figure 5.4**) where the cumulative frequencies of the decay times for both the AMC (A) and SE (B) populations have been plotted. Here, no real change is noted in the AMC populations, while a very subtle shift to the right is observed in the SE data.

The differences present between the two populations once again indicate a disease specific action of CBD, especially in these young juvenile/adolescent animals – as was suggested by the LFP data present in the previous chapter (**Chapter 4**).

Taken together, the LFP and sIPSC data proffered demonstrate CBD as an age- and disease-specific compound, which decreases network excitability (observed in the LFP data through the suppression of gamma oscillations) and, neuronal excitability (sIPSC data presented here). The significant results obtained in the SE data are suggestive of a subtle effect of CBD on the IEI and kinetics of inhibitory events, one similar to that of a benzodiazepine agonist. This effect is most likely caused by increasing the inhibition on pyramidal cells, either on the postsynaptic terminal, through increasing the $GABA_AR$ opening time (increased decay time observed here) or through increased GABA neurotransmission from presynaptic interneurons.

5.3.2 Rat sIPSC show decreased inhibitory charge transfer in response to CBDV

In contrast to the LFP data, CBDV causes no effect on either the AMC, or much of the SE sIPSC kinetics. This is somewhat surprising as CBDV produced a general suppressive effect across the LFP data in each population and disease condition (excepting the 24-hour AMC animals). There is however one area of this analysis where CBDV does produce an effect, especially in the SE population, which is in the relative NICT values (**Figure 5.7.Biv**).

The SE NICT response shows a significant decline in value, indicative of an actual drug induced effect, both from the small standard error but also the tighter range and consistent decrease in NICT value across all respondents. As well as being a significant effect, it is also a surprising one, as it is suggestive of CBDV inducing less inhibition of pyramidal cells, which would subsequently indicate a higher excitation of the neurons. When paired with the LFP data previous, which suggests CBDV causes a flat decrease in gamma oscillation regardless of age/disease, plus other studies (Hill et al., 2013), it is puzzling as to how CBDV is able to possess an anti-convulsant effect.

The PCA presented (**Figure 5.8**) for this dataset is slightly different to those produced for the addition of CBD, with alterations to amplitude and rise time appearing to have more of an effect on the differences between baseline and cannabinoid addition, highly suggestive of differing MOAs between CBD and CBDV.

A considerably smaller n number is presented for each population here compared to the CBD data, mostly due to time constraints, as well as greater interest in the CBD portion of this project and, as such, this is the final experiment on the CBDV portion of the project.

5.3.3 Human sIPSC responses to CBD are similar to those of the rat

The human tissue samples we receive provide some of the most interesting results of this chapter, and indeed this whole project, as it is difficult to obtain and study in the manner we have been fortunate to.

The data obtained from, nominally, principal HT cells (determined by morphological observations and location within the slice, therefore not fool proof; **Figure 5.10**) are largely, and intriguingly, in agreement with the SE rat tissue data. That is, there are no significant differences after CBD application in the mean median amplitude nor in the mean median IEI in HT, though a significant decrease in IEI was observed in the rat data. There is however, a highly significant increase in the current decay times similar to the rat observation, though the change itself was relatively small, alongside a significant increase in the NICT value as well.

The significance relationship is the reverse of that present in the rat data, with the decay showing a lesser significance while the NICT value showed higher. Nonetheless, both experimental samples display increased decay times and increased NICT values. This allows several observations to be made, one, that the RISE model is successfully mimicking the human epilepsy condition (as touched on in the AMC v SE section previously, **Chapter 3**), through the common responses to CBD, not observed in the rat AMC population. Secondly, that CBD is interacting, directly or indirectly, with $GABA_AR$ in some manner to produce increased decay times, reminiscent of a benzodiazepine effect. Thirdly, that either through increased decay times or via another mechanism, CBD is able to produce increased inhibition transfer into the neurons. Most likely this is due to the increased open time of the $GABA_AR$, though that is not necessarily the only mechanism responsible, as suggested before, it could also be due to larger presynaptic GABA release.

Due to human tissue being so infrequent and rare as a resource, more n numbers could not be achieved within the timeframe of this project. With a higher number it is possible that the IEI would see a similar significant decrease to that observed in the rat data. It would also be possible to run specific experiments to try and determine the cause of increased inhibition in HT neurons. Interestingly, significance in the HT cells has been achieved with a much lower n than that of the SE rat data, which may suggest CBD is more effective in raising inhibition in HT cells than in the rat.

5.3.4 No effect of CBD on sEPSC responses

Due to the success of the sIPSC experiments with regards to CBD effect, we explored its effect on excitatory mechanisms by recording spontaneous excitatory post-synaptic currents (sEPSCs). These were performed in both the AMC and SE populations (**Figure 5.13**). The

same analysis parameters were utilised again, with NICT converted to normalised excitatory charge transfer (NECT), though the formula used was the same.

Here no significant effects of CBD were observed in either population in any of the parameters observed, with no real trends observed either. These data are highly suggestive that CBD is not inducing its observed effect in SE afflicted tissue, noted in the LFP and sIPSC experiments so far, through excitatory mechanisms. Due to this, no further sEPSC data was collected.

It is interesting to note, however, that the SE animals show higher amplitudes and lower IEI (higher frequency) than the AMC rats, even in the baseline (sEPSC) portion of the experiments, which again is another indication that this epilepsy model is a successful imitation of that observed in humans, where hyperexcitability is noted (Scharfman, 2007). This implication has been further discussed in **Chapter 3**.

5.4 General discussion and future work

Here we have demonstrated CBD as increasing SE mEC layer II single pyramidal cell inhibition through, most likely, increasing mean median decay time and as such greater Cl^- entry. Further to this, we have shown that this response is successfully observed in epileptic HT cells in response to CBD addition. Moreover, we have demonstrated that CBD application has no effect on AMC mEC layer II pyramidal cell sIPSC recordings or, spontaneous excitatory currents (sEPSCs). All of which is highly suggestive of the reported anti-convulsant CBD effect occurring through inducing increased inhibition in pyramidal cells. These data also further support the disease specific effect postulated in **Chapter 4**, as SE responses at 24-hours post-induction show significance while the AMC population does not. Interesting directions this data could be used in in future include: expanding the HT work to show CBD responses in specific epilepsy cases (FCD vs. TLE etc.), binding study assays to assess the binding site of CBD and, developmental studies to assess possible targets shown in the juvenile SE tissue that are not present in the comparable AMC population.

CBDV responses here do not display any effects on the AMC sIPSC recordings. Indeed, CBDV only displayed a significant effect on the normalised inhibitory charge transfer parameter in the SE tissue. In contrast to the CBD data, a decrease in NICT value was observed suggestive that CBDV may produce its noted effect of **Chapter 4** via excitatory mechanisms of some description. A somewhat interesting experiment for the CBDV data may be to perform CBDV responses in AMC and SE sEPSC recordings to note any differences between the two.

Chapter 6

Pharmacological modulation of the CBD effect

6.1 Introduction

6.1.1 CBD has a benzodiazepine-like effect on $GABA_AR$

The previous chapter implicates CBD as having a benzodiazepine-like effect on $GABA_AR$, as noted through the increased decay time present in both the SE rat and HT neuronal responses. This effect has been noted in a recent study on CBD binding (Bakas et al., 2017), where CBD was found exert a benzodiazepine (BZ) effect on $GABA_AR$, though it does not bind to the classical BZ binding site at the alpha/gamma subunit interface of $GABA_ARs$. This observation concurs with our own experiments, presented below (**Section 5.2**), raising the question of where and how is CBD able to bind to influence this response?

The classical BZ binding site of the canonical $GABA_AR$ composition (α, β, γ in a 2:2:1 ratio), shown in **Figure 1.14**, is at the interface between the αγ2 subunits. 1,4-benzodiazepine agonists, such as diazepam, increase Cl^- entry into the neuron, through increasing the receptor ion channel open time, resulting in augmented hyperpolarisation and a suppression of neuronal excitability (Otis and Mody, 1992). Subsequent addition of BZ antagonists/inverse agonists, such as flumazenil, work in reverse to this, decreasing the length of time $GABA_AR$ remain open and thereby decreasing Cl^- entry and reducing hyperpolarisation. This effect was only noted as being observed in the presence of a BZ agonist, flumazenil having shown no effect when applied alone (Otis and Mody, 1992). More recent research, however, has shown flumazenil is capable of possessing augmentation effects in the absence of BZs most likely through competition with endozepines. Indeed, it appears as though flumazenil may act as an inverse agonist at the BZ site due to its inhibition of tonic GABA, instead of as a benzodiazepine antagonist, as it is commonly described (Cortelli et al., 2005; Prokic et al., 2015).

Alongside BZ modulation of $GABA_AR$ open time, barbiturate agonists are also noted as capable of increasing receptor open time (Otis and Mody, 1992). It was a reasonable suggestion to surmise that CBD was binding to the BZ/barbiturate site to affect an increased opening time of the receptor, as observed in **Chapter 4** upon CBD addition, explaining the BZ-like effect CBD possesses. Due to recent binding studies we now know this is unlikely, as CBD has been demonstrated to not show affinity at the BZ site (Bakas et al., 2017; plus, recent unpublished GW pharma binding data), while our work here suggests no affinity at the barbiturate site either. An alternative theory may suggest CBD is binding to different allosteric site on $GABA_ARs$, of which there are many, as suggested in Bakas et al, (2017).

6.1.2 Neurosteroids and the $GABA_AR$

Neurosteroids are a class of endogenous steroids synthesised in multiple areas of the body, including the brain, gonads and adrenal glands (Wang, 2011). There are a variety of different neurosteroids, with most acting as positive or negative allosteric modulators (PAM or NAM)l

either positively or negatively modulating receptor function in the presence of a classical agonist. Many neurosteroid allosteric modulators have potent effects on $GABA_AR$s, for example the PAM allopregnanolone (3α-OH-5α-pregnan-20-one), increases GABA-mediated Cl^- entry. Neurosteroids are thought to bind at sites different to the GABA, BZ, picrotoxin or barbiturate sites (Mitchell et al., 2008; Wang, 2011).

It has been proposed that every different subunit composition of $GABA_AR$ is able to bind some neurosteroid ligands. This has been demonstrated through neurosteroid modulation of GABA signalling across a variety of neuronal types many of which possess distinct compositions of $GABA_AR$s (Mitchell et al., 2008). Recombinant $GABA_AR$ binding studies previously performed also back this assessment, with neurosteroids displaying a plethora of effects on a variety of $GABA_AR$ compositions, all of which suggest that neurosteroid binding sites are conserved across $GABA_AR$ compositions (Puia et al., 1993; Lambert et al., 1996; Maitra and Reynolds, 1999; Belelli et al., 2002). It has been demonstrated that the α subunit is critical for the binding of neurosteroid PAM, explaining the conservation of neurosteroid binding across $GABA_AR$ compositions (Hosie et al., 2006, 2009; Akk et al., 2008; Li et al., 2009). The binding of NAM is rather more disputed, with several mechanisms proposed, though current thinking highlights two amino acids (α1 V256S and β2 A252S) as critical in *C. Elegans* studies, though whether this translates to mammalian $GABA_AR$ is as of yet unknown (Akk et al., 2001; Wang et al., 2006, 2007; Wardell et al., 2006). A definite neurosteroid binding site location, for either PAM or NAM is yet to be discovered.

6.1.3 CBD directly or indirectly interacting with NMDARs to influence GABA signalling/release

Published work by Xue et al, (2011), has raised the possibility of NMDARs being able to modulate GABA signalling and GABA release probabilities. This study showed that focal application of NMDA induced an enhancement of $GABA_AR$ mediated inhibitory transmission in CA1 neurons (between interneuron and pyramidal cells). Two mechanisms for NMDAR modulation of GABA neurotransmission were defined, one highlighted the activation of presynaptic NMDARs which contributed to NMDA-induced GABA release. The other was a postsynaptic mechanism, whereby activation of postsynaptic pyramidal cell NMDARs was linked to the synthesis/release of retrograde messengers, most likely nitric oxide (NO), which diffuses across the synaptic cleft to enhance presynaptic GABA release from interneurons (Xue et al., 2011).

This work is pertinent to this project, as the results presented in **Chapter 4** could be explained by CBD interacting with NMDAR receptors to produce an effect similar to the NMDA modulation of GABA response observed in this publication.

6.1.4 CBD has a lack of affinity for CBRs

As mentioned in the introduction section of this project (**Section 1.6.6**), CBD lacks affinity for both CB1 and CB2 receptors (Showalter et al., 1996; Thomas et al., 1998; Pertwee, 1999; Bisogno et al., 2001; Thomas et al., 2004), which would suggest that the CBD induced effect noted in the previous chapter as not arising via either CB receptors. This suggestion is further enhanced by recent published work, which states that the action of both CBD and CBDV are independent of CB1Rs (Wallace et al., 2008; Hill et al., 2013), while CBD has also previously been shown to compete weakly with the synthetic cannabinoid ^{3}[H] CP55940 at CB1R and CB2R (Griffin et al., 1998; Thomas et al., 1998). CBD, however, has recently been demonstrated to possess high affinity for the allosteric site of CB1R and, is purported to be a negative allosteric modulator at this site (Laprairie et al., 2015). Furthermore, CBD has also been shown to be a high affinity antagonist for the agonists at the orthosteric CB1R binding site (Thomas et al., 2007). Either of these findings may have implications in the anti-convulsant effect of CBD. Though CB2Rs have been documented to be located in the mEC (Morgan et al., 2009), the lack of affinity CBD displays for these receptors would suggest they are not involved in the CBD effect observed. Both CBR1 and CB2R are, however, able to modulate GABA signalling and therefore we probed for potential indirect roles at these receptors in the observed CBD effect.

6.1.5 FAAH as an intracellular target of CBD and modulator of GABA signalling

As CBD is a highly lipophilic molecule, it is able to diffuse across the cell membrane. This fact may mean that CBD is able to interact with a multitude of intracellular targets, any number of which may be able to alter GABA signalling via second messenger systems or signalling cascades.

One intracellular interaction partner of CBD is thought to be the enzyme, fatty acid amine hydrolyse (FAAH) (Bisogno et al., 2001; Massi et al., 2008; De Petrocellis et al., 2011; Ibeas Bih et al., 2015). FAAH is involved in catabolism of fatty acid amides, such as anandamide. CBD interaction with FAAH is somewhat disputed across literature, with only limited studies on the interaction. Some of these studies report an inhibitory effect at higher doses, with excitatory or stimulatory effects upon lower dosages (Bisogno et al., 2001; De Petrocellis et al., 2011). Cell culture systems suggest a CBD induced FAAH activation, whereas membrane extract assays depict CBD induced inhibition, which suggest that CBD induced effects are reliant on the physiological environment. These data imply that more than one mechanism is involved, one producing fast-acting effects, and the other longer-term effects (Massi et al., 2008).

Due to the relatively high concentration of CBD required to produce a result in our *in vitro* experiments and in the previous studies, we were interested in whether CBD interaction with FAAH may be responsible for the induced effects we have observed. A possible mechanism for these effects through FAAH inhibition could be a rise in anandamide, due to decreased catabolism, with anandamide acting to increase GABA release and uptake, resulting in a higher amount of inhibition and a subsequent decrease in neuronal excitability.

Here we have performed preliminary experiments to look at whether interaction between FAAH and CBD could be responsible for the effects of CBD on IEI, decay time and NICT values noted in the SE animals. As such, we have used the FAAH inhibitor URB597 to inhibit FAAH and then subsequently added CBD afterward. The data presented once more has a small n number (animal n = 3; n = 4).

All of the experiments performed in this chapter have only been done so on SE animals of the same age as the previous chapter (p19-26) due to the observed lack of effect of CBD on the AMC animals.

6.2 Results

6.2.1 Modulation of the $GABA_AR$

6.2.1.1 Benzodiazepine site modulation

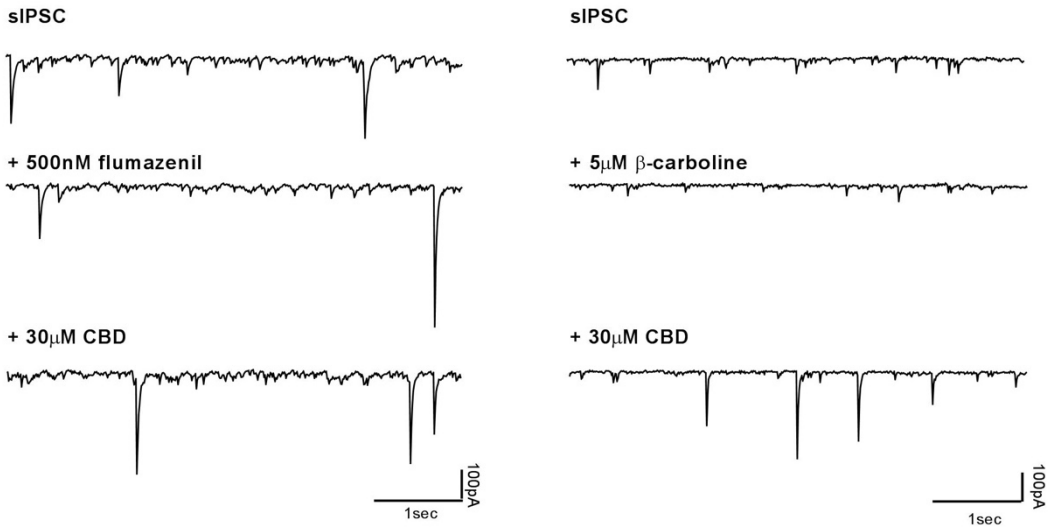

Figure 6.1 Raw sIPSC traces from SE rat tissue with BZ-site blockers.
Left 500nM flumazenil, right 1μM β-carboline.

Here we have applied BZ inverse agonists, in the form of flumazenil and β-carboline, and agonists at the BZ site, clobazam and the non-BZ BZ-site agonist zolpidem, to observe their effects on sIPSC in the presence and absence of CBD. Alongside BZs, we also investigated whether CBD was binding to the barbiturate binding site by the addition of the barbiturate site potentiator pentobarbital.

As stated, we probed the possible CBD interaction with $GABA_AR$ at the benzodiazepine (BZ) binding site, due to the increased decay times observed upon its addition in SE rats and HT samples. We therefore blocked the BZ site using 500nM flumazenil (n = 7, animal n = 5), and separately, 5μM β-carboline (n = 5, animal n = 3), both benzodiazepine site inverse agonists. Each was bath applied and left for at least 15 minutes before 30μM CBD addition. The results of each are presented in **Figure 6.2.Ai-Biv**.

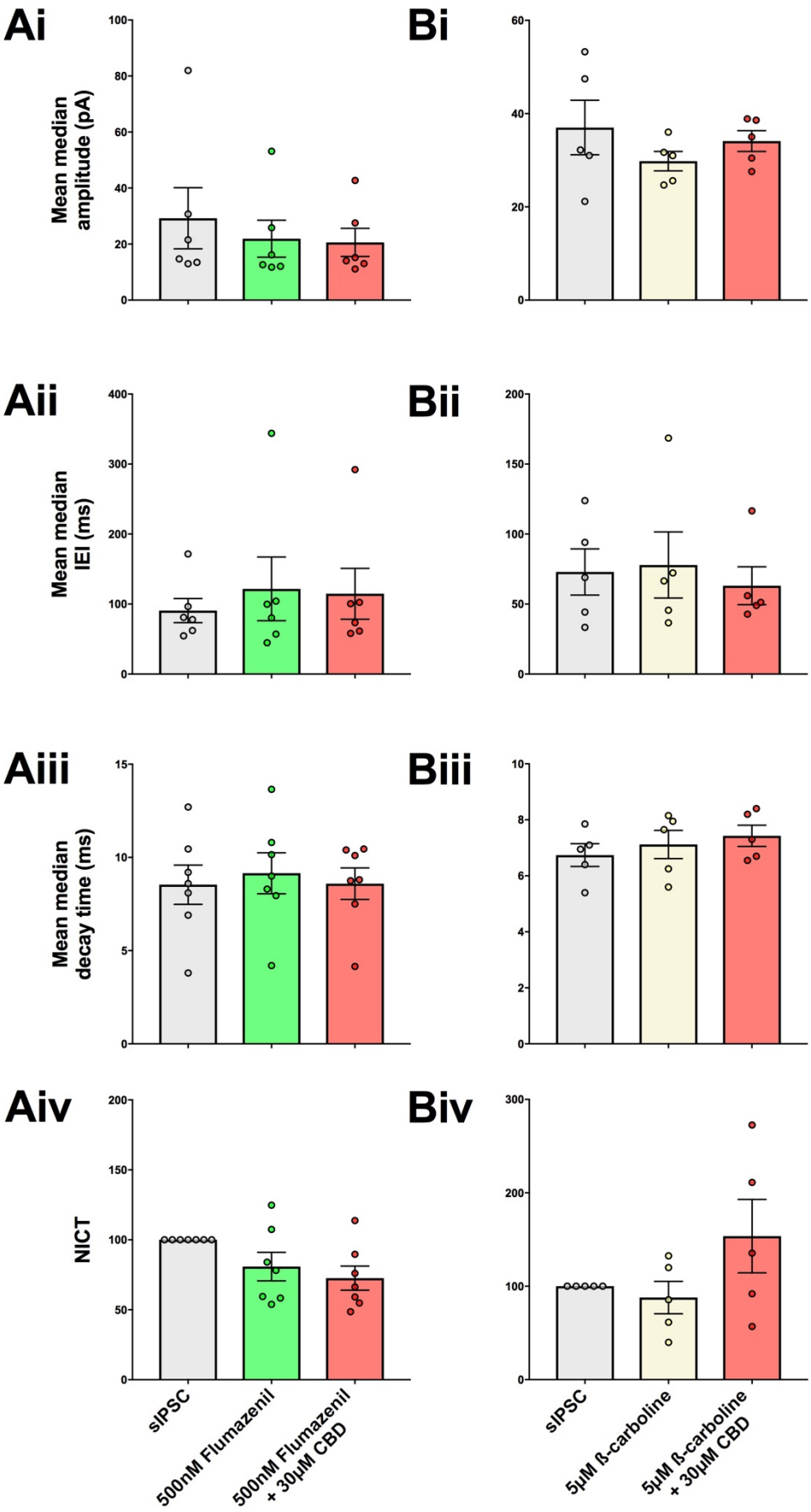

Figure 6.2 Histogram showing the responses of sIPSCs to BZ site blockers previous to CBD. The BZ site inverse agonists flumazenil (Ai-iv) and β-carboline (Bi-iv) were applied. Parameters analysed include mean median amplitude (Ai/Bi), IEI (Aii/Bii) and decay time (Aiii/Biii) as well as NICT values (Aiv/Biv).

Figure 6.2.Ai highlights the mean median amplitude response of the sIPSCs upon flumazenil addition, and subsequently CBD application. The mean median values showed no significant decreased upon 500nM flumazenil addition and no significant change after CBD application either (29.2 ± 10.5 – 21.9 ± 6.63 – 20.6 ± 4.79; ranges: 13.0-82.0; 11.8-53.1; 11.1-42.7 respectively). The overall p value returned was 0.052, while the post-hoc test reveals a p value of 0.063 when comparing the baseline to 500nM flumazenil, with the same p value shown for the comparison between baseline and 500nM flumazenil + 30μM CBD. **Aii** shows the mean median IEI responses, where no change was observed between the flumazenil or CBD additions and baseline (86.0 ± 15.3 – 115 ± 39.0 – 110 ± 31.1; range: 54.6-172; 44.8-344; 58.1-292). An overall p value of 0.49 was returned for this dataset, with the multiple comparison post-hoc also producing no significance.

The mean median decay times are presented in **Aiii** and, though a trending increase upon the addition of flumazenil was shown, no significance was noted in either flumazenil or once CBD was applied (8.54 ± 1.06 – 9.15 ± 0.85 – 8.59 ± 0.85; range: 3.8-12.7; 4.2-13.7; 4.15-10.5). This dataset produced an overall p value of $p = 0.051$, with the post-hoc analysis highlighting the comparison between baseline and 500nM flumazenil as having a p value of 0.069, suggestive of a trending increase. **Aiv** presents the mean NICT values for each drug condition. No change in value was shown in 500nM flumazenil (80.9 ± 10.2; range: 53.8-124), which continued when CBD was applied (72.6 ± 8.60; range: 48.6-114). An overall p value of 0.19 was produced from this dataset, while the post-hoc analysis shows no significance either.

Bi-iv represents sIPSC responses to the addition of 5μM β-carboline-3-carboxylic acid N-methylamide (β-carboline) previous to the addition of CBD. **Bi** shows the mean median amplitude response, where no change upon the addition of β-carboline was observed (37.0 ± 5.84 – 29.8 ± 2.09 – 34.1 ± 2.23; range: 21.2-53.3; 24.7-36.0; 27.6-38.9). The overall p value for this data was 0.69, with the post-hoc analysis showing no significance here either. **Bii** highlights the mean median IEI response, where no change was noted in either β-carboline or CBD (72.9 ± 16.5 – 77.9 ± 23.6 – 63.1 ± 13.5 - 42.8-116; range: 33.4-124; 36.6-169. The overall p value here was 0.37, with no post-hoc comparisons approaching significance.

Biii represents the mean median decay time responses, where the addition of β-carboline had no effect (6.74 ± 0.41 – 7.12 ± 0.50; range: 5.40-7.85; 5.60-8.15). The addition of CBD also provided no change (7.43 ± 0.38; range: 6.55-8.40). A p value of 0.69 was returned, with the post-hoc analysis showing no significance. **Biv** shows the relative NICT values for each drug condition, where the addition of β-carboline caused no change (87.9 ± 17.4; range: 39.9-133), while the application of CBD caused a visually large increase, however this was not reflected in the statistical analysis, most likely due to the large variance among the responses (154 ±

39.4; range: 56.9-273). The overall p value was 0.52, with no significance shown in the post-hoc analysis either.

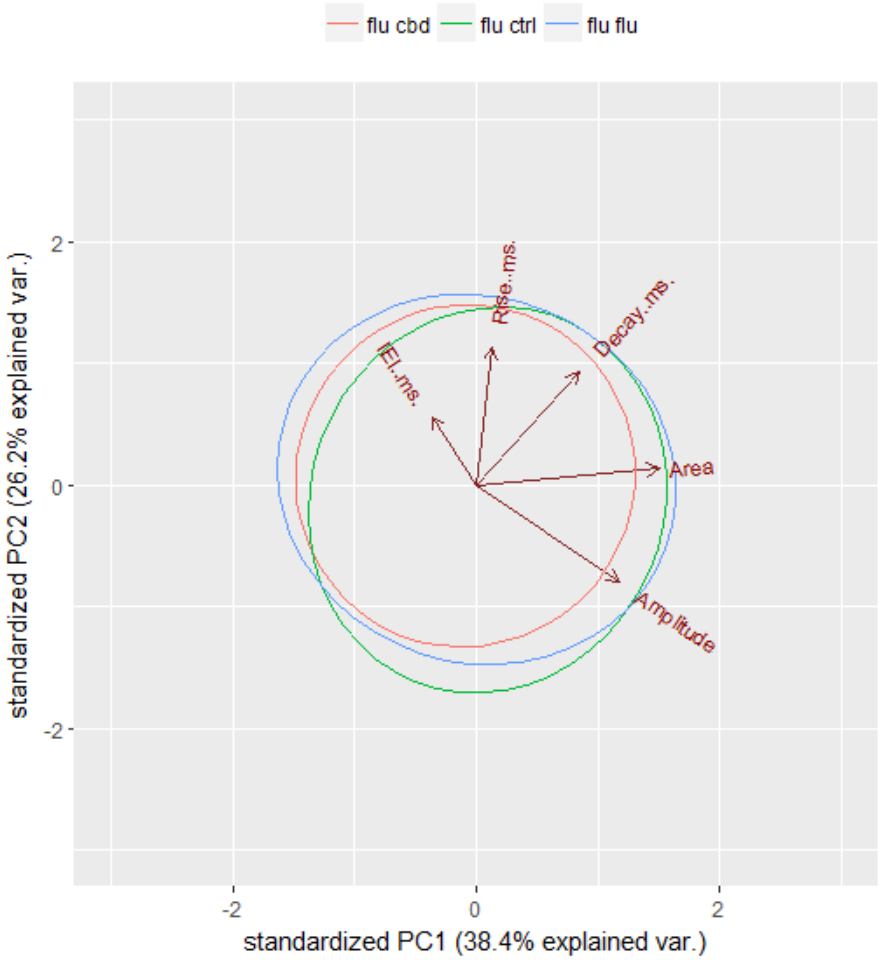

Figure 6.3 PCA of flumazenil data.
Green circle is the baseline, blue is flumazenil and, red CBD.

PCA computations were also performed for the flumazenil experimental data, to observe the components responsible for the largest variation (**Figure 6.3**). As with the CBD only addition (**Chapter 5**), the area component was the first principal component, as evidenced by the shifting of the circle and size of arrow (red circle against blue circle). Amplitude and decay time are the second and third principal components, which are the two parameters used to find the area. This again, therefore, highly suggests that increases in event area, through alterations to decay time and amplitude, are occurring in the presence of CBD. The addition of flumazenil does not seem affect variation here too much, though the circle has shifted downward somewhat, suggesting that amplitude many be the component causing the most variance here.

A ‘positive control’ experiment was then performed, applying CBD before flumazenil to see if it is able to inhibit CBD induced effects on sIPSC responses (n = 8, animal n = 8), the results of which are presented in **Figure 6.5.Ai-iv**.

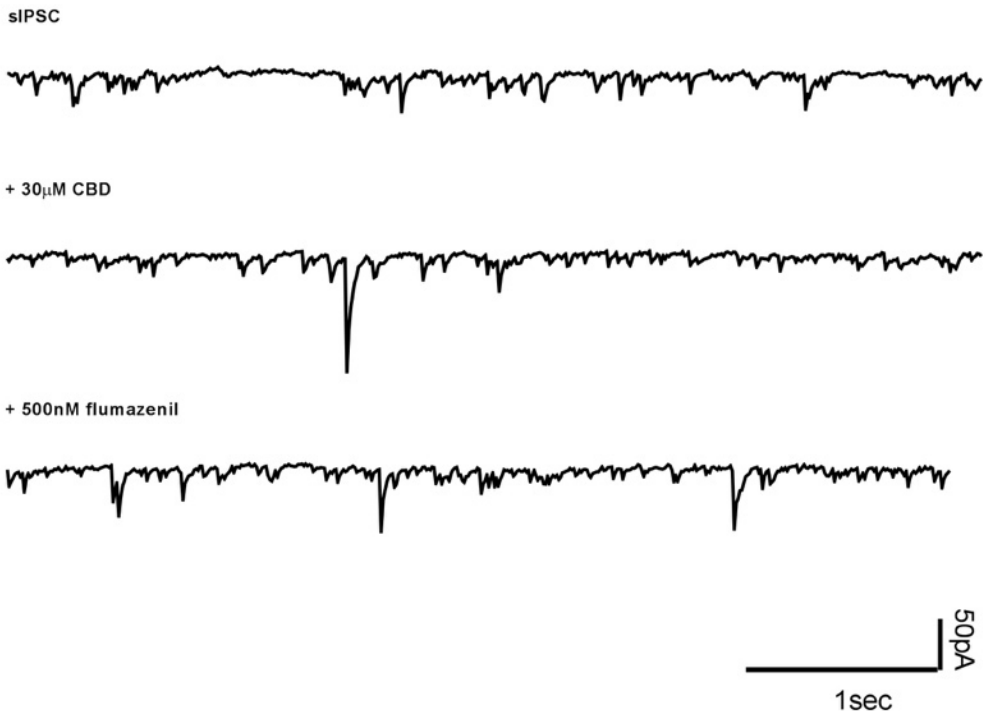

Figure 6.4 Raw trace of sIPSCs from a flumazenil positive control experiment
Here 30μM CBD has been added before 500nM flumazenil

As can be observed in **Ai**, there was no change to the mean median amplitude when CBD or flumazenil was applied (27.9 ± 4.06 – 28.4 ± 4.07 – 29.6 ± 4.46; range: 14.2-46.6; 15.4-48.8; 16.2-49.8). The overall p value returned was 0.53, with no significance in the post-hoc analysis. **Aii** highlights the mean median IEI, where a significant decrease is noted upon CBD addition (59.7 ± 5.80 – 51.7 ± 4.83; range: 33.5-84.5; 29.5-65.8). This significance was lost once flumazenil was added, with a recovery back toward the baseline value (58.0 ± 5.26; range: 32.8-71.8). The overall p value for this dataset was 0.001, with the post-hoc Dunn’s multiple comparison showing significance between baseline and 30μM CBD (p = 0.0035). When 30μM CBD was compared to 30μM CBD + 500nM flumazenil condition the p value was 0.053, suggesting a trending increase.

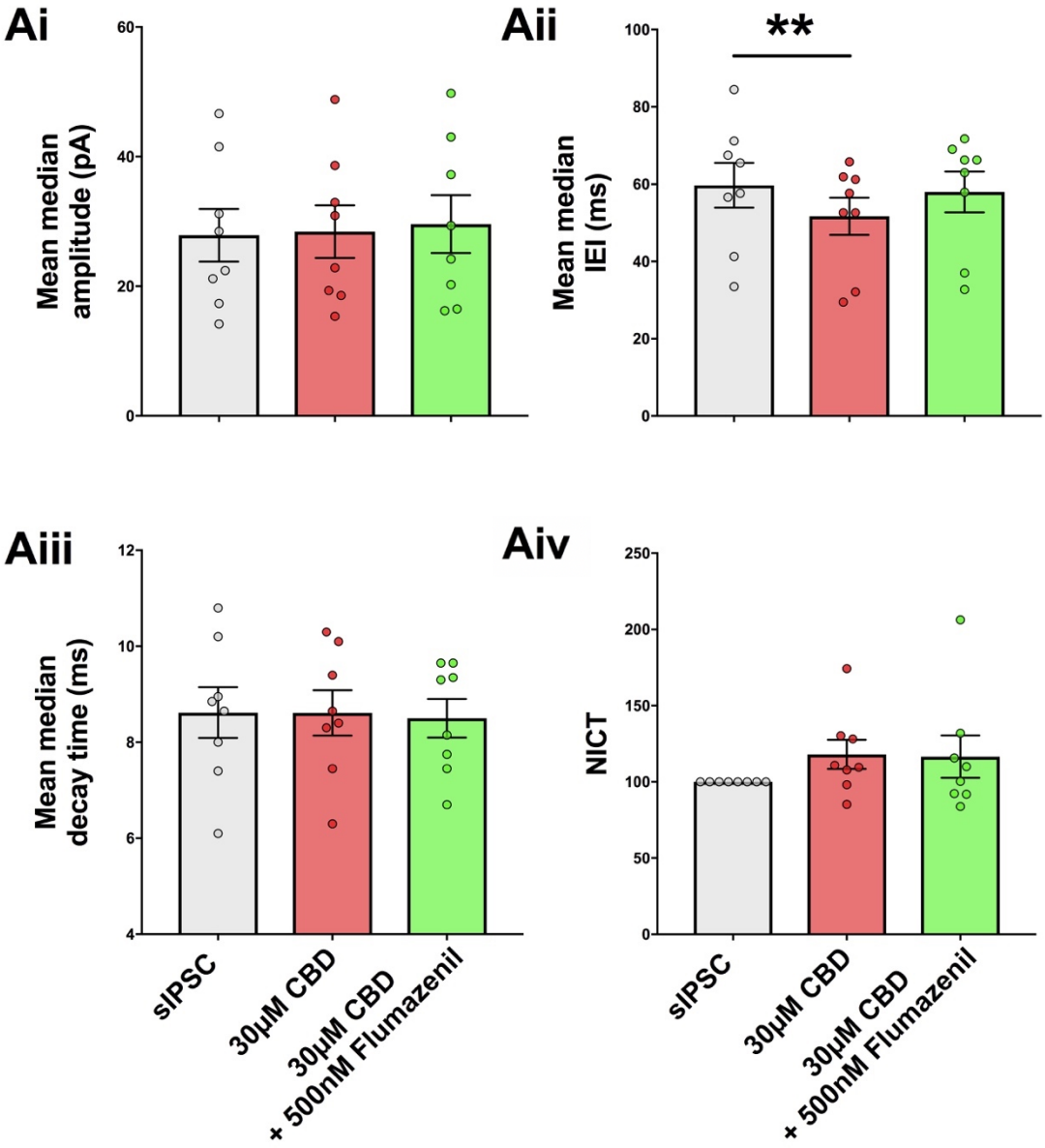

Figure 6.5 Histogram of flumazenil positive control experiments
Parameters analysed include Ai - mean median amplitude; Aii - mean median IEI; Aii - mean median decay time; Aiv - NICT values. ** $p < 0.01$.

Aiii shows the mean median decay time responses, where surprisingly there was no change when CBD was added (8.62 ± 0.53 – 8.61 ± 0.48; range: 6.1-10.8; 6.3-10.3). Similarly, the addition of 500nM flumazenil also caused no alteration to the mean median value (8.50 ± 0.40; range: 6.70-9.65). The p value returned here equalled 0.76, with the post-hoc showing no significance. **Aiv** presents the relative NICT values, with again no change upon CBD (118 ± 9.56; range: 85.3-174), or flumazenil addition (117 ± 13.9; range: 83.8-206) noted. The overall p value was 0.36, with the post-hoc analysis shows no significance between any of the comparisons.

6.2.1.2 Additive effects of CBD at $GABA_AR$

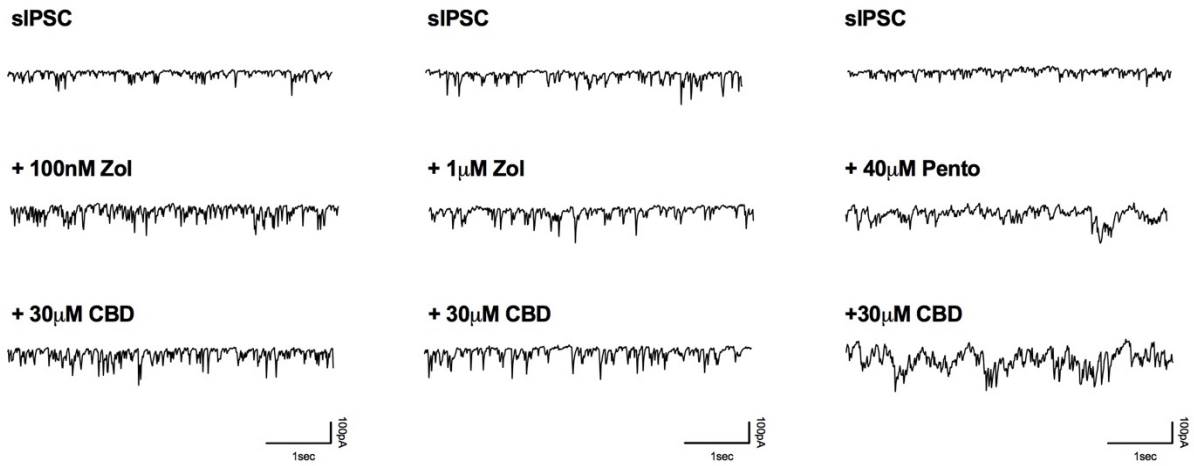

Figure 6.6 Raw traces of sIPSC from 100nM, 1μM zolpidem and 40μM pentobarbital treatments.

To test whether the effect of CBD observed was acting at the BZ site or at another allosteric site varying zolpidem doses were applied (a well-known BZ site agonist). Two doses of zolpidem were employed for this, a minimal 100nM dose (n = 6, animal n = 5) and a maximal 1μM dose (n = 6, animal n = 5), as this would allow us to observe whether the effect of CBD would be additive with the zolpidem effect, suggesting a differential binding location, or competitive (**Figure 6.7.Ai-Biv**). An additive effect would be observed by CBD increasing the decay time and NICT values when added after the 100nM zolpidem dose, a competitive effect would most likely show no change. A third drug treatment was also employed, 40μM pentobarbital (n = 4, animal n = 3), a potentiator at $GABA_AR$ receptors, specifically binding to the α1 subunit barbiturate site. Pentobarbital was selected to investigate whether CBD was interacting at the barbiturate binding site present on many $GABA_AR$ conformations to exert its effect (**Ci-iv**).

The first histograms presented are the 100nM zolpidem addition (**Ai-iv**), where no significant effect was observed in relation to the mean median amplitude responses (**Ai**) (29.8 ± 3.79 – 35.0 ± 5.34 – 36.0 ± 5.17; range: 20.0-41.6; 23.7-59.3; 25.3-59.9). An overall p value of 0.14 was returned from this dataset, with the lowest p value observed in the post-hoc comparison between the baseline and 100nM zolpidem + 30μM CBD (p = 0.13). **Aii** shows the mean median IEI responses, with little differences observed across either zolpidem or CBD treatments (57.0 ± 9.60 – 54.1 ± 10.8 – 53.2 ± 10.1; range: 33.1-100; 29.9-104; 33.0-103). A p value of 0.43 overall was returned, with no significance shown in the post-hoc comparison.

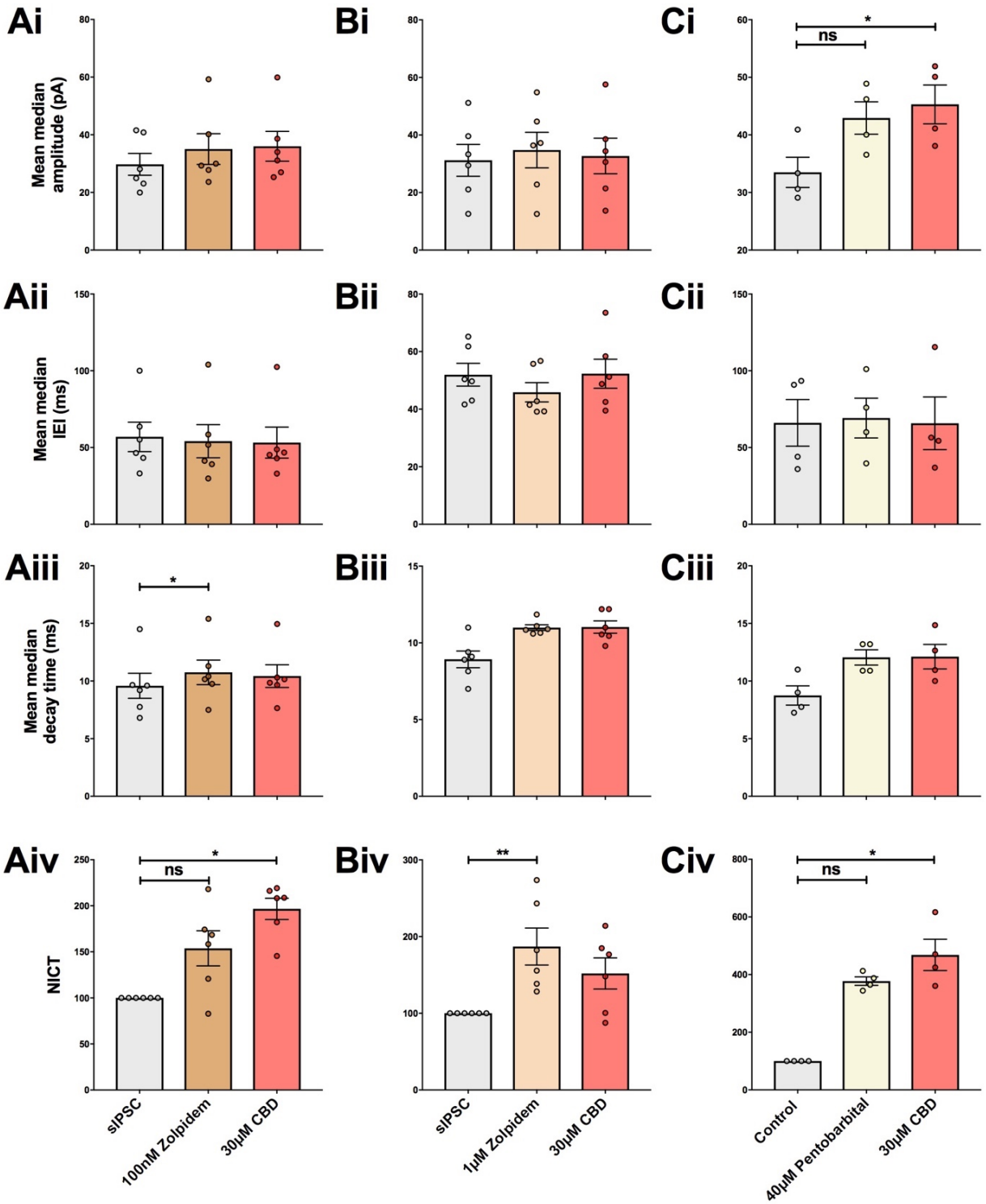

Figure 6.7 Histograms for BZ/barbiturate site agonists effect on SE tissue.
Parameters analysed for the addition of BZ and barbiturate agonists, being 100nM zolpidem (A), 1μM zolpidem (B) and, 40μM pentobarbital (C) including Ai-Ci: mean median amplitude; Aii-Cii: mean median IEI; Aiii-Ciii: mean median decay time; Aiv-Civ: NICT values. * $p < 0.05$, ** $p < 0.01$.

Aiii highlights the mean median decay time responses, where an increase was observed upon 100nM zolpidem addition (9.58 ± 1.10 – 10.8 ± 1.06; range: 6.8-14.5; 7.5-15.4). A slight decrease to lose significance was then noted upon CBD application (10.4 ± 0.99; range: 7.65-14.9). A p value of 0.006 overall is returned, with Dunn's multiple comparison post-hoc analysis showing significance between the baseline and 100nM zolpidem ($p = 0.012$). A p value of

0.0628 was shown for the comparison of baseline to 100nM zolpidem + 30μM CBD suggesting a trending increase from baseline. Relative NICT values are presented in **Aiv**, with a significant increase observed in only the CBD condition (100nM zolpidem: 154 ± 19.1; range: 82.8-218; CBD: 197 ± 11.5; range: 146-219). A p value of 0.012 was returned overall, with significance observed only in baseline vs. 100nM zolpidem + 30μM CBD (p = 0.012).

Bi-iv presents the 1μM zolpidem sIPSC responses. **Bi** highlights the mean median amplitude responses, where no changes were noted upon the addition of zolpidem (31.2 ± 5.56 – 34.8 ± 6.18; range: 12.6-51.2; 12.6-54.8), or CBD (32.7 ± 6.18; range: 13.7-57.6). No significance was noted for this dataset, either overall (p = 0.43), or through post-hoc analysis. **Bii** shows the mean median IEI responses, with again no alterations noted upon zolpidem addition (52.0 ± 3.95 – 45.9 ± 3.34; range: 41.6-65.2; 39.1-56.8), or CBD addition (52.3 ± 5.03; range: 39.5-73.5). A p value of 0.14 overall was returned, with the post-hoc comparison showing a p value of 0.13 between baseline and 1μM zolpidem.

In **Biii** the mean median decay times are represented, where a visually large, trending increase was observed upon the addition of 1μM zolpidem and, remained high after the addition of CBD (8.93 ± 0.54 – 11.0 ± 0.19 – 11.0 ± 0.40; range: 7.00-11.0; 10.6-11.9; 9.80-12.2). A p value of 0.052 overall was returned suggesting a trending increase, with the multiple comparison post-hoc also producing a trending p value of 0.063 between the baseline and zolpidem + 30μM CBD. The final histogram (**Biv**) shows the mean NICT value for each drug treatment, with a large, highly significant increase observed upon zolpidem addition (187 ± 24.1; range: 128-274), which subsequently decreased once CBD was applied to lose significance (152 ± 20.3; range: 87.6-214). The overall p value was 0.0017, with the post-hoc returning a value of 0.0045 for the comparison of baseline and 1μM zolpidem. There was no significance observed between the baseline and 1μM zolpidem + 30μM CBD condition.

Figure 6.7.Ci-iv highlights the effect of 40μM pentobarbital on the various kinetic parameters. **Ci** shows the mean median amplitude response, which showed a relatively large visual increase upon the addition of pentobarbital (33.5 ± 2.62 – 42.9 ± 2.82; range: 29.1-40.9; 36.6-48.9). A subsequent significant increase was observed upon the application of CBD (45.3±3.37; range: 38.1-51.9). An overall p value of 0.0046 was produced by this dataset, with the post-hoc analysis highlighting significance arose only between the baseline and 40μM pentobarbital + 30μM CBD condition. The mean median IEI responses are shown in **Cii**, where little alterations were noted in either the pentobarbital or CBD treatments (66.1 ± 15.1 – 69.2 ± 13.0 – 65.8 ± 17.1; range: 36.0-93.4; 39.7-101; 36.9-116). The p value for this dataset was 0.43 overall, while the post-hoc analysis displayed no significance.

Mean median decay time responses are presented in **Ciii**, where no changes were present upon the addition of pentobarbital (8.75 ± 0.84 – 12.1 ± 0.66; range: 7.25-11.0; 10.9-13.2 respectively) or following CBD addition (12.1 ± 1.06; range: 10.0-14.9). Despite the seemingly large increase between baseline and 40μM pentobarbital, the returned p value was 0.27, with no significance observed in the post-hoc analysis. The final histogram of this set displays the mean NICT values (**Civ**), where surprisingly no change was noted upon pentobarbital addition (377 ± 14.8; range: 344-413), though a significant increase was noted once CBD was applied (468 ± 54.4; range: 361-617). The overall p value produced was 0.0046, though in spite of the large increase noted upon pentobarbital addition, no significance was noted (p = 0.47). Significance was, however, presented between baseline and 40μM pentobarbital + 30μM CBD (p = 0.014). The reason for the lack of significance when pentobarbital is added is due to the statistical test used, non-parametric, chosen as NICT values are composed of not normally distributed data (amplitude (pA) * decay time (ms)).

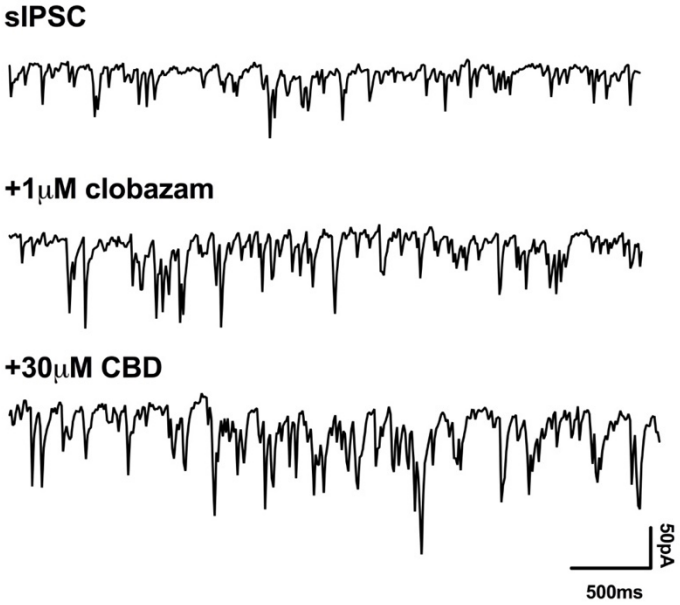

Figure 6.8 Raw traces showing the addition of clobazam before CBD.

Clobazam is a member of the 1,5-beznodiazepine class and, binds to an allosteric interface (the BZ site) between the α- and γ2- subunits of $GABA_AR$s, as a partial agonist. As an agonist of the $GABA_AR$, clobazam binding causes an increase in ionic channel opening, resulting in hyperpolarisation and enhancement of the postsynaptic GABA effect.

The effect of CBD in collaboration with clobazam has been investigated here as clobazam is currently used as an anti-epileptic drug. Clobazam is specifically used in the treatment of Lennox-Gastaut syndrome, a syndrome CBD purportedly has beneficial effects in as well, therefore opening the possibility of co-application of these two drugs if applicable. Alongside this, collaborators investigating CBD *in vitro* in cell culture using recombinant human $GABA_AR$ in HEC cells, have noted clobazam is able to potentiate the CBD effect (R Harvey, personal communication).

Figure 6.9 highlights the results found from the application of 1μM clobazam previous to the addition of CBD to the sIPSC parameters. An n of 10, animal n = 6 has been used in these results.

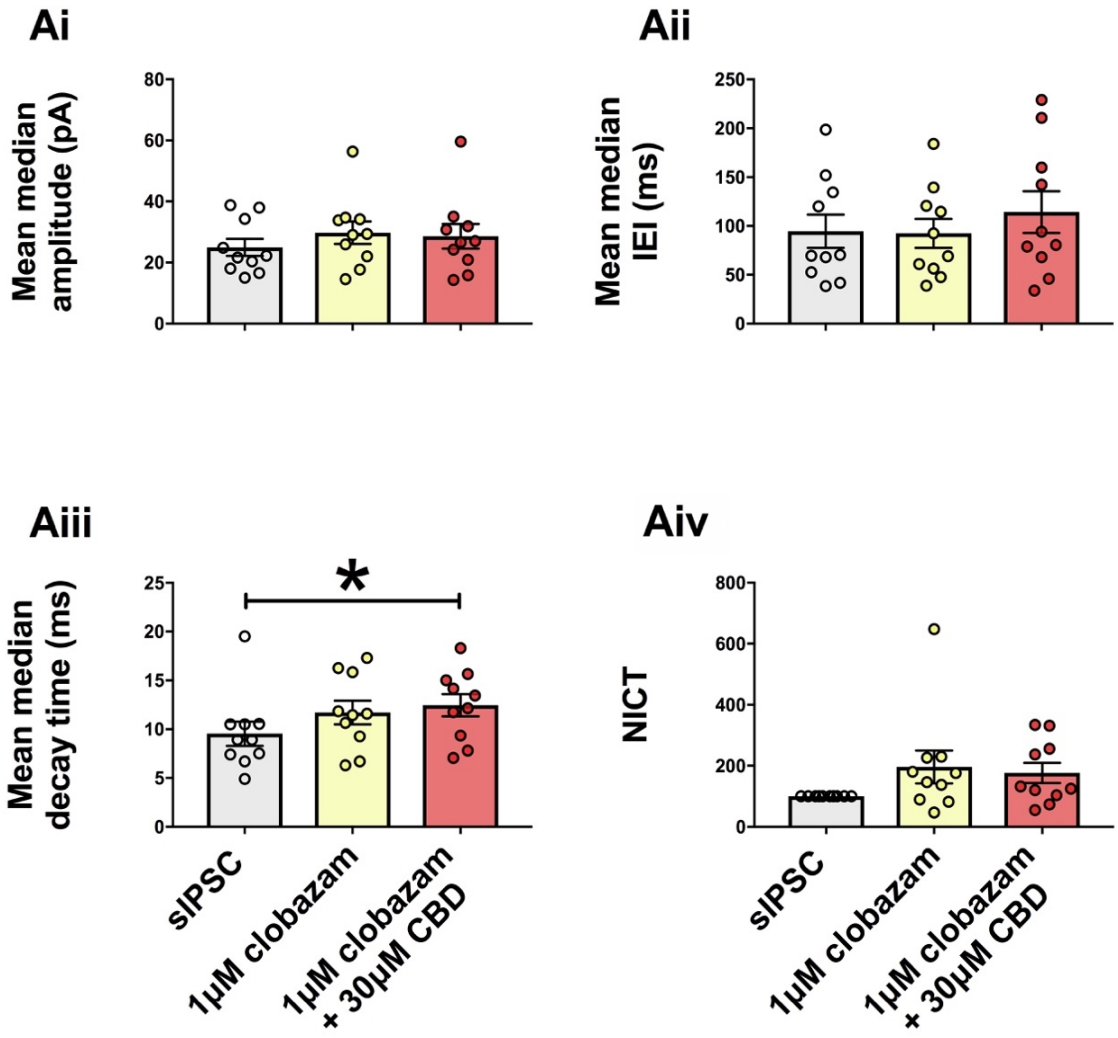

Figure 6.9 Histograms showing the effect of 1μM clobazam on sIPSCs
Parameters analysed include, Ai: mean median amplitude; Aii: mean median IEI; Aiii: mean median decay time; Aiv: NICT values. * $p < 0.05$.

Ai shows the mean median amplitude responses, where the addition of clobazam and CBD had no effect (25.0 ± 2.80 – 29.8 ± 3.68 – 28.6 ± 4.04; range: 15.1-38.8; 14.6-56.4; 14.3-59.6). A p value of 0.19 was presented overall, with the lowest p value returned in multiple comparison post-hoc shown when clobazam was added ($p = 0.22$). **Aii** highlights the mean median IEI responses, where little alterations were noted upon the application of clobazam or CBD (94.5 ± 17.0 – 92.4 ± 14.8 – 114 ± 21.5; range: 38.4-199; 38.8-184; 33.8-229). An identical p value to that of the mean median amplitude was noted here ($p = 0.19$), both overall and from the post-hoc analysis.

Aiii presents the mean median decay time, where no differences were noted with clobazam addition, though a significant increase was shown when CBD was applied (9.54 ± 1.25 – 11.7 ± 1.21 – 12.5 ± 1.34; range: 4.90-19.5; 6.30-17.3; 7.05-18.3). A p value of 0.012 was returned overall, with baseline vs. 1μM clobazam + 30μM CBD showing significance (p = 0.011). The final histogram presented shows the NICT values (**Aiv**), where no effect of the addition of clobazam was observed (196 ± 53.6; range: 46.9-647), nor when CBD was applied (177 ± 32.9; range: 54.9-334). The overall p value was 0.19, with a low occurring between baseline vs. 1μM clobazam + 30μM CBD in the post-hoc (p = 0.22).

6.2.1.3 Modulation of the neurosteroid site

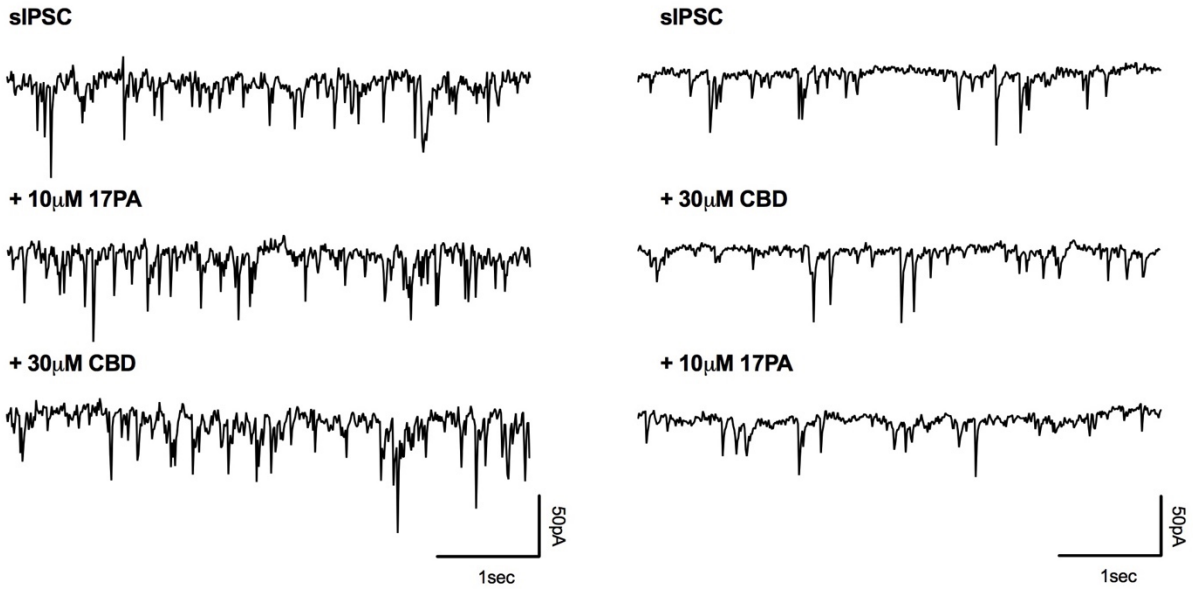

Figure 6.10 Raw traces of 17PA addition before (left) and after (right) CBD addition.

As our data suggest a $GABA_AR$ binding site for CBD that is not one of the well-known sites, we investigated whether CBD was binding at a neurosteroid site. To investigate this, we applied the known neurosteroid NAM, 17-Phenylandrostenol (17PA) to observe its effects on CBD action. 17PA was applied at a dose of 10μM, bath applied, either before (n = 3, animal n = 2) or after (n = 4, animal n = 3) the 30μM CBD application. The n numbers for this experimental dataset are low due to time constraints of the project, though some useful information can be interpreted despite this, though they are limited in nature.

Figure 6.11 presents the results for this dataset, with **Ai-iv** showing the 17PA application before CBD and **Bi-iv** the reverse.

Ai shows the effect on mean median amplitude, where little change was shown (33.9 ± 3.86 – 36.3 ± 4.12 – 35.0 ± 2.71; range: 28.1-41.2; 31.4-44.5; 30.0-39.3). An overall p value of 0.36 was produced, with the post-hoc analysis showing this was derived mainly from the initial 17PA addition (p = 0.31). Once more, no alterations were noted in the mean median IEI response (**Aii**) by either 17PA or CBD addition (37.9 ± 3.98 – 40.0 ± 5.47 – 37.5 ± 5.45; range: 30.6-44.3; 30.6-49.6; 28.8-47.5 respectively). The overall p value was 0.19, with the multiple comparison post-hoc showing a p value of 0.31 between the baseline and 17PA condition.

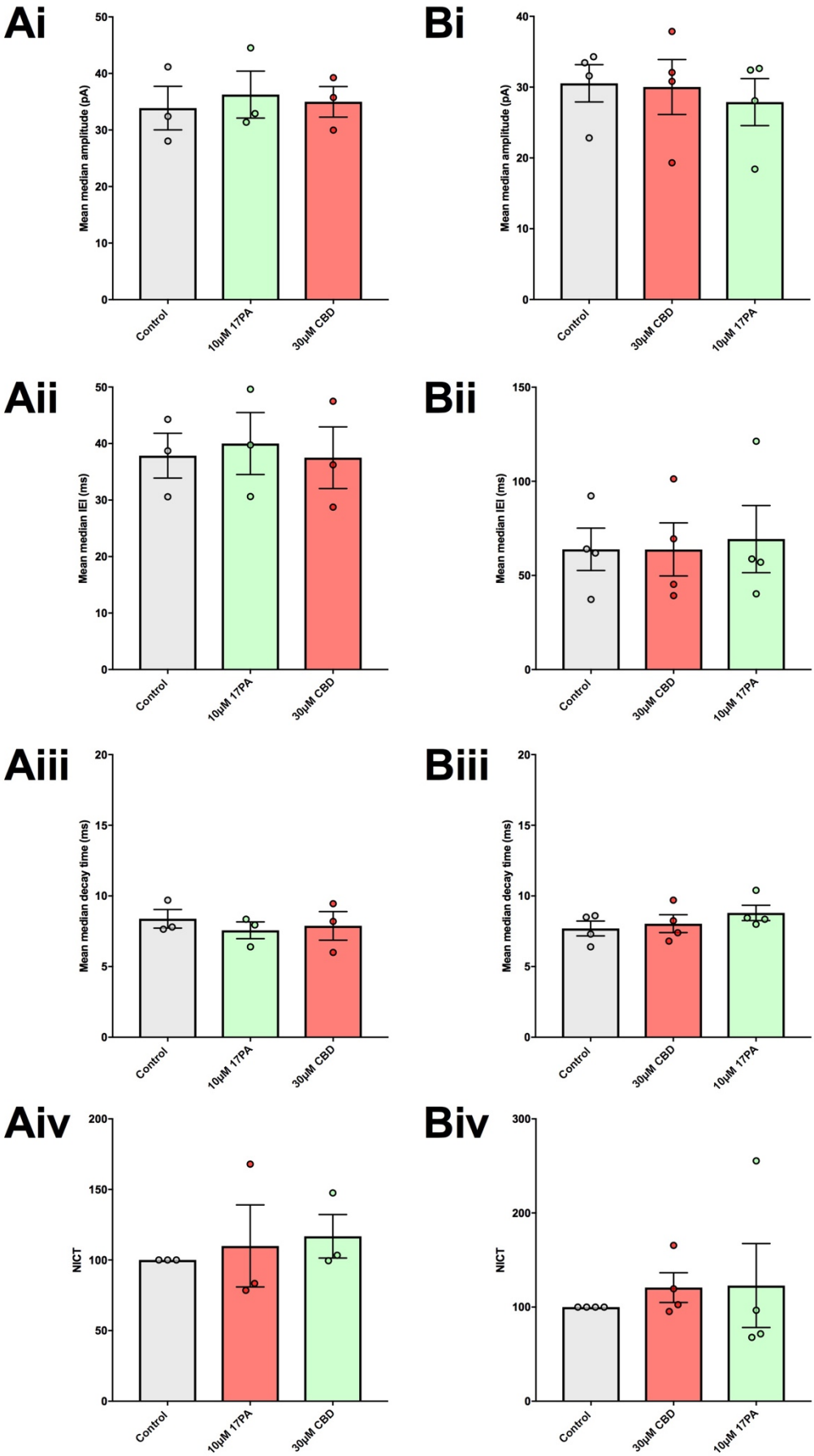

Figure 6.11 Histograms showing the effect of the neurosteroid 17PA on sIPSCs. Parameters analysed with 17PA addition before (left) and after (right) CBD addition, include, Ai-Bi: mean median amplitude; Aii-Bii: mean median IEI; Aiii-Biii: mean median decay time; Aiv-Biv: NICT values.

No effect on mean median decay was observed upon 17PA or CBD addition (**Aiii**; 8.38 ± 0.66 – 7.57 ± 0.59 – 7.88 ± 1.01). Observing the distribution of population responses, CBD application caused a wider spreading of responses post 17PA addition, with one increasing, one remaining constant and one decreasing (range: 7.65-9.70; 6.40-8.35; 6.00-9.45 respectively across the conditions). The NICT (**Aiv**) parameter showed no change upon either 17PA or CBD addition (110 ± 29.0 – 117 ± 15.4; range: 78.6-168; 99.5-148). The overall p value returned p = 0.94, with no significance among the post-hoc comparisons.

Bi displays the mean median amplitude, where little differences were noted upon CBD addition (30.5 ± 2.63 – 30.0 ± 3.88; range: 22.8-34.3; 19.3-37.9). The subsequent addition of 17PA also displayed no effect on the value (27.9 ± 3.32; range: 18.4-32.7). A p value of 0.13 overall was returned, with the post-hoc analysis showing a p value of 0.10 between the baseline and 30μM CBD + 10μM 17PA condition. **Bii** highlights the mean median IEI responses, where no alterations were noted upon CBD addition (63.9 ± 11.3 – 63.8 ± 14.1; range: 37.3-92.3; 39.3-101). The 17PA addition caused no change to the response either (69.3 ± 17.8; range: 40.3-121). There was no hint of significance here, with an overall p value of 0.93 and no trends observed in the post-hoc calculations.

This pattern is repeated in the mean median decay time (**Biii**), with no changes upon CBD or 17PA addition (7.70 ± 0.52 – 8.04 ± 0.63 – 8.80 ± 0.54; range: 6.40-8.60; 6.80-9.70; 8.00-10.4. **Biv** highlights the NICT responses, where no change was noted upon CBD addition (121 ± 15.8), with the range showing 2 of the 4 responses increased relatively substantially, while another rose slightly, and the final response remained unchanged (range: 95.3-166). This lack of effect endured upon 17PA application (123 ± 44.6), though closer examination showed a large increase of one response while the other three all decreased from their CBD values (68.0-255). With an increased n number it would be interesting to observe what the results of this experiment may be.

6.2.1.4 Summary of $GABA_AR$ modulation on CBD effects

Table 6.1 below shows a summary of the effects noted by CBD with (and without) GABAAR modulation. In brief, there was a lack of effect on the AMC animals by CBD, while the SE animals showed a significant decrease in IEI and, significant increases to both decay time and NICT values. All experiments after were only performed in SE animals.

The use of $GABA_AR$ inverse agonists in SE animals inhibit the effects of CBD (Flumazenil and β-carboline rows). A low dose of zolpidem (100nM) alone increases the decay time, while the subsequent addition of CBD increases the NICT value significantly, while the decay time alteration is lost. The larger zolpidem dose (1μM) showed a large increase in NICT value, which was subsequently lost after CBD addition. Pentobarbital addition showed no significant

changes to any parameter alone, while the subsequent addition of CBD showed significant increase in both amplitude and NICT values. Finally, the addition of clobazam showed no effect alone, while the addition of CBD afterward showed an increase to decay time. Modulation of the neurosteriod site using 17-PA showed no effect at all when added previous to CBD.

Two positive controls were also performed (where the drug was added after CBD). The flumazenil control showed a significant decrease in the IEI when CBD was applied (+ Flumazenil row), but otherwise no other effects in either CBD or + flumazenil conditions. The 17-PA control showed no effect on kinetics in either drug.

Drug used	+ Drug				+ 30µM CBD			
	Amp	IEI	Decay	NICT	Amp	IEI	Decay	NICT
AMC	N/A	N/A	N/A	N/A	-	-	-	-
SE	N/A	N/A	N/A	N/A	-	↓	↑	↑
Flumazenil	-	-	-	-	-	-	-	-
β-carboline	-	-	-	-	-	-	-	-
100nM Zolpidem	-	-	↑	-	-	-	-	↑
1µM Zolpidem	-	-	-	↑↑	-	-	-	-
Pentobarbital	-	-	-	-	↑	-	-	↑
Clobazam	-	-	-	-	-	-	↑	-
17-PA	-	-	-	-	-	-	-	-
	+ 30µM CBD				+ Drug			
	Amp	IEI	Decay	NICT	Amp	IEI	Decay	NICT
+ Flumazenil	-	↓↓	-	-	-	-	-	-
+17-PA	-	-	-	-	-	-	-	-

Table 6.1 Summary of $GABA_AR$ modulation effects on CBD influence on sIPSC kinetics
Ages, condition of animals and, drugs used are noted on the left, with the sIPSC kinetic parameters noted horizontally across the top. The arrows have been used to show the level of significance achieved at that dose (1 arrow = 0.05, 2 = 0.01), with the direction of the arrow also representing the direction of change in value.

6.2.2 Modulation of the NMDAR

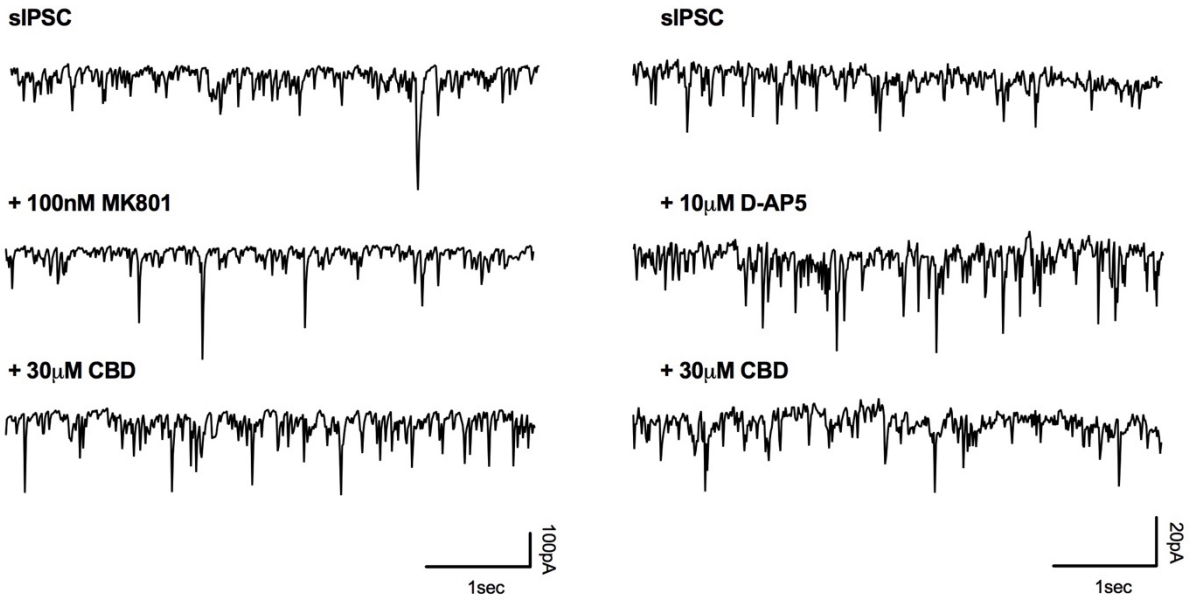

Figure 6.12 Raw traces of sIPSC responses when two separate NMDAR antagonists are added. One non-competitive (MK801; left) and one competitive (D-AP5; right).

Concurrently with the $GABA_AR$ investigations, we also examined the possible role of NMDAR-CBD interactions, due to the possible links between NMDARs and their possible modulation of $GABA_AR$ function detailed in the previous section (**Section 6.1**). With regards to this possible NMDAR interaction, we were interested in the effect antagonistic inhibition of NMDARs had on the CBD response. As such we added a variety of NMDAR antagonists, both competitive and non-competitive, as well as subunit specific antagonists to observe their effect on the induced CBD effect. To do so, we used two NMDAR antagonists initially, one non-competitive antagonist (100nM MK801; n = 8; animal n = 6), the other a competitive antagonist (50μM D-AP5; n = 6; animal n = 3), the results of which are displayed in **Figure 6.13**.

Exploring first the effects of 100nM MK801 on CBD response (**Ai-Aiv**), it is obvious that its application is sufficient to block the CBD responses observed in **Figure 5.2**.**Ai** displays the mean median amplitude responses, where no effect of either MK801 or CBD was observed (26.1 ± 3.60 – 26.7 ± 4.56 – 28.2 ± 5.50). The ranges of response did increase slightly upon application of both MK801 and CBD however (15.2-46.7; 11.3-54.3; 12.2-63.4). The overall p value returned here was 0.97, with no effects observed in the post-hoc analysis. Examining next **Aii**, no change in mean median IEI was observed upon the addition of MK801, with CBD unable to exert an effect either (75.5 ± 18.9 – 88.4 ± 21.7 – 90.5 ± 24.8), the ranges of the responses remained relatively stable (32.4-180; 34.1-198; 30.5-207). A p value of $p > 0.99$ was returned with no trends noted in the post-hoc.

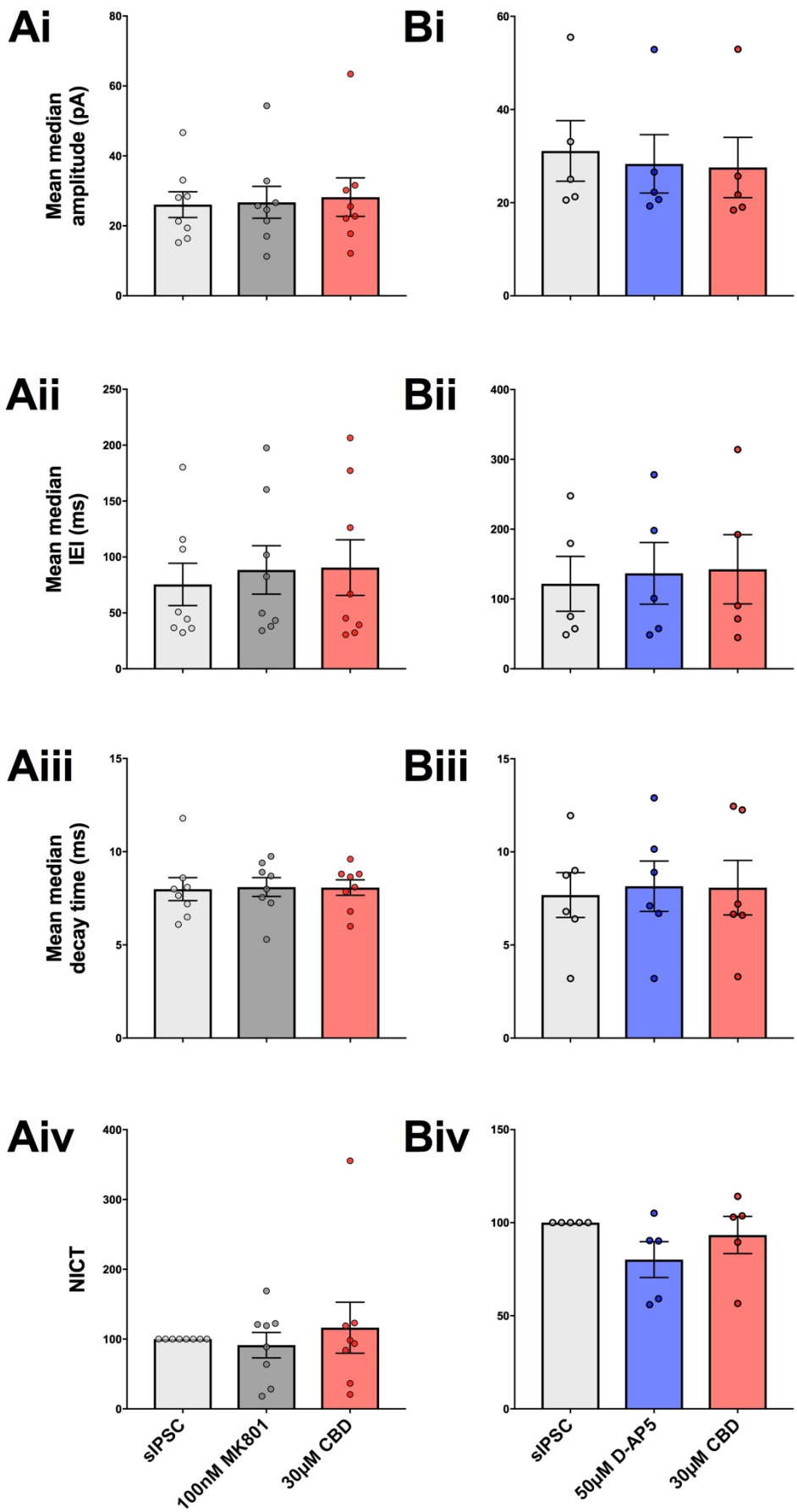

Figure 6.13 Histograms showing MK801 and D-AP5 experiment responses.
Mean median amplitude (Ai-Bi), IEI (Aii-Bii), decay time (Aiii-Biii) as well as NICT values (Aiv-Biv) have been analysed. MK801 (left), AP-5 (right).

The mean median decay time responses are highlighted in **Aiii**, where again, no changes were noted in either of the drug conditions (7.99 ± 0.62 – 8.11 ± 0.51 – 8.08 ± 0.42; range: 6.10-11.8; 5.30-9.75; 6.00-9.60). The p value for this dataset was 0.97, with no significance observed in the post-hoc analysis. **Aiv** notes the NICT values, where neither the MK801 or CBD treatments showed any effect (91.3 ± 18.3 – 116 ± 36.5; range: 18.2-169; 20.7-356). A p value of 0.79 was returned, with no trends noted in the post-hoc. If the possible anomalous data from the CBD treatment is removed (356) along with its paired data points the mean NICT values fall to 87.1 ± 20.5 in MK801 and 82.2 ± 14.9 in CBD, while the overall p value becomes 0.62 with no trends of note in the post-hoc analysis. Due to the lack of change from its removal and consistent values displayed from this respondent in the other parameters analysed, this dataset has been kept in the analysis pool.

Bi displays the mean median amplitude response upon addition of D-AP5 prior to CBD. Little change was noted when D-AP5 was added, or upon the application of CBD (33.2 ± 5.72 – 32.6 ± 6.63 – 26.6 ± 5.37 respectively), the ranges also remained relatively constant (20.6-55.5; 19.3-53.6; 18.4-53.0). The overall p value was 0.14, with the lowest p value in the post-hoc observed between baseline and 50μM D-AP5 + 30μM CBD at p = 0.13. **Bii** highlights the mean median IEI responses, with no change observed in either the D-AP5 or CBD applications (113 ± 33.18 – 126 ± 37.7 – 146 ± 40.6; range: 48.8-248; 48.6-278; 44.8-314). The overall p value returned for this dataset was 0.43, with the lowest p value in the post-hoc observed between baseline and 50μM D-AP5 + 30μM CBD at p = 0.45.

Examining next the mean median decay times (**Biii**), no changes were noted in either drug application (7.68 ± 1.21 – 8.16 ± 1.35 – 8.08 ± 1.47; range: 3.20-11.9; 3.20-12.9; 3.30-12.4). An overall p value of 0.52 was found for this dataset, with no change in the post-hoc. The final histogram presented here represents the NICT values (**Biv**), with no change in either D-AP5 (83.8 ± 8.66; range: 55.9-105) or CBD (81.9 ± 14.0; range: 24.8-114.1) shown. A p value of 0.96 was found here, with no trends observed in the post-hoc analysis.

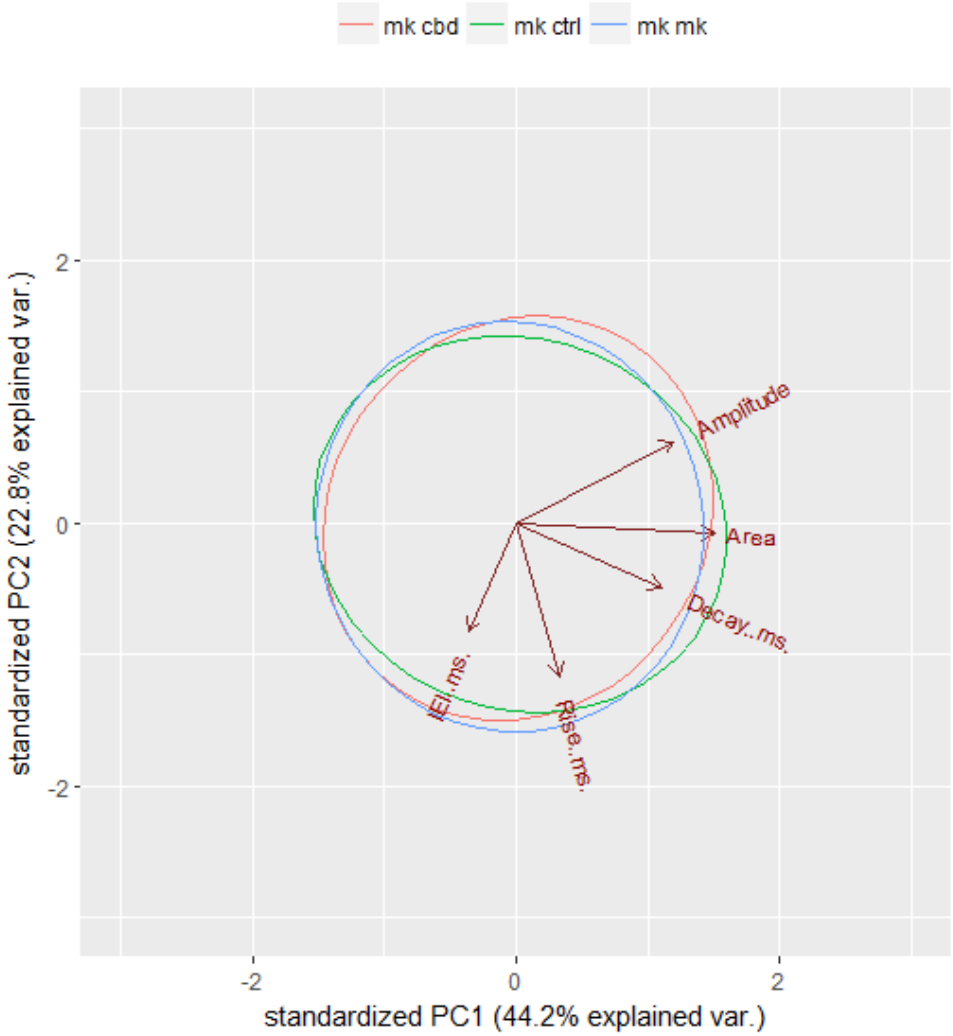

Figure 6.14 PCA of MK801 application effect on CBD response.
The green circle is the baseline, blue MK801 and red CBD.

PCA was performed on the MK801 dataset to observe whether the inhibition of the CBD effect was due to a restriction in area, amplitude and decay time by MK801. **Figure 6.14** represents this, and as can be observed, the amount of variation between the concentric rings is lower than that of the PCA of CBD alone (**Figure 5.5**), highly suggestive of MK801 successfully blocking CBDs ability to increase decay time, amplitude and, therefore, area values.

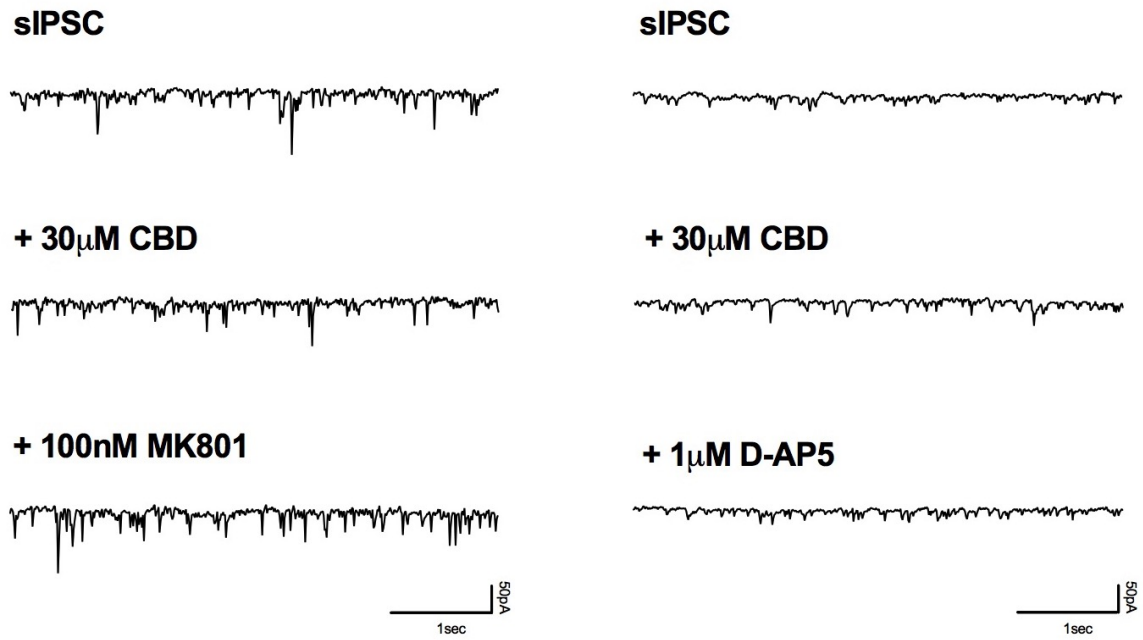

Figure 6.15 Raw traces of both NMDAR antagonists being added after CBD. MK801 on the right, D-AP5 on the left.

As with the $GABA_AR$ dataset, positive controls were also performed on the NMDAR antagonists at the same concentrations used previously (**Figure 6.16**), with CBD being applied before the antagonist (MK801: n = 7; animal n = 5; D-AP5: n = 5, animal n = 4).

As presented, there was no change in the mean median amplitude (**Ai**) upon CBD addition (22.7 ± 5.07 – 19.7 ± 3.41 – 21.3 ± 4.81; range: 9.74-45.9; 11.2-37.5; 11.0-47.9). A p value of 0.49 was shown, with a lowest p value of 0.54 observed post-hoc between the baseline and 30μM CBD + 100nM MK801. Examining the mean median IEI responses (**Aii**), no effect was observed in the presence of CBD (94.7 ± 13.3 – 84.2 ± 10.9; range: 35.5-126; 44.8-116), or in the presence of MK801 (104 ± 17.6; range: 42.5-183). No significance was found, with an overall p value of 0.19 returned and a low of p = 0.18 produced by the post-hoc test comparison between CBD alone and CBD + MK801 treatments. **Aiii** displays the mean median decay time responses, where little change was present across the drug treatments (7.97 ± 1.03 – 7.96 ± 0.78 – 7.77 ± 0.88; range: 4.00-11.3; 4.30-10.6; 4.45-10.9 respectively). Here, a p value of 0.96 was shown, with no trends observed in the post-hoc test. The final histogram of the MK801 positive control dataset highlights the comparative NICT values (**Aiv**), where once more no effect by CBD (125 ± 25.7; range: 34.3-250), or MK801 was present (107 ± 27.1; range: 27.0-249). The returned p value here was 0.19, with the comparison between the two drug treatments producing the lowest p value (p = 0.18).

The mean median amplitude for the D-AP5 positive control responses are shown in **Bi**, where no effects of CBD or the subsequent addition of D-AP5 were noted (25.3 ± 3.50 – 20.5 ± 1.68 – 19.7 ± 1.76; range: 16.9-34.2; 17.8-27.0; 16.6-26.6). A p value of 0.37 was shown, with a lowest p value of 0.34 observed post-hoc between the baseline and 30μM CBD + 50μM D-

AP5 condition. **Bii** shows the mean median IEI responses, where little change was observed upon CBD or D-AP5 addition (80.1 ± 22.6 – 81.2 ± 17.6 – 87.8 ± 12.0; range: 37.7-166; 42.9-146; 50.5-119 respectively). Here a p value of 0.99 was shown with, unsurprisingly, no trends in the post-hoc analysis.

Biii presents the mean median decay times for this dataset, with no changes again presented for either the addition of CBD or D-AP5 (8.47 ± 1.19 – 8.97 ± 1.06 – 8.98 ± 0.95; ranges: 5.25-12.4; 5.75-12.0; 6.45-11.7 respectively). The p value produced overall was 0.37, with the lowest p value in the multiple comparisons being 0.34 observed between baseline and the 30μM CBD + 50μM D-AP5 condition. The final histogram of this figure (**Biv**), once more shows the NICT values, where no change was produced by CBD (105 ± 15.4; range: 73.2-148) or observed in AP-5 (86.7 ± 19.3; range: 26.7-139). This returned an overall p value of 0.69, no trends were noted in the post-hoc analysis.

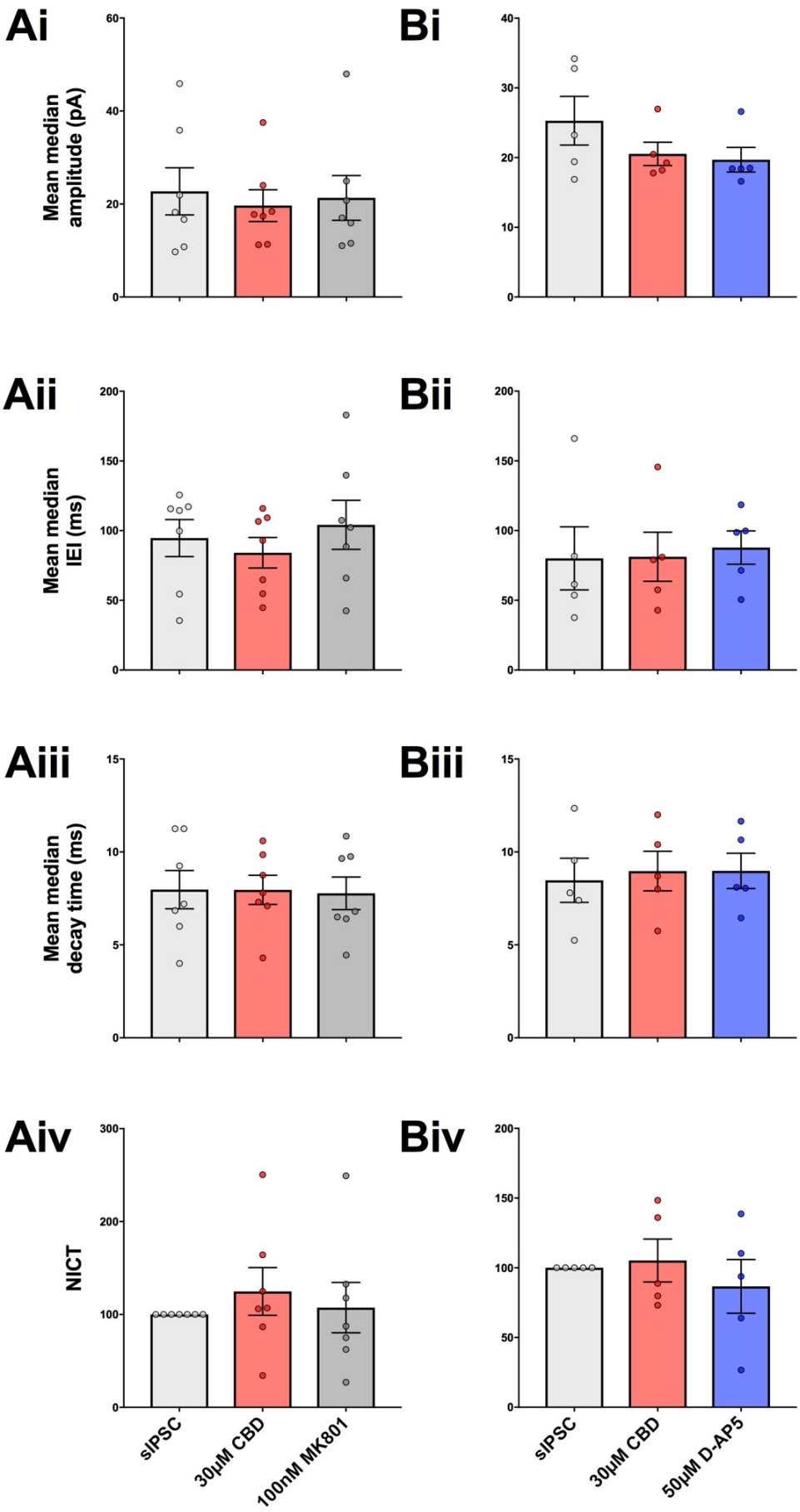

Figure 6.16 Histogram showing MK801 and D-AP5 positive control experiment responses
Mean median amplitude (Ai-Bi), IEI (Aii-Bii), decay time (Aiii-Biii) as well as NICT values (Aiv-Biv) presented. Ai-iv shows MK801 addition, while Bi-iv shows D-AP5.

6.2.2.1 Subunit specific modulation of the NMDAR

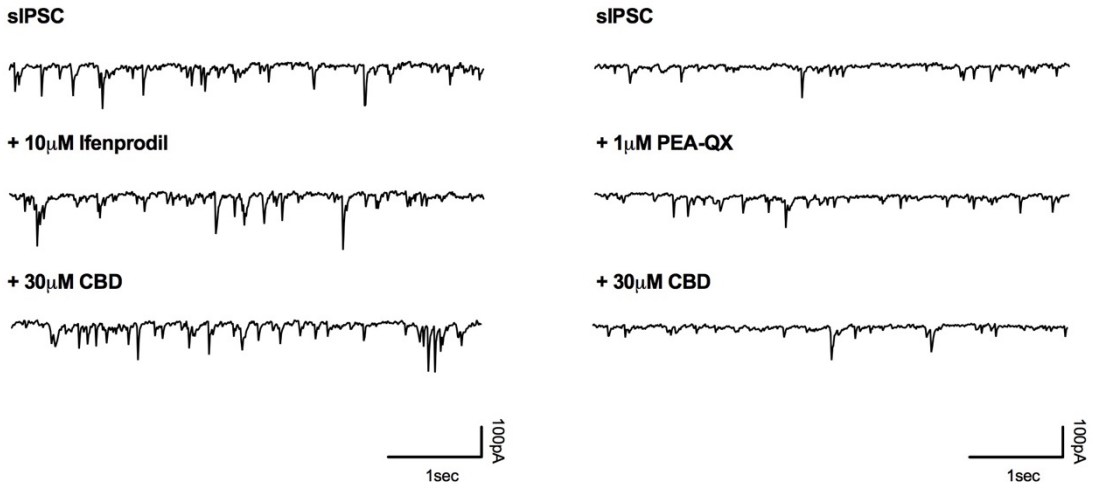

Figure 6.17 Raw traces from sIPSC with NMDAR subunit specific antagonists and CBD.

Due to this possible inhibition of the induced CBD effect by NMDAR antagonists, we were interested to uncover whether a specific NMDAR subunit was responsible. NMDARs are composed of two GluN1 subunits plus two NR2 subunits, most commonly in mature CNS one each of GluN2A and N2B (**Chapter 1, section 1.3.1.2**); therefore, we utilised subunit specific antagonists for this purpose (10μM ifenprodil targeting NR2B, **Ai-iv**; and 1μM PEA-QX for NR2A, **Bi-iv**). The outcomes of these experiments are displayed in **Figure 6.18**.

As can be observed in **Ai**, ifenprodil application (n = 8; animal n = 8) had no effect on the mean median amplitude, neither did addition of CBD (23.9 ± 0.69 – 23.6 ± 0.72 – 20.8 ± 0.53; ranges: 12.1-63.8; 3.20-101; 9.46-57.0). The overall p value was p = 0.79, with no trends observed in the post-hoc. **Aii** displays the mean median IEI responses, where once more ifenprodil and CBD both had little effect on the overall value (61.7 ± 11.5 – 63.6-14.5 – 59.9 ± 10.2; range: 33.2-128; 32.6-151; 32.3-114). The resulting p value was 0.53, with the lowest p value found in the post-hoc analysis between baseline and 10μM ifendprodil + 30μM CBD at p = 0.63.

The mean median decay time comparison is presented in **Aiii**, where relative stability across the drug treatments was observed in terms of mean median values (8.21 ± 0.51 – 8.29 ± 0.73 – 8.59 ± 0.71; range: 5.70-10.8; 5.50-12.5; 5.70-11.9). The p value returned for this dataset was p = 0.35, with the lowest p value observed between the two drug treatments (10μM ifenprodil vs. 10μM ifenprodil + 30μM CBD; p = 0.51). NICT values are shown in **Aiv**, where again no change was found in either ifenprodil or CBD (102 ± 9.97 – 108.4 ± 17.0; range: 61.9-147; 37.3-170), with a p value return of 0.97 overall with no changes noted in the post-hoc analysis.

The right-hand side of this figure (**Bi-iv**) displays the sIPSC responses when exposed to the NR2A antagonist PEA-QX (1μM; n = 10, animal n = 8). **Bi** presents the mean median amplitude

comparisons, where no change was shown in either PEA-QX or CBD addition (28.9 ± 2.52 – 29.7 ± 2.38 – 31.4 ± 2.53; range: 16.3-38.9; 20.0-41.6; 22.6-43.7 respectively). The resulting p value was 0.83, with no alterations observed in Dunn's multiple comparison post-hoc test. The mean median IEI values are highlighted in **Bii**, where neither the addition of PEA-QX or CBD caused any changes to be observed (63.2 ± 8.40 – 58.5 ± 8.96 – 61.6 ± 8.04; range: 29.8-106; 30.6-119; 35.9-106). The p value here was 0.14, with the lowest p value of the post-hoc analysis occurring between the two drug conditions (1μM PEA-QX vs. 1μM PEA-QX + 30μM CBD; p = 0.13).

The penultimate histogram shows the mean median decay time values (**Biii**), where once more there was little change from baseline when PEA-QX or CBD were applied (8.54 ± 0.79 – 8.46 ± 0.69 – 8.44 ± 1.40; range: 6.45-14.2; 6.40-12.7; 6.80-11.2). A p value of 0.37 was produced here, with both the baseline vs. 1μM PEA-QX + 30μM CBD, and the 1μM PEA-QX vs. 1μM PEA-QX + 30μM CBD comparisons producing an identical p value of 0.54. **Biv** presents the NICT values for both drug groups, where PEA-QX returned a value of 117 ± 14.0 (range: 75.7-205) whilst the addition of CBD produced a value of 122 ± 17.8 (range: 61.7-261), neither of which are significant. A p value of 0.60 was shwon overall, with the lowest p value produced by the post-hoc occurring at the baseline vs. 1μM PEA-QX + 30μM CBD comparison (p = 0.79).

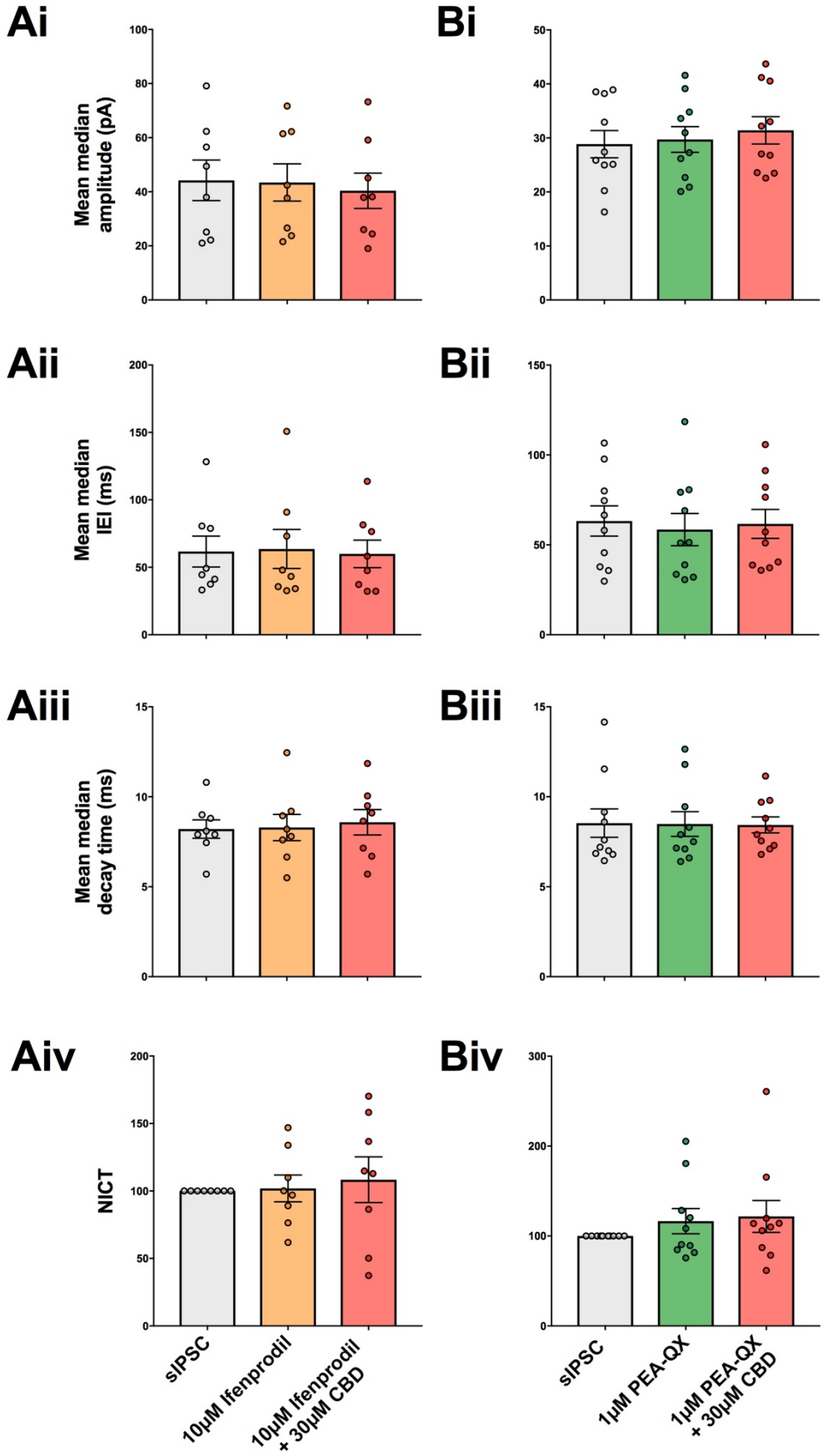

Figure 6.18 Histograms displaying NMDAR subunit antagonist experiments.
Parameters analysed include: mean median amplitude (A-Bi), IEI (A-Bii), decay time (A-Biii) as well as NICT values (A-Biv) presented. Ai-iv shows ifenprodil effect, Bi-iv shows PEA-QX.

6.2.2.2 Summary of NMDAR modulation on CBD effects

A summary of the effect NMDAR modulation had on CBD is shown in **Table 6.2** below. Once more the AMC and SE results are shown to act as a reference, with no effects observed in the AMC when CBD was applied. Changes to IEI, decay time and NICT values are noted in the SE population when CBD was added.

Modulation of the NMDAR by MK801 and D-AP5 antagonists showed no changes to sIPSC kinetics in either drug or CBD conditions. This was also true for the subunit specific antagonists ifenprodil and PEA-QX. Furthermore, CBD before drug or "positive controls" were also performed, with no effect of either CBD or MK801/D-AP5 noted.

Drug used	+ Drug				+ 30µM CBD			
	Amp	IEI	Decay	NICT	Amp	IEI	Decay	NICT
AMC	N/A	N/A	N/A	N/A	-	-	-	-
SE	N/A	N/A	N/A	N/A	-	↓	↑	↑
MK801	-	-	-	-	-	-	-	-
D-AP5	-	-	-	-	-	-	-	-
Ifenprodil	-	-	-	-	-	-	-	-
PEA-QX	-	-	-	-	-	-	-	-
	+ 30µM CBD				+ Drug			
	Amp	IEI	Decay	NICT	Amp	IEI	Decay	NICT
+ MK801	-	-	-	-	-	-	-	-
+ D-AP5	-	-	-	-	-	-	-	-

Table 6.2 Summary table of NMDAR modulation and its influence on the CBD effect.
Ages, condition of animals and, drugs used are noted on the left, with the sIPSC kinetic parameters noted horizontally across the top. The arrows have been used to show the level of significance achieved at that dose (1 arrow = 0.05, 2 = 0.01), with the direction of the arrow also representing the direction of change in value.

6.2.3 The role of CBRs and FAAH in the effect of CBD

Alongside the $GABA_AR$ and NMDAR specific investigations, we also tested the possibility of interaction at other known CBD targets, as well as other cannabinoid-interacting targets, such as CB1R. CBRs are known modulators of neurotransmission and as such we determined that they may be responsible for the changes observed in this report. Furthermore, CBD has been shown to interact with FAAH, and here preliminary investigations into the effect of this interaction *in vitro* were performed. Specifically, both CB1R and CB2R were targeted using the inverse agonists AM251 (n = 5, animal n = 4) and AM630 (n = 3, animal n = 3) at doses of 1µM and 50nM respectively. In addition, fatty acid amine hydrolase (FAAH) was also inhibited, employing 1µM URB597 (n = 4, animal n = 3) to do so. The effects of these drugs addition are shown in **Figure 6.20**.

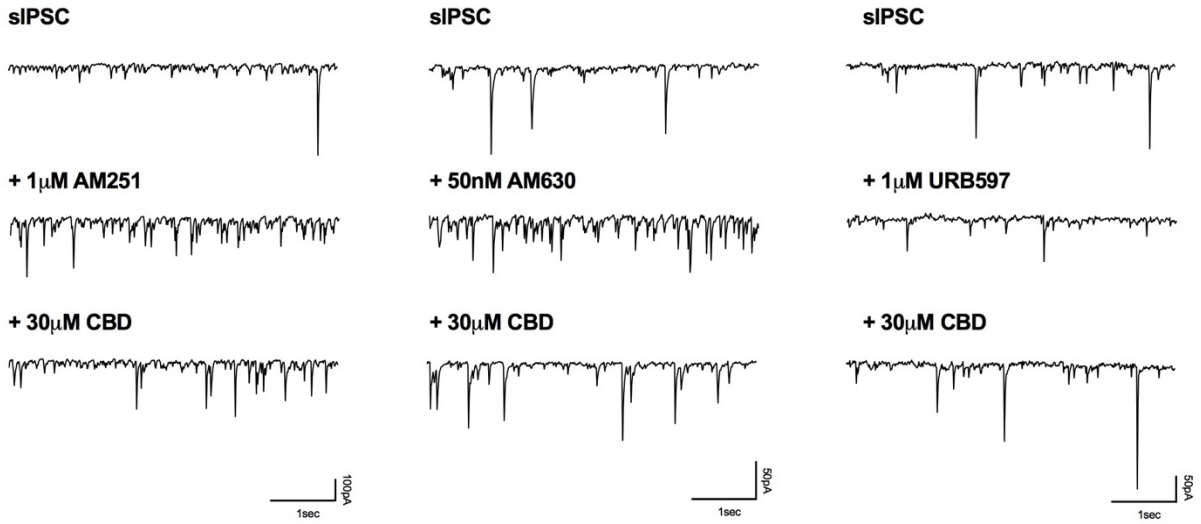

Figure 6.19 Raw traces of 1μM AM251, 50nM AM630 and 1μM URB597 on sISPCs. AM251 left, AM630 middle, URB597 right.

The effect of AM251 on mean median amplitude is observed (**Ai**), where neither AM251 addition nor CBD had any significant effect (21.7 ± 3.50 – 26.3 ± 2.94 – 20.2 ± 3.07; range: 14.5-34.6; 16.7-32.9; 14.0-30.9). The p value was 0.37, with the comparison between AM251 addition and AM251 + CBD producing a p value of 0.34. This lack of effect was also observed in the mean median IEI comparisons as well (**Aii**) (62.2 ± 7.91 – 54.1 ± 4.75 – 63.5 ± 4.20; range: 35.3-83.7; 36.8-64.0; 55.5-76.8). The p value returned here was 0.37, with the baseline vs. 1μM producing a p value of p = 0.34. **Aiii** displays the mean median decay times, where once more no alterations upon AM251 addition were noted, with no change observed upon CBD addition either (7.78 ± 0.20 – 8.38 ± 0.36 – 8.03 ± 0.20; range: 7.34-8.50; 7.66-9.70; 7.58-8.80). The p value produced for this dataset was 0.74, with no changes noted in the post-hoc analysis. **Aiv** shows the NICT values, where visually a very large, though ultimately non-significant increase was present in AM251 (241 ± 81.5; range: 85.5-636), which was then decreased by the addition of CBD (133 ± 34.8; range: 26.3-275). A p value of 0.14 was produced here, with the baseline vs. 1μM AM251 showing the lowest p value (p = 0.13).

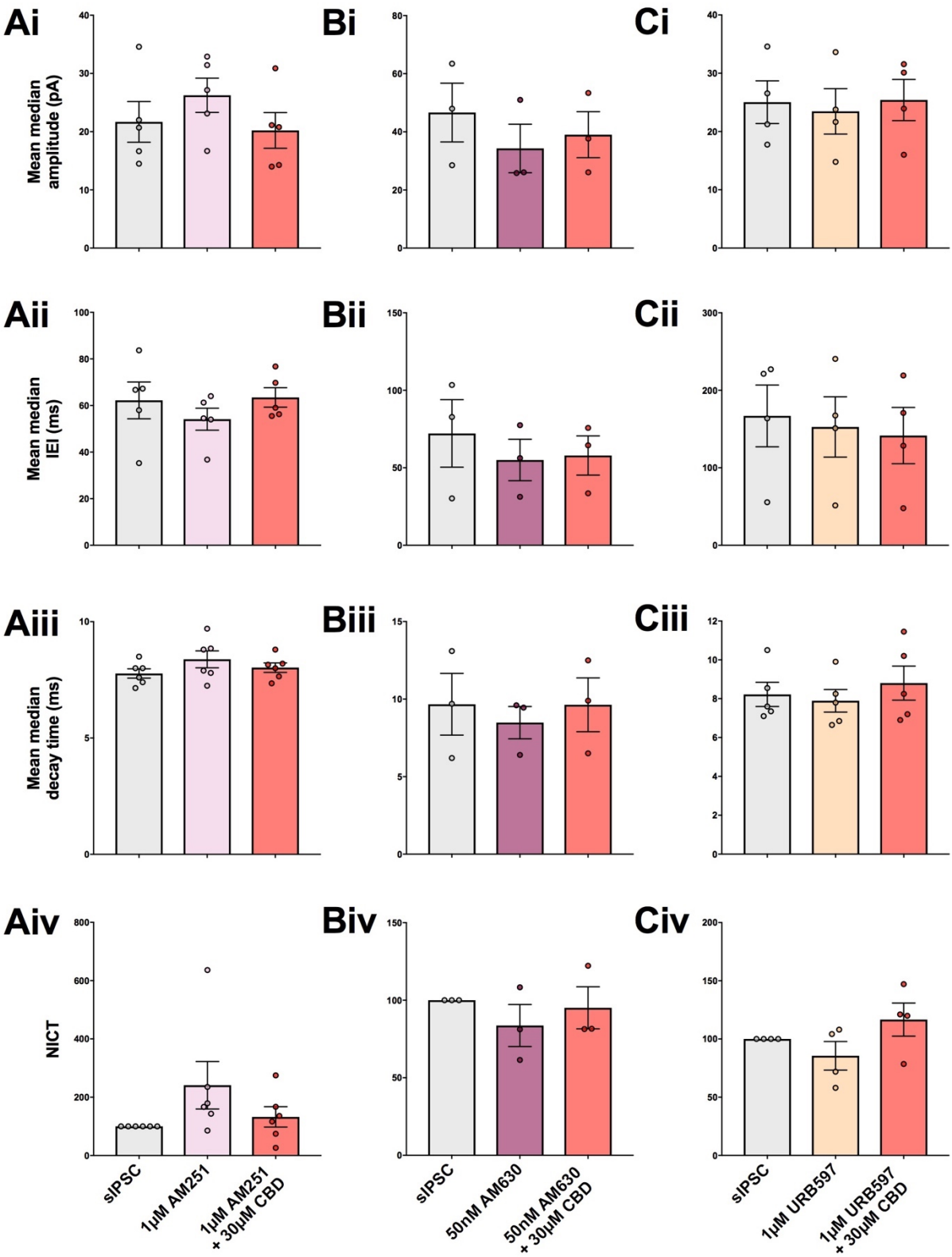

Figure 6.20 Histograms showing sIPSC responses to CB1R, CB2R and FAAH inhibitors. Parameters analysed include: mean median amplitude (A-Ci), IEI (A-Cii), decay time (A-Ciii) as well as NICT values (A-Civ) presented. AM251 shown Ai-iv, AM630 Bi-iv and, URB59 Ci-iv.

AM630 application (**Bi-iv**) delivered no significant change in response across any of the analysed parameters. In the mean median amplitude (**Bi**) no alterations were present in either 50nM AM630 addition or the subsequent 30μM CBD addition (46.7 ± 10.1 – 34.3 ± 8.35 – 39.0

± 7.92; range: 28.5-63.5; 25.8-51.0; 26.1-53.4), with a p value of 0.39 returned and no trends in the post-hoc. The mean median IEI values are presented in (**Bii**) where a similar pattern iwa observed (72.1 ± 21.8 – 55.0 ± 13.4 – 57.9 ± 12.6; range: 30.3-103; 31.3-77.5; 33.5-75.8). A p value of 0.94 is returned, with no trends in the post-hoc. The mean median decay time (**Biii**) shows a similar lack of effect in either AM630 or CBD (9.67 ± 1.99 – 8.48 ± 1.04 – 9.63 ± 1.74; range: 6.20-13.1; 6.40-9.60; 6.50-12.5). A p value of 0.36 was produced, with AM630 vs. AM630 + CBD comparison providing the lowest p value in the post-hoc analysis (p = 0.31). No significant changes are noted in NICT (**Biv**) values upon AM251 application (83.7 ± 13.6; range: 61.5-108), where the presence of CBD showed no alterations (95.1 ± 13.6; range: 81.4-122). The resulting p value was 0.94, with no trends observed in the post-hoc test.

The inhibitory effects of URB597 on FAAH, and their subsequent influence on CBD effects are displayed in **Ci-iv**. The application of URB597 had very little effect on mean median amplitude values (**Ci**), as neither did CBD (25.0 ± 3.66 – 23.5 ± 3.89 – 25.4 ± 3.54; range: 17.8 - 34.6; 14.8-33.6; 16.0-31.6). A p value of 0.65 was shown, with baseline vs. URB597 and, baseline vs. URB597 + CBD treatment showing identical p values of 0.87. In the mean median IEI comparison (**Cii**), neither URB597 or CBD were able to elicit a significant response (167 ± 39.8 – 153 ± 38.9 – 142 ± 36.3; range: 55.6-227; 51.5-241; 47.9-219). A p value of 0.13 was noted overall, with baseline vs. 1μM URB597 + 30μM CBD producing p = 0.10 in the post-hoc analysis. The mean median decay time responses (**Ciii**) were again unaffected by either the application of URB597 or the subsequent addition of CBD (7.65 ± 0.32 – 7.39 ± 0.38 – 8.45 ± 1.04; range: 7.10-8.55; 6.65-8.25; 6.90-11.45). A p value of 0.28 was produced with the lowest p value shown to occur between baseline and 1μM URB597 (p = 0.34). The NICT values are presented in **Civ**, where URB597 produced no effect (85.6 ± 12.3; range: 58.1-108), as neither did CBD (117 ± 14.2; range: 78.5-147). A p value of 0.27 was produced overall with the post-hoc showing the comparison between the two drug treatments producing the lowest p value (p = 0.23).

6.2.4 The response of human cells to antagonism of NMDAR or $GABA_AR$ before CBD application is similar to those observed in rat tissue

In addition to the rat data presented previously, we have also been fortunate enough to be able to perform some preliminary experiments of MK801 (n=4; sample n = 4) and flumazenil (n = 2; sample n = 1) effects on CBD response in HT samples. The results of these initial experiments are laid out in **Figure 6.22**.

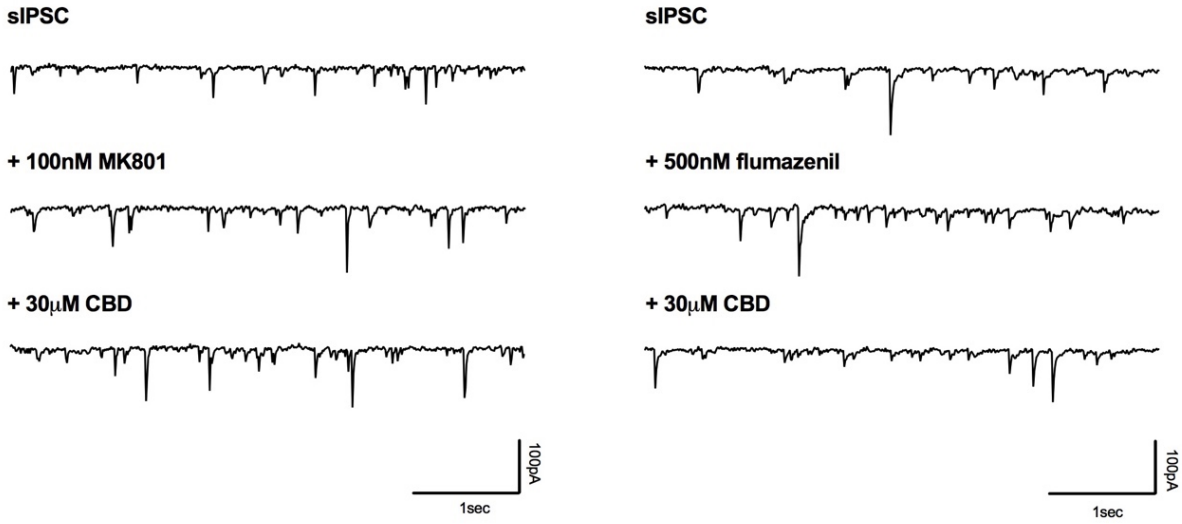

Figure 6.21 Raw traces showing the application of MK801 and flumazenil previous to CBD. MK801 addition on the left, flumazenil on the right.

Ai-iv show the MK801 drug treatment responses. In general, similar results to those presented in the rat tissue are observed (**Figure 6.14.Ai-iv**), with MK801 addition sufficient to block CBD effects. No changes were observed in the mean median amplitude parameter (**Ai**), though MK801 and CBD addition caused a larger variation in population responses (25.5 ± 2.41 – 25.6 ± 3.64 – 26.3 ± 5.28; range: 19.0-30.5; 18.9-33.8; 16.5 – 38.6). A p value of $p > 0.99$ was returned, with the same result in the post-hoc. MK801 had a no effect on sIPSC mean median IEI (**Aii**), as neither did CBD addition (200 ± 79.2 – 188 ± 66.1 – 252 ± 74.7; range: 73.1-429; 94.1-376; 100-421). A p value of 0.43 was produced, with the post-hoc showing the lowest p value between the two drug treatments ($p = 0.47$). The mean median decay time (**Aiii**), showed little effect by MK801 or CBD addition (8.71 ± 1.04 – 9.16 ± 1.43 – 10.75 ± 1.93; range: 5.95-10.8; 6.65-12.9; 7.60-15.9). A p value of 0.27 was produced, with the lowest p value noted from the post-hoc analysis being baseline vs. 100nM MK801 + 30μM CBD ($p = 0.23$) No change to NICT (**Aiv**) was present when MK801 was added (110 ± 20.9; range: 58.0-156), though visually a very large increase was observed when CBD is added, the standard error is similarly large (280 ± 206; range: 39.3-898). A p value of 0.93 is returned, with no change in the post-hoc test observed. This substantial increase is due to one, most likely anomalous result (126 – 896 MK801 to CBD response). This result has been included due paucity of HT

cells obtained, and the similar nature of this data set to the other collected in the other parameters when compared to the other results. Despite the large increase, the error bars are correspondingly large, ensuring this is apparent increase is not statistically verifiable. For reference, the results without this most likely anomalous result produced an NICT value of 105 ± 28.5 in MK801 (range: 58.0-156) and, 75.2 ± 25.8 in CBD (range: 39.3-125). This provided an overall p value of 0.53, with the multiple comparison post-hoc showing the base vs. MK801 + CBD and, MK801 vs. MK801 + CBD treatments having an identical p value of 0.66.

The more limited flumazenil data is presented from **Figure 6.22.Bi-iv**. Again, the data shown here was similar to that found in the rat mEC data. No effect on the mean median amplitude was observed upon flumazenil addition (**Bi**), consistent with the lack of CBD effect (23.3 ± 1.79 – 26.1 ± 3.48 – 25.2 ± 1.13; range: 21.5-25.1; 22.6-29.6; 24.1-26.4). No changes to the mean median IEI (**Bii**) were shown with flumazenil or CBD addition (130 ± 34.8 – 103 ± 22.0 – 115 ± 37.7; range: 95.0-165; 81.0-125; 77.5-153). Decay times were also relatively unaffected (**Biii**), by either the addition of flumazenil or CBD (9.40 ± 1.90 – 9.10 ± 1.55 – 9.76 ± 2.00; range: 7.50-11.3; 7.55-10.7; 7.80-11.8). The addition of flumazenil had little effect on the NICT value (**Biv**; 128 ± 6.45), with both responses closely clustered together (range: 121-134), which remains at a similar level upon CBD addition (133 ± 36.6), though the two responses have separately increased and decreased resulting in a much larger variance (range: 96.7-170). Due to the limited data set no statistical analysis could be performed.

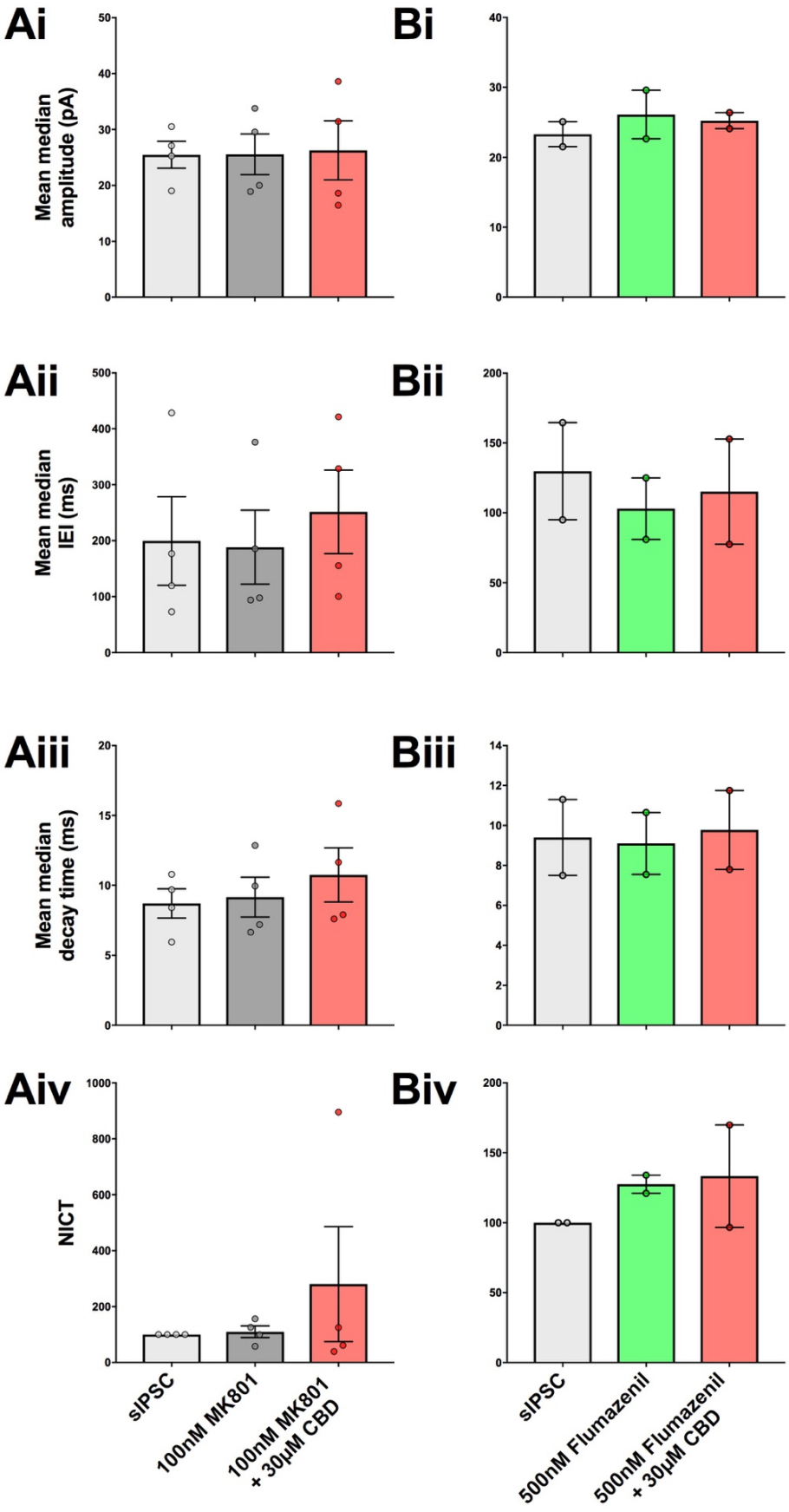

Figure 6.22 Histograms of MK801 and flumazenil effects on CBD responses in HT tissue. Parameters analysed include: mean median amplitude (A-Bi), IEI (A-Bii), decay time (A-Biii) as well as NICT values (A-Biv) presented. Ai-iv shows MK801 effect, Bi-iv shows flumazenil.

6.3 Discussion

6.3.1 CBD interaction with $GABA_ARs$

Due to the BZ-like effect of increased decay times and increased NICT values observed when CBD was applied to SE rat and HT tissue (**Chapter 5**), the effect of CBD in the presence of BZ antagonists/inverse agonists (flumazenil and β-carboline) investigated. Here, block of the BZ-site also blocked of the effects of CBD on both decay time and NICT, with the effect of CBD blocked when flumazenil was added either before or after CBD. This action is suggestive of direct interaction between CBD and the BZ site of $GABA_ARs$. Recently, a study by Bakas et al, (2017) has postulated that CBD possesses a BZ-like effect, though rules out binding to the classical BZ-site of canonical $GABA_ARs$. The Bakas study utilised two-electrode voltage clamp experiments performed on 10 recombinant human $GABA_ARs$ expressed in *Xenopus* oocytes. The data showed both CBD and 2-AG acted as positive allosteric modulators (PAM) at each of the $GABA_ARs$ expressing an α subunit, though each displayed a higher efficacy for $\alpha2$ containing receptors. Indeed, CBD displayed a higher efficacy at the α2β2γ2L and α2β3γ2L containing receptors than α2β1γ2L receptors, indicating a preference for β2/3 over β1 subunits, with a rank order of β3 > β2 > β1. To demonstrate that CBD activity does not rely upon the classical BZ-site located at the α-γ2L interface, the modulatory effects of CBD on binary α1β2 and α2β2 receptors were observed. Here, no significant change in relative EC50 was noted when α1β2 were used, while a significant increase in potency was noted in α2β2 studies. In addition, unpublished work by GW pharmaceuticals utilising radioligand binding studies, with radioactive ^{3}[H] flunitrazepam show a similar lack of binding between CBD and the BZ-site.

6.3.1.1 An additive effect of CBD and BZ agonists on $GABA_ARs$

Previous to the publication of the Bakas et al, (2017) data, confirming no direct binding between CBD and the classical BZ site, we were interested in whether CBD acted in a competitive or additive manner at the BZ-site (as well as the barbiturate site). By determining whether CBD acted in collaboration or competition with BZ/barbiturates, information on the specific interaction between CBD and $GABA_ARs$ could be inferred. Here we have shown that at low doses of zolpidem CBD displays an additive effect, increasing both decay time and NICT values, while at near maximal zolpidem levels this effect of CBD is occluded. Furthermore, experiments with clobazam highlight a similar relationship, with CBD addition subsequent to clobazam inducing increased decay time values, though not an increase in NICT. These data suggest that CBD and BZ have a similar final common path in augmenting channel function, though not achieved through binding at identical binding sites. CBD also displayed an additive effect with pentobarbital, with significant increases noted in both amplitude and NICT values when CBD is added subsequent to pentobarbital, again suggestive of CBD also operating allosterically to augment $GABA_AR$ function.

BZ are able to functionally modulate the canonical $GABA_AR$s composed of alpha/beta/gamma ($\alpha\beta\gamma$), binding with a high affinity to the allosteric BZ-site, located on the extracellular N-terminal at the alpha/gamma ($\alpha\gamma2$) interface (Sigel, 2002). The extracellular N-terminal of $GABA_AR$ subunits is noted in receptor assembly and the formation of orthosteric and allosteric binding sites, three of its four transmembrane spanning domains are linked with small loops (TM1-3), while TM4 is connected to TM3 via a larger cytoplasmic loop – implicated in cell signalling and trafficking pathways (Kittler and Moss, 2003). TM2 is the domain that lines the central pore (Xu and Akabas, 1996; Goren et al., 2004).

The exact mechanism of BZ interaction is still under intensive examination. Traditionally, BZ agonist binding "locks" the $GABA_AR$ into a conformational shape, where the affinity to GABA is much increased, eliciting a potentiation of Cl^- currents and, indeed this is still a popular notion (Berezhnoy et al., 2005). The two GABA binding sites of the $\alpha\beta\gamma$ $GABA_AR$ are located in the extracellular domains of the $\alpha\beta$ interface (Sigel et al., 1992; Amin and Weiss, 1993; Westh-Hansen et al., 1997; Wagner and Czajkowski, 2001; Boileau et al., 2002). BZ action was thought to occur due to BZ increasing the affinity of GABA agonists, though did not affect channel open time (Study and Barker, 1981). A more concise mechanism was proposed of BZ action, with diazepam specifically thought to increase the opening of mono-ligand bound $GABA_AR$s, though generally two GABA molecules must bind to cause an opening of the pore (Twyman et al., 1989; Rogers et al., 1994). Further to this, publications have proposed that the binding of allosteric BZs causes an increase in GABA affinity at, at least, one of the GABA agonist binding sites (Gallager and Tallman, 1983; Serfozo and Cash, 1992; Lavoie and Twyman, 1996). BZ agonists are described as positive allosteric modulators (PAMs), enhancing $GABA_AR$ currents, while BZ antagonists are generally inverse agonists, inhibiting GABA currents, most likely through structural mechanisms (Hanson and Czajkowski, 2008).

At saturating concentrations of partial GABA agonists, however, BZs are able to potentiate GABA responses, as well as directly gate spontaneously active $GABA_AR$s (Maksay et al., 2000; Bianchi and Macdonald, 2001; Downing et al., 2005; Rusch and Forman, 2005; Campo-Soria et al., 2006). The emergence of these effects suggests that the traditional view of BZs as solely increasing GABA binding affinity was incomplete and another allosteric mechanism of BZ was considered. Indeed, later published work has shown that BZs are able to modulate $GABA_AR$s channel opening by modulating the equilibrium between ligand-bound resting states and pre-activated states, suggesting it is this switch to pre-activated states that produces an appearance of increased GABA affinity (Gielen et al., 2012). This translates to BZs agonists increasing the frequency of channel, and burst, opening at non-saturating concentrations of GABA and, increased decay time in saturating GABA concentrations (Lévi et al., 2015).

Conformational changes in $GABA_AR$ are an accepted part of its activation, with the three most commonly discussed being resting/closed, active/open and desensitised, which occur in the presence of GABA agonists. Activation of a resting $GABA_A$ receptor induces conformational change at the extracellular domains of the alpha/beta/gamma subunits to trap the agonist (Bianchi and Macdonald, 2001; Teissere and Czajkowski, 2001; Wagner and Czajkowski, 2001; Bera et al., 2002; Boileau et al., 2002; Newell and Czajkowski, 2003) and, subsequently cause movement in the transmembrane (TM) portions of the receptor, with TM2-3 linker changes causing movement in the TM2 segments to open the central pore (Xu and Akabas, 1996; O'Shea and Harrison, 2000; Horenstein et al., 2001; Kash et al., 2003, 2004). BZ binding alone has been demonstrated to be unable to open the pore of $GABA_AR$, but may possibly cause a conformational change, to a transitional pre-activated state, between the resting and open states, that potentiates $GABA_AR$ function (Gielen et al., 2012).

From the data presented so far, CBD is able to mimic certain aspects of BZ effects, most notably the increased decay time, which would suggest that CBD is able to bind the $GABA_AR$ at an allosteric site to produce a similar effect. From the information known about how BZs exert their effect on $GABA_ARs$, namely eliciting a conformational change in the receptor to increase apparent GABA affinity, one would assume CBD is having a similar conformational effect. Indeed, from our own data and those of Bakas et al, 2017, it seems most likely that CBD is acting as a PAM at the $GABA_AR$, being able to functionally modulate inhibitory signalling mechanisms through this interaction. A notable feature of CBD presented in **Chapter 5 & 6**, is the lack of consistency of response and seemingly subtle nature of the effect. A possible factor in this is the presence of endozopines, interacting or inhibiting the CBD effect by binding to the BZ site, leading to variation in the CBD effect across the experiments performed. Previous work in the laboratory has shown that endogenous dopamine levels vary greatly between slices *in vitro* (G Woodhall, personal communication), and this may also be true for endogenous BZ ligands.

Endozepines are endogenous benzodiazepine-like ligands and have been theorised since the discovery of the $GABA_AR$ BZ site (Iversen, 1977; Costa and Guidotti, 1985). Indeed, several molecules fitting this description have been uncovered since including: oleamides, non-peptidic enzodiazepines and, a protein dubbed diazepam-binding inhibitor (DBI), with DBI being the most extensively studied of these (Costa and Guidotti, 1985; Rothstein et al., 1992; Cravatt et al., 1995). The majority of endozepines are NAMs at the $GABA_AR$ (Costa and Guidotti, 1985; Alfonso et al., 2012), though more recent research now suggests DBI as possessing some PAM capabilities (Christian et al., 2013). Taking DBI as an example of an endozepine, the NAM capabilities of this molecule have been widely detailed, with reports suggesting increases in anxiety, aggression and, neurogenesis (by a DBI fragment peptide), while also decreasing sleep (Guidotti et al., 1983; Kavaliers and Hirst, 1986; De Mateos-

Verchere et al., 1998; Dong et al., 1999; Alfonso et al., 2012). Examples of PAM by DBI are less numerous, though have also been shown, with DBI demonstrated as potentiating GABAergic synaptic transmission in thalamic reticular nucleus neurons (Christian et al., 2013). Endozepines, such as DBI, may be binding at $GABA_AR$ to alter functional conformations of the receptor, precluding CBD from binding or, CBD actions from occurring, which may be a factor in the variation noted across the single cell CBD experiments performed here.

Taken together, the presented data are suggestive of an importance of the BZ site within the action of CBD. The use of inverse agonists here, flumazenil and β-carboline, fits with our assessment of CBD as a PAM; there is, though, speculation over the correct status of flumazenil, with it historically defined as an antagonist at BZ site of $GABA_AR$. Flumazenil has been comprehensively shown to competitively bind at the BZ site, blocking action of NAMs and PAMs, and was thought to not display any intrinsic effect on GABA actions itself (Hunkeler et al., 1981), however a more recent study by the host lab has shown flumazenil to display more inverse agonist-like effects on tonic GABA actions (Prokic et al., 2015), possibly through constitutive activity at the BZ site by endozepines (Christian et al., 2013). Similarly, a recent study on recombinant receptors has shown that long-term exposure to flumazenil may cause $GABA_AR$ internalisation (Kuver and Smith, 2016). Classical inverse agonists at the BZ site, such as β-carboline, cause reductions in GABA actions and have been theorised to be able to lock $GABA_ARs$ in a conformational state that precludes the effects of any allosteric modulation (Farzampour et al., 2015). If CBD were acting in an allosteric modulatory role the inclusion of inverse agonists would abolish these effects, as has been observed here.

The barbiturate, pentobarbital, is a potentiator at the $GABA_AR$ at low micromolar doses, able to open the central pore at high micromolar doses, while at millimolar doses it is able to block the channel (Akaike et al., 1987; Akk and Steinbach, 2000; Serafini et al., 2000). Barbiturates bind at an allosteric site on $GABA_AR$ to induce their effects; here a low micromolar dose of pentobarbital has been applied and, caused potentiation of the GABA currents. The subsequent addition of CBD has shown a further potentiation of the GABA response, again, highly suggestive of an additive effect for CBD at the $GABA_AR$ via allosteric mechanisms.

It seems likely then, that CBD acts as a PAM at the $GABA_AR$ to produce the effects described in this project. One clear candidate for endogenous allosteric modulation of $GABA_AR$ function is the neurosteroids. As such, we performed investigations into a possible CBD effect via the steroid binding site on the $GABA_AR$. Using the negative modulatory neurosteroid, 17PA, we blocked the steroid binding site. As of yet, no work on the effect of 17PA on sIPSCs has been published, as such we determined to characterise its effect on sIPSCs and, the CBD effect. The presented data shows there is little effect of either CBD or 17PA on sIPSCs, though this is most likely due to the limited n number provided. The data presented here requires further

replication before any definite conclusions could be made about the actions of 17PA on sIPSCs and, any influence it may have on the CBD effect.

The results presented here, in conjunction with the findings of Bakas et al, (2017), are highly suggestive of a direct interaction of CBD at the $GABA_AR$, most likely acting as a PAM. The mechanism of this action though, is not accomplished through binding of CBD at the classical benzodiazepine site (located at the interface between α-γ2L subunits), nor the barbiturate site, and most likely not, the neurosteroid site, though it cannot yet be definitively ruled out. Our hypothesis, therefore, is that CBD most likely binds to another, as of yet, unknown allosteric site on postsynaptic pyramidal cell $GABA_ARs$ to induce increased decay time by prolonging channel open time, and as such, increased inhibitory charge transfer into the neuron, resulting in decreased neuronal excitability.

6.3.1.1.1 *Possible anomalous results*

In the 1μM application of zolpidem there interestingly appears to be what should be a significant increase again in the mean median decay times (**Figure 6.7.Biii**) when zolpidem is applied ($p = 0.13$). There is what could be constituted as an outlier, apparent when viewing the baseline especially (11.00 – 10.60 – 12.20), which when removed does allow significance to be reached (8.51 ± 0.43 – 11.01 ± 0.23; $p = 0.034$), however, this cell produces 'normal' values, in line with those observed in the other cell responses, across the other parameter analyses, making its exclusion difficult to justify.

It could also be argued that there is an outlier present in the NICT values of the clobazam experiment (**Figure 6.9.Aiv**), especially notable in the clobazam condition, where a value of 647.3 is present, this decreases once CBD is applied to 334.2, which is more in line with some of the other values observed in the CBD condition. If this result set is removed from the population, the means change quite dramatically, with a value of 146.1 ± 21.26 returned for clobazam only and, 159.6 ± 31.34 in the clobazam + CBD treatment. In these circumstances, an overall p value of 0.28 returned, with the multiple comparison post-hoc showing a value of $p = 0.72$ for clobazam only and, $p = 0.30$ once CBD is also applied.

6.3.2 Direct CBD interaction with NMDARs

Due to the factors discussed in the introduction (**Section 6.1.3**), we also pursued whether CBD was interacting with NMDARs to exert its effect. Little published work has been performed on the effect of CBD at NMDARs and as such, there is little to compare this work with. Previous published work however, has demonstrated links between CB1R and NMDARs, which may provide some indication of how CBD exerts the noted effect it has on sIPSCs (Sánchez-Blázquez et al., 2013; Rodríguez-Muñoz et al., 2016). Recent effects discovered between CBD

and CB1Rs have been documented in the section below. It may be possible that CBD is able to interact either, directly with NMDARs to influence GABAergic signalling, as detailed in Xue et al, (2011) or alternatively, indirectly via CB1R, acting as a NAM, as suggested in Laprairie et al, (2015), to influence NMDAR signalling via CB1R-NMDAR interactions or, at another target to modulate NMDAR signalling.

To test possible direct CBD interactions at NMDARs, we initially employed the use of two NMDAR antagonists, one competitive (D-AP5), the other non-competitive (MK801). Indeed, both orthosteric and allosteric inhibition of the NMDARs were sufficient in abolishing the CBD effect (**Figure 6.13.Ai-iv**). In the 'positive control' experiments for each of these antagonists (**Figure 6.16**), CBD was once more unable to replicate the results observed in **Chapter 5** on decay time and NICT. Due to this, it is difficult to assess the ability of MK801 and D-AP5 to reduce CBD induced inhibition. This lack of CBD response with smaller n numbers once more highlights the need of a large n number pool, to allow detection of the significant increases observed in both decay time and NICT values and, is highly indicative of CBD possessing only subtle effects.

As both competitive and non-competitive NMDAR antagonists were successful in blocking CBD, we were interested to ascertain whether a certain NMDAR subunit was responsible. As such, GluN2A and N2B were targeted, with PEA-QX and ifenprodil used to inhibit each respectively. The data presented in **Figure 6.18** show either subunit antagonist is sufficient in blocking the induced CBD effect, with no real alterations in any of the values observed across the dataset in either of the antagonists, nor upon CBD addition

The data collected from the NMDAR inhibition experiments suggest that blockade of the orthosteric, allosteric and, specific GluN2 subunits of NMDARs are sufficient to inhibit the CBD effect in SE tissue, however, we must admit that the CBD response is unseen in the positive control experiments. It is somewhat plausible that CBD may be able to bind to GluN1 subunits in some manner and, as the canonical CNS NMDAR is composed of 2x GluN1, 1x GluN2A, 1 x GluN2B, inhibition of either GluN2 subunits is thus able to cause a conformational change that limits CBD access to this site. Indeed, a recent publication has shown that ifenprodil addition causes a change in conformational state of NMDARs from open to closed (Tajima et al., 2016). Perhaps this conformational change is sufficient to block the GluN1 site for CBD, ergo no effect of CBD noted after the inclusion of specific GluN2 antagonists.

Reasons for why NMDAR inhibition is effective in blockade of CBD effects could be due to the link between NMDAR and GABAergic signalling discussed in the introduction and highlighted in Xue et al, (2011), with inhibition of presynaptic NMDARs able to lower GABA release from interneurons. It may be a case of CBD enhancing NMDAR-mediated GABA release from the

presynaptic terminal by activating presynaptic NMDAR located on mEC, therefore, increasing inhibitory ion entry into the postsynaptic bouton and, decreasing neuronal excitability. NMDAR inhibition would interrupt this CBD-NMDAR interaction, reducing NMDAR mediated GABA release and inhibiting the observed CBD effect on sIPSCs. Postsynaptic CBD interactions with NMDARs are also possible causes of the noted effects here. Plausible mechanisms by which this may occur may include CBD interaction with NMDARs to influence production of postsynaptic signalling molecules, for instance nitric oxide (NO), increasing NO synthesis and retrograde transmission across the synapse. This retrograde signalling would then result in increased uptake presynaptically and, subsequently, elevated GABA neurotransmission, this is another signalling pathway suggested in Xue et al, (2011). Blockade of NMDARs in this case reduces NMDAR-CBD interaction, ceasing or limiting synthesis of postsynaptic signalling molecules enough to sufficiently inhibit the noted CBD effect.

6.3.3 CBRs, FAAH and the effects of CBD

Previous published studies have ruled out CB1R interaction with CBD (and CBDV) to produce the anticonvulsant effects observed by each (Wallace et al., 2008; Hill et al., 2012). Each of these studies utilised orthosteric antagonists, which were unable to inhibit the actions of either phytocannabinoid. As specified in the previous section CBD has a well-established low affinity for the CB1R orthosteric site however, recent work has demonstrated that at low doses (< 2μM) CBD possesses high affinity as a NAM for CB1R *in vitro* (Laprairie et al., 2015). At higher doses (> 2μM), CBD has been noted to possibly possess weak partial agonist capabilities, with CBD documented to increase PLCβ3 signalling and, ERK phosphorylation while limiting CB1R internalisation, though evidence for this is limited (Mechoulam et al., 2007; McPartland et al., 2015). Alongside this CBD has been shown to potentiate the effect of THC at CB1Rs via a CB1R-dependent mechanism (Hayakawa et al., 2008). These factors may be implicated in the noted CBD effect, for instance it is possible that CBD is causing an increased internalisation of CB1Rs, which would result in a greater amount of neurotransmission.

Blockade of CB1Rs by the inverse agonist AM251, which competes at the orthosteric site of CB1R, was sufficient in inhibiting the CBD effect here, though a relatively small n number (n = 5) was completed. A suggestion of interaction between CBD and CB1R can be taken from this as the noted CBD effect is lost, though this may be more due to the lack of n, as CBD has been shown to only possess subtle effects noticeable across a high population of responses. The pattern of the responses is interesting however, as AM251 seemingly increases both amplitude and decay times, while decreasing IEI, resulting in a larger NICT value, while CBD appears to reverse these trends, conversely to the effects observed by CBD previously. None of these AM251 effects are significant, and as such it is impossible to be sure of these results, however it may be that the loss in CB1R function due to inverse agonism of the receptor allows for greater synaptic transmission, which leads to an increase in inhibition at the postsynapse.

The subsequent addition of CBD and its reversal of these effects is puzzling, as if it were acting upon solely $GABA_A$Rs and NMDARs to produce its effects, CB1R blockade should not impede this. It would be interesting to increase the n number of this experiment to observe whether the initial effects remain in a more robust sample. Completion of which would clarify any interaction between CBD and CB1Rs, and whether it is of importance for the subtle effects noted in this project.

A limited set of experiments were also run on CB2R interaction with CBD, again employing the use of an inverse agonist, in this case AM630, though the n number provided here was very small (n = 3). Little previous work has been performed on CB2R and CBD in the CNS, most likely due to the well reported lack of affinity CBD possesses for CB2R (Thomas et al., 2007). The data provided here is unable to support any definite conclusions, due to the low nature of the sample, however, observing the population responses suggests that blockade of CB2R is unlikely to inhibit CBD effect, most likely confirmed if performed on an adequate n number.

Recent research has also implicated CBD as interacting with FAAH (Ibeas Bih et al., 2015), and as CBD is a highly lipophilic molecule it could be possible that this interaction with FAAH is inducing the effect of CBD we have observed. CBD interaction with FAAH, generally thought to be an inhibitory one, would result in an increased amount of AEA, AEA binding to CB1Rs would then decrease neurotransmission from the postsynapse, which is a plausible explanation of the anticonvulsant nature of CBD (Pertwee, 2005; Vaughan and Christie, 2005; Campos et al., 2012; Patel et al., 2016). This possible interaction would not provide the effects noted due to CBD throughout this project, increased decay times and NICT values, as those findings are highly suggestive of either increased GABA release and uptake or, increased GABA sensitivity.

Here the FAAH inhibitor URB597 has been applied, though again only a small n number has been produced (n = 4). The single cell population responses show FAAH inhibition as generally decreasing baseline values, while CBD is able to reverse this effect in many of the cells tested. Again, more n numbers are required to state this as a complete conclusion, though it looks as though FAAH inhibition is not responsible for the CBD effects we have observed.

6.3.4 Human tissue neurons follow a similar pattern to the rat tissue

The human tissue data, **Figure 6.22**, shows a similar pattern to that presented in the rat tissue (**Figures 6.2** & **6.13**), albeit with an understandably smaller n (n = 4). Here, MK801 (**Ai-iv**) shows adequate blockade of the CBD effect observed in the previous HT data (**Figure 5.11**), though slight increases are noted in both the decay time and NICT values. These increases are largely due to the increase in one respondent, as explained in the results section previous (**Section 5.2.5**). The removal of this result shows a decrease in NICT value upon CBD addition,

though decay time remains elevated. As such, these data are very similar to the rat tissue results presented previously, and it would be interesting to be able to observe this data at a similar n (n = 7/8). The flumazenil addition (**Bi-iv**), shows a different pattern to that identified in the rat tissue, with increases in amplitude and NICT values and, decreases to IEI and decay time upon flumazenil addition. CBD appears to reverse these effects; however, these data are highly speculative due to only an n of 2; a much larger n is required for any concrete conclusion to be drawn here.

6.4 General discussion and future experiments

It is possible that CBD is acting upon a multitude of different receptor targets to exert the increased postsynaptic inhibition shown here due to its inherent promiscuous nature, indeed, many different research groups are investigating purported CBD effects at a variety of receptors including: GPR55, $5HT_{1A}$, $5HT_3$, glycine receptors (Russo et al., 2005; Pertwee, 2008; Xiong et al., 2014) alongside other intracellular targets such as mTOR, vDAC and, NPY (Gamber et al., 2005; Shrivastava et al., 2011; Rimmerman et al., 2013; Giacoppo et al., 2017). Further to this, recent publications have shown CBD interaction with the epilepsy-associated sodium channels NaV1.6 channels that are mutated in the Dravet syndrome form of epilepsy (Patel et al., 2016). Here CBD acts to reduce neuronal excitability by selectively inhibiting the resurgent current over the peak transient current, in both wild-type and mutated NaV1.6 channels. As CBD has been noted to reduce seizure number in clinical trials of children with Dravet syndrome (Devinsky et al., 2016), this link may be crucial for understanding the anticonvulsant mechanism of CBD.

The work presented here, however, shows CBD's BZ-like response is able to be effectively inhibited by either $GABA_AR$ BZ site inhibition, via inverse agonism, or NMDAR inhibition by both general and subunit specific antagonists. CBD has also been demonstrated to act in an additive manner when applied subsequent to BZ-site agonists, which is indicative of allosteric binding by CBD to the BZ site, something corroborated by recent binding studies (Bakas et al., 2017). Together these data suggest an interaction between CBD and, both $GABA_AR$ and NMDARs. Most likely, there is a direct interaction of CBD in the case of $GABA_AR$, though both direct and indirect interaction with NMDARs could be possible. Our current working hypothesis is that CBD has a plethora of multimodal effects which combine to provide the anticonvulsant effects noted, and the increased levels of inhibition shown throughout this report. We theorise that CBD is able to interact either directly or indirectly with presynaptic NMDARs, most likely on GABAergic interneurons to positively modulate GABA neurotransmission, possibly through mechanisms similar to those proposed in Xue et al, (2011). Concomitantly, we also suggest that CBD is directly interacting with postsynaptic pyramidal cell $GABA_ARs$ at an as of yet unknown allosteric binding site as a PAM, to increase one, or a combination of, GABA binding, uptake and, sensitivity, thereby increasing inhibitory activity in the postsynapse terminal, and as such decreasing neuronal excitability. Roles for CB1R, CB2R and FAAH seem unlikely

given the data provided here and published elsewhere, though interaction at CB1R, possibly as an NAM looks likely.

Future experiments that could be performed here include, further binding studies to try and elucidate the binding site of CBD on $GABA_AR$, specifically looking at whether application of inverse agonists such as flumazenil or β-carboline are able to diminish CBD binding at $GABA_ARs$ compared to control. Alternatively, similar binding experiments could be run with zolpidem instead of an inverse agonist to look at CBD binding, again compared to control. Binding studies could also be performed between CBD and NMDAR which would help to distinguish whether this interaction is direct. Moreover, CBD could be applied in collaboration with NMDA, to establish whether an additive effect in NMDA-mediated GABA neurotransmission, reported by Xue et al, (2011), is noted.

Chapter 7

General Discussion

The overarching aim of this project was to characterise the reported anti-epileptic mechanism of CBD(V) *in vitro* (Jones et al., 2010, 2012, Hill et al., 2012, 2013; Devinsky et al., 2016). Little *in vitro* investigation has been performed with either CBD or CBDV, and as such we sought to determine the effect of CBD(V) on neural oscillations and single cell properties.

To do so, we utilised the RISE model of TLE (Modebadze et al., 2016) alongside AMC animals, focusing our attention on the mEC, due to its crucial link to epileptogenesis and its role as a gatekeeper for information processing to the hippocampus (Amaral and Witter, 1995; Witter et al., 2000; Vago and Kesner, 2008). Furthermore, we endeavoured to assess CBD(V) at several time points along the epileptogenesis pathway, to observe whether a consistent cannabinoid effect was observed.

Initally, comparisons between the AMC and SE rat tissues were made across both LFP and whole-cell voltage-clamp techniques to uncover any induced changes in the baseline conditions caused by the RISE model (**Chapter 3**). Here, little effects were noted in the LFP experiments, with only the peak frequency significantly decreased in 24-hour SE animals compared to AMC rats of this time, most likely a result of the procedure itself causing insult to the mEC neurons. No significant effects were observed across any of the sIPSC patch-clamp experimental parameters. Significant changes were noted, however, in the sEPSC baseline conditions, with an increase in mean median amplitude and excitatory charge transfer (ECT), indicative of an increase in excitatory neurotransmission and, when coupled with the sIPSC data, a shift in inhibitory-excitatory balance (I-E) towards excitation. This shift is present and known in human epilepsy conditions (Scharfman, 2007), and as such highlights the effectiveness of the RISE model as a template for human TLE.

Our initial phytocannabinoid experimental work focused on the pharmacologically induced gamma response of both AMC and SE rat mEC to CBD(V), using gamma oscillations as a marker of neuronal activity. The application kainic acid reliably induced persistent gamma oscillations within the mEC layer II networks of rats at all ages (**Chapter 4**). Network neuronal oscillations were used as a sensitive measure of network function that includes both inhibitory and excitatory aspects, as epilepsy is a neurological disease characterised by pathological oscillations and abnormal synchronous activity (Uhlhaas and Singer, 2006). Also, no information was available on whether CBD(V) were able to effect both physiological and pathological oscillations in a similar manner and, as such, we endeavoured to investigate whether this occurred.

Application of CBD(V) reliably decreased gamma oscillation power (using nAUC as a measure) in each age group and disease state, excepting the 24-hour AMC populations for both CBD and CBDV, at the maximal 30μM dose. The lack of response to CBD(V) in the AMC juvenile

(24-hour) animals may be due to the lack of maturity in glutamatergic and GABAergic signalling systems, including the inhibitory and excitatory receptor presence at this time and, their responses to neurotransmitters (Walther et al., 1986; Kriegstein et al., 1987; Ben-Ari et al., 1989; Michelson et al., 1989; Cherubini et al., 1990; Luhmann and Prince, 1990a, 1990b; Kleckner and Dingledine, 1991). Indeed, with regards to CBD, an increasing sensitivity is noted with age in the AMC rats, with the delta peak gamma power showing a high amount of significance across the time points tested. It is most likely that these changes are due to the receptor targets of CBD(V) being expressed at these time points and, are influential in the mechanisms of gamma oscillations.

On the other hand, the SE population shows no significant difference in sensitivity with age to CBD. This lack of difference with regards to CBD sensitivity with age in SE animals, is indicative of disease specific effects of CBD, with these data highlighting changes occur upon the initial insult. This change seemingly results in alterations to neuronal or synaptic organisation and composition, allowing targets of CBD to be present before they would normally appear, as CBD only shows an effect in the AMC animals from the 1-week time point (P26), while is present from the earliest SE time point. Collaborative investigations with the Henley lab have shown differing level of protein expression for each of the ionotropic glutamate receptors at various time points on the epileptogenesis pathway used here (**Appendix 2**).

Alongside LFP investigation, we also employed use of whole-cell voltage-clamp electrophysiology techniques to assess single mEC layer II pyramidal cell current responses to CBD(V) 24-hours to 1-week post-induction (**Chapter 5**). Assessing CBD effect on spontaneous excitatory postsynaptic currents (sEPSCs), no differences were observed in any parameter of sEPSC analysis in either AMC or SE populations, indicative of CBD having no effect on excitatory neurotransmitter release to exert its effect.

In contrast, a significant decrease in the interevent interval (IEI) and, significant increase in decay time was noted in SE populations when spontaneous inhibitory postsynaptic currents (sIPSCs) were exposed to 30μM CBD. Alongside this, an overall normalised inhibitory charge transfer (NICT) increase was noted. Such increases were not noted in the comparable AMC animals when assessing sIPSCs (**Chapter 5**). These results suggest that CBD is able to increase inhibitory activity onto the postsynaptic neuron, either through increased $GABA_AR$ receptor open time, indicated by longer decay times of sIPSC events or, through increased GABA neurotransmitter release by presynaptic interneurons. Previous work has also shown NMDARs are able to influence and modulate GABA release, via both pre- and postsynaptic mechanisms (Xue et al., 2011). When this information is combined with the protein expression assays performed by the Henley lab on 24-hour SE rats, where an upregulation in GluN1 is noted, the two may be related, especially once CBD is applied. It is plausible that CBD is either

directly or indirectly interacting with GluN1-containing NMDARs, on either the presynaptic element or postsynaptic terminal, to cause a modulation or, increase in GABA release from the presynapse, mostly likely through NOS retrograde signalling presynaptically, or indirectly through second messenger systems postsynaptically (Xue et al., 2011).

To explore these results further, we investigated whether direct inhibition of either of these receptors were sufficient for blockade of the CBD response noted in sIPSC experiments (**Chapter 6**). As such, both $GABA_AR$ inverse agonists and NMDAR antagonists were employed. The blockade of the $GABA_AR$ benzodiazepine site by inverse agonists (flumazenil/β-carboline) was successful in blocking the induced CBD effect. This result was highly suggestive of CBD binding either directly to this site or at an allosteric site on the $GABA_AR$. Furthermore, the use of competitive (D-AP5) and non-competitive (MK801) NMDAR antagonists proved to be sufficient for inhibition of the induced CBD effect, once more suggesting that NMDARs are influential in its mechanism.

These $GABA_AR$/NMDAR results provided us with two viable targets for CBD mechanisms of action, and as such we investigated their involvement further. In terms of the influence of $GABA_AR$, we were interested to observe whether CBD produced an additive or competitive effect at the benzodiazepine (BZ) site, as this would provide information on whether CBD was binding directly at the BZ site. We therefore used a benzodiazepine site agonist (zolpidem) at two different concentrations to observe CBD effects when it was added subsequently. The results achieved here were indicative of CBD displaying an additive effect, as CBD acted to enhance the response when a minimal (100nM) zolpidem dose was used and, had little effect when a maximal (1μM) dose was applied. The additive effect observed lends support to the hypothesis of CBD binding to an allosteric site as a positive allosteric modulator (PAM) on $GABA_ARs$ to exert an effect similar to a benzodiazepine, a finding also posited in Bakas et al., (2017). Further to this, possible CBD binding at the barbiturate site was observed, using pentobarbital, a potentiator at this site, the results of which showed CBD providing an additive effect here also. Finally, we used a neurosteriod site NAM to observe if its addition was detrimental to CBD influence. Unfortunately, only a small n number was performed here, so little can be taken from this data as is. The current trends would suggest that a neurosteriod NAM may be not be sufficient for CBD inhibition, though this conclusion requires further n numbers to be stated with confidence.

To investigate NMDAR involvement in the observed CBD effect, we utilised subunit specific antagonists to observe whether CBD inhibition by MK801 + D-AP5 was subunit related. The most common NMDAR subunits expressed in the mEC, alongside GluN1 isoforms, are N2A and N2B (Schorge and Colquhoun, 2003; Furukawa et al., 2005; Parsons and Raymond, 2014). As such we inhibited both of these subunits in individual experiments, using the subunit

specific antagonists PEA-QX (N2A) and ifenprodil (N2B). Initially, PEA-QX was described as a highly selective N2A antagonist, displaying >100-fold selectivity for N2A over N2B (Auberson et al., 2002). More recently however, the activity of PEA-QX at N2A has been suggested to be more in the region of ~5/10 fold selectivity over N2B and, as such, the 1μM PEA-QX used here, may have also inhibited N2B (Neyton and Paoletti, 2006; Lind et al., 2017). Ifenprodil is a well characterised N2B blocker, displaying ~400 fold selectivity for N2B over N2A (Williams, 1993, 2001). Nevertheless, the results from the antagonism of N2B, and possibly N2A, was sufficient to block CBD induced effects on sIPSCs. This result shows that CBD's action is definitely blocked by antagonism at N2B and, possibly N2A subunits, which suggests interaction for CBD at N2B and, possibly at GluN1 subunits, if antagonism of both GluN2 subunits is sufficient for inhibition of the CBD effect this may suggest a role for GluN1 in the CBD effect, though whether this is via specific binding would require further experiments to be completed. Indeed, further work could be performed here, with the CBD added after the application of NMDA to observe the effect of CBD on NMDA-induced GABA neurotransmission (Xue et al., 2011), similar to the $GABA_AR$ experiments performed with zolpidem. This may allow an assessment of whether CBD is directly or indirectly interaction/binding to NMDARs. Specific NMDAR-CBD binding studies could also be performed to assess whether this interaction is via direct binding of CBD to NMDAR or indirect via second messenger/cell signalling pathways.

Alongside these NMDAR and $GABA_AR$ experiments, we were interested in whether CBD was interacting with CBRs in the mEC to produce an effect, with recent evidence has suggested CBD has high affinity NAM abilities at CB1R (Laprairie et al., 2015). As such, known orthosteric inverse agonists to both CB1R (AM251) and CB2R (AM630) were used to block the cannabinoid binding site on these receptors (Pertwee, 2005). Low n numbers were performed for each of these drug treatments making any definite conclusions difficult to state, though the addition of both was sufficient in blockade of the CBD effects noted previously. Whether these results were due to low n numbers or inhibition of the CBD effect by CBR blockade requires further replication. Alongside these data, the FAAH inhibitor URB597 and its effect on CBD addition was also investigated. Once more, a small n number was produced, however observation of the population responses suggests that this inhibition looked to have little effect on CBD. Again, for these experiments to have definitive conclusions further n numbers are required, though for reference, GW pharmaceuticals believe there to be no involvement of CBRs in the anticonvulsant effect of CBD.

In addition to rat experiments, human tissue (HT) samples where sIPSCs had been recorded from pyramidal cells show remarkably similar results to those of the SE rats, with increased decay times and NICT values when CBD was added alone (**Chapter 5**). Indeed, a lower n number than the rat data was performed, suggestive of CBD possessing a higher efficacy in

the HT samples. This result suggests similar mechanisms of CBD action between the two species, as well as validating the RISE model of epilepsy as an adequate model of TLE and human epilepsy. Due to this, preliminary antagonist experiments were also performed on HT samples (**Chapter 6**), however the scarcity of this resource has meant that only a small n could be provided here. Despite that, similar responses to those observed in the SE rat tissue have been seen here. The MK801 addition appears effective at blocking any CBD induced responses in the HT samples, especially so in the decay time and NICT parameters (though here only once an obvious anomalous result is removed). This is indicative of the importance NMDARs have in CBD responses, as this effect is present in both SE rat tissue and HT cells. Flumazenil appears to block CBD induced increases in decay time and NICT, though as only an n of 2 is shown here this is difficult to state with any certainty.

CBDV was only used briefly in whole-cell voltage-clamp experiments (**Chapter 5**), where no changes in sIPSC responses were noted in AMC tissue. In the SE tissue CBDV appeared ineffective across the event kinetic parameters, though a significant decrease in NICT values was observed, highly suggestive of a different mechanism of action to that of CBD. This decrease in NICT also possibly indicates a role in excitatory neurotransmission machinery for CBDV effects noted in the LFP data (**Chapter 4**). Further experiments could involve looking at the effect of CBDV on sEPSC kinetics to uncover whether this is where CBDV is effective.

From the results we have achieved, we hypothesise CBD as acting concurrently at either presynaptic or postsynaptic NMDARs and, postsynaptic pyramidal cell $GABA_A$Rs. At NMDARs, CBD may be interacting directly or indirectly to influence NMDAR gating and increase NMDAR-mediated GABA release, through driving Ca^{2+} entry presynaptically to result in increased presynaptic GABA release. If acting at postsynaptic NMDARs, CBD interaction is most likely fuelling second messenger systems, eliciting the synthesis of retrograde signalling molecules, such as NO, which subsequently diffuse across the synaptic cleft to drive the release of GABA from presynaptic boutons. At postsynaptic $GABA_A$Rs, CBD is most likely acting as a PAM, binding to an as of yet unknown allosteric site to decrease IEI times and, increase channel open times, resulting in an increase in inhibitory activity at the postsynaptic terminal and, therefore, a decrease in neuronal excitability. CBD certainly displays subtle effects, requiring a large number of n to be visible on a single cell level, the result of which has made its study more difficult as significant effects are not often noted at low n number (n =7/8). CBDV is most likely causing a suppression of gamma oscillations through excitatory mechanisms in SE tissue, suggested by the decrease in mean NICT values noted in sEPSC experiments (**Chapter 5**), though what these may be has not been clarified in this report. The RISE model of epilepsy shows significant changes in excitatory neurotransmission, suggesting it is a competent model of TLE.

Chapter 8

References

Abel EL (1980) Marijuana: The First Twelve Thousand Years. Springer.
Aghajanian GK, Rasmussen K (1989) Intracellular studies in the facial nucleus illustrating a simple new method for obtaining viable motoneurons in adult rat brain slices. Synapse 3:331–338.
Aimone JB, Li Y, Lee SW, Clemenson GD, Deng W, Gage FH (2014) Regulation and function of adult neurogenesis: from genes to cognition. Physiol Rev 94:991–1026.
Akaike N, Maruyama T, Tokutomi N (1987) Kinetic properties of the pentobarbitone-gated chloride current in frog sensory neurones. J Physiol 394:85–98.
Akazawa C, Shigemoto R, Bessho Y, Nakanishi S, Mizuno N (1994) Differential expression of five N-methyl-D-aspartate receptor subunit mRNAs in the cerebellum of developing and adult rats. J Comp Neurol 347:150–160.
Akk G, Bracamontes J, Steinbach JH (2001) Pregnenolone sulfate block of GABA(A) receptors: mechanism and involvement of a residue in the M2 region of the alpha subunit. J Physiol 532:673–684.
Akk G, Li P, Bracamontes J, Reichert DE, Covey DF, Steinbach JH (2008) Mutations of the GABA-A receptor alpha1 subunit M1 domain reveal unexpected complexity for modulation by neuroactive steroids. Mol Pharmacol 74:614–627.
Akk G, Steinbach JH (2000) Activation and block of recombinant GABA(A) receptors by pentobarbitone: a single-channel study. Br J Pharmacol 130:249–258.
Aksoy-Aksel A, Manahan-Vaughan D (2013) The temporoammonic input to the hippocampal CA1 region displays distinctly different synaptic plasticity compared to the Schaffer collateral input in vivo: significance for synaptic information processing. Front Synaptic Neurosci 5:5 Available at: http://www.ncbi.nlm.nih.gov/pmc/articles/PMC3750210/.
Alexander SPH (2012) So what do we call GPR18 now? Br J Pharmacol 165:2411–2413.
Alfonso J, Le Magueresse C, Zuccotti A, Khodosevich K, Monyer H (2012) Diazepam binding inhibitor promotes progenitor proliferation in the postnatal SVZ by reducing GABA signaling. Cell Stem Cell 10:76–87.
Alonso A, Klink R (1993) Differential electroresponsiveness of stellate and pyramidal-like cells of medial entorhinal cortex layer II. J Neurophysiol 70:128–143.
Alonso A, Llinás RR (1989) Subthreshold Na+-dependent theta-like rhythmicity in stellate cells of entorhinal cortex layer II. Nature 342:175 Available at: http://dx.doi.org/10.1038/342175a0.
Amaral D, Witter M (1995) Hippocampal formation In: The Rat Nervous System (Paxinos G, ed)., 2nd editio. San Diego: Academic Press.
Amaral DG, Ishizuka N, Claiborne B (1990) Neurons, numbers and the hippocampal network. Prog Brain Res 83:1–11.
Amaral DG, Scharfman HE, Lavenex P (2007) The dentate gyrus: fundamental neuroanatomical organization (dentate gyrus for dummies). Prog Brain Res 163:3–22 Available at: http://www.ncbi.nlm.nih.gov/pmc/articles/PMC2492885/.
Amaral DG, Witter MP (1989) The three-dimensional organization of the hippocampal formation: a review of anatomical data. Neuroscience 31:571–591.
Amaral, DG & Lavenex P (2007) Hippocampal Neuroanatomy. In: The Hippocampus Book. New York: Oxford University Press.
Amin J, Weiss DS (1993) GABAA receptor needs two homologous domains of the beta-subunit for activation by GABA but not by pentobarbital. Nature 366:565–569.
Andersen P, Bliss T V, Skrede KK (1971) Lamellar organization of hippocampal pathways. Exp Brain Res 13:222–238.
Andersen P, Holmqvist B, Voorhoeve PE (1966) Excitatory Synapses on Hippocampal Apical Dendrites Activated by Entorhinal Stimulation. Acta Physiol Scand 66:461–472 Available at: http://dx.doi.org/10.1111/j.1748-1716.1966.tb03224.x.
Andreasen NC (2000) Schizophrenia: the fundamental questions. Brain Res Brain Res Rev 31:106–112.
Annegers JF, Hauser WA, Coan SP, Rocca WA (1998) A Population-Based Study of Seizures after Traumatic Brain Injuries. N Engl J Med 338:20–24 Available at: http://www.nejm.org/doi/full/10.1056/NEJM199801013380104.
Arrigoni E, Greene RW (2004) Schaffer collateral and perforant path inputs activate different subtypes of NMDA receptors on the same CA1 pyramidal cell. Br J Pharmacol 142:317–322 Available at: http://www.ncbi.nlm.nih.gov/pmc/articles/PMC1574942/.
Auberson YP, Allgeier H, Bischoff S, Lingenhoehl K, Moretti R, Schmutz M (2002) 5-

Phosphonomethylquinoxalinediones as competitive NMDA receptor antagonists with a preference for the human 1A/2A, rather than 1A/2B receptor composition. Bioorg Med Chem Lett 12:1099–1102.
Avoli M, Barbarosie M, Lucke A, Nagao T, Lopantsev V, Kohling R (1996) Synchronous GABA-mediated potentials and epileptiform discharges in the rat limbic system in vitro. J Neurosci 16:3912–3924.
Babb TL, Kupfer WR, Pretorius JK, Crandall PH, Levesque MF (1991) Synaptic reorganization by mossy fibers in human epileptic fascia dentata. Neuroscience 42:351–363.
Bailey SJ, Dhillon A, Woodhall GL, Jones RSG (2004) Lamina-specific differences in GABA(B) autoreceptor-mediated regulation of spontaneous GABA release in rat entorhinal cortex. Neuropharmacology 46:31–42.
Bakas T, van Nieuwenhuijzen PS, Devenish SO, McGregor IS, Arnold JC, Chebib M (2017) The direct actions of cannabidiol and 2-arachidonoyl glycerol at GABAA receptors. Pharmacol Res 119:358–370.
Banks MI, Pearce RA (2000) Kinetic differences between synaptic and extrasynaptic GABA(A) receptors in CA1 pyramidal cells. J Neurosci 20:937–948.
Bartlett TE, Bannister NJ, Collett VJ, Dargan SL, Massey P V, Bortolotto ZA, Fitzjohn SM, Bashir ZI, Collingridge GL, Lodge D (2007) Differential roles of NR2A and NR2B-containing NMDA receptors in LTP and LTD in the CA1 region of two-week old rat hippocampus. Neuropharmacology 52:60–70.
Bartos M, Vida I, Frotscher M, Meyer A, Monyer H, Geiger JR, Jonas P (2002) Fast synaptic inhibition promotes synchronized gamma oscillations in hippocampal interneuron networks. Proc Natl Acad Sci U S A 99:13222–13227.
Bazelot M, Dinocourt C, Cohen I, Miles R (2010) Unitary inhibitory field potentials in the CA3 region of rat hippocampus. J Physiol 588:2077–2090 Available at: http://www.ncbi.nlm.nih.gov/pubmed/20403979.
Behrens CJ, van den Boom LP, de Hoz L, Friedman A, Heinemann U (2005) Induction of sharp wave-ripple complexes in vitro and reorganization of hippocampal networks. Nat Neurosci 8:1560–1567.
Belelli D, Casula A, Ling A, Lambert JJ (2002) The influence of subunit composition on the interaction of neurosteroids with GABA(A) receptors. Neuropharmacology 43:651–661.
Belelli D, Harrison NL, Maguire J, Macdonald RL, Walker MC, Cope DW (2009) Extrasynaptic GABAA receptors: form, pharmacology, and function. J Neurosci 29:12757–12763.
Bell GS, Sander JW (2001) CPD — Education and self-assessment The epidemiology of epilepsy: the size of the problem. Seizure - Eur J Epilepsy 10:306–316 Available at: http://dx.doi.org/10.1053/seiz.2001.0584.
Beltramo M, Bernardini N, Bertorelli R, Campanella M, Nicolussi E, Fredduzzi S, Reggiani A (2006) CB2 receptor-mediated antihyperalgesia: possible direct involvement of neural mechanisms. Eur J Neurosci 23:1530–1538.
Ben-Ari Y, Cherubini E, Corradetti R, Gaiarsa JL (1989) Giant synaptic potentials in immature rat CA3 hippocampal neurones. J Physiol 416:303–325.
Ben-Ari Y, Cossart R (2000) Kainate, a double agent that generates seizures: two decades of progress. Trends Neurosci 23:580–587.
Ben-Ari Y, Tremblay E, Ottersen OP (1980) Injections of kainic acid into the amygdaloid complex of the rat: an electrographic, clinical and histological study in relation to the pathology of epilepsy. Neuroscience 5:515–528.
Benard G et al. (2012) Mitochondrial CB(1) receptors regulate neuronal energy metabolism. Nat Neurosci 15:558–564.
Bera AK, Chatav M, Akabas MH (2002) GABA(A) receptor M2-M3 loop secondary structure and changes in accessibility during channel gating. J Biol Chem 277:43002–43010.
Berezhnoy D, Baur R, Gonthier A, Foucaud B, Goeldner M, Sigel E (2005) Conformational changes at benzodiazepine binding sites of GABAA receptors detected with a novel technique. J Neurochem 92:859–866 Available at: http://dx.doi.org/10.1111/j.1471-4159.2004.02913.x.
Berger H (1929) Über das Elektrenkephalogramm des Menschen. [On the electroencephalogram of humans]. Arch für Psychiatr und Nervenkrankheiten 87.
Berger H (1929) Über das Elektrenkephalogramm des Menschen. [On the

electroencephalogram of humans]. Arch für Psychiatr und Nervenkrankheiten 87.
Bernasconi N, Bernasconi A, Andermann F, Dubeau F, Feindel W, Reutens DC (1999) Entorhinal cortex in temporal lobe epilepsy: a quantitative MRI study. Neurology 52:1870–1876.
Bernasconi N, Bernasconi A, Caramanos Z, Andermann F, Dubeau F, Arnold DL (2000) Morphometric MRI analysis of the parahippocampal region in temporal lobe epilepsy. Ann N Y Acad Sci 911:495–500.
Bernier R, Dawson G, Webb S, Murias M (2007) EEG mu rhythm and imitation impairments in individuals with autism spectrum disorder. Brain Cogn 64:228–237.
Berretta N, Jones RS (1996) A comparison of spontaneous EPSCs in layer II and layer IV-V neurons of the rat entorhinal cortex in vitro. J Neurophysiol 76:1089–1100.
Bertram EH, Cornett JF (1994) The evolution of a rat model of chronic spontaneous limbic seizures. Brain Res 661:157–162 Available at: http://www.sciencedirect.com/science/article/pii/0006899394911924.
Bettler B, Kaupmann K, Mosbacher J, Gassmann M (2004) Molecular structure and physiological functions of GABA(B) receptors. Physiol Rev 84:835–867.
Bianchi MT, Macdonald RL (2001) Agonist Trapping by GABA_A Receptor Channels. J Neurosci 21:9083 LP-9091 Available at: http://www.jneurosci.org/content/21/23/9083.abstract.
Bianchi MT, Macdonald RL (2002) Slow phases of GABA(A) receptor desensitization: structural determinants and possible relevance for synaptic function. J Physiol 544:3–18.
Bisogno T, Hanus L, De Petrocellis L, Tchilibon S, Ponde DE, Brandi I, Moriello AS, Davis JB, Mechoulam R, Di Marzo V (2001) Molecular targets for cannabidiol and its synthetic analogues: effect on vanilloid VR1 receptors and on the cellular uptake and enzymatic hydrolysis of anandamide. Br J Pharmacol 134:845–852.
Blair HT, Welday AC, Zhang K (2007) Scale-invariant memory representations emerge from moire interference between grid fields that produce theta oscillations: a computational model. J Neurosci 27:3211–3229.
Blair MG, Nguyen NN-Q, Albani SH, L'Etoile MM, Andrawis MM, Owen LM, Oliveira RF, Johnson MW, Purvis DL, Sanders EM, Stoneham ET, Xu H, Dumas TC (2013) Developmental changes in structural and functional properties of hippocampal AMPARs parallels the emergence of deliberative spatial navigation in juvenile rats. J Neurosci 33:12218–12228.
Bledsoe D, Tamer C, Mesic I, Madry C, Klein BG, Laube B, Costa BM (2017) Positive Modulatory Interactions of NMDA Receptor GluN1/2B Ligand Binding Domains Attenuate Antagonists Activity. Front Pharmacol 8:229.
Bliss TVP, Lømo T (1973) Long-lasting potentiation of synaptic transmission in the dentate area of the anaesthetized rabbit following stimulation of the perforant path. J Physiol 232:331–356 Available at: http://dx.doi.org/10.1113/jphysiol.1973.sp010273.
Blumcke I et al. (2011) The clinicopathologic spectrum of focal cortical dysplasias: a consensus classification proposed by an ad hoc Task Force of the ILAE Diagnostic Methods Commission. Epilepsia 52:158–174.
Boggan WO, Steele RA, Freedman DX (1973) 9 -Tetrahydrocannabinol effect on audiogenic seizure susceptibility. Psychopharmacologia 29:101–106.
Boileau AJ, Newell JG, Czajkowski C (2002) GABA(A) receptor beta 2 Tyr97 and Leu99 line the GABA-binding site. Insights into mechanisms of agonist and antagonist actions. J Biol Chem 277:2931–2937.
Bortolotto ZA, Clarke VR, Delany CM, Parry MC, Smolders I, Vignes M, Ho KH, Miu P, Brinton BT, Fantaske R, Ogden A, Gates M, Ornstein PL, Lodge D, Bleakman D, Collingridge GL (1999) Kainate receptors are involved in synaptic plasticity. Nature 402:297–301.
Bouaboula M, Dussossoy D, Casellas P (1999) Regulation of peripheral cannabinoid receptor CB2 phosphorylation by the inverse agonist SR 144528. Implications for receptor biological responses. J Biol Chem 274:20397–20405.
Bourgeois B (2008) General concepts of medical intractability, In: HO Luders, Epilepsy surgery, 2nd ed. informa healthcare.
Bouvard S, Costes N, Bonnefoi F, Lavenne F, Mauguiere F, Delforge J, Ryvlin P (2005) Seizure-related short-term plasticity of benzodiazepine receptors in partial epilepsy: a

[11C]flumazenil-PET study. Brain 128:1330–1343.
Bowe MA, Nadler J V (1990) Developmental increase in the sensitivity to magnesium of NMDA receptors on CA1 hippocampal pyramidal cells. Brain Res Dev Brain Res 56:55–61.
Bowery NG, Bettler B, Froestl W, Gallagher JP, Marshall F, Raiteri M, Bonner TI, Enna SJ (2002) International Union of Pharmacology. XXXIII. Mammalian gamma-aminobutyric acid(B) receptors: structure and function. Pharmacol Rev 54:247–264.
Bowery NG, Hill DR, Hudson AL, Doble A, Middlemiss DN, Shaw J, Turnbull M (1980) (-)Baclofen decreases neurotransmitter release in the mammalian CNS by an action at a novel GABA receptor. Nature 283:92–94.
Bragin A, Jando G, Nadasdy Z, Hetke J, Wise K, Buzsaki G (1995) Gamma (40-100 Hz) oscillation in the hippocampus of the behaving rat. J Neurosci 15:47–60.
Bressler SL, Freeman WJ (1980) Frequency analysis of olfactory system EEG in cat, rabbit, and rat. Electroencephalogr Clin Neurophysiol 50:19–24.
Brooks-Kayal AR, Shumate MD, Jin H, Rikhter TY, Coulter DA (1998) Selective changes in single cell GABA(A) receptor subunit expression and function in temporal lobe epilepsy. Nat Med 4:1166–1172.
Brown JT, Davies CH, Randall AD (2007) Synaptic activation of GABAB receptors regulates neuronal network activity and entrainment. Eur J Neurosci 25:2982–2990 Available at: http://dx.doi.org/10.1111/j.1460-9568.2007.05544.x.
Brown N, Kerby J, Bonnert TP, Whiting PJ, Wafford KA (2002) Pharmacological characterization of a novel cell line expressing human alpha(4)beta(3)delta GABA(A) receptors. Br J Pharmacol 136:965–974.
Buchheim K, Schuchmann S, Siegmund H, Weissinger F, Heinemann U, Meierkord H (2000) Comparison of intrinsic optical signals associated with low Mg2+-and 4-aminopyridine-induced seizure-like events reveals characteristic features in adult rat limbic system. Epilepsia 41:635–641.
Buckmaster PS, Zhang GF, Yamawaki R (2002) Axon sprouting in a model of temporal lobe epilepsy creates a predominantly excitatory feedback circuit. J Neurosci 22:6650–6658.
Buhl DL, Harris KD, Hormuzdi SG, Monyer H, Buzsaki G (2003) Selective impairment of hippocampal gamma oscillations in connexin-36 knock-out mouse in vivo. J Neurosci 23:1013–1018.
Burgard EC, Dahl D, Sarvey JM (1990) NMDA receptor antagonists reduce medial, but not lateral, perforant path-evoked EPSPs in dentate gyrus of rat hippocampal slice. Exp brain Res 83:172–177.
Burgess N, Barry C, O'Keefe J (2007) An oscillatory interference model of grid cell firing. Hippocampus 17:801–812.
Burton BG, Economo MN, Lee GJ, White JA (2008) Development of Theta Rhythmicity in Entorhinal Stellate Cells of the Juvenile Rat. J Neurophysiol 100:3144–3157 Available at: https://doi.org/10.1152/jn.90424.2008.
Buzsaki G (2006) Rhythms of the Brain. Oxford University Press. Available at: https://books.google.co.uk/books?id=ldz58irprjYC.
Buzsaki G (2011) Hippocampus. Scholarpedia 6:1468.
Buzsaki G, Anastassiou CA, Koch C (2012) The origin of extracellular fields and currents--EEG, ECoG, LFP and spikes. Nat Rev Neurosci 13:407–420 Available at: http://www.ncbi.nlm.nih.gov/pubmed/22595786.
Buzsáki G, Chrobak JJ (1995) Temporal structure in spatially organized neuronal ensembles: a role for interneuronal networks. Curr Opin Neurobiol 5:504–510.
Buzsaki G, Leung LW, Vanderwolf CH (1983) Cellular bases of hippocampal EEG in the behaving rat. Brain Res 287:139–171.
Buzsaki G, Traub R, Pedley T (2003) The cellular synaptic generation of EEG activity. Curr Partice Clin Enceph 3:1–11.
Buzsaki G, Wang XJ (2012) Mechanisms of gamma oscillations. Annu Rev Neurosci 35:203–225.
Camacho DL, Castillo M (2007) MR imaging of temporal lobe epilepsy. Semin Ultrasound CT MR 28:424–436.
Campo-Soria C, Chang Y, Weiss DS (2006) Mechanism of action of benzodiazepines on GABAA receptors. Br J Pharmacol 148:984–990.
Campos AC, Guimaraes FS (2008) Involvement of 5HT1A receptors in the anxiolytic-like

effects of cannabidiol injected into the dorsolateral periaqueductal gray of rats. Psychopharmacology (Berl) 199:223–230.
Campos AC, Moreira FA, Gomes F V, Del Bel EA, Guimaraes FS (2012) Multiple mechanisms involved in the large-spectrum therapeutic potential of cannabidiol in psychiatric disorders. Philos Trans R Soc L B Biol Sci 367:3364–3378.
Canto CB, Wouterlood FG, Witter MP (2008) What does anatomical organization of entorhinal cortex tell us? Neural Plast 2008.
Carayon P, Marchand J, Dussossoy D, Derocq JM, Jbilo O, Bord A, Bouaboula M, Galiegue S, Mondiere P, Penarier G, Fur GL, Defrance T, Casellas P (1998) Modulation and functional involvement of CB2 peripheral cannabinoid receptors during B-cell differentiation. Blood 92:3605–3615.
Cavalheiro EA, Riche DA, Le Gal La Salle G (1982) Long-term effects of intrahippocampal kainic acid injection in rats: a method for inducing spontaneous recurrent seizures. Electroencephalogr Clin Neurophysiol 53:581–589.
Chakrabarti A, Onaivi ES, Chaudhuri G (1995) Cloning and sequencing of a cDNA encoding the mouse brain-type cannabinoid receptor protein. DNA Seq 5:385–388.
Chapman AG (1998) Glutamate receptors in epilepsy. Prog Brain Res 116:371–383.
Charpak S, Pare D, Llinas R (1995) The entorhinal cortex entrains fast CA1 hippocampal oscillations in the anaesthetized guinea-pig: role of the monosynaptic component of the perforant path. Eur J Neurosci 7:1548–1557.
Cherubini E, Rovira C, Gaiarsa JL, Corradetti R, Ben Ari Y (1990) GABA mediated excitation in immature rat CA3 hippocampal neurons. Int J Dev Neurosci 8:481–490.
Chittajallu R, Braithwaite SP, Clarke VRJ, Henley JM (1999) Kainate receptors: subunits, synaptic localization and function. Trends Pharmacol Sci 20:26–35 Available at: http://www.sciencedirect.com/science/article/pii/S0165614798012863.
Christian CA, Herbert AG, Holt RL, Peng K, Sherwood KD, Pangratz-Fuehrer S, Rudolph U, Huguenard JR (2013) Endogenous positive allosteric modulation of GABA(A) receptors by diazepam binding inhibitor. Neuron 78:1063–1074.
Chrobak JJ, Amaral DG (2007) Entorhinal cortex of the monkey: VII. intrinsic connections. J Comp Neurol 500:612–633.
Chrobak JJ, Buzsaki G (1998) Gamma oscillations in the entorhinal cortex of the freely behaving rat. J Neurosci 18:388–398.
Ciabarra AM, Sullivan JM, Gahn LG, Pecht G, Heinemann S, Sevarino KA (1995) Cloning and characterization of chi-1: a developmentally regulated member of a novel class of the ionotropic glutamate receptor family. J Neurosci 15:6498–6508.
Clifford DB, Olney JW, Maniotis A, Collins RC, Zorumski CF (1987) The functional anatomy and pathology of lithium-pilocarpine and high-dose pilocarpine seizures. Neuroscience 23:953–968.
Cobb SR, Buhl EH, Halasy K, Paulsen O, Somogyi P (1995) Synchronization of neuronal activity in hippocampus by individual GABAergic interneurons. Nature 378:75–78.
Cobb SR, Halasy K, Vida I, Nyiri G, Tamas G, Buhl EH, Somogyi P (1997) Synaptic effects of identified interneurons innervating both interneurons and pyramidal cells in the rat hippocampus. Neuroscience 79:629–648.
Cohen AS, Lin DD, Quirk GL, Coulter DA (2003) Dentate granule cell GABA(A) receptors in epileptic hippocampus: enhanced synaptic efficacy and altered pharmacology. Eur J Neurosci 17:1607–1616.
Cohen MX, Elger CE, Fell J (2009) Oscillatory activity and phase-amplitude coupling in the human medial frontal cortex during decision making. J Cogn Neurosci 21:390–402.
Cohen SM, Tsien RW, Goff DC, Halassa MM (2015) The impact of NMDA Receptor hypofunction on GABAergic interneurons in the pathophysiology of schizophrenia. Schizophr Res 167:98–107 Available at: http://www.ncbi.nlm.nih.gov/pmc/articles/PMC4724170/.
Colombo N, Tassi L, Galli C, Citterio A, Lo Russo G, Scialfa G, Spreafico R (2003) Focal cortical dysplasias: MR imaging, histopathologic, and clinical correlations in surgically treated patients with epilepsy. AJNR Am J Neuroradiol 24:724–733.
Consroe P, Benedito MA, Leite JR, Carlini EA, Mechoulam R (1982) Effects of cannabidiol on behavioral seizures caused by convulsant drugs or current in mice. Eur J Pharmacol 83:293–298.
Cortelli P, Avallone R, Baraldi M, Zeneroli ML, Mandrioli J, Corsi L, Riva R, Tinuper P,

Lugaresi E, Baruzzi A, Montagna P (2005) Endozepines in recurrent stupor. Sleep Med Rev 9:477–487.
Costa E, Guidotti A (1985) Endogenous ligands for benzodiazepine recognition sites. Biochem Pharmacol 34:3399–3403.
Coutts AA, Anavi-Goffer S, Ross RA, MacEwan DJ, Mackie K, Pertwee RG, Irving AJ (2001) Agonist-induced internalization and trafficking of cannabinoid CB1 receptors in hippocampal neurons. J Neurosci 21:2425–2433.
Cravatt BF, Prospero-Garcia O, Siuzdak G, Gilula NB, Henriksen SJ, Boger DL, Lerner RA (1995) Chemical characterization of a family of brain lipids that induce sleep. Science 268:1506–1509.
Creutzfeldt OD (1995) The allocortex and limbic system. In: Cortex Cerebri. Oxford: Oxford University Press. Available at: http://www.oxfordscholarship.com/10.1093/acprof:oso/9780198523246.001.0001/acprof-9780198523246-chapter-9.
Croci T, Manara L, Aureggi G, Guagnini F, Rinaldi-Carmona M, Maffrand JP, Le Fur G, Mukenge S, Ferla G (1998) In vitro functional evidence of neuronal cannabinoid CB1 receptors in human ileum. Br J Pharmacol 125:1393–1395.
Csicsvari J, Jamieson B, Wise KD, Buzsaki G (2003) Mechanisms of gamma oscillations in the hippocampus of the behaving rat. Neuron 37:311–322.
Cull-Candy S, Brickley S, Farrant M (2001) NMDA receptor subunits: diversity, development and disease. Curr Opin Neurobiol 11:327–335.
Cunha JM, Carlini EA, Pereira AE, Ramos OL, Pimentel C, Gagliardi R, Sanvito WL, Lander N, Mechoulam R (1980) Chronic administration of cannabidiol to healthy volunteers and epileptic patients. Pharmacology 21:175–185.
Cunningham MO, Davies CH, Buhl EH, Kopell N, Whittington MA (2003) Gamma oscillations induced by kainate receptor activation in the entorhinal cortex in vitro. J Neurosci 23:9761–9769.
Cunningham MO, Hunt J, Middleton S, LeBeau FEN, Gillies MJ, Davies CH, Maycox PR, Whittington MA, Racca C (2006) Region-specific reduction in entorhinal gamma oscillations and parvalbumin-immunoreactive neurons in animal models of psychiatric illness. J Neurosci 26:2767–2776.
Curia G, Longo D, Biagini G, Jones RS, Avoli M (2008) The pilocarpine model of temporal lobe epilepsy. J Neurosci Methods 172:143–157.
Curia G, Lucchi C, Vinet J, Gualtieri F, Marinelli C, Torsello A, Costantino L, Biagini* G (2014) Pathophysiogenesis of Mesial Temporal Lobe Epilepsy: Is Prevention of Damage Antiepileptogenic? Curr Med Chem 21:663–688.
D'Arcangelo G, Tancredi V, Avoli M (2001) Intrinsic optical signals and electrographic seizures in the rat limbic system. Neurobiol Dis 8:993–1005.
De Felipe MC, Molinero MT, Del Rio J (1989) Long-lasting neurochemical and functional changes in rats induced by neonatal administration of substance P antiserum. Brain Res 485:301–308.
De Mateos-Verchere JG, Leprince J, Tonon MC, Vaudry H, Costentin J (1998) The octadecaneuropeptide ODN induces anxiety in rodents: possible involvement of a shorter biologically active fragment. Peptides 19:841–848.
De Petrocellis L, Ligresti A, Moriello AS, Allara M, Bisogno T, Petrosino S, Stott CG, Di Marzo V (2011) Effects of cannabinoids and cannabinoid-enriched Cannabis extracts on TRP channels and endocannabinoid metabolic enzymes. Br J Pharmacol 163:1479–1494.
De Petrocellis L, Marini P, Matias I, Moriello AS, Starowicz K, Cristino L, Nigam S, Di Marzo V (2007) Mechanisms for the coupling of cannabinoid receptors to intracellular calcium mobilization in rat insulinoma beta-cells. Exp Cell Res 313:2993–3004.
Deans MR, Gibson JR, Sellitto C, Connors BW, Paul DL (2001) Synchronous activity of inhibitory networks in neocortex requires electrical synapses containing connexin36. Neuron 31:477–485.
Derkach VA, Oh MC, Guire ES, Soderling TR (2007) Regulatory mechanisms of AMPA receptors in synaptic plasticity. Nat Rev Neurosci 8:101–113.
Destexhe A, Pare D (1999) Impact of network activity on the integrative properties of neocortical pyramidal neurons in vivo. J Neurophysiol 81:1531–1547.
Devane WA, Dysarz FA 3rd, Johnson MR, Melvin LS, Howlett AC (1988) Determination and

characterization of a cannabinoid receptor in rat brain. Mol Pharmacol 34:605–613.
Devane WA, Hanus L, Breuer A, Pertwee RG, Stevenson LA, Griffin G, Gibson D, Mandelbaum A, Etinger A, Mechoulam R (1992) Isolation and structure of a brain constituent that binds to the cannabinoid receptor. Science (80-) 258:1946–1949.
Devinsky O et al. (2016) Cannabidiol in patients with treatment-resistant epilepsy: an open-label interventional trial. Lancet Neurol 15:270–278 Available at: http://www.ncbi.nlm.nih.gov/pubmed/26724101.
Devinsky O, Cilio MR, Cross H, Fernandez-Ruiz J, French J, Hill C, Katz R, Di Marzo V, Jutras-Aswad D, Notcutt WG, Martinez-Orgado J, Robson PJ, Rohrback BG, Thiele E, Whalley B, Friedman D (2014) Cannabidiol: Pharmacology and potential therapeutic role in epilepsy and other neuropsychiatric disorders. Epilepsia 55:791–802.
Dhillon A, Jones RS (2000) Laminar differences in recurrent excitatory transmission in the rat entorhinal cortex in vitro. Neuroscience 99:413–422.
Di Marzo V (2008) Targeting the endocannabinoid system: to enhance or reduce? Nat Rev Drug Discov 7:438–455.
Di Marzo V, Bifulco M, Petrocellis L De (2004) The endocannabinoid system and its therapeutic exploitation. Nat Rev Drug Discov 3:771 Available at: http://dx.doi.org/10.1038/nrd1495.
Di Marzo V, De Petrocellis L, Bisogno T (2005) The biosynthesis, fate and pharmacological properties of endocannabinoids. Handb Exp Pharmacol:147–185.
Diana MA, Marty A (2004) Endocannabinoid-mediated short-term synaptic plasticity: depolarization-induced suppression of inhibition (DSI) and depolarization-induced suppression of excitation (DSE). Br J Pharmacol 142:9–19 Available at: http://www.ncbi.nlm.nih.gov/pmc/articles/PMC1574919/.
Dietzel I, Heinemann U, Lux HD (1989) Relations between slow extracellular potential changes, glial potassium buffering, and electrolyte and cellular volume changes during neuronal hyperactivity in cat brain. Glia 2:25–44.
Dolorfo CL, Amaral DG (1998a) Entorhinal cortex of the rat: organization of intrinsic connections. J Comp Neurol 398:49–82.
Dolorfo CL, Amaral DG (1998b) Entorhinal cortex of the rat: topographic organization of the cells of origin of the perforant path projection to the dentate gyrus. J Comp Neurol 398:25–48.
Dong E, Matsumoto K, Tohda M, Watanabe H (1999) Involvement of diazepam binding inhibitor and its fragment octadecaneuropeptide in social isolation stress-induced decrease in pentobarbital sleep in mice. Life Sci 64:1779–1784.
Douglas RJ, Martin KAC (2007) Mapping the Matrix: The Ways of Neocortex. Neuron 56:226–238 Available at: http://dx.doi.org/10.1016/j.neuron.2007.10.017.
Downing SS, Lee YT, Farb DH, Gibbs TT (2005) Benzodiazepine modulation of partial agonist efficacy and spontaneously active GABA(A) receptors supports an allosteric model of modulation. Br J Pharmacol 145:894–906.
Dragoi G, Harris KD, Buzsáki G (2003) Place Representation within Hippocampal Networks Is Modified by Long-Term Potentiation. Neuron 39:843–853 Available at: http://www.sciencedirect.com/science/article/pii/S0896627303004653.
Drexel M, Preidt AP, Sperk G (2012) Sequel of spontaneous seizures after kainic acid-induced status epilepticus and associated neuropathological changes in the subiculum and entorhinal cortex. Neuropharmacology 63:806–817.
Du F, Eid T, Lothman EW, Kohler C, Schwarcz R (1995) Preferential neuronal loss in layer III of the medial entorhinal cortex in rat models of temporal lobe epilepsy. J Neurosci 15:6301–6313.
Du F, Schwarcz R (1992) Aminooxyacetic acid causes selective neuronal loss in layer III of the rat medial entorhinal cortex. Neurosci Lett 147:185–188 Available at: http://www.sciencedirect.com/science/article/pii/030439409290591T.
Du F, Whetsell Jr. WO, Abou-Khalil B, Blumenkopf B, Lothman EW, Schwarcz R (1993) Preferential neuronal loss in layer III of the entorhinal cortex in patients with temporal lobe epilepsy. Epilepsy Res 16:223–233.
Dudek F, Clark S, Williams P, Grabenstatter H (2005) Kainate-induced status epilepticus: A chronic model of acquired epilepsy. In: Models of seizures and epilepsy, pp 415–432. New York, NY, USA: Elsevier.
Dudek FE, Shao L-R (2004) Mossy fiber sprouting and recurrent excitation: direct

electrophysiologic evidence and potential implications. Epilepsy Curr 4:184–187.
Durand GM, Bennett M V, Zukin RS (1993) Splice variants of the N-methyl-D-aspartate receptor NR1 identify domains involved in regulation by polyamines and protein kinase C. Proc Natl Acad Sci U S A 90:6731–6735 Available at: http://www.ncbi.nlm.nih.gov/pmc/articles/PMC47006/.
Durand GM, Gregor P, Zheng X, Bennett M V, Uhl GR, Zukin RS (1992) Cloning of an apparent splice variant of the rat N-methyl-D-aspartate receptor NMDAR1 with altered sensitivity to polyamines and activators of protein kinase C. Proc Natl Acad Sci U S A 89:9359–9363.
Dutar P, Nicoll RA (1988) Pre- and postsynaptic GABAB receptors in the hippocampus have different pharmacological properties. Neuron 1:585–591.
El-Alfy AT, Ivey K, Robinson K, Ahmed S, Radwan M, Slade D, Khan I, ElSohly M, Ross S (2010) Antidepressant-like effect of delta9-tetrahydrocannabinol and other cannabinoids isolated from Cannabis sativa L. Pharmacol Biochem Behav 95:434–442.
Farrant M, Nusser Z (2005) Variations on an inhibitory theme: phasic and tonic activation of GABA(A) receptors. Nat Rev Neurosci 6:215–229.
Farrar SJ, Whiting PJ, Bonnert TP, McKernan RM (1999) Stoichiometry of a ligand-gated ion channel determined by fluorescence energy transfer. J Biol Chem 274:10100–10104.
Farzampour Z, Reimer RJ, Huguenard J (2015) Endozepines. Adv Pharmacol 72:147–164.
Fauser S, Huppertz H-J, Bast T, Strobl K, Pantazis G, Altenmueller D-M, Feil B, Rona S, Kurth C, Rating D, Korinthenberg R, Steinhoff BJ, Volk B, Schulze-Bonhage A (2006) Clinical characteristics in focal cortical dysplasia: a retrospective evaluation in a series of 120 patients. Brain 129:1907–1916.
Fell J, Klaver P, Lehnertz K, Grunwald T, Schaller C, Elger CE, Fernandez G (2001) Human memory formation is accompanied by rhinal-hippocampal coupling and decoupling. Nat Neurosci 4:1259–1264.
FG. Wouterlood (2002) Spotlight on the neurones (I): cell types, local connectivity, microcircuits and distribution of markers, In: The Parahippocampal Region: Organization and role in cogitive function. Oxford: Oxford University Press.
Fisahn A, Contractor A, Traub RD, Buhl EH, Heinemann SF, McBain CJ (2004) Distinct roles for the kainate receptor subunits GluR5 and GluR6 in kainate-induced hippocampal gamma oscillations. J Neurosci 24:9658–9668.
Fisahn A, Pike FG, Buhl EH, Paulsen O (1998) Cholinergic induction of network oscillations at 40 Hz in the hippocampus in vitro. Nature 394:186–189.
Fisher RS, Acevedo C, Arzimanoglou A, Bogacz A, Cross JH, Elger CE, Engel JJ, Forsgren L, French JA, Glynn M, Hesdorffer DC, Lee BI, Mathern GW, Moshe SL, Perucca E, Scheffer IE, Tomson T, Watanabe M, Wiebe S (2014) ILAE official report: a practical clinical definition of epilepsy. Epilepsia 55:475–482.
Fisher RS, Cross JH, French JA, Higurashi N, Hirsch E, Jansen FE, Lagae L, Moshe SL, Peltola J, Roulet Perez E, Scheffer IE, Zuberi SM (2017) Operational classification of seizure types by the International League Against Epilepsy: Position Paper of the ILAE Commission for Classification and Terminology. Epilepsia 58:522–530.
Fisher RS, van Emde Boas W, Blume W, Elger C, Genton P, Lee P, Engel JJ (2005) Epileptic seizures and epilepsy: definitions proposed by the International League Against Epilepsy (ILAE) and the International Bureau for Epilepsy (IBE). Epilepsia 46:470–472.
Freiman TM, Eismann-Schweimler J, Frotscher M (2011) Granule cell dispersion in temporal lobe epilepsy is associated with changes in dendritic orientation and spine distribution. Exp Neurol 229:332–338.
French JA, Williamson PD, Thadani VM, Darcey TM, Mattson RH, Spencer SS, Spencer DD (1993) Characteristics of medial temporal lobe epilepsy: I. Results of history and physical examination. Ann Neurol 34:774–780.
Freund TF, Martin KA, Smith AD, Somogyi P (1983) Glutamate decarboxylase-immunoreactive terminals of Golgi-impregnated axoaxonic cells and of presumed basket cells in synaptic contact with pyramidal neurons of the cat's visual cortex. J Comp Neurol 221:263–278.
Friedman LK, Pellegrini-Giampietro DE, Sperber EF, Bennett M V, Moshe SL, Zukin RS (1994) Kainate-induced status epilepticus alters glutamate and GABAA receptor gene expression in adult rat hippocampus: an in situ hybridization study. J Neurosci 14:2697–

2707.
Fries P, Neuenschwander S, Engel AK, Goebel R, Singer W (2001) Rapid feature selective neuronal synchronization through correlated latency shifting. Nat Neurosci 4:194–200.
Fritsch B, Reis J, Gasior M, Kaminski RM, Rogawski MA (2014) Role of GluK1 Kainate Receptors in Seizures, Epileptic Discharges, and Epileptogenesis. J Neurosci 34:5765–5775 Available at: http://www.ncbi.nlm.nih.gov/pmc/articles/PMC3996208/.
Froestl W (2010) Chemistry and pharmacology of GABAB receptor ligands. Adv Pharmacol 58:19–62.
Furukawa H, Singh SK, Mancusso R, Gouaux E (2005) Subunit arrangement and function in NMDA receptors. Nature 438:185–192.
Galarreta M, Hestrin S (2001) Spike transmission and synchrony detection in networks of GABAergic interneurons. Science 292:2295–2299.
Galiegue S, Mary S, Marchand J, Dussossoy D, Carriere D, Carayon P, Bouaboula M, Shire D, Le Fur G, Casellas P (1995) Expression of central and peripheral cannabinoid receptors in human immune tissues and leukocyte subpopulations. Eur J Biochem 232:54–61.
Gallager DW, Tallman JF (1983) Consequences of benzodiazepine receptor occupancy. Neuropharmacology 22:1493–1498.
Gamber KM, Macarthur H, Westfall TC (2005) Cannabinoids augment the release of neuropeptide Y in the rat hypothalamus. Neuropharmacology 49:646–652.
Gaoni Y, Mechoulam R (1964) Isolation, structure and partial synthesis of an active constituent of hashish. J Am Chem soceity:1646–1647.
Gerard CM, Mollereau C, Vassart G, Parmentier M (1991) Molecular cloning of a human cannabinoid receptor which is also expressed in testis. Biochem J 279 (Pt 1:129–134.
Germroth P, Schwerdtfeger WK, Buhl EH (1989) Morphology of identified entorhinal neurons projecting to the hippocampus. A light microscopical study combining retrograde tracing and intracellular injection. Neuroscience 30:683–691 Available at: http://www.sciencedirect.com/science/article/pii/0306452289901619.
Germroth P, Schwerdtfeger WK, Buhl EH (1991) Ultrastructure and aspects of functional organization of pyramidal and nonpyramidal entorhinal projection neurons contributing to the perforant path. J Comp Neurol 305:215–231.
Giacoppo S, Pollastro F, Grassi G, Bramanti P, Mazzon E (2017) Target regulation of PI3K/Akt/mTOR pathway by cannabidiol in treatment of experimental multiple sclerosis. Fitoterapia 116:77–84.
Gielen MC, Lumb MJ, Smart TG (2012) Benzodiazepines Modulate GABA_A Receptors by Regulating the Preactivation Step after GABA Binding. J Neurosci 32:5707 LP-5715 Available at: http://www.jneurosci.org/content/32/17/5707.abstract.
Gillies MJ, Traub RD, LeBeau FEN, Davies CH, Gloveli T, Buhl EH, Whittington MA (2002) A model of atropine-resistant theta oscillations in rat hippocampal area CA1. J Physiol 543:779–793.
Giocomo LM, Zilli EA, Fransén E, Hasselmo ME (2007) Temporal Frequency of Subthreshold Oscillations Scales with Entorhinal Grid Cell Field Spacing. Science 315:1719–1722 Available at: http://www.ncbi.nlm.nih.gov/pmc/articles/PMC2950607/.
Glass M, Dragunow M, Faull RL (1997) Cannabinoid receptors in the human brain: a detailed anatomical and quantitative autoradiographic study in the fetal, neonatal and adult human brain. Neuroscience 77:299–318.
Glickfeld LL, Roberts JD, Somogyi P, Scanziani M (2009) Interneurons hyperpolarize pyramidal cells along their entire somatodendritic axis. Nat Neurosci 12:21–23.
Glien M, Brandt C, Potschka H, Voigt H, Ebert U, Loscher W (2001) Repeated low-dose treatment of rats with pilocarpine: low mortality but high proportion of rats developing epilepsy. Epilepsy Res 46:111–119.
Gloveli T, Dugladze T, Saha S, Monyer H, Heinemann U, Traub RD, Whittington MA, Buhl EH (2005) Differential involvement of oriens/pyramidale interneurones in hippocampal network oscillations in vitro. J Physiol 562:131–147.
Gloveli T, Dugladze T, Schmitz D, Heinemann U (2001) Properties of entorhinal cortex deep layer neurons projecting to the rat dentate gyrus. Eur J Neurosci 13:413–420.
Gloveli T, Schmitz D, Empson RM, Dugladze T, Heinemann U (1997) Morphological and electrophysiological characterization of layer III cells of the medial entorhinal cortex of

the rat. Neuroscience 77:629–648.
Goddard G V (1967) Development of epileptic seizures through brain stimulation at low intensity. Nature 214:1020–1021.
Goddard G V, McIntyre DC, Leech CK (1969) A permanent change in brain function resulting from daily electrical stimulation. Exp Neurol 25:295–330 Available at: http://www.sciencedirect.com/science/article/pii/0014488669901289.
Gomes I, Grushko JS, Golebiewska U, Hoogendoorn S, Gupta A, Heimann AS, Ferro ES, Scarlata S, Fricker LD, Devi LA (2009) Novel endogenous peptide agonists of cannabinoid receptors. FASEB J Off Publ Fed Am Soc Exp Biol 23:3020–3029.
Gong J-P, Onaivi ES, Ishiguro H, Liu Q-R, Tagliaferro PA, Brusco A, Uhl GR (2006) Cannabinoid CB2 receptors: immunohistochemical localization in rat brain. Brain Res 1071:10–23.
Goren EN, Reeves DC, Akabas MH (2004) Loose protein packing around the extracellular half of the GABA(A) receptor beta1 subunit M2 channel-lining segment. J Biol Chem 279:11198–11205.
Gray CM (1994) Synchronous oscillations in neuronal systems: mechanisms and functions. J Comput Neurosci 1:11–38.
Gray H, Lewis WH (1918) Anatomy of the Human Body. Lea & Febiger. Available at: https://books.google.co.uk/books?id=uaQMAAAAYAAJ.
Greenhill SD, Chamberlain SEL, Lench A, Massey PV, Yuill KH, Woodhall GL, Jones RSG (2014) Background synaptic activity in rat entorhinal cortex shows a progressively greater dominance of inhibition over excitation from deep to superficial layers. PLoS One 9:e85125.
Greenhill SD, Jones RSG (2007) Simultaneous estimation of global background synaptic inhibition and excitation from membrane potential fluctuations in layer III neurons of the rat entorhinal cortex in vitro. Neuroscience 147:884–892 Available at: http://www.sciencedirect.com/science/article/pii/S0306452207006574.
Greenhill SD, Jones RSG (2010) Diverse antiepileptic drugs increase the ratio of background synaptic inhibition to excitation and decrease neuronal excitability in neurones of the rat entorhinal cortex in vitro. Neuroscience 167:456–474.
Greenhill SD, Morgan NH, Massey P V, Woodhall GL, Jones RSG (2012) Ethosuximide modifies network excitability in the rat entorhinal cortex via an increase in GABA release. Neuropharmacology 62:807–814.
Grimwood S, Le Bourdellès B, Whiting PJ (1995) Recombinant Human NMDA Homomeric NR1 Receptors Expressed in Mammalian Cells Form a High-Affinity Glycine Antagonist Binding Site. J Neurochem 64:525–530 Available at: http://dx.doi.org/10.1046/j.1471-4159.1995.64020525.x.
Guidotti A, Forchetti CM, Corda MG, Konkel D, Bennett CD, Costa E (1983) Isolation, characterization, and purification to homogeneity of an endogenous polypeptide with agonistic action on benzodiazepine receptors. Proc Natl Acad Sci U S A 80:3531–3535.
Haas KF, Macdonald RL (1999) GABAA receptor subunit gamma2 and delta subtypes confer unique kinetic properties on recombinant GABAA receptor currents in mouse fibroblasts. J Physiol 514 (Pt 1:27–45.
Hafting T, Fyhn M, Molden S, Moser M-B, Moser EI (2005) Microstructure of a spatial map in the entorhinal cortex. Nature 436:801 Available at: http://dx.doi.org/10.1038/nature03721.
Hajos N, Katona I, Naiem SS, MacKie K, Ledent C, Mody I, Freund TF (2000) Cannabinoids inhibit hippocampal GABAergic transmission and network oscillations. Eur J Neurosci 12:3239–3249.
Hajos N, Ledent C, Freund TF (2001) Novel cannabinoid-sensitive receptor mediates inhibition of glutamatergic synaptic transmission in the hippocampus. Neuroscience 106:1–4.
Hajos N, Palhalmi J, Mann EO, Nemeth B, Paulsen O, Freund TF (2004) Spike timing of distinct types of GABAergic interneuron during hippocampal gamma oscillations in vitro. J Neurosci 24:9127–9137.
Hajos N, Paulsen O (2009) Network mechanisms of gamma oscillations in the CA3 region of the hippocampus. Neural Networks 22:1113–1119.
Halgren E, Babb TL, Crandall PH (1977) Responses of human limbic neurons to induced changes in blood gases. Brain Res 132:43–63.

Hamam BN, Amaral DG, Alonso AA (2002) Morphological and electrophysiological characteristics of layer V neurons of the rat lateral entorhinal cortex. J Comp Neurol 451:45–61.
Hamam BN, Kennedy TE, Alonso A, Amaral DG (2000) Morphological and electrophysiological characteristics of layer V neurons of the rat medial entorhinal cortex. J Comp Neurol 418:457–472.
Hamilton SE, Loose MD, Qi M, Levey AI, Hille B, McKnight GS, Idzerda RL, Nathanson NM (1997) Disruption of the m1 receptor gene ablates muscarinic receptor-dependent M current regulation and seizure activity in mice. Proc Natl Acad Sci U S A 94:13311–13316.
Hamon B, Heinemann U (1988) Developmental changes in neuronal sensitivity to excitatory amino acids in area CA1 of the rat hippocampus. Brain Res 466:286–290.
Hand KS, Baird VH, Van Paesschen W, Koepp MJ, Revesz T, Thom M, Harkness WF, Duncan JS, Bowery NG (1997) Central benzodiazepine receptor autoradiography in hippocampal sclerosis. Br J Pharmacol 122:358–364.
Hanson SM, Czajkowski C (2008) Structural Mechanisms Underlying Benzodiazepine Modulation of the GABA_A Receptor. J Neurosci 28:3490 LP-3499 Available at: http://www.jneurosci.org/content/28/13/3490.abstract.
Harsch A, Robinson HP (2000) Postsynaptic variability of firing in rat cortical neurons: the roles of input synchronization and synaptic NMDA receptor conductance. J Neurosci 20:6181–6192.
Hasselmo ME, Eichenbaum H (2005) Hippocampal mechanisms for the context-dependent retrieval of episodes. Neural Netw 18:1172–1190.
Hausser M, Clark BA (1997) Tonic synaptic inhibition modulates neuronal output pattern and spatiotemporal synaptic integration. Neuron 19:665–678.
Hayakawa K, Mishima K, Hazekawa M, Sano K, Irie K, Orito K, Egawa T, Kitamura Y, Uchida N, Nishimura R, Egashira N, Iwasaki K, Fujiwara M (2008) Cannabidiol potentiates pharmacological effects of Delta(9)-tetrahydrocannabinol via CB(1) receptor-dependent mechanism. Brain Res 1188:157–164.
Hayakawa K, Mishima K, Nozako M, Ogata A, Hazekawa M, Liu A-X, Fujioka M, Abe K, Hasebe N, Egashira N, Iwasaki K, Fujiwara M (2007) Repeated treatment with cannabidiol but not Delta9-tetrahydrocannabinol has a neuroprotective effect without the development of tolerance. Neuropharmacology 52:1079–1087.
Headley DB, Paré D (2017) Common oscillatory mechanisms across multiple memory systems. npj Sci Learn 2:1 Available at: https://doi.org/10.1038/s41539-016-0001-2.
Hendry SH, Jones EG, Emson PC, Lawson DE, Heizmann CW, Streit P (1989) Two classes of cortical GABA neurons defined by differential calcium binding protein immunoreactivities. Exp brain Res 76:467–472.
Henson MA, Roberts AC, Pérez-Otaño I, Philpot BD (2010) Influence of the NR3A subunit on NMDA receptor functions. Prog Neurobiol 91:23–37 Available at: http://www.ncbi.nlm.nih.gov/pmc/articles/PMC2883719/.
Herkenham M, Lynn AB, Johnson MR, Melvin LS, de Costa BR, Rice KC (1991) Characterization and localization of cannabinoid receptors in rat brain: a quantitative in vitro autoradiographic study. J Neurosci 11:563–583.
Herkenham M, Lynn AB, Little MD, Johnson MR, Melvin LS, de Costa BR, Rice KC (1990) Cannabinoid receptor localization in brain. Proc Natl Acad Sci U S A 87:1932–1936.
Hill AJ, Mercier MS, Hill TD, Glyn SE, Jones NA, Yamasaki Y, Futamura T, Duncan M, Stott CG, Stephens GJ, Williams CM, Whalley BJ (2012) Cannabidivarin is anticonvulsant in mouse and rat. Br J Pharmacol 167:1629–1642.
Hill TDM, Cascio MG, Romano B, Duncan M, Pertwee RG, Williams CM, Whalley BJ, Hill a. J (2013) Cannabidivarin-rich cannabis extracts are anticonvulsant in mouse and rat via a CB1 receptor-independent mechanism. Br J Pharmacol 170:679–692.
Hirai H, Kirsch J, Laube B, Betz H, Kuhse J (1996) The glycine binding site of the N-methyl-D-aspartate receptor subunit NR1: identification of novel determinants of co-agonist potentiation in the extracellular M3-M4 loop region. Proc Natl Acad Sci U S A 93:6031–6036.
Ho N, Destexhe A (2000) Synaptic background activity enhances the responsiveness of neocortical pyramidal neurons. J Neurophysiol 84:1488–1496.
Hoffman SN, Prince DA (1995) Epileptogenesis in immature neocortical slices induced by 4-

aminopyridine. Brain Res Dev Brain Res 85:64–70.
Hollmann M, Boulter J, Maron C, Beasley L, Sullivan J, Pecht G, Heinemann S (1993) Zinc potentiates agonist-induced currents at certain splice variants of the NMDA receptor. Neuron 10:943–954.
Hollmann M, Hartley M, Heinemann S (1991) Ca2+ permeability of KA-AMPA--gated glutamate receptor channels depends on subunit composition. Science 252:851–853.
Hollrigel GS, Soltesz I (1997) Slow kinetics of miniature IPSCs during early postnatal development in granule cells of the dentate gyrus. J Neurosci 17:5119–5128.
Hopper MW, Vogel FS (1976) The limbic system in Alzheimer's disease. A neuropathologic investigation. Am J Pathol 85:1–20 Available at: http://www.ncbi.nlm.nih.gov/pmc/articles/PMC2032549/.
Horenstein J, Wagner DA, Czajkowski C, Akabas MH (2001) Protein mobility and GABA-induced conformational changes in GABA(A) receptor pore-lining M2 segment. Nat Neurosci 4:477–485.
Hosie AM, Clarke L, da Silva H, Smart TG (2009) Conserved site for neurosteroid modulation of GABA A receptors. Neuropharmacology 56:149–154.
Hosie AM, Wilkins ME, da Silva HMA, Smart TG (2006) Endogenous neurosteroids regulate GABAA receptors through two discrete transmembrane sites. Nature 444:486–489.
Howlett AC (1987) Cannabinoid inhibition of adenylate cyclase: relative activity of constituents and metabolites of marihuana. Neuropharmacology 26:507–512.
Howlett AC (1998) The CB1 cannabinoid receptor in the brain. Neurobiol Dis 5:405–416.
Howlett AC (2002) The cannabinoid receptors. Prostaglandins Other Lipid Mediat 68–69:619–631.
Howlett AC (2004) Efficacy in CB1 receptor-mediated signal transduction. Br J Pharmacol 142:1209–1218.
Howlett AC (2005) Cannabinoid receptor signaling. Handb Exp Pharmacol:53–79.
Howlett AC, Barth F, Bonner TI, Cabral G, Casellas P, Devane WA, Felder CC, Herkenham M, Mackie K, Martin BR, Mechoulam R, Pertwee RG (2002) International Union of Pharmacology. XXVII. Classification of cannabinoid receptors. Pharmacol Rev 54:161–202.
Howlett AC, Fleming RM (1984) Cannabinoid inhibition of adenylate cyclase. Pharmacology of the response in neuroblastoma cell membranes. Mol Pharmacol 26:532–538.
Howlett AC, Qualy JM, Khachatrian LL (1986) Involvement of Gi in the inhibition of adenylate cyclase by cannabimimetic drugs. Mol Pharmacol 29:307–313.
Hubbard J, Llinas R, Quastel D (1969) Electrophysiological Analysis of Synaptic Transmission. London.
Hume RI, Dingledine R, Heinemann SF (1991) Identification of a site in glutamate receptor subunits that controls calcium permeability. Science 253:1028–1031.
Hunkeler W, Mohler H, Pieri L, Polc P, Bonetti EP, Cumin R, Schaffner R, Haefely W (1981) Selective antagonists of benzodiazepines. Nature 290:514–516.
Ibeas Bih C, Chen T, Nunn AVW, Bazelot M, Dallas M, Whalley BJ (2015) Molecular Targets of Cannabidiol in Neurological Disorders. Neurotherapeutics 12:699–730.
Iijima T, Witter MP, Ichikawa M, Tominaga T, Kajiwara R, Matsumoto G (1996) Entorhinal-hippocampal interactions revealed by real-time imaging. Science 272:1176–1179.
Inada H, Maejima T, Nakahata Y, Yamaguchi J, Nabekura J, Ishibashi H (2010) Endocannabinoids contribute to metabotropic glutamate receptor-mediated inhibition of GABA release onto hippocampal CA3 pyramidal neurons in an isolated neuron/bouton preparation. Neuroscience 165:1377–1389 Available at: http://www.sciencedirect.com/science/article/pii/S0306452209019654.
Irving AJ, Coutts AA, Harvey J, Rae MG, Mackie K, Bewick GS, Pertwee RG (2000) Functional expression of cell surface cannabinoid CB(1) receptors on presynaptic inhibitory terminals in cultured rat hippocampal neurons. Neuroscience 98:253–262.
Ishizuka N, Weber J, Amaral DG (1990) Organization of intrahippocampal projections originating from CA3 pyramidal cells in the rat. J Comp Neurol 295:580–623 Available at: http://dx.doi.org/10.1002/cne.902950407.
Iversen L (1977) Anti-anxiety receptors in the brain? Nature 266:678 Available at: http://dx.doi.org/10.1038/266678a0.
Jackson J, Goutagny R, Williams S (2011) Fast and Slow Gamma Rhythms Are Intrinsically and Independently Generated in the Subiculum. J Neurosci 31:12104 LP-12117

Available at: http://www.jneurosci.org/content/31/34/12104.abstract.
Jane DE, Lodge D, Collingridge GL (2009) Kainate receptors: pharmacology, function and therapeutic potential. Neuropharmacology 56:90–113.
Johnston GA (1996) GABAc receptors: relatively simple transmitter -gated ion channels? Trends Pharmacol Sci 17:319–323.
Jones KA et al. (1998) GABA(B) receptors function as a heteromeric assembly of the subunits GABA(B)R1 and GABA(B)R2. Nature 396:674–679.
Jones NA, Glyn SE, Akiyama S, Hill TD, Hill AJ, Weston SE, Burnett MD, Yamasaki Y, Stephens GJ, Whalley BJ, Williams CM (2012) Cannabidiol exerts anti-convulsant effects in animal models of temporal lobe and partial seizures. Seizure 21:344–352.
Jones NA, Hill AJ, Smith I, Bevan SA, Williams CM, Whalley BJ, Stephens GJ (2010) Cannabidiol displays antiepileptiform and antiseizure properties in vitro and in vivo. J Pharmacol Exp Ther 332:569–577.
Jones RS (1996) Short- and long-term alterations in glutamate transmission in the entorhinal cortex: relevance to epileptogenesis. Epilepsy Res Suppl 12:229–237.
Jones RS, Buhl EH (1993) Basket-like interneurones in layer II of the entorhinal cortex exhibit a powerful NMDA-mediated synaptic excitation. Neurosci Lett 149:35–39.
Jones RS, Heinemann U (1989) Spontaneous activity mediated by NMDA receptors in immature rat entorhinal cortex in vitro. Neurosci Lett 104:93–98.
Jones RS, Lambert JD (1990a) The role of excitatory amino acid receptors in the propagation of epileptiform discharges from the entorhinal cortex to the dentate gyrus in vitro. Exp brain Res 80:310–322.
Jones RS, Lambert JD (1990b) Synchronous discharges in the rat entorhinal cortex in vitro: site of initiation and the role of excitatory amino acid receptors. Neuroscience 34:657–670.
Jones RSG, Woodhall GL (2005) Background synaptic activity in rat entorhinal cortical neurones: differential control of transmitter release by presynaptic receptors. J Physiol 562:107–120.
Kabat J, Krol P (2012) Focal cortical dysplasia - review. Polish J Radiol 77:35–43.
Kajiwara R, Takashima I, Mimura Y, Witter MP, Iijima T (2003) Amygdala input promotes spread of excitatory neural activity from perirhinal cortex to the entorhinal-hippocampal circuit. J Neurophysiol 89:2176–2184.
Kallarackal AJ, Kvarta MD, Cammarata E, Jaberi L, Cai X, Bailey AM, Thompson SM (2013) Chronic stress induces a selective decrease in AMPA receptor-mediated synaptic excitation at hippocampal temporoammonic-CA1 synapses. J Neurosci 33:15669–15674.
Kapur A, Zhao P, Sharir H, Bai Y, Caron MG, Barak LS, Abood ME (2009) Atypical responsiveness of the orphan receptor GPR55 to cannabinoid ligands. J Biol Chem 284:29817–29827.
Kash TL, Dizon M-JF, Trudell JR, Harrison NL (2004) Charged residues in the beta2 subunit involved in GABAA receptor activation. J Biol Chem 279:4887–4893.
Kash TL, Jenkins A, Kelley JC, Trudell JR, Harrison NL (2003) Coupling of agonist binding to channel gating in the GABA(A) receptor. Nature 421:272–275.
Kathmann M, Flau K, Redmer A, Trankle C, Schlicker E (2006) Cannabidiol is an allosteric modulator at mu- and delta-opioid receptors. Naunyn Schmiedebergs Arch Pharmacol 372:354–361.
Katona I, Freund TF (2012) Multiple functions of endocannabinoid signaling in the brain. Annu Rev Neurosci 35:529–558.
Katona I, Sperlagh B, Sik A, Kafalvi A, Vizi ES, Mackie K, Freund TF (1999) Presynaptically located CB1 cannabinoid receptors regulate GABA release from axon terminals of specific hippocampal interneurons. J Neurosci 19:4544–4558.
Katona I, Urbán GM, Wallace M, Ledent C, Jung K-M, Piomelli D, Mackie K, Freund TF (2006) Molecular Composition of the Endocannabinoid System at Glutamatergic Synapses. J Neurosci 26:5628–5637 Available at: http://www.ncbi.nlm.nih.gov/pmc/articles/PMC1698282/.
Kaupmann K, Huggel K, Heid J, Flor PJ, Bischoff S, Mickel SJ, McMaster G, Angst C, Bittiger H, Froestl W, Bettler B (1997) Expression cloning of GABA(B) receptors uncovers similarity to metabotropic glutamate receptors. Nature 386:239–246.
Kaupmann K, Malitschek B, Schuler V, Heid J, Froestl W, Beck P, Mosbacher J, Bischoff S,

Kulik A, Shigemoto R, Karschin A, Bettler B (1998) GABA(B)-receptor subtypes assemble into functional heteromeric complexes. Nature 396:683–687.
Kavaliers M, Hirst M (1986) An octadecaneuropeptide (ODN) derived from diazepam binding inhibitor increases aggressive interactions in mice. Brain Res 383:343–349.
Kawahara Y, Ito K, Sun H, Kanazawa I, Kwak S (2003) Low editing efficiency of GluR2 mRNA is associated with a low relative abundance of ADAR2 mRNA in white matter of normal human brain. Eur J Neurosci 18:23–33.
Kawamura Y, Fukaya M, Maejima T, Yoshida T, Miura E, Watanabe M, Ohno-Shosaku T, Kano M (2006) The CB1 cannabinoid receptor is the major cannabinoid receptor at excitatory presynaptic sites in the hippocampus and cerebellum. J Neurosci 26:2991–3001.
Kirischuk S, Akyeli J, Iosub R, Grantyn R (2003) Pre- and postsynaptic contribution of GABAC receptors to GABAergic synaptic transmission in rat collicular slices and cultures. Eur J Neurosci 18:752–758.
Kittler JT, Moss SJ (2003) Modulation of GABAA receptor activity by phosphorylation and receptor trafficking: implications for the efficacy of synaptic inhibition. Curr Opin Neurobiol 13:341–347.
Kleckner NW, Dingledine R (1991) Regulation of hippocampal NMDA receptors by magnesium and glycine during development. Brain Res Mol Brain Res 11:151–159.
Klink R, Alonso A (1997) Morphological characteristics of layer II projection neurons in the rat medial entorhinal cortex. Hippocampus 7:571–583 Available at: http://dx.doi.org/10.1002/(SICI)1098-1063(1997)7:5%3C571::AID-HIPO12%3E3.0.CO.
Kloosterman F, Van Haeften T, Witter MP, Lopes Da Silva FH (2003) Electrophysiological characterization of interlaminar entorhinal connections: an essential link for re-entrance in the hippocampal-entorhinal system. Eur J Neurosci 18:3037–3052.
Koepp MJ, Richardson MP, Labbe C, Brooks DJ, Cunningham VJ, Ashburner J, Van Paesschen W, Revesz T, Duncan JS (1997) 11C-flumazenil PET, volumetric MRI, and quantitative pathology in mesial temporal lobe epilepsy. Neurology 49:764–773.
Köfalvi A (2008) Cannabinoids and the Brain. New York City: Axel Springer AG.
Kohler C (1986) Intrinsic connections of the retrohippocampal region in the rat brain. II. The medial entorhinal area. J Comp Neurol 246:149–169.
Kohler C (1988) Intrinsic connections of the retrohippocampal region in the rat brain: III. The lateral entorhinal area. J Comp Neurol 271:208–228.
Kohler C, Chan-Palay V (1983) Somatostatin and vasoactive intestinal polypeptide-like immunoreactive cells and terminals in the retrohippocampal region of the rat brain. Anat Embryol (Berl) 167:151–172.
Kohler C, Eriksson L, Davies S, Chan-Palay V (1986) Neuropeptide Y innervation of the hippocampal region in the rat and monkey brain. J Comp Neurol 244:384–400.
Kohler C, Wu JY, Chan-Palay V (1985) Neurons and terminals in the retrohippocampal region in the rat's brain identified by anti-gamma-aminobutyric acid and anti-glutamic acid decarboxylase immunocytochemistry. Anat Embryol (Berl) 173:35–44.
Kopell N, Ermentrout B (2004) Chemical and electrical synapses perform complementary roles in the synchronization of interneuronal networks. Proc Natl Acad Sci U S A 101:15482–15487.
Kopell N, Ermentrout GB, Whittington MA, Traub RD (2000) Gamma rhythms and beta rhythms have different synchronization properties. Proc Natl Acad Sci U S A 97:1867–1872.
Kovacs FE, Knop T, Urbanski MJ, Freiman I, Freiman TM, Feuerstein TJ, Zentner J, Szabo B (2012) Exogenous and endogenous cannabinoids suppress inhibitory neurotransmission in the human neocortex. Neuropsychopharmacology 37:1104–1114.
Kreitzer AC, Regehr WG (2001) Retrograde inhibition of presynaptic calcium influx by endogenous cannabinoids at excitatory synapses onto Purkinje cells. Neuron 29:717–727.
Kriegstein AR, Suppes T, Prince DA (1987) Cellular and synaptic physiology and epileptogenesis of developing rat neocortical neurons in vitro. Brain Res 431:161–171.
Kumar SS, Buckmaster PS (2006) Hyperexcitability, interneurons, and loss of GABAergic synapses in entorhinal cortex in a model of temporal lobe epilepsy. J Neurosci 26:4613–4623.
Kunos G, Osei-Hyiaman D, Batkai S, Sharkey KA, Makriyannis A (2009) Should peripheral

CB(1) cannabinoid receptors be selectively targeted for therapeutic gain? Trends Pharmacol Sci 30:1–7.
Kuver A, Smith SS (2016) Flumazenil decreases surface expression of alpha4beta2delta GABAA receptors by increasing the rate of receptor internalization. Brain Res Bull 120:131–143.
Kwak S, Hideyama T, Yamashita T, Aizawa H (2010) AMPA receptor-mediated neuronal death in sporadic ALS. Neuropathology 30:182–188.
Kwak S, Kawahara Y (2005) Deficient RNA editing of GluR2 and neuronal death in amyotropic lateral sclerosis. J Mol Med (Berl) 83:110–120.
Kwak S, Weiss JH (2006) Calcium-permeable AMPA channels in neurodegenerative disease and ischemia. Curr Opin Neurobiol 16:281–287.
Kwan P, Arzimanoglou A, Berg AT, Brodie MJ, Allen Hauser W, Mathern G, Moshé SL, Perucca E, Wiebe S, French J (2010) Definition of drug resistant epilepsy: Consensus proposal by the ad hoc Task Force of the ILAE Commission on Therapeutic Strategies. Epilepsia 51:1069–1077 Available at: http://dx.doi.org/10.1111/j.1528-1167.2009.02397.x.
Kwan P, Schachter SC, Brodie MJ (2011) Drug-resistant epilepsy. N Engl J Med 365:919–926.
Lakatos P, Shah AS, Knuth KH, Ulbert I, Karmos G, Schroeder CE (2005) An oscillatory hierarchy controlling neuronal excitability and stimulus processing in the auditory cortex. J Neurophysiol 94:1904–1911.
Lambert JJ, Belelli D, Peden DR, Vardy AW, Peters JA (2003) Neurosteroid modulation of GABAA receptors. Prog Neurobiol 71:67–80.
Lancaster B, Wheal H V (1982) A comparative histological and electrophysiological study of some neurotoxins in the rat hippocampus. J Comp Neurol 211:105–114.
Laprairie RB, Bagher AM, Kelly MEM, Denovan-Wright EM (2015) Cannabidiol is a negative allosteric modulator of the cannabinoid CB1 receptor. Br J Pharmacol 172:4790–4805 Available at: http://dx.doi.org/10.1111/bph.13250.
Lau CG, Zukin RS (2007) NMDA receptor trafficking in synaptic plasticity and neuropsychiatric disorders. Nat Rev Neurosci 8:413–426.
Laube B, Hirai H, Sturgess M, Betz H, Kuhse J (1997) Molecular determinants of agonist discrimination by NMDA receptor subunits: analysis of the glutamate binding site on the NR2B subunit. Neuron 18:493–503.
Lauckner JE, Hille B, Mackie K (2005) The cannabinoid agonist WIN55,212-2 increases intracellular calcium via CB1 receptor coupling to Gq/11 G proteins. Proc Natl Acad Sci U S A 102:19144–19149.
Lauckner JE, Jensen JB, Chen H-Y, Lu H-C, Hille B, Mackie K (2008) GPR55 is a cannabinoid receptor that increases intracellular calcium and inhibits M current. Proc Natl Acad Sci U S A 105:2699–2704.
Lavoie AM, Twyman RE (1996) Direct evidence for diazepam modulation of GABAA receptor microscopic affinity. Neuropharmacology 35:1383–1392.
Lee T-S, Mane S, Eid T, Zhao H, Lin A, Guan Z, Kim JH, Schweitzer J, King-Stevens D, Weber P, Spencer SS, Spencer DD, de Lanerolle NC (2007) Gene expression in temporal lobe epilepsy is consistent with increased release of glutamate by astrocytes. Mol Med 13:1–13.
Leonardi M, Ustun TB (2002) The global burden of epilepsy. Epilepsia 43 Suppl 6:21–25.
Leroy C, Poisbeau P, Keller AF, Nehlig A (2004) Pharmacological plasticity of GABA(A) receptors at dentate gyrus synapses in a rat model of temporal lobe epilepsy. J Physiol 557:473–487.
Leung LS (1982) Nonlinear feedback model of neuronal populations in hippocampal CAl region. J Neurophysiol 47:845–868.
Levesque M, Avoli M (2013) The kainic acid model of temporal lobe epilepsy. Neurosci Biobehav Rev 37:2887–2899.
Lévi S, Le Roux N, Eugène E, Poncer JC (2015) Benzodiazepine ligands rapidly influence GABAA receptor diffusion and clustering at hippocampal inhibitory synapses. Neuropharmacology 88:199–208 Available at: http://www.sciencedirect.com/science/article/pii/S002839081400224X.
Li G-D, Chiara DC, Cohen JB, Olsen RW (2009) Neurosteroids allosterically modulate binding of the anesthetic etomidate to gamma-aminobutyric acid type A receptors. J Biol

Chem 284:11771–11775.
Lim C, Blume HW, Madsen JR, Saper CB (1997) Connections of the hippocampal formation in humans: I. The mossy fiber pathway. J Comp Neurol 385:325–351.
Lind GE, Mou T-C, Tamborini L, Pomper MG, De Micheli C, Conti P, Pinto A, Hansen KB (2017) Structural basis of subunit selectivity for competitive NMDA receptor antagonists with preference for GluN2A over GluN2B subunits. Proc Natl Acad Sci 114:E6942 LP-E6951 Available at: http://www.pnas.org/content/114/33/E6942.abstract.
Lingenhohl K, Finch DM (1991) Morphological characterization of rat entorhinal neurons in vivo: soma-dendritic structure and axonal domains. Exp brain Res 84:57–74.
Lisman J (2012) Excitation, inhibition, local oscillations, or large-scale loops: what causes the symptoms of schizophrenia? Curr Opin Neurobiol 22:537–544.
Lisman JE, Jensen O (2013) The Theta-Gamma Neural Code. Neuron 77:1002–1016.
Lisman JE, Otmakhova NA (2001) Storage, recall, and novelty detection of sequences by the hippocampus: elaborating on the SOCRATIC model to account for normal and aberrant effects of dopamine. Hippocampus 11:551–568.
Liu L, Wong TP, Pozza MF, Lingenhoehl K, Wang Y, Sheng M, Auberson YP, Wang YT (2004) Role of NMDA receptor subtypes in governing the direction of hippocampal synaptic plasticity. Science 304:1021–1024.
Liu SJ, Zukin RS (2007) Ca2+-permeable AMPA receptors in synaptic plasticity and neuronal death. Trends Neurosci 30:126–134.
Llano I, Leresche N, Marty A (1991) Calcium entry increases the sensitivity of cerebellar Purkinje cells to applied GABA and decreases inhibitory synaptic currents. Neuron 6:565–574 Available at: http://www.sciencedirect.com/science/article/pii/0896627391900599.
Llinas R, Ribary U, Contreras D, Pedroarena C (1998) The neuronal basis for consciousness. Philos Trans R Soc L B Biol Sci 353:1841–1849.
Lomo T (1971) Patterns of activation in a monosynaptic cortical pathway: the perforant path input to the dentate area of the hippocampal formation. Exp brain Res 12:18–45.
Lorente de Nó R (1933) Anatomy of the eighth nerve. The central projection of the nerve endings of the internal ear. Laryngoscope 43:1–38.
Lorgen J-O, Egbenya DL, Hammer J, Davanger S (2017) PICK1 facilitates lasting reduction in GluA2 concentration in the hippocampus during chronic epilepsy. Epilepsy Res 137:25–32.
Lothman EW, Bertram EH, Kapur J, Stringer JL (1990) Recurrent spontaneous hippocampal seizures in the rat as a chronic sequela to limbic status epilepticus. Epilepsy Res 6:110–118 Available at: http://www.sciencedirect.com/science/article/pii/092012119090085A.
Lu W, Shi Y, Jackson AC, Bjorgan K, During MJ, Sprengel R, Seeburg PH, Nicoll RA (2009) Subunit composition of synaptic AMPA receptors revealed by a single-cell genetic approach. Neuron 62:254–268 Available at: http://www.ncbi.nlm.nih.gov/pmc/articles/PMC3632349/.
Luchicchi A, Pistis M (2012) Anandamide and 2-arachidonoylglycerol: pharmacological properties, functional features, and emerging specificities of the two major endocannabinoids. Mol Neurobiol 46:374–392.
Luhmann HJ, Prince DA (1990a) Control of NMDA receptor-mediated activity by GABAergic mechanisms in mature and developing rat neocortex. Brain Res Dev Brain Res 54:287–290.
Luhmann HJ, Prince DA (1990b) Transient expression of polysynaptic NMDA receptor-mediated activity during neocortical development. Neurosci Lett 111:109–115.
Lüscher C, Jan LY, Stoffel M, Malenka RC, Nicoll RA (1997) G Protein-Coupled Inwardly Rectifying K+ Channels (GIRKs) Mediate Postsynaptic but Not Presynaptic Transmitter Actions in Hippocampal Neurons. Neuron 19:687–695 Available at: http://www.sciencedirect.com/science/article/pii/S0896627300803815.
Maitra R, Reynolds JN (1999) Subunit dependent modulation of GABAA receptor function by neuroactive steroids. Brain Res 819:75–82.
Maksay G, Thompson SA, Wafford KA (2000) Allosteric modulators affect the efficacy of partial agonists for recombinant GABA(A) receptors. Br J Pharmacol 129:1794–1800.
Mann EO, Mody I (2010) Control of hippocampal gamma oscillation frequency by tonic inhibition and excitation of interneurons. Nat Neurosci 13:205–212.
Mann EO, Suckling JM, Hajos N, Greenfield SA, Paulsen O (2005) Perisomatic feedback

inhibition underlies cholinergically induced fast network oscillations in the rat hippocampus in vitro. Neuron 45:105–117.
Margineanu DG (2012) Systems biology impact on antiepileptic drug discovery. Epilepsy Res 98:104–115.
Marinelli S, Pacioni S, Bisogno T, Di Marzo V, Prince DA, Huguenard JR, Bacci A (2008) The endocannabinoid 2-arachidonoylglycerol is responsible for the slow self-inhibition in neocortical interneurons. J Neurosci 28:13532–13541.
Marks MD, Tian L, Wenger JP, Omburo SN, Soto-Fuentes W, He J, Gang DR, Weiblen GD, Dixon RA (2009) Identification of candidate genes affecting Δ(9)-tetrahydrocannabinol biosynthesis in Cannabis sativa. J Exp Bot 60:3715–3726 Available at: http://www.ncbi.nlm.nih.gov/pmc/articles/PMC2736886/.
Martin LJ, Blackstone CD, Levey AI, Huganir RL, Price DL (1993) AMPA glutamate receptor subunits are differentially distributed in rat brain. Neuroscience 53:327–358.
Massi P, Valenti M, Vaccani A, Gasperi V, Perletti G, Marras E, Fezza F, Maccarrone M, Parolaro D (2008) 5-Lipoxygenase and anandamide hydrolase (FAAH) mediate the antitumor activity of cannabidiol, a non-psychoactive cannabinoid. J Neurochem 104:1091–1100.
Mathern GW, Babb TL, Vickrey BG, Melendez M, Pretorius JK (1995) The clinical-pathogenic mechanisms of hippocampal neuron loss and surgical outcomes in temporal lobe epilepsy. Brain 118 (Pt 1:105–118.
Matsuda L a, Lolait SJ, Brownstein MJ, Young a C, Bonner TI (1990) Structure of a cannabinoid receptor and functional expression of the cloned cDNA. Nature 346:561–564.
Mattson MP, Lee RE, Adams ME, Guthrie PB, Kater SB (1988) Interactions between entorhinal axons and target hippocampal neurons: a role for glutamate in the development of hippocampal circuitry. Neuron 1:865–876.
McBain CJ, Mayer ML (1994) N-methyl-D-aspartic acid receptor structure and function. Physiol Rev 74:723–760.
McHugh D, Page J, Dunn E, Bradshaw HB (2012a) Delta(9) -Tetrahydrocannabinol and N-arachidonyl glycine are full agonists at GPR18 receptors and induce migration in human endometrial HEC-1B cells. Br J Pharmacol 165:2414–2424.
McHugh D, Wager-Miller J, Page J, Bradshaw HB (2012b) siRNA knockdown of GPR18 receptors in BV-2 microglia attenuates N-arachidonoyl glycine-induced cell migration. J Mol Signal 7:10.
McIntyre DC, Gilby KL (2006) Parahippocampal networks, intractability, and the chronic epilepsy of kindling. Adv Neurol 97:77–83.
McIntyre DC, Nathanson D, Edson N (1982) A new model of partial status epilepticus based on kindling. Brain Res 250:53–63.
McNaughton BL, Barnes CA (1977) Physiological identification and analysis of dentate granule cell responses to stimulation of the medial and lateral perforant pathways in the rat. J Comp Neurol 175:439–453 Available at: http://dx.doi.org/10.1002/cne.901750404.
McPartland JM, Duncan M, Di Marzo V, Pertwee RG (2015) Are cannabidiol and Δ(9)-tetrahydrocannabivarin negative modulators of the endocannabinoid system? A systematic review. Br J Pharmacol 172:737–753 Available at: http://www.ncbi.nlm.nih.gov/pmc/articles/PMC4301686/.
Mechoulam R (1986) The pharmacohistory of Cannabis sativa. (Mechoulam R, ed). Boca Raton, FL: CRC Press.
Mechoulam R, Ben-Shabat S, Hanus L, Ligumsky M, Kaminski NE, Schatz AR, Gopher A, Almog S, Martin BR, Compton DR, al. et (1995) Identification of an endogenous 2-monoglyceride, present in canine gut, that binds to cannabinoid receptors. Biochem Pharmacol 50:83–90.
Mechoulam R, Hanus L (2000) A historical overview of chemical research on cannabinoids. Chem Phys Lipids 108:1–13.
Mechoulam R, Hanuš LO, Pertwee R, Howlett AC (2014) Early phytocannabinoid chemistry to endocannabinoids and beyond. Nat Rev Neurosci 15:757–764 Available at: http://www.nature.com/doifinder/10.1038/nrn3811.
Mechoulam R, Peters M, Murillo-rodriguez E, Hanus LO (2007) Cannabidiol – Recent Advances. 4:1678–1692.
Meguro H, Mori H, Araki K, Kushiya E, Kutsuwada T, Yamazaki M, Kumanishi T, Arakawa M,

Sakimura K, Mishina M (1992) Functional characterization of a heteromeric NMDA receptor channel expressed from cloned cDNAs. Nature 357:70–74.
Meldrum BS (2000) Glutamate as a neurotransmitter in the brain: review of physiology and pathology. J Nutr 130:1007S–15S.
Meldrum BS, Rogawski MA (2007) Molecular targets for antiepileptic drug development. Neurotherapeutics 4:18–61.
Mercer A, Trigg HL, Thomson AM (2007) Characterization of neurons in the CA2 subfield of the adult rat hippocampus. J Neurosci 27:7329–7338.
Meyer AH, Katona I, Blatow M, Rozov A, Monyer H (2002) In vivo labeling of parvalbumin-positive interneurons and analysis of electrical coupling in identified neurons. J Neurosci 22:7055–7064.
Michelson HB, Kapur J, Lothman EW (1989) Reduction of paired pulse inhibition in the CA1 region of the hippocampus by pilocarpine in naive and in amygdala-kindled rats. Exp Neurol 104:264–271.
Miettinen M, Pitkanen A, Miettinen R (1997) Distribution of calretinin-immunoreactivity in the rat entorhinal cortex: coexistence with GABA. J Comp Neurol 378:363–378.
Miles R, Wong RK (1986) Excitatory synaptic interactions between CA3 neurones in the guinea-pig hippocampus. J Physiol 373:397–418.
Milgram NW, Michael M, Cammisuli S, Head E, Ferbinteanu J, Reid C, Murphy MP, Racine R (1995) Development of spontaneous seizures over extended electrical kindling. II. Persistence of dentate inhibitory suppression. Brain Res 670:112–120.
Mintz IM, Bean BP (1993) GABAB receptor inhibition of P-type Ca2+ channels in central neurons. Neuron 10:889–898.
Mishima K, Hayakawa K, Abe K, Ikeda T, Egashira N, Iwasaki K, Fujiwara M (2005) Cannabidiol prevents cerebral infarction via a serotonergic 5-hydroxytryptamine1A receptor-dependent mechanism. Stroke 36:1077–1082.
Mishina M, Mori H, Araki K, Kushiya E, Meguro H, Kutsuwada T, Kashiwabuchi N, Ikeda K, Nagasawa M, Yamazaki M (1993) Molecular and functional diversity of the NMDA receptor channel. Ann N Y Acad Sci 707:136–152.
Mitchell EA, Herd MB, Gunn BG, Lambert JJ, Belelli D (2008) Neurosteroid modulation of GABAA receptors: molecular determinants and significance in health and disease. Neurochem Int 52:588–595.
Mody I (2001) Distinguishing between GABA(A) receptors responsible for tonic and phasic conductances. Neurochem Res 26:907–913.
Mody I, De Koninck Y, Otis TS, Soltesz I (1994) Bridging the cleft at GABA synapses in the brain. Trends Neurosci 17:517–525.
Monyer H, Burnashev N, Laurie DJ, Sakmann B, Seeburg PH (1994) Developmental and regional expression in the rat brain and functional properties of four NMDA receptors. Neuron 12:529–540.
Monyer H, Seeburg PH, Wisden W (1991) Glutamate-operated channels: developmentally early and mature forms arise by alternative splicing. Neuron 6:799–810.
Monyer H, Sprengel R, Schoepfer R, Herb A, Higuchi M, Lomeli H, Burnashev N, Sakmann B, Seeburg PH (1992) Heteromeric NMDA receptors: molecular and functional distinction of subtypes. Science 256:1217–1221.
Morgan NH, Stanford IM, Woodhall GL (2009) Functional CB2 type cannabinoid receptors at CNS synapses. Neuropharmacology 57:356–368 Available at: http://dx.doi.org/10.1016/j.neuropharm.2009.07.017.
Mori H, Mishina M (1995) Structure and function of the NMDA receptor channel. Neuropharmacology 34:1219–1237.
Moriconi A, Cerbara I, Maccarrone M, Topai A (2010) GPR55: Current knowledge and future perspectives of a purported “Type-3” cannabinoid receptor. Curr Med Chem 17:1411–1429.
Morimoto K, Fahnestock M, Racine RJ (2004) Kindling and status epilepticus models of epilepsy: Rewiring the brain. Prog Neurobiol 73:1–60.
Morishita W, Lu W, Smith GB, Nicoll RA, Bear MF, Malenka RC (2007) Activation of NR2B-containing NMDA receptors is not required for NMDA receptor-dependent long-term depression. Neuropharmacology 52:71–76.
Moriyoshi K, Masu M, Ishii T, Shigemoto R, Mizuno N, Nakanishi S (1991) Molecular cloning and characterization of the rat NMDA receptor. Nature 354:31–37.

Moser EI, Roudi Y, Witter MP, Kentros C, Bonhoeffer T, Moser M-B (2014) Grid cells and cortical representation. Nat Rev Neurosci 15:466 Available at: http://dx.doi.org/10.1038/nrn3766.
Moser VC, McCormick JP, Creason JP, MacPhail RC (1988) Comparison of chlordimeform and carbaryl using a functional observational battery. Fundam Appl Toxicol 11:189–206.
Munro S, Thomas KL, Abu-Shaar M (1993) Molecular characterization of a peripheral receptor for cannabinoids. Nature 365:61–65.
Murakami S, Zhang T, Hirose A, Okada YC (2002) Physiological origins of evoked magnetic fields and extracellular field potentials produced by guinea-pig CA3 hippocampal slices. J Physiol 544:237–251.
Nadler J V, Perry BW, Cotman CW (1978) Intraventricular kainic acid preferentially destroys hippocampal pyramidal cells. Nature 271:676–677.
Nadler JV (2003) The recurrent mossy fiber pathway of the epileptic brain. Neurochem Res 28:1649–1658.
Netzeband JG, Conroy SM, Parsons KL, Gruol DL (1999) Cannabinoids enhance NMDA-elicited Ca2+ signals in cerebellar granule neurons in culture. J Neurosci 19:8765–8777.
Newell JG, Czajkowski C (2003) The GABAA receptor alpha 1 subunit Pro174-Asp191 segment is involved in GABA binding and channel gating. J Biol Chem 278:13166–13172.
Neyton J, Paoletti P (2006) Relating NMDA receptor function to receptor subunit composition: limitations of the pharmacological approach. J Neurosci 26:1331–1333.
Nishi M, Hinds H, Lu HP, Kawata M, Hayashi Y (2001) Motoneuron-specific expression of NR3B, a novel NMDA-type glutamate receptor subunit that works in a dominant-negative manner. J Neurosci 21:RC185.
Noebels JL, Jasper HH (2012) Jasper's Basic Mechanisms of the Epilepsies. Oxford University Press, USA. Available at: https://books.google.co.uk/books?id=T2_LVTB7ftgC.
O'Shea SM, Harrison NL (2000) Arg-274 and Leu-277 of the gamma-aminobutyric acid type A receptor alpha 2 subunit define agonist efficacy and potency. J Biol Chem 275:22764–22768.
Ohno-Shosaku T, Maejima T, Kano M (2001) Endogenous cannabinoids mediate retrograde signals from depolarized postsynaptic neurons to presynaptic terminals. Neuron 29:729–738.
Olsen RW, Sieghart W (2008) International Union of Pharmacology. LXX. Subtypes of γ-Aminobutyric Acid_A Receptors: Classification on the Basis of Subunit Composition, Pharmacology, and Function. Update. Pharmacol Rev 60:243 LP-260 Available at: http://pharmrev.aspetjournals.org/content/60/3/243.abstract.
Orban G, Kiss T, Lengyel M, Erdi P (2001) Hippocampal rhythm generation: gamma-related theta-frequency resonance in CA3 interneurons. Biol Cybern 84:123–132.
Ormandy GC, Song L, Jope RS (1991) Analysis of the convulsant-potentiating effects of lithium in rats. Exp Neurol 111:356–361.
Otis TS, Mody I (1992) Modulation of decay kinetics and frequency of GABAA receptor-mediated spontaneous inhibitory postsynaptic currents in hippocampal neurons. Neuroscience 49:13–32.
Otis TS, Staley KJ, Mody I (1991) Perpetual inhibitory activity in mammalian brain slices generated by spontaneous GABA release. Brain Res 545:142–150.
Pachernegg S, Strutz-Seebohm N, Hollmann M (2012) GluN3 subunit-containing NMDA receptors: not just one-trick ponies. Trends Neurosci 35:240–249.
Pagano A, Rovelli G, Mosbacher J, Lohmann T, Duthey B, Stauffer D, Ristig D, Schuler V, Meigel I, Lampert C, Stein T, Prezeau L, Blahos J, Pin J, Froestl W, Kuhn R, Heid J, Kaupmann K, Bettler B (2001) C-terminal interaction is essential for surface trafficking but not for heteromeric assembly of GABA(b) receptors. J Neurosci 21:1189–1202.
Palmini A, Najm I, Avanzini G, Babb T, Guerrini R, Foldvary-Schaefer N, Jackson G, Luders HO, Prayson R, Spreafico R, Vinters H V (2004) Terminology and classification of the cortical dysplasias. Neurology 62:S2-8.
Paré D, Lang EJ, Destexhe A (1998a) Inhibitory control of somatodendritic interactions underlying action potentials in neocortical pyramidal neurons in vivo: an intracellular and computational study. Neuroscience 84:377–402.

Paré D, Shink E, Gaudreau H, Destexhe A, Lang EJ (1998b) Impact of Spontaneous Synaptic Activity on the Resting Properties of Cat Neocortical Pyramidal Neurons In Vivo. J Neurophysiol 79:1450–1460 Available at: https://doi.org/10.1152/jn.1998.79.3.1450.
Parsons CG, Stoffler A, Danysz W (2007) Memantine: a NMDA receptor antagonist that improves memory by restoration of homeostasis in the glutamatergic system--too little activation is bad, too much is even worse. Neuropharmacology 53:699–723.
Parsons MP, Raymond LA (2014) Extrasynaptic NMDA receptor involvement in central nervous system disorders. Neuron 82:279–293.
Pascual MR (2007) Temporal lobe epilepsy: clinical semiology and neurophysiological studies. Semin Ultrasound CT MR 28:416–423.
Patel RR, Barbosa C, Brustovetsky T, Brustovetsky N, Cummins TR (2016) Aberrant epilepsy-associated mutant Nav1.6 sodium channel activity can be targeted with cannabidiol. Brain 139:2164–2181 Available at: http://dx.doi.org/10.1093/brain/aww129.
Patten AR, Yau SY, Fontaine CJ, Meconi A, Wortman RC, Christie BR (2015) The Benefits of Exercise on Structural and Functional Plasticity in the Rodent Hippocampus of Different Disease Models. Brain Plast 1:97–127 Available at: http://www.medra.org/servlet/aliasResolver?alias=iospress&doi=10.3233/BPL-150016.
Paulsen O, Moser EI (1998) A model of hippocampal memory encoding and retrieval: GABAergic control of synaptic plasticity. Trends Neurosci 21:273–278.
Peinado A, Yuste R, Katz LC (1993) Extensive dye coupling between rat neocortical neurons during the period of circuit formation. Neuron 10:103–114.
Pellegrini-Giampietro DE, Bennett M V, Zukin RS (1992) Are Ca(2+)-permeable kainate/AMPA receptors more abundant in immature brain? Neurosci Lett 144:65–69.
Peng Z, Huang CS, Stell BM, Mody I, Houser CR (2004) Altered expression of the delta subunit of the GABAA receptor in a mouse model of temporal lobe epilepsy. J Neurosci 24:8629–8639.
Pennifold J (2016) Oscillatory and epileptiform activity in human an rodent cortical regions in vitro.
Penttonen M, Kamondi A, Acsady L, Buzsaki G (1998) Gamma frequency oscillation in the hippocampus of the rat: intracellular analysis in vivo. Eur J Neurosci 10:718–728.
Perez-Otano I, Ehlers MD (2004) Learning from NMDA receptor trafficking: clues to the development and maturation of glutamatergic synapses. Neurosignals 13:175–189.
Pérez-Otaño I, Schulteis CT, Contractor A, Lipton SA, Trimmer JS, Sucher NJ, Heinemann SF (2001) Assembly with the NR1 Subunit Is Required for Surface Expression of NR3A-Containing NMDA Receptors. J Neurosci 21:1228 LP-1237 Available at: http://www.jneurosci.org/content/21/4/1228.abstract.
Pertwee RG (2001a) Cannabinoid receptors and pain. Prog Neurobiol 63:569–611.
Pertwee RG (2001b) Cannabinoids and the gastrointestinal tract. Gut 48:859–867.
Pertwee RG (2005a) The therapeutic potential of drugs that target cannabinoid receptors or modulate the tissue levels or actions of endocannabinoids. Aaps j 7:E625-54.
Pertwee RG (2005b) Inverse agonism and neutral antagonism at cannabinoid CB1 receptors. Life Sci 76:1307–1324 Available at: http://www.sciencedirect.com/science/article/pii/S0024320504009737.
Pertwee RG (2006) Cannabinoid pharmacology: The first 66 years. Br J Pharmacol 147.
Pertwee RG (2007) GPR55: a new member of the cannabinoid receptor clan? Br J Pharmacol 152:984–986.
Pertwee RG (2008) The diverse CB1 and CB2 receptor pharmacology of three plant cannabinoids: delta9-tetrahydrocannabinol, cannabidiol and delta9-tetrahydrocannabivarin. Br J Pharmacol 153:199–215.
Pertwee RG (2009) Emerging strategies for exploiting cannabinoid receptor agonists as medicines. Br J Pharmacol 156:397–411 Available at: http://www.ncbi.nlm.nih.gov/pmc/articles/PMC2697681/.
Pertwee RG, Howlett AC, Abood ME, Alexander SPH, Di Marzo V, Elphick MR, Greasley PJ, Hansen HS, Kunos G, Mackie K, Mechoulam R, Ross RA (2010) International Union of Basic and Clinical Pharmacology. LXXIX. Cannabinoid receptors and their ligands: beyond CB(1) and CB(2). Pharmacol Rev 62:588–631.
Petrini EM, Marchionni I, Zacchi P, Sieghart W, Cherubini E (2004) Clustering of extrasynaptic GABA(A) receptors modulates tonic inhibition in cultured hippocampal

neurons. J Biol Chem 279:45833–45843.
Pettit DA, Harrison MP, Olson JM, Spencer RF, Cabral GA (1998) Immunohistochemical localization of the neural cannabinoid receptor in rat brain. J Neurosci Res 51:391–402.
Pierce KL, Premont RT, Lefkowitz RJ (2002) Seven-transmembrane receptors. Nat Rev Mol Cell Biol 3:639–650.
Pinault D, Deschenes M (1992) Voltage-dependent 40-Hz oscillations in rat reticular thalamic neurons in vivo. Neuroscience 51:245–258.
Pinheiro PS, Mulle C (2008) Presynaptic glutamate receptors: physiological functions and mechanisms of action. Nat Rev Neurosci 9:423 Available at: http://dx.doi.org/10.1038/nrn2379.
Pinteaux-Jones F, Sevastou IG, Fry VAH, Heales S, Baker D, Pocock JM (2008) Myelin-induced microglial neurotoxicity can be controlled by microglial metabotropic glutamate receptors. J Neurochem 106:442–454.
Piomelli D (2003) The molecular logic of endocannabinoid signalling. Nat Rev Neurosci 4:873–884.
Pitler TA, Alger BE (1992) Postsynaptic spike firing reduces synaptic GABAA responses in hippocampal pyramidal cells. J Neurosci 12:4122–4132.
Pitler TA, Alger BE (1994) Depolarization-induced suppression of GABAergic inhibition in rat hippocampal pyramidal cells: G protein involvement in a presynaptic mechanism. Neuron 13:1447–1455.
Pittman-Polletta BR, Kocsis B, Vijayan S, Whittington MA, Kopell NJ (2015) Brain rhythms connect impaired inhibition to altered cognition in schizophrenia. Biol Psychiatry 77:1020–1030.
Prokic EJ, Weston C, Yamawaki N, Hall SD, Jones RS, Stanford IM, Ladds G, Woodhall GL (2015) Cortical oscillatory dynamics and benzodiazepine-site modulation of tonic inhibition in fast spiking interneurons. Neuropharmacology 95:192–205 Available at: http://www.ncbi.nlm.nih.gov/pubmed/25797493.
Puia G, Ducic I, Vicini S, Costa E (1993) Does neurosteroid modulatory efficacy depend on GABAA receptor subunit composition? Receptors Channels 1:135–142.
Quilichini P, Sirota A, Buzsáki G (2010) Intrinsic circuit organization and theta-gamma oscillation dynamics in the entorhinal cortex of the rat. J Neurosci 30:11128–11142 Available at: http://www.ncbi.nlm.nih.gov/pmc/articles/PMC2937273/.
Rachline J, Perin-Dureau F, Le Goff A, Neyton J, Paoletti P (2005) The micromolar zinc-binding domain on the NMDA receptor subunit NR2B. J Neurosci 25:308–317.
Racine RJ (1972) Modification of seizure activity by electrical stimulation. II. Motor seizure. Electroencephalogr Clin Neurophysiol 32:281–294.
Rafiq A, DeLorenzo RJ, Coulter DA (1993) Generation and propagation of epileptiform discharges in a combined entorhinal cortex/hippocampal slice. J Neurophysiol 70:1962–1974.
Rakic P (2009) Evolution of the neocortex: Perspective from developmental biology. Nat Rev Neurosci 10:724–735 Available at: http://www.ncbi.nlm.nih.gov/pmc/articles/PMC2913577/.
Rall W, Shepherd GM (1968) Theoretical reconstruction of field potentials and dendrodendritic synaptic interactions in olfactory bulb. J Neurophysiol 31:884–915.
Remondes M, Schuman EM (2004) Role for a cortical input to hippocampal area CA1 in the consolidation of a long-term memory. Nature 431:699–703.
Resstel LBM, Tavares RF, Lisboa SFS, Joca SRL, Correa FMA, Guimaraes FS (2009) 5-HT1A receptors are involved in the cannabidiol-induced attenuation of behavioural and cardiovascular responses to acute restraint stress in rats. Br J Pharmacol 156:181–188.
Rimmerman N, Ben-Hail D, Porat Z, Juknat A, Kozela E, Daniels MP, Connelly PS, Leishman E, Bradshaw HB, Shoshan-Barmatz V, Vogel Z (2013) Direct modulation of the outer mitochondrial membrane channel, voltage-dependent anion channel 1 (VDAC1) by cannabidiol: a novel mechanism for cannabinoid-induced cell death. Cell Death Dis 4:e949 Available at: http://www.ncbi.nlm.nih.gov/pmc/articles/PMC3877544/.
Rinaldi-Carmona M, Barth F, Heaulme M, Shire D, Calandra B, Congy C, Martinez S, Maruani J, Neliat G, Caput D, al. et (1994) SR141716A, a potent and selective antagonist of the brain cannabinoid receptor. FEBS Lett 350:240–244.
Rioult-Pedotti MS, Friedman D, Donoghue JP (2000) Learning-induced LTP in neocortex. Science 290:533–536.

Rodríguez-Muñoz M, Sánchez-Blázquez P, Merlos M, Garzón-Niño J (2016) Endocannabinoid control of glutamate NMDA receptors: the therapeutic potential and consequences of dysfunction. Oncotarget 7:55840–55862 Available at: http://www.ncbi.nlm.nih.gov/pmc/articles/PMC5342457/.
Rogawski MA, Loscher W (2004) The neurobiology of antiepileptic drugs. Nat Rev Neurosci 5:553–564.
Rogers CJ, Twyman RE, Macdonald RL (1994) Benzodiazepine and beta-carboline regulation of single GABAA receptor channels of mouse spinal neurones in culture. J Physiol 475:69–82 Available at: http://dx.doi.org/10.1113/jphysiol.1994.sp020050.
Rolls ET, Kesner RP (2006) A computational theory of hippocampal function, and empirical tests of the theory. Prog Neurobiol 79:1–48.
Room P, Groenewegen HJ, Lohman AH (1984) Inputs from the olfactory bulb and olfactory cortex to the entorhinal cortex in the cat. I. Anatomical observations. Exp brain Res 56:488–496.
Rosenberg EC, Tsien RW, Whalley BJ, Devinsky O (2015) Cannabinoids and Epilepsy. Neurotherapeutics 12:747–768.
Ross RA, Coutts AA, McFarlane SM, Anavi-Goffer S, Irving AJ, Pertwee RG, MacEwan DJ, Scott RH (2001) Actions of cannabinoid receptor ligands on rat cultured sensory neurones: implications for antinociception. Neuropharmacology 40:221–232.
Rothstein JD, Garland W, Puia G, Guidotti A, Weber RJ, Costa E (1992) Purification and characterization of naturally occurring benzodiazepine receptor ligands in rat and human brain. J Neurochem 58:2102–2115.
Rozenfeld R, Devi LA (2008) Regulation of CB1 cannabinoid receptor trafficking by the adaptor protein AP-3. FASEB J Off Publ Fed Am Soc Exp Biol 22:2311–2322.
Rusch D, Forman SA (2005) Classic benzodiazepines modulate the open-close equilibrium in alpha1beta2gamma2L gamma-aminobutyric acid type A receptors. Anesthesiology 102:783–792.
Russo EB, Burnett A, Hall B, Parker KK (2005) Agonistic properties of cannabidiol at 5-HT1a receptors. Neurochem Res 30:1037–1043.
Rutecki PA, Grossman RG, Armstrong D, Irish-Loewen S (1989) Electrophysiological connections between the hippocampus and entorhinal cortex in patients with complex partial seizures. J Neurosurg 70:667–675.
Ryberg E, Larsson N, Sjogren S, Hjorth S, Hermansson N-O, Leonova J, Elebring T, Nilsson K, Drmota T, Greasley PJ (2007) The orphan receptor GPR55 is a novel cannabinoid receptor. Br J Pharmacol 152:1092–1101.
Ryvlin P, Bouvard S, Le Bars D, De Lamerie G, Gregoire MC, Kahane P, Froment JC, Mauguiere F (1998) Clinical utility of flumazenil-PET versus [18F]fluorodeoxyglucose-PET and MRI in refractory partial epilepsy. A prospective study in 100 patients. Brain 121 (Pt 1:2067–2081.
Salin PA, Prince DA (1996) Spontaneous GABAA receptor-mediated inhibitory currents in adult rat somatosensory cortex. J Neurophysiol 75:1573–1588.
Sánchez-Blázquez P, Rodríguez-Muñoz M, Garzón J (2013) The cannabinoid receptor 1 associates with NMDA receptors to produce glutamatergic hypofunction: implications in psychosis and schizophrenia. Front Pharmacol 4:169 Available at: http://www.ncbi.nlm.nih.gov/pmc/articles/PMC3877778/.
Sans N, Vissel B, Petralia RS, Wang Y-X, Chang K, Royle GA, Wang C-Y, O'Gorman S, Heinemann SF, Wenthold RJ (2003) Aberrant formation of glutamate receptor complexes in hippocampal neurons of mice lacking the GluR2 AMPA receptor subunit. J Neurosci 23:9367–9373.
Sans NA, Montcouquiol ME, Raymond J (2000) Postnatal developmental changes in AMPA and NMDA receptors in the rat vestibular nuclei. Brain Res Dev Brain Res 123:41–52.
Sargolini F, Fyhn M, Hafting T, McNaughton BL, Witter MP, Moser M-B, Moser EI (2006) Conjunctive Representation of Position, Direction, and Velocity in Entorhinal Cortex. Science (80-) 312:758 LP-762 Available at: http://science.sciencemag.org/content/312/5774/758.abstract.
Sauvage MM, Nakamura NH, Beer Z (2013) Mapping memory function in the medial temporal lobe with the immediate-early gene Arc. Behav Brain Res 254:22–33 Available at: http://www.sciencedirect.com/science/article/pii/S0166432813002568.
Savic I, Persson A, Roland P, Pauli S, Sedvall G, Widen L (1988) In-vivo demonstration of

reduced benzodiazepine receptor binding in human epileptic foci. Lancet (London, England) 2:863–866.
Saxena NC, Macdonald RL (1994) Assembly of GABAA receptor subunits: role of the delta subunit. J Neurosci 14:7077–7086.
Scharfman HE (2007) The Neurobiology of Epilepsy. Curr Neurol Neurosci Rep 7:348–354 Available at: http://www.ncbi.nlm.nih.gov/pmc/articles/PMC2492886/.
Schatz AR, Lee M, Condie RB, Pulaski JT, Kaminski NE (1997) Cannabinoid receptors CB1 and CB2: a characterization of expression and adenylate cyclase modulation within the immune system. Toxicol Appl Pharmacol 142:278–287.
Schorge S, Colquhoun D (2003) Studies of NMDA receptor function and stoichiometry with truncated and tandem subunits. J Neurosci 23:1151–1158.
Schultz C, Engelhardt M (2014) Anatomy of the hippocampal formation. Front Neurol Neurosci 34:6–17.
Schwerdtfeger WK, Buhl EH, Germroth P (1990) Disynaptic olfactory input to the hippocampus mediated by stellate cells in the entorhinal cortex. J Comp Neurol 292:163–177 Available at: http://dx.doi.org/10.1002/cne.902920202.
Sedley W, Cunningham MO (2013) Do cortical gamma oscillations promote or suppress perception? An under-asked question with an over-assumed answer. Front Hum Neurosci 7:595 Available at: http://www.ncbi.nlm.nih.gov/pmc/articles/PMC3778316/.
Serafini R, Bracamontes J, Steinbach JH (2000) Structural domains of the human GABAA receptor 3 subunit involved in the actions of pentobarbital. J Physiol 524 Pt 3:649–676.
Serfozo P, Cash DJ (1992) Effect of a benzodiazepine (chlordiazepoxide) on a GABAA receptor from rat brain. Requirement of only one bound GABA molecule for channel opening. FEBS Lett 310:55–59.
Sheng M, Cummings J, Roldan LA, Jan YN, Jan LY (1994) Changing subunit composition of heteromeric NMDA receptors during development of rat cortex. Nature 368:144–147.
Shrivastava A, Kuzontkoski PM, Groopman JE, Prasad A (2011) Cannabidiol induces programmed cell death in breast cancer cells by coordinating the cross-talk between apoptosis and autophagy. Mol Cancer Ther 10:1161–1172.
Shu Y, Hasenstaub A, McCormick DA (2003) Turning on and off recurrent balanced cortical activity. Nature 423:288 Available at: http://dx.doi.org/10.1038/nature01616.
Sieghart W, Ramerstorfer J, Sarto-Jackson I, Varagic Z, Ernst M (2012) A novel GABA(A) receptor pharmacology: drugs interacting with the α(+)β(−) interface. Br J Pharmacol 166:476–485 Available at: http://www.ncbi.nlm.nih.gov/pmc/articles/PMC3417481/.
Sigel E (2002) Mapping of the benzodiazepine recognition site on GABA(A) receptors. Curr Top Med Chem 2:833–839.
Sigel E, Baur R, Kellenberger S, Malherbe P (1992) Point mutations affecting antagonist affinity and agonist dependent gating of GABAA receptor channels. EMBO J 11:2017–2023.
Sik A, Penttonen M, Ylinen A, Buzsaki G (1995) Hippocampal CA1 interneurons: an in vivo intracellular labeling study. J Neurosci 15:6651–6665.
Singer W (1993) Synchronization of cortical activity and its putative role in information processing and learning. Annu Rev Physiol 55:349–374.
Smolders I, Bortolotto ZA, Clarke VRJ, Warre R, Khan GM, O'Neill MJ, Ornstein PL, Bleakman D, Ogden A, Weiss B, Stables JP, Ho KH, Ebinger G, Collingridge GL, Lodge D, Michotte Y (2002) Antagonists of GLU(K5)-containing kainate receptors prevent pilocarpine-induced limbic seizures. Nat Neurosci 5:796–804.
Soltesz I, Smetters DK, Mody I (1995) Tonic inhibition originates from synapses close to the soma. Neuron 14:1273–1283.
Somogyi P (1977) A specific "axo-axonal" interneuron in the visual cortex of the rat. Brain Res 136:345–350 Available at: http://www.sciencedirect.com/science/article/pii/0006899377908083.
Soriano E, Martinez A, Farinas I, Frotscher M (1993) Chandelier cells in the hippocampal formation of the rat: the entorhinal area and subicular complex. J Comp Neurol 337:151–167.
Spencer SS, Spencer DD (1994) Entorhinal-hippocampal interactions in medial temporal lobe epilepsy. Epilepsia 35:721–727.
Squire LR, Stark CEL, Clark RE (2004) The medial temporal lobe. Annu Rev Neurosci 27:279–306.

Stacey WC, Durand DM (2001) Synaptic noise improves detection of subthreshold signals in hippocampal CA1 neurons. J Neurophysiol 86:1104–1112.
Stagg CJ, Bestmann S, Constantinescu AO, Moreno Moreno L, Allman C, Mekle R, Woolrich M, Near J, Johansen-Berg H, Rothwell JC (2011) Relationship between physiological measures of excitability and levels of glutamate and GABA in the human motor cortex. J Physiol 589:5845–5855 Available at: http://dx.doi.org/10.1113/jphysiol.2011.216978.
Stander S, Schmelz M, Metze D, Luger T, Rukwied R (2005) Distribution of cannabinoid receptor 1 (CB1) and 2 (CB2) on sensory nerve fibers and adnexal structures in human skin. J Dermatol Sci 38:177–188.
Stevens CF, Zador AM (1998) Input synchrony and the irregular firing of cortical neurons. Nat Neurosci 1:210–217.
Study RE, Barker JL (1981) Diazepam and (--)-pentobarbital: fluctuation analysis reveals different mechanisms for potentiation of gamma-aminobutyric acid responses in cultured central neurons. Proc Natl Acad Sci 78:7180 LP-7184 Available at: http://www.pnas.org/content/78/11/7180.abstract.
Sucher NJ, Akbarian S, Chi CL, Leclerc CL, Awobuluyi M, Deitcher DL, Wu MK, Yuan JP, Jones EG, Lipton SA (1995) Developmental and regional expression pattern of a novel NMDA receptor-like subunit (NMDAR-L) in the rodent brain. J Neurosci 15:6509–6520.
Sugihara H, Moriyoshi K, Ishii T, Masu M, Nakanishi S (1992) Structures and properties of seven isoforms of the NMDA receptor generated by alternative splicing. Biochem Biophys Res Commun 185:826–832.
Sutula T, Cascino G, Cavazos J, Parada I, Ramirez L (1989) Mossy fiber synaptic reorganization in the epileptic human temporal lobe. Ann Neurol 26:321–330.
Suzuki E, Kessler M, Arai AC (2008) The fast kinetics of AMPA GluR3 receptors is selectively modulated by the TARPs gamma 4 and gamma 8. Mol Cell Neurosci 38:117–123.
Swann JW, Smith KL, Brady RJ (1993) Localized excitatory synaptic interactions mediate the sustained depolarization of electrographic seizures in developing hippocampus. J Neurosci 13:4680–4689.
Szabadics J, Lorincz A, Tamas G (2001) Beta and gamma frequency synchronization by dendritic gabaergic synapses and gap junctions in a network of cortical interneurons. J Neurosci 21:5824–5831.
Szabo B, Dorner L, Pfreundtner C, Norenberg W, Starke K (1998) Inhibition of GABAergic inhibitory postsynaptic currents by cannabinoids in rat corpus striatum. Neuroscience 85:395–403.
Tahvildari B, Alonso A (2005) Morphological and electrophysiological properties of lateral entorhinal cortex layers II and III principal neurons. J Comp Neurol 491:123–140.
Tajima N, Karakas E, Grant T, Simorowski N, Diaz-Avalos R, Grigorieff N, Furukawa H (2016) Activation of NMDA receptors and the mechanism of inhibition by ifenprodil. Nature 534:63 Available at: http://dx.doi.org/10.1038/nature17679.
Takahashi T, Kajikawa Y, Tsujimoto T (1998) G-Protein-Coupled Modulation of Presynaptic Calcium Currents and Transmitter Release by a GABA_B Receptor. J Neurosci 18:3138 LP-3146 Available at: http://www.jneurosci.org/content/18/9/3138.abstract.
Tamas G, Buhl EH, Lorincz A, Somogyi P (2000) Proximally targeted GABAergic synapses and gap junctions synchronize cortical interneurons. Nat Neurosci 3:366–371.
Tang FR, Chen PM, Tang YC, Tsai MC, Lee WL (2007) Two-methyl-6-phenylethynyl-pyridine (MPEP), a metabotropic glutamate receptor 5 antagonist, with low doses of MK801 and diazepam: a novel approach for controlling status epilepticus. Neuropharmacology 53:821–831.
Tao W, Higgs MH, Spain WJ, Ransom CB (2013) Postsynaptic GABAB receptors enhance extrasynaptic GABAA receptor function in dentate gyrus granule cells. J Neurosci 33:3738–3743.
Tassi L, Colombo N, Garbelli R, Francione S, Lo Russo G, Mai R, Cardinale F, Cossu M, Ferrario A, Galli C, Bramerio M, Citterio A, Spreafico R (2002) Focal cortical dysplasia: neuropathological subtypes, EEG, neuroimaging and surgical outcome. Brain 125:1719–1732.
Taura F, Sirikantaramas S, Shoyama Y, Yoshikai K, Shoyama Y, Morimoto S (2007) Cannabidiolic-acid synthase, the chemotype-determining enzyme in the fiber-type

Cannabis sativa. FEBS Lett 581:2929–2934 Available at: http://www.sciencedirect.com/science/article/pii/S0014579307005728.
Taylor DC, Falconer MA, Bruton CJ, Corsellis JA (1971) Focal dysplasia of the cerebral cortex in epilepsy. J Neurol Neurosurg Psychiatry 34:369–387.
Teissere JA, Czajkowski C (2001) A (beta)-strand in the (gamma)2 subunit lines the benzodiazepine binding site of the GABA A receptor: structural rearrangements detected during channel gating. J Neurosci 21:4977–4986.
Thomas A, Baillie GL, Phillips AM, Razdan RK, Ross RA, Pertwee RG (2007) Cannabidiol displays unexpectedly high potency as an antagonist of CB1 and CB2 receptor agonists in vitro. Br J Pharmacol 150:613–623.
Traub RD, Whittington MA (2010) Cortical Oscillations in Health and Disease. Oxford University Press .
Traub RD, Whittington MA, Buhl EH, Jefferys JG, Faulkner HJ (1999) On the mechanism of the gamma --> beta frequency shift in neuronal oscillations induced in rat hippocampal slices by tetanic stimulation. J Neurosci 19:1088–1105.
Traub RD, Whittington MA, Buhl EH, LeBeau FE, Bibbig A, Boyd S, Cross H, Baldeweg T (2001) A possible role for gap junctions in generation of very fast EEG oscillations preceding the onset of, and perhaps initiating, seizures. Epilepsia 42:153–170.
Traub RD, Whittington MA, Colling SB, Buzsáki G, Jefferys JG (1996a) Analysis of gamma rhythms in the rat hippocampus in vitro and in vivo. J Physiol 493:471–484 Available at: http://jp.physoc.org/content/493/Pt_2/471.abstract.
Traub RD, Whittington MA, Stanford IM, Jefferys JG (1996b) A mechanism for generation of long-range synchronous fast oscillations in the cortex. Nature 383:621–624.
Tremblay E, Roisin MP, Represa A, Charriaut-Marlangue C, Ben-Ari Y (1988) Transient increased density of NMDA binding sites in the developing rat hippocampus. Brain Res 461:393–396.
Treves A (2004) Computational constraints between retrieving the past and predicting the future, and the CA3-CA1 differentiation. Hippocampus 14:539–556.
Tsien JZ, Huerta PT, Tonegawa S (1996) The essential role of hippocampal CA1 NMDA receptor-dependent synaptic plasticity in spatial memory. Cell 87:1327–1338.
Tsou K, Brown S, Sanudo-Pena MC, Mackie K, Walker JM (1998) Immunohistochemical distribution of cannabinoid CB1 receptors in the rat central nervous system. Neuroscience 83:393–411.
Tudor M, Tudor L, Tudor KI (2005) [Hans Berger (1873-1941)--the history of electroencephalography]. Acta Med Croat 59:307–313.
Turski WA, Cavalheiro EA, Schwarz M, Czuczwar SJ, Kleinrok Z, Turski L (1983a) Limbic seizures produced by pilocarpine in rats: behavioural, electroencephalographic and neuropathological study. Behav Brain Res 9:315–335.
Turski WA, Czuczwar SJ, Kleinrok Z, Turski L (1983b) Cholinomimetics produce seizures and brain damage in rats. Experientia 39:1408–1411.
Twyman RE, Rogers CJ, Macdonald RL (1989) Differential regulation of gamma-aminobutyric acid receptor channels by diazepam and phenobarbital. Ann Neurol 25:213–220.
Uhlhaas PJ, Singer W (2006) Neural Synchrony in Brain Disorders: Relevance for Cognitive Dysfunctions and Pathophysiology. Neuron 52:155–168 Available at: http://www.sciencedirect.com/science/article/pii/S0896627306007276.
Uhlhaas PJ, Singer W (2015) Oscillations and neuronal dynamics in schizophrenia: the search for basic symptoms and translational opportunities. Biol Psychiatry 77:1001–1009.
Vago DR, Kesner RP (2008) Disruption of the direct perforant path input to the CA1 subregion of the dorsal hippocampus interferes with spatial working memory and novelty detection. Behav Brain Res 189:273–283.
van Groen T, Miettinen P, Kadish I (2003) The entorhinal cortex of the mouse: Organization of the projection to the hippocampal formation. Hippocampus 13:133–149 Available at: http://dx.doi.org/10.1002/hipo.10037.
van Groen T, Wyss JM (1990) Extrinsic projections from area CA1 of the rat hippocampus: Olfactory, cortical, subcortical, and bilateral hippocampal formation projections. J Comp Neurol 302:515–528 Available at: http://dx.doi.org/10.1002/cne.903020308.
van Haeften T, Baks-te-Bulte L, Goede PH, Wouterlood FG, Witter MP (2003) Morphological

and numerical analysis of synaptic interactions between neurons in deep and superficial layers of the entorhinal cortex of the rat. Hippocampus 13:943–952.
van Sickle MD, Duncan M, Kingsley PJ, Mouihate A, Urbani P, Mackie K, Stella N, Makriyannis A, Piomelli D, Davison JS, Marnett LJ, Di Marzo V, Pittman QJ, Patel KD, Sharkey KA (2005) Identification and functional characterization of brainstem cannabinoid CB2 receptors. Science 310:329–332.
Varela F, Lachaux JP, Rodriguez E, Martinerie J (2001) The brainweb: phase synchronization and large-scale integration. Nat Rev Neurosci 2:229–239.
Vaughan CW, Christie MJ (2005) Retrograde signalling by endocannabinoids. Handb Exp Pharmacol:367–383.
Vivash L, Tostevin A, Liu DSH, Dalic L, Dedeurwaerdere S, Hicks RJ, Williams DA, Myers DE, O'Brien TJ (2011) Changes in hippocampal GABAA/cBZR density during limbic epileptogenesis: relationship to cell loss and mossy fibre sprouting. Neurobiol Dis 41:227–236.
Wagner DA, Czajkowski C (2001) Structure and dynamics of the GABA binding pocket: A narrowing cleft that constricts during activation. J Neurosci 21:67–74.
Wagner JA, Jarai Z, Batkai S, Kunos G (2001) Hemodynamic effects of cannabinoids: coronary and cerebral vasodilation mediated by cannabinoid CB(1) receptors. Eur J Pharmacol 423:203–210.
Wallace MJ, Wiley JL, Martin BR, DeLorenzo RJ (2001) Assessment of the role of CB1 receptors in cannabinoid anticonvulsant effects. Eur J Pharmacol 428:51–57.
Walther H, Lambert JD, Jones RS, Heinemann U, Hamon B (1986) Epileptiform activity in combined slices of the hippocampus, subiculum and entorhinal cortex during perfusion with low magnesium medium. Neurosci Lett 69:156–161.
Wang J, Ueda N (2009) Biology of endocannabinoid synthesis system. Prostaglandins Other Lipid Mediat 89:112–119 Available at: http://www.sciencedirect.com/science/article/pii/S1098882308000890.
Wang M (2011) Neurosteroids and GABA-A Receptor Function. Front Endocrinol (Lausanne) 2:44 Available at: http://www.ncbi.nlm.nih.gov/pmc/articles/PMC3356040/.
Wang M-D, Rahman M, Zhu D, Backstrom T (2006) Pregnenolone sulphate and Zn2+ inhibit recombinant rat GABA(A) receptor through different channel property. Acta Physiol (Oxf) 188:153–162.
Wang M-D, Rahman M, Zhu D, Johansson I-M, Backstrom T (2007) 3Beta-hydroxysteroids and pregnenolone sulfate inhibit recombinant rat GABA(A) receptor through different channel property. Eur J Pharmacol 557:124–131.
Wang X-J, Rinzel J (1992) Alternating and Synchronous Rhythms in Reciprocally Inhibitory Model Neurons. Neural Comput 4:84–97 Available at: http://dx.doi.org/10.1162/neco.1992.4.1.84.
Wang XJ, Buzsaki G (1996) Gamma oscillation by synaptic inhibition in a hippocampal interneuronal network model. J Neurosci 16:6402–6413.
Wardell B, Marik PS, Piper D, Rutar T, Jorgensen EM, Bamber BA (2006) Residues in the first transmembrane domain of the Caenorhabditis elegans GABA(A) receptor confer sensitivity to the neurosteroid pregnenolone sulfate. Br J Pharmacol 148:162–172.
Watanabe M, Inoue Y, Sakimura K, Mishina M (1992) Developmental changes in distribution of NMDA receptor channel subunit mRNAs. Neuroreport 3:1138–1140.
Weissinger F, Buchheim K, Siegmund H, Heinemann U, Meierkord H (2000) Optical imaging reveals characteristic seizure onsets, spread patterns, and propagation velocities in hippocampal-entorhinal cortex slices of juvenile rats. Neurobiol Dis 7:286–298.
Wennberg R, Arruda F, Quesney LF, Olivier A (2002) Preeminence of Extrahippocampal Structures in the Generation of Mesial Temporal Seizures: Evidence from Human Depth Electrode Recordings. Epilepsia 43:716–726 Available at: http://dx.doi.org/10.1046/j.1528-1157.2002.31101.x.
Wenzel A, Scheurer L, Kunzi R, Fritschy JM, Mohler H, Benke D (1995) Distribution of NMDA receptor subunit proteins NR2A, 2B, 2C and 2D in rat brain. Neuroreport 7:45–48.
Westh-Hansen SE, Rasmussen PB, Hastrup S, Nabekura J, Noguchi K, Akaike N, Witt MR, Nielsen M (1997) Decreased agonist sensitivity of human GABA(A) receptors by an amino acid variant, isoleucine to valine, in the alpha1 subunit. Eur J Pharmacol 329:253–257.

White WF, Nadler J V, Hamberger A, Cotman CW, Cummins JT (1977) Glutamate as transmitter of hippocampal perforant path. Nature 270:356–357.
Whitlock JR, Heynen AJ, Shuler MG, Bear MF (2006) Learning induces long-term potentiation in the hippocampus. Science 313:1093–1097.
Whittington MA, Stanford IM, Colling SB, Jefferys JGR, Traub RD (1997) Spatiotemporal patterns of γ frequency oscillations tetanically induced in the rat hippocampal slice. J Physiol 502:591–607 Available at: http://dx.doi.org/10.1111/j.1469-7793.1997.591bj.x.
Whittington MA, Traub RD (2003) Interneuron diversity series: inhibitory interneurons and network oscillations in vitro. Trends Neurosci 26:676–682.
Whittington MA, Traub RD, Jefferys JG (1995) Synchronized oscillations in interneuron networks driven by metabotropic glutamate receptor activation. Nature 373:612–615.
Whittington MA, Traub RD, Kopell N, Ermentrout B, Buhl EH (2000) Inhibition-based rhythms: experimental and mathematical observations on network dynamics. Int J Psychophysiol 38:315–336.
WHO (2015) Epilepsy Fact Sheet no.999. Available at: http://www.who.int/mediacentre/factsheets/fs999/en/.
Williams K (1993) Ifenprodil discriminates subtypes of the N-methyl-D-aspartate receptor: selectivity and mechanisms at recombinant heteromeric receptors. Mol Pharmacol 44:851–859.
Williams K (2001) Ifenprodil, a novel NMDA receptor antagonist: site and mechanism of action. Curr Drug Targets 2:285–298.
Wilson HR, Cowan JD (1972) Excitatory and inhibitory interactions in localized populations of model neurons. Biophys J 12:1–24.
Wilson RI, Nicoll RA (2001) Endogenous cannabinoids mediate retrograde signalling at hippocampal synapses. Nature 410:588–592.
Witter M (1989) Connectivity of the rat hippocampus, In: The Hippcampus: New vistas. New York, NY, USA.
Witter M, Wouterlood F, Naber P, Van Haeften T (2000) Anatomical Organization of the Parahippocampal-Hippocampal Network. Ann N Y Acad Sci 911:1–24 Available at: http://dx.doi.org/10.1111/j.1749-6632.2000.tb06716.x.
Witter MP, Groenewegen HJ, Lopes da Silva FH, Lohman AHM (1989) Functional organization of the extrinsic and intrinsic circuitry of the parahippocampal region. Prog Neurobiol 33:161–253 Available at: http://www.sciencedirect.com/science/article/pii/0301008289900099.
Witter MP, Moser EI (2006) Spatial representation and the architecture of the entorhinal cortex. Trends Neurosci 29:671–678 Available at: http://dx.doi.org/10.1016/j.tins.2006.10.003.
Witter MP, Naber PA, van Haeften T, Machielsen WCM, Rombouts SARB, Barkhof F, Scheltens P, Lopes da Silva FH (2000) Cortico-hippocampal communication by way of parallel parahippocampal-subicular pathways. Hippocampus 10:398–410 Available at: http://dx.doi.org/10.1002/1098-1063(2000)10:4%3C398::AID-HIPO6%3E3.0.CO.
Witter MP, Room P, Groenewegen HJ, Lohman AH (1986) Connections of the parahippocampal cortex in the cat. V. Intrinsic connections; comments on input/output connections with the hippocampus. J Comp Neurol 252:78–94.
Wong D, Kuwabara H, Horti A, Brasic J, Raymont V, Nandi A, Rahmin A, Gean E, Dannals R, Casella N (2012) Cannabinoid receptor subtype 1 (CB1) distribution correlates with neuropsychiatric ratings. Soc biolocigal psychiatry Abstr.
Wong M (2009) The Window of Epileptogenesis: Looking Beyond the Latent Period. Epilepsy Curr 9:144–145.
Wood TB, Spivey WTN, Easterfield TH (1897) Charas, the resin of Indian hemp. J Chem Soc:539–546.
Woodhall GL, Bailey SJ, Thompson SE, Evans DIP, Jones RSG (2005) Fundamental differences in spontaneous synaptic inhibition between deep and superficial layers of the rat entorhinal cortex. Hippocampus 15:232–245.
Woodhams PL, Celio MR, Ulfig N, Witter MP (1993) Morphological and functional correlates of borders in the entorhinal cortex and hippocampus. Hippocampus 3 Spec No:303–311.
Wouterlood FG, Hartig W, Bruckner G, Witter MP (1995) Parvalbumin-immunoreactive neurons in the entorhinal cortex of the rat: localization, morphology, connectivity and

ultrastructure. J Neurocytol 24:135–153.
Wouterlood FG, Nederlof J (1983) Terminations of olfactory afferents on layer II and III neurons in the entorhinal area: Degeneration-golgi-electron microscopic study in the rat. Neurosci Lett 36:105–110 Available at: http://www.sciencedirect.com/science/article/pii/0304394083902501.
Wouterlood FG, van Denderen JC, van Haeften T, Witter MP (2000) Calretinin in the entorhinal cortex of the rat: distribution, morphology, ultrastructure of neurons, and co-localization with gamma-aminobutyric acid and parvalbumin. J Comp Neurol 425:177–192.
Wulff P, Ponomarenko A a, Bartos M, Korotkova TM, Fuchs EC, Bähner F, Both M, Tort ABL, Kopell NJ, Wisden W, Monyer H (2009) Hippocampal theta rhythm and its coupling with gamma oscillations require fast inhibition onto parvalbumin-positive interneurons. Proc Natl Acad Sci U S A 106:3561–3566.
Xie CW, McGinty JF, Lee PH, Mitchell CL, Hong JS (1991) A glutamate antagonist blocks perforant path stimulation-induced reduction of dynorphin peptide and prodynorphin mRNA levels in rat hippocampus. Brain Res 562:243–250.
Xiong W, Chen S-R, He L, Cheng K, Zhao Y-L, Chen H, Li D-P, Homanics GE, Peever J, Rice KC, Wu L, Pan H-L, Zhang L (2014) Presynaptic glycine receptors as a potential therapeutic target for hyperekplexia disease. Nat Neurosci 17:232 Available at: http://dx.doi.org/10.1038/nn.3615.
Xu M, Akabas MH (1996) Identification of channel-lining residues in the M2 membrane-spanning segment of the GABA(A) receptor alpha1 subunit. J Gen Physiol 107:195–205.
Xu Z, Chen R-Q, Gu Q-H, Yan J-Z, Wang S-H, Liu S-Y, Lu W (2009) Metaplastic regulation of long-term potentiation/long-term depression threshold by activity-dependent changes of NR2A/NR2B ratio. J Neurosci 29:8764–8773.
Xue JG, Masuoka T, Gong XD, Chen KS, Yanagawa Y, Law SK, Konishi S (2011) NMDA receptor activation enhances inhibitory GABAergic transmission onto hippocampal pyramidal neurons via presynaptic and postsynaptic mechanisms. J Neurophysiol 105:2897–2906 Available at: http://www.ncbi.nlm.nih.gov/pubmed/21471392.
Yamawaki N, Stanford IM, Hall SD, Woodhall GL (2008) Pharmacologically induced and stimulus evoked rhythmic neuronal oscillatory activity in the primary motor cortex in vitro. Neuroscience 151:386–395.
Yang L, Benardo LS (2002) Laminar properties of 4-aminopyridine-induced synchronous network activities in rat neocortex. Neuroscience 111:303–313.
Yeckel MF, Berger TW (1990) Feedforward excitation of the hippocampus by afferents from the entorhinal cortex: redefinition of the role of the trisynaptic pathway. Proc Natl Acad Sci U S A 87:5832–5836 Available at: http://www.ncbi.nlm.nih.gov/pmc/articles/PMC54422/.
Yoshida M, Teramura M, Sakai M, Karasawa N, Nagatsu T, Nagatsu I (1987) Immunohistochemical visualization of glutamate- and aspartate-containing nerve terminal pools in the rat limbic structures. Brain Res 410:169–173.
Zanelati T V, Biojone C, Moreira FA, Guimaraes FS, Joca SRL (2010) Antidepressant-like effects of cannabidiol in mice: possible involvement of 5-HT1A receptors. Br J Pharmacol 159:122–128.
Zijlmans M, Jiruska P, Zelmann R, Leijten FSS, Jefferys JGR, Gotman J (2012) High-Frequency Oscillations as a New Biomarker in Epilepsy. Ann Neurol 71:169–178 Available at: http://www.ncbi.nlm.nih.gov/pmc/articles/PMC3754947/.
Zilles K (1990) The Human Nervous System (G P, ed). San Diego: Academic Press.

Chapter 9

Appendix

9.1 Appendix 1

Principal component analysis code:

```
> log.ht <- log(ht[, 1:5])
> ht.cat <- ht[, 6]
> ht.pca <- prcomp(log.ht, center = TRUE, scale. = TRUE)
> print(ggbiplot(ht.pca, scale = 0, obs.scale = 0, var.scale = 0, groups = ht.cat, ellipse = TRUE, alpha = 0))
```

Performed in R with the Rcmder (Rcommander) and ggbiplot packages installed.

Here ht refers to the dataset used (in this case all human tissue cell parameter responses). Included parameters: Amplitude (pA), Rise time (ms), Decay time (ms), Area (AUC) and, IEI (ms), which represented columns 1 – 5 respectively. These responses were sorted into categories based upon which condition they were selected from (baseline or CBD) and labelled in column 6.

The first line of code shows the parameter responses being logged. The second shows the categories being used to label the two groups. The third is the PCA computation, with “prcomp” the command for this.

The final line is how the graphs were displayed with the arguments corresponding to the list below:

scale - covariance biplot (scale = 1), form biplot (scale = 0).

obs.scale - scale factor to apply to observations

var.scale - scale factor to apply to variables

groups - optional factor variable indicating the groups that the observations belong to. If provided the points will be coloured according to groups

ellipse - draw a normal data ellipse for each group?

alpha - alpha transparency value for the points (0 = transparent, 1 = opaque) – show all data points or not

circle - draw a correlation circle? (only applies when prcomp was called with scale = TRUE and when var.scale = 1

9.2 Appendix 2

Protein expression investigations performed by the Henley lab at the University of Bristol were described in **Chapter 3** of this thesis. The following figures have been reproduced with the permission of the lab, showing the changes in protein expression levels over the course of epileptogenesis from the RISE induction. Here the same time points as presented throughout this thesis have been used, with time point 1 referring to the 24-hour post-induction, time point 2 the latent period or 1-week post-induction phase, with time point 3 relating to the chronic/SRS population (3-months post-induction).

The histograms presented here show the responses of the SE rats when compared to normalised AMC animals (shown with the dotted line). Western blots show individual protein expression comparisons between AMC and SE rats.

Materials and methods

AMC and SE rat brains were provided by this lab, from three epileptogenesis time points (24-hours post, 1-week post, 3-months post/SRS). The brains were dissected after decapitation and placed into ice-cold normal aCSF (**Chapter 2**). From here the brains were separated into individual brain regions (cerebellum, frontal lobe, somatosensory cortex, temporal lobe, hippocampus and striatum), placed into 1ml Eppendorf tubes and snap frozen in liquid nitrogen to prevent degeneration and in preparation for travel.

All rat brain samples were homogenised using liquid nitrogen to keep samples from degenerating, and a pestle and mortar for crushing into a fine powder. Samples were resuspended in lysis buffer (50mM Tris pH 7.4, 150mM NaCl, 1% Triton, 1X Protease Inhibitor) then sonicated, vortexed briefly, and left on ice for 30 minutes. Samples were then centrifuged (13.2 rpm, 20 minutes, 4$_{o}$C) and the pellet discarded. Total protein concentration was quantified using a bicinchoninic acid (BCA) assay.

Following preparation, protein samples were boiled at 95$_{o}$C for 5 minutes in the presence of sample buffer (2X). 30µg of total protein was loaded on 10% SDS-PAGE gels, separated (150V, 1.5 hours), and transferred onto PVDF membranes (activated with methanol) with transfer buffer (29mM glycine, 58mM Tris-HCl pH 7.5, 0.0375% (w/v) SDS, 20% (v/v) methanol) using a wet transfer system (400mAmps, 70min). Membranes were blocked for 1 hour in milk (5% w/v in T-PBS) and incubated overnight in milk (5% (w/v) in T-PBS) containing the appropriate primary antibody (see figure legends) at 4°C. Membranes were washed extensively with T-8

PBS (10X PBS, 1% (v/v) Tween) and probed with appropriate secondary HRP-antibodies (RT, 1 hour). Blots were washed extensively with T-PBS and developed using an Odyssey Fc Imaging System (LI-COR). For reprobing, membranes were stripped by incubating for 15 minutes at 55$_o$C with Restore PLUS Western Blot Stripping Buffer (Thermo Scientific), then washed extensively with T-PBS and blocked in milk (5% w/v in T-PBS) for 30 minutes at RT. Membranes were then incubated with the appropriate primary and secondary antibodies and developed as above. Blots were analysed, and bands quantified using Image Studio Lite (LI-COR). A list of proteins probed for, along with their molecular weights and function or role in this study are shown in Table 1.1.

GraphPad Prism 7 software was used to perform statistical analysis on results of all quantitative experiments, as detailed in figure legends. One sample t-tests were used to calculate and determine statistical significance between observed differences. Error bars show the standard deviation. A p-value less than 0.05 was considered significant for all experiments ($p<0.05$ = *, $p<0.01$ = **, $p<0.001$ = ***, $p<0.0001$ = ****).

Protein	Molecular Weight (kDa)	Function/Role in Study
B-Actin	42	Loading Control
B-Tubulin	55	Loading Control
EGFR	170	Surface Receptor - Control
GluA1	100	AMPA Receptor Subunit
GluA2	100	AMPA Receptor Subunit
GluK2	120	Kainate Receptor Subunit
GluK5	130	Kainate Receptor Subunit
GluN1	120	NMDA Receptor Subunit
ADAR2 (Adenosine Deaminase acting on RNA 2)	100	A- to I- RNA Editing Enzyme
SENP3 (SUMO-Specific Protease 3)	70	De-SUMOylation Enzyme
PSD95	95	Post-synaptic Marker
Synaptophysin	40	Pre-synaptic Marker

Table 9.1 Summary of proteins screened.
All proteins for which expression levels were measured in SE and AMC rat brains using appropriate primary and secondary antibodies, their molecular weights in kDa for reference, and a description of their function or role in this study.

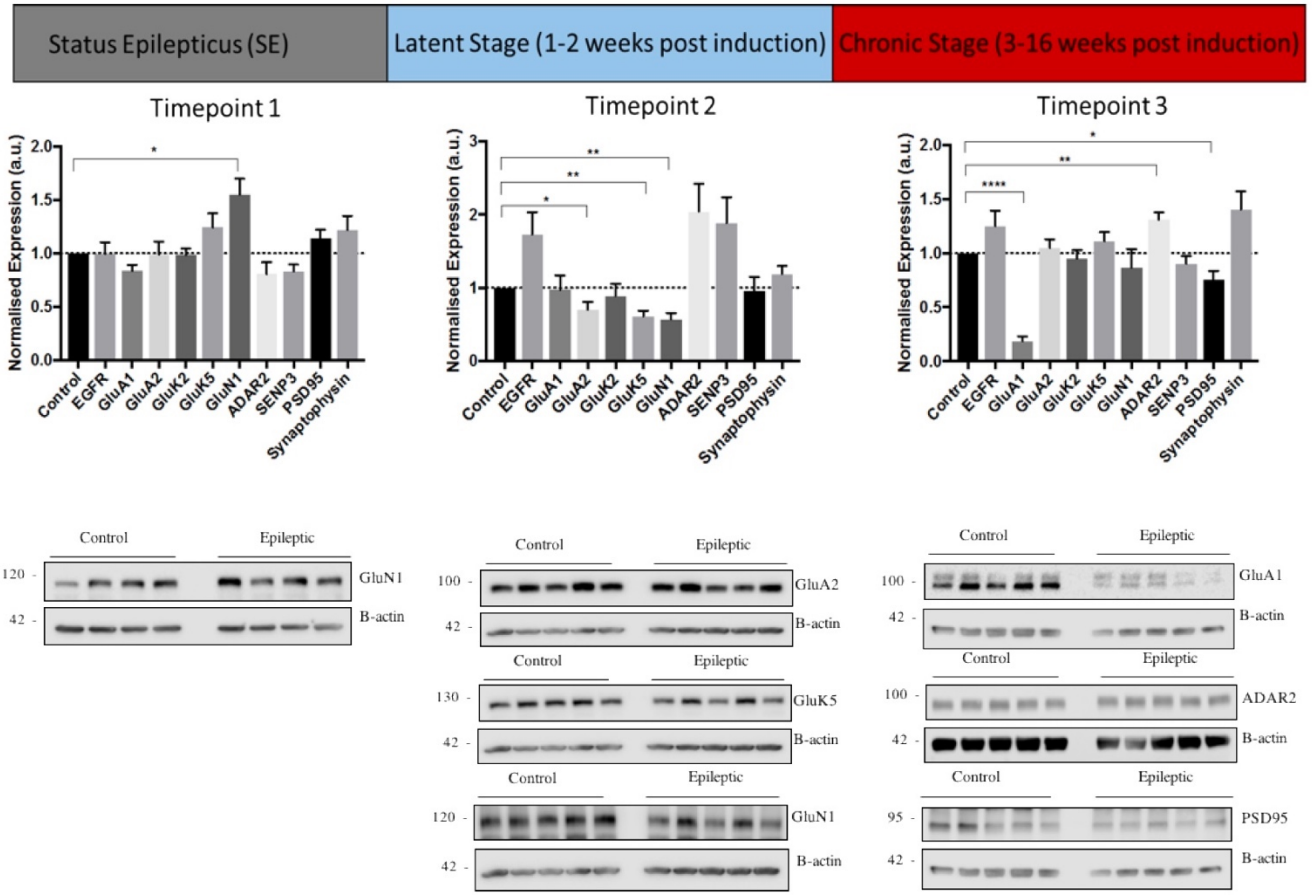

Figure 9.1 Protein expression changes in the TL.
Western blotting analysis was carried out on the TL of SE and AMC rat brain samples (n=4 (time point 1), n=5 (time points 2 & 3)) from across 3x time points, using appropriate primary and HRP-conjugated secondary antibodies to compare protein expression levels for the proteins listed in Table 1. Histograms show expression levels of all proteins relative to the average expression level for the AMC, and blots are shown for proteins displaying altered relative expression levels in SE samples. See Table 8.2 for p-values.

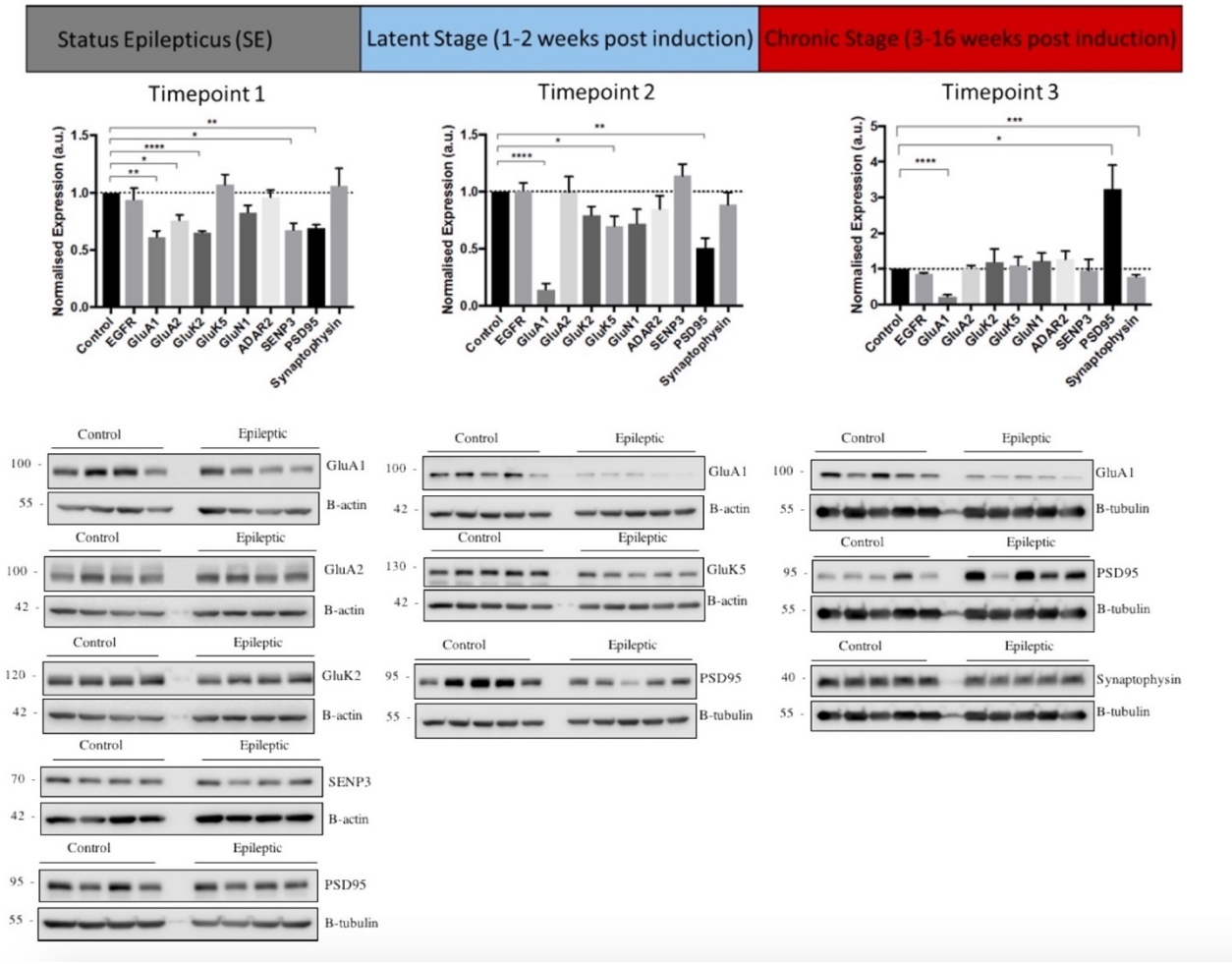

Figure 9.2 Protein expression change in the hippocampus.
Western blotting analysis was carried out on the hippocampi of SE and AMC rat brain samples across 3x time points (n=4 (timepoint 1), n=5 (timepoints 2 & 3)), using appropriate primary and HRP-conjugated secondary antibodies to compare protein expression levels for the proteins listed in Table 1.1. Histograms show expression levels of all proteins relative to the AMC, and blots are shown for proteins displaying altered relative expression levels in SE samples. See Table 8.2 for p-values

Region	Timepoint	Protein	Significance	P-value
Temporal Lobe	1	GluN1	*	0.0360
Temporal Lobe	2	GluA2 GluN1 GluK5	* ** **	0.0454 0.0073 0.0075
Temporal Lobe	3	GluA1 ADAR2 PSD95	**** ** *	<0.0001 0.0101 0.0412
Hippocampus	1	GluA1 GluA2 GluK2 SENP3 PSD95	** * **** * **	0.0058 0.0149 0.0001 0.0139 0.0014
Hippocampus	2	GluA1 GluK5 PSD95	**** * *	<0.0001 0.0253 0.0045
Hippocampus	3	GluA1 PSD95 Synaptophysin	**** * ***	<0.0001 0.0461 0.0007

Table 9.2 Protein expression changes.
A summary of the region, time point, level of significance, and p-values for all proteins whose expression levels were altered in SE rats compared to AMC rats (graphs and blots shown in Figures 8.1 (temporal lobe) and 8.2 (hippocampus).